Satellite Power System: Concept Development and Evaluation Program

Volume III - Power Transmission and Reception Technical Summary and Assessment

R. H. Dietz, G. D. Arndt, J. W. Seyl,
L. Leopold, and J. S. Kelley

JULY 1981

NASA

NASA Reference Publication 1076

Satellite Power System: Concept Development and Evaluation Program

Volume III - Power Transmission and Reception Technical Summary and Assessment

R. H. Dietz, G. D. Arndt, J. W. Seyl,
L. Leopold, and J. S. Kelley
Lyndon B. Johnson Space Center
Houston, Texas

CONTENTS

v

TABLES

FIGURES

ABBREVIATIONS AND ACRONYMS

A	amplifier
ac	alternating current
ACQ	acquisition
AGC	automatic gain control
AMO	air mass zero
AMP	amplifier
ARA	active retrodirective array
ARL	Applied Research Laboratory
BPF	band-pass filter
BW	bandwidth
CCIR	International Radio Consultative Committee
CDEP	Concept Development and Evaluation Program
CFA	crossed-field amplifier
CMT	coherent multiple tone
Cont	controller
CR	concentration ratio
CTE	coefficient of thermal expansion
CW	continuous wave
dBc	decibels below carrier level
dBm	decibels referenced to 1 milliwatt
dBW	decibels referenced to 1 watt
dc	direct current
DCA	direct coupled amplifier
DEC	decision
Det	detector

DIP	diplexer
DOE	Department of Energy
DWG	distribution waveguide
ECM	electronic countermeasures
EDL	electric discharge laser
EIRP	effective isotropic radiated power
EM	electromagnet; electromagnetic
EMI	electromagnetic interference
EOTV	electric orbital transfer vehicle
ERP	effective radiated power
ESTL	Electronic Systems Test Laboratory
E-W	east-west
feb	focused electron beam
FEL	free electron laser
FET	field-effect transistor
GBED	Ground-Based Exploratory Development
GEN	generator
GEO	geosynchronous orbit
HLLV	heavy lift launch vehicle
HPA	high-power amplifier
IC	integrated circuit
i.f.	intermediate frequency
IMPATT	impact avalanche transit time
IPC	interferometric phase control
IRU	interface return unit
ISM	industrial, scientific, and medical

ITS	Institute for Telecommunication Sciences
IVPO	inside vapor phase oxidation
JPL	Jet Propulsion Laboratory
JSC	Lyndon B. Johnson Space Center
KSA	K-band single access
LEMSCO	Lockheed Engineering and Management Services Company
LEO	low Earth orbit
LJ	location jitter
L.O.	local oscillator
LPF	low-pass filter
MA	multiple access
MBG	multibandgap
MESFET	metal Schottky barrier field-effect transistor
MJ	megajoule
MLI	multilayer insulation
mod	modulation
MOS	metal-oxide semiconductor
MPE	mechanical pointing error
MPJ	jitter on mechanical pointing
MPTS	microwave power transmission system
MSFC	George C. Marshall Space Flight Center
MSRTS	master slave returnable timing system
MTBF	mean time between failures
N.A.	numerical aperture
NASA	National Aeronautics and Space Administration
Navsat	navigation satellite

NBS	National Bureau of Standards
NEC	Nippon Electric Company
N-S	north-south
OSC	oscillator
PA	power amplifier
P/A	power amplifier
PCC	phase control center
PCU	power control unit
PD	phase detector
PLV	personnel launch vehicle
PM	permanent magnet
PMA	phase-measurement antenna
PN	pseudonoise
PNSS	PN synchronization system
POTV	personnel orbital transfer vehicle
PPM	periodic permanent magnet
PTAR	power transmission and reception
PTU	phase tracking unit
RCA	Radio Corporation of America
RCR	resonant cavity radiator
RCVR	receiver
rectenna	rectifying antenna
rf	radiofrequency
RFI	radiofrequency interference
rms	root mean square
RPDS	reference phase distribution system

rss	root sum square
RWG	radiating waveguide
SA	single access
S/A	Scientific Atlanta
SCU	signal-conditioning unit
SMART	solar microwave array technology
S/N	signal-to-noise ratio
SOA	state of the art
spacetenna	space-based transmission antenna
SPS	solar power satellite
SS	spread spectrum
SSA	S-band single access
SYNC	synchronization
TDRSS	Tracking and Data Relay Satellite System
TE	transverse electric
TECU	total electron content unit
TRAPATT	trapped plasma avalanche triggered transit
TT&C	tracking, telemetry, and command
TWT	traveling-wave tube
typ.	typical
VCO	voltage-controlled oscillator
VSWR	voltage standing-wave ratio
XMTR	transmitter
XPDR	transponder

SYMBOLS

A	amplitude of pilot signal (fig. III-12); quantity defined in equation (25)
Al	aluminum
B	surface brightness
B/B_o	ratio of magnetic field to design value
$b = e^2/(2\varepsilon_o m)$	quantity used in equation (7)
$b, \bar{b}$	AGC bias control inputs
c	speed of light in a vacuum
CO	carbon monoxide
CO_2	carbon dioxide
D	antenna directivity; antenna diameter
E	electric field vector
e	electron charge
e(t)	time function in figure IV-1
f	frequency
f_c	center frequency
f_D	downlink frequency
f_o	carrier frequency; center frequency (fig. III-76)
f(p)	low-pass filter transfer function
f_p	pilot carrier frequency; plasma frequency
f_r	reference frequency
f_{r1}, f_{r2}	generating frequencies
f_u	uplink frequency
G	antenna gain
GaAs	gallium arsenide

$G(s)$	signal gain
G_A	1-kilometer-diameter antenna gain at 2.45 gigahertz
G_H	1-kilometer-diameter antenna gain at n-th harmonic
G_K	antenna gain of average klystron power module
G_{LH}	harmonic antenna gain relative to fundamental
G_{SS}	antenna gain of average solid-state power module
g	slot conductance
H	magnetic field vector
$H(S)$	loop filter function
I	current
I^2R	power dissipated as heat
I_D	design current
I_R	coherent power beam signal power
I_T	total isolation
K_D	quantity representing ionospheric effects on downlink signal
K_u	quantity representing ionospheric effects on uplink signal
K_1, K_2	antenna gains
L	physical path length
L_1	inner scale length of variations
L_2	thickness of irregularity region
ℓ	path length; slot length
M	PN code length
m	shift-register sequence; electron mass (eq. (7))
N	electron density
N_c	electron columnar content
N_U	number of units

n	refractive index
P_D	power density
P_H	n-th harmonic power transmitted
P_{H-gr}	harmonic power density at the ground
P_{LH}	harmonic power relative to fundamental
P_r	received power
P_T	fundamental (2.45 gigahertz) power transmitted; total power (fig. III-57)
$P_{T-K(N)}$	transmitted noise power from klystron antenna
$P_{T-SS(N)}$	transmitted noise power from solid-state antenna
P_U	unit power
R	resistance; range; radius of curvature (eq. (34))
R_c	PN chip rate
$r(t)$	time function in figure IV-1
r_B	boresight radius
r_e	classical radius of the electron
r_o	Fresnel zone radius
$S(f)$	power spectrum
S_p	pilot signal received power level
s	slope; path
$s(t)$	time function in figure IV-1
s_1, s_{r1}	signals transmitted from reference transmitter
s_2	signal transmitted by power module being phase tuned
$TE_{m,o}$	electromagnetic field propagation configuration, $1 \leq m \leq 10$
t	time
U_{max}	maximum radiation intensity

$\bar{U}$	average radiation intensity
V	voltage
V_D	design voltage
V_G	gate bias voltage
w_r	ring width
$x(t)$	time function in figure IV-1
$y(t)$	time function in figure IV-1
Δ	change; phase change due to path distance (fig. IV-1)
ΔN_{rms}	rms density perturbation
$\delta\phi_A = \phi_2 - \phi_1$	quantity defined in equation (14)
$\delta\phi_B = \phi_1 - \phi_3$	quantity defined in equation (15)
$\delta_2\phi = \delta\phi_A - \delta\phi_B$	quantity defined in equation (16)
ε_o	free-space permittivity
η	efficiency
η_c	collector recovery efficiency
η_{CCT}	circuit efficiency
η_e	electronic efficiency
θ	inclination angle; azimuth angle variable (Sec. IV)
θ_i	beam width
θ_J	phase jitter
θ_o	reference-signal phase
θ_R	reference-signal phase (fig. IV-6)
λ	wavelength
$\lambda = 360°$	parameter used for estimating antenna location jitter
λ_g	waveguide wavelength
λ_o	free-space wavelength

σ_{GJ}	carrier recovery loop phase jitter
ϕ	phase; elevation angle variable (Sec. IV)
ϕ_i	received pilot signal phase (fig. IV-6)
ϕ_M	reference-signal phase
ϕ_o	initial VCO phase
ϕ_s	transferred phase
ϕ_1	channel-induced phase shift at $f_o + \Delta f$
ϕ_2	channel-induced phase shift at $f_o - \Delta f$
ϕ^*	conjugated phase
Ω	angular space
ω	angular frequency
ω_o	reference-signal radian frequency

Superscripts

R	receiver
T	transmitter

Subscript

down	downlink

SUMMARY

The solar power satellite Concept Development and Evaluation Program was conducted jointly by the National Aeronautics and Space Administration and the Department of Energy. With respect to the power transmission and reception system, the purpose of the program was to refine concepts within the initial constraints of providing electricity at minimum cost and maximum efficiency and of maintaining a transmitting antenna power density limit of 23 kW/m^2, a maximum radiofrequency power density in the ionosphere of 23 mW/cm^2, and a power transmission frequency of 2.45 gigahertz. On the basis of these constraints, the basic klystron reference configuration was optimized at 5 gigawatts power delivered to the utility grid, a 1-kilometer-diameter transmitting antenna, and a 10-kilometer-diameter ground rectifying antenna. System sizing trade-off studies were performed, and alternative concepts such as solid-state power amplifiers were considered. Certain critical supporting investigations were performed to develop a better understanding of hardware implications in the areas of phase control, power amplifiers, and radiating elements. Finally, a workshop was held to evaluate the results of the program and to make recommendations for subsequent development efforts.

I. INTRODUCTION

This report is a summary of the technical assessment activities on the solar power satellite (SPS) power transmission and reception (PTAR) system which took place during the Department of Energy (DOE)/NASA Concept Development and Evaluation Program (CDEP). It is one of a series of SPS CDEP technical summary and assessment reports. Three major topics are treated: PTAR system studies, experimental investigations, and conclusions. Within the PTAR system studies area (Section III) is a section on each of the major subsystems (system performance, phase control, power amplifiers, radiating elements, and rectenna) plus a section on solid-state configurations.

One of the major outputs of the assessment activities was the SPS reference configuration as documented in reference 1. Assessment activities performed after the issuance of the reference configuration report are documented herein. Changes to the reference configuration are discussed, alternative concepts for each subsystem are presented, the system workshop is discussed, conclusions are presented, and remaining issues are identified.

Section II contains an overview of all PTAR system assessment activities during the SPS CDEP. Section III contains a section on each of the major subsystems. Each of those sections includes a discussion on alternate approaches, changes to the reference configuration as applicable, and the conclusions reached and issues identified. Section IV contains a discussion of the critical technology supporting investigations performed in the areas of phase control, power amplifiers, and radiating elements. The conclusions reached and the issues identified on the PTAR system level are presented in Section V.

In compliance with the NASA's publication policy, the original units of measure have been converted to the equivalent value in the Système International d'Unités (SI). As an aid to the reader, the SI units are written first and the original units are written parenthetically thereafter.

II. OVERVIEW

Definition and assessment of the SPS PTAR system has been an important part of the DOE/NASA Concept Development and Evaluation Program (ref. 2). A detailed description of the microwave PTAR system is contained in the SPS reference system report (ref. 1) as well as discussions of system and subsystem trade-offs which led to the reference system. Since then, major system assessment activities have been in support of (1) solid-state PTAR system studies, (2) critical technology supporting investigations, and (3) continued PTAR system and subsystem trade-offs. Preliminary laser concepts have been analyzed for overall SPS integration feasibility but not to the depth of the microwave system analysis. A discussion of laser concepts is contained in references 3 and 4.

System assessments have generally resulted in the conclusion that transferring gigawatt power levels between two points using microwaves is technically feasible. Certain changes are recommended to the reference concept regarding phase control to the power module level, allowable amplitude jitter on the antenna, and startup/shutdown procedures. Alternative concepts have been studied in each subsystem area as follows.

1. System performance - smaller systems, multiple beams

2. Phase control - retrodirective, ground based

3. Power amplifiers - klystron, magnetron, and solid state

4. Radiating elements - slotted waveguide, resonant cavity, aluminum (Al), metal-matrix composites

5. Rectenna - dipole/diode, yagi-uda/diode, other higher gain receive elements

Certain critical supporting investigations have developed a better understanding of the hardware implications in the phase control, power amplifier, and radiating-element areas. The subsystem studies are summarized in subsequent sections. The microwave system conclusions and remaining issues are documented in the last section.

A. SYSTEM ASSESSMENT ACTIVITIES

A considerable body of information has been developed as part of the joint DOE/NASA program; this material will serve as an excellent data base for future activities in this area. Most activities have been contracted efforts through the two NASA SPS centers, the Lyndon B. Johnson Space Center (JSC) and the George C. Marshall Space Flight Center (MSFC). Also, a considerable amount of in-house effort has been devoted to special projects. All these efforts were tied together in a major peer review and assessment process at the SPS Workshop on Microwave Power Transmission and Reception (ref. 5).

1. SOLAR POWER SATELLITE CONTRACTED EFFORTS

System evaluation activities fall into three major areas, each of which received an approximately equal share of funding: (a) microwave system studies (including that portion of the overall SPS system definition studies concentrated on the microwave system and subsystems) conducted primarily by Boeing Aerospace Company and Rockwell International; (b) independent subsystem studies (including phase control, power amplifiers, antenna, rectenna, and ionospheric effects) conducted by a variety of contractors; and (c) experimental critical supporting investigations conducted by various contractors in the areas of phase control, solid state, magnetron, waveguide, and ionospheric effects.

2. IN-HOUSE NASA EFFORTS

The NASA in-house efforts have consisted of both contracted studies and experiments funded with non-SPS funds and special studies conducted by NASA personnel. A sonic simulator of the microwave system has been evaluated for possible use in investigating effects of the disturbed ionosphere on the phase control uplink pilot signal. The rectenna has been modeled to evaluate levels and patterns resulting from harmonic and fundamental reradiation. System interference and environmental effects due to radiofrequency (rf) beat-frequency generation from multiple SPS's have been investigated. Also, metal-matrix composites (e.g., graphite aluminum) have been evaluated in several areas: (a) capability to maintain the close tolerances required by the SPS waveguides under thermal stress, (b) rf performance characteristics, (c) fabrication techniques, and (d) reproducibility.

Some of the special studies conducted by NASA personnel have included technical and economic trade-offs of small SPS systems configured with larger antennas, smaller rectennas, and less power to the grid. Also, potential areas of interference have been investigated including SPS to SPS, SPS to Tracking and Data Relay Satellite System (TDRSS), power beam to uplink pilot signal, and covert interference. Results indicate the existence of sufficient signal-to-interference margins.

3. SYSTEM WORKSHOP

As part of the system assessment activities, the SPS Workshop on Microwave Power Transmission and Reception was held at JSC on January 15 to 18, 1980. This workshop evaluated all the efforts funded as part of the DOE/ NASA SPS Concept Development and Evaluation Program as well as historical data in some areas. Peer review was accommodated by having the workshop material assessed and critiqued by a review panel consisting of prominent individuals in the field. Additional evaluations made following the workshop addressed some of the areas critiqued by the review panel. These evaluations are contained in this report.

a. Workshop Organization

The objectives of the workshop were (1) to assess and critique the assumptions, methodologies, and conclusions of the investigations

and (2) to assess and critique the critical issues identified and the recommended follow-on work. The workshop addressed all aspects of microwave PTAR system activities including studies, analyses, and laboratory investigations. It was organized into eight sessions as follows: General, System Performance, Phase Control, Power Amplifiers, Radiating Elements, Rectenna, Solid-State Configurations, and Planned Program Activities. As part of the documentation of the workshop, summary papers were published and distributed (ref. 5).

b. Review Panel Report: Summary

The consensus of the workshop review panel was that a 5-gigawatt microwave PTAR system would probably be technically feasible; however, a large amount of work was believed to be necessary in a number of areas to establish certainty and to determine system efficiency, reliability, rf compatibility, security, safety, longevity, and cost. The panel believed that the final system may not resemble the current reference system and urged NASA to recognize this difference in all future planning. The Ground-Based Exploratory Development (GBED) program appeared to be excessively integrated with the reference system.

The panel recommended more attention to system engineering, failure analysis, sensitivity studies to optimize cost effectiveness, system security and antijamming features, and periodic overall design reviews to update critical design parameters. In view of the magnitude and potential importance of the SPS, the panel recommended major program management status and a single program office within NASA for greater coordination of the contractor efforts.

Finally, the panel recognized the outstanding effort to date by the SPS team and the very good progress made. The complete review panel report is included in this document as an appendix.

B. SYSTEM OPTIONS

Investigation of concepts for power transmission and reception has been concentrated on microwaves as a transport means, although preliminary laser concepts have recently been analyzed for overall SPS integration feasibility. Although the use of lasers offers several potential advantages (smaller blocks of power; not subject to possible long-term, low-level microwave effects), these are offset by major difficulties (achieving high-efficiency power transfer, laser system complexity, atmospheric propagation characteristics, and general state of technology development). Only microwave system concepts are considered herein.

Microwave transmission can be accomplished in a variety of ways. Five options are illustrated in figure II-1. The power amplifiers (rf converters) can be located on an antenna which is separate from the photovoltaic array or they can be an integral part of the photovoltaic array. In turn, the separate antenna can be designed to accommodate all three types of power amplifiers: linear beam amplifiers, crossed-field amplifiers (CFA's), and solid-state devices. The primary advantage of the separate antenna

RF Converter   **Antenna mounted**   **Solar cell mounted (concentration ratio = 3)**
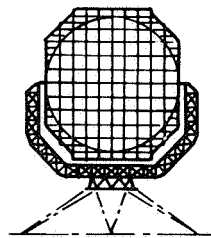
                                           Optical reflector   **rf reflector**
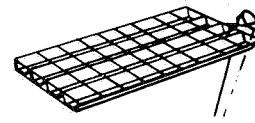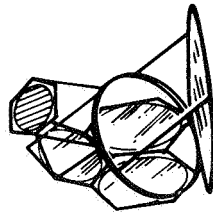
SPS Design	**Klystron or CFA**	**Solid state**	**Solid state**	**Solid state**
Power output to grid	5 GW	2.5 GW	1.2 GW	0.2 GW per km^2 solar cells
Space antenna diameter	1 km	1.4 km	1.77 km	High-power waveguide
Rectenna diameter at 23 mW/cm^2	10 km	7.1 km	5.0 km	Not determined
Antenna	10 dB taper	10 dB taper	Uniform	Advanced horn feb paraboloid

Figure II-1.- Microwave system options. (feb is focused electron beam.)

is that it can accommodate maximum packing density of the power amplifiers up to the thermal dissipation limit. Because of the power thermal limits (channel temperature) on solid-state amplifiers, transmitted power is not as great and the antenna is larger when compared to a tube configuration. This disadvantage is even greater for the integrated photovoltaic/solid-state power amplifier option since this configuration is limited by area and prime power rather than by temperature. Overall size per delivered kilowatt of this configuration is also larger. The major anticipated advantages of the solid-state concept (both separate and integrated antenna) are higher relia-bility (and thus lower maintenance costs) and greater amenability to mass manufacturing.

The integrated solid-state rf reflector option results in conversion of photovoltaic direct current (dc) immediately to rf and in rf distribution along the array to a reflector antenna. This option was dropped from further consideration because of the difficult technology development requirements anticipated in the disciplines of rf waveguides and rf reflectors.

Of the five options illustrated, the antenna-mounted klystron config-uration has been thoroughly evaluated and developed into the current SPS ref-erence system. Within the last several years, projected efficiency, gain, and power output of solid-state devices have made them attractive for application to the SPS concept. The separate antenna configuration and the integrated photovoltaic/power amplifier (so-called "sandwich") configuration were evalua-ted for technical and cost effectiveness. To the depth studied, it appears that cost per kilowatt may be somewhat higher than that of the reference sys-tem, although, as cost estimates have been refined, the costs have trended toward convergence.

C. SYSTEM DEFINITION DRIVERS

Several basic assumptions and constraints affect the total microwave PTAR system definition. The current klystron reference configuration was optimized at 5 gigawatts delivered to the utility grid, a 1-kilometer-diameter transmit antenna, and a 10-kilometer-diameter rectenna. This opti-mization was based on two assumptions and three assumed constraints (based on analyses) as follows.

1. Minimum cost of electricity

2. Projections of system efficiencies

3. Transmit antenna rf power density limit of 23 kW/m^2

4. Maximum rf power density in the ionosphere of 23 mW/cm^2

5. Power transmission frequency of 2.45 gigahertz

These assumptions are the same for the solid-state configurations except that (1) the operating temperature is in the range 373 to 398 K (100° to 125° C) and (2) the projected system efficiencies are based on the use of solid-state amplifiers. These assumptions and assumed constraints are based on best

available analyses and experimental data; if they are changed, definition of the system also changes. For example, if the ionospheric limit is changed to 54 mW/cm^2, the rectenna diameter can be reduced to 6.8 kilometers, with an increase in transmit antenna diameter to 1.5 kilometers and an increase in cost of electricity of 17 percent. This change in the reference sizing may be an acceptable alternative; however, the critical requirement is a realistic assessment of the actual ionospheric power density limit. Various tradeoffs using different assumptions and constraints have been made and are discussed in Section III.A.4 and documented in reference 6.

D. REFERENCE SYSTEM UPDATES AND STUDIES

The microwave system is defined in reference 1. The concept for power transmission is shown in figure II-2. In this concept, the linear beam klystron is used to convert from dc to rf energy. The 70-kilowatt klystron together with a cooling system, slotted-waveguide radiators, phase control receiver and conjugation electronics, and other necessary hardware comprise the transmit antenna power module. There are 4 to 36 power modules in an antenna subarray depending on the subarray location with respect to the overall tapered antenna array. There are 7220 subarrays in the 1-kilometer-diameter array.

The receiving array (rectenna) on the ground is characterized by immediate rectification from rf to dc. A typical configuration is shown in figure II-3. Individual dipole antennas are used as the receiving element, and, since rectification takes place immediately, dc power is collected from each element and fed into parallel and series strings to build up the voltage and current levels. Figure II-4 is an illustration of the overall microwave PTAR concept and shows subsystem interrelationships in both the transmit and the receive arrays.

As a result of continuing NASA and contractor system investigations and trade-offs since 1978, the following changes are made to the reference system: (1) phase conjugation is performed at the power module level (101 552 points) rather than at the subarray level (7220 points) (fig. II-4), (2) allowable amplitude jitter across the surface of a subarray is changed from ±1 decibel to ±1 percent, and (3) to ensure that SPS startup/shutdown procedures produce side-lobe levels lower than steady-state levels, the three allowable sequences are random, incoherent phasing, and center-to-edge concentric rings. In addition to the investigations that resulted in these changes, a considerable number of other studies have contributed to a better understanding of the SPS concept and to the microwave PTAR data base. These studies are highlighted in the following paragraphs and discussed in more detail in subsequent sections.

1. SYSTEM PERFORMANCE

System performance studies were concentrated on (a) parametric effects for all elements in the efficiency chain, (b) ionospheric analyses and test results from Arecibo, Puerto Rico, and Platteville, Colorado, (c) radiofrequency interference (RFI)/electromagnetic interference (EMI) for the transmit array and the rectenna, (d) reshaping of the power beam, and (e) multiple beams from one transmit array.

10

Subarray

70-kW
heat-pipe-
cooled klystron

Power module

Main structure

Transmit
antenna array

Power processing
and distribution
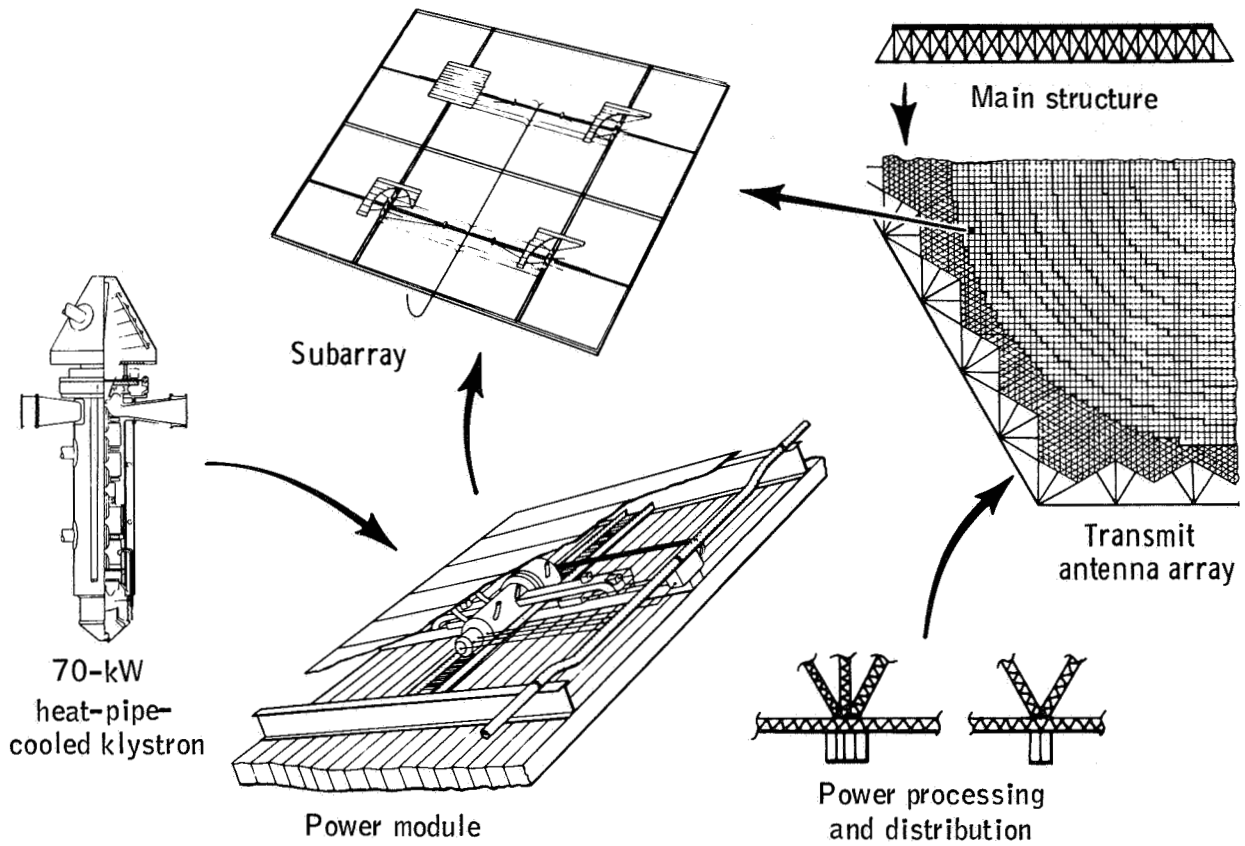
Figure II-2.- Microwave power transmission design concept.

Backstop
screen

Electrical
power out

Dipole
antenna
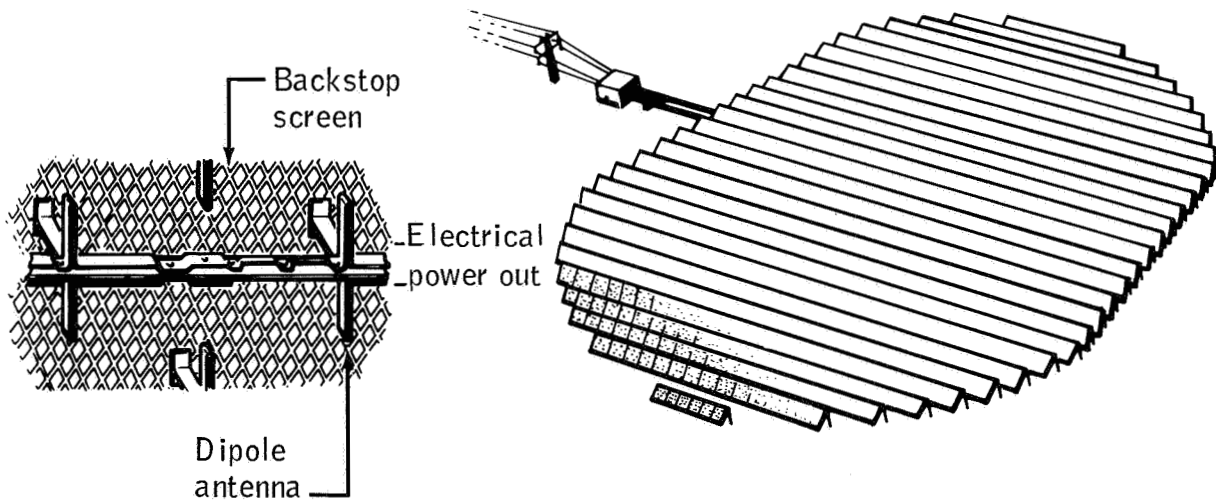
Figure II-3.- Typical rectenna configuration.

11

Reference SPS
microwave system

Rectenna

Rectenna
inverter
blocks

Rectenna arrays,
panels, units,
and groups

Rectenna
element

├ Antenna element
├ Rectifier
├ Filters
└ Termination

Power-
combining
networks

Radiating module
One/power module
101 552/array

├ Feedguides
├ Diplexer
└ Cross guides

Solid state

Transmit antenna array

Antenna subarray
7220/array

Power module
4 to 36/subarray
101 552/array

Microwave
power
amplifier

70-kW klystron
One/power XPDR
101 552/array

Thermal control
├ Heat pipe
└ Radiators

Reference phase
distr system

├ Phase control
   centers
├ Distribution
   "cables"

Power transponder
One/power module
101 552/array

├ Pilot recovery
   and conjugation
   receiver
└ P/A phase control
   and noise-
   suppression
   loop

Figure II-4.- Reference SPS microwave system. (XPDR is transponder;
P/A is power amplifier.)

2. PHASE CONTROL

Work in the phase control area was concentrated on defining the reference phase control system for SPS. Alternate concepts also were studied including interferometer and coherent multiple-tone ground-based systems (refs. 5, 7, and 8). A major concern for all the phase control system concepts was the lack of analytical or experimental data on the ionosphere usable for predicting phase errors in the presence of ionospheric disturbances.

3. POWER AMPLIFIERS

Besides the investigations into the klystron and its integration into the system, power amplifier study efforts were concentrated on solid-state amplifiers and the magnetron. Considerable advancement in gallium arsenide (GaAs) field-effect transistors (FET's) over the past several years has indicated that projected parameters of efficiency, power output, and gain may be suitable for use in the SPS concept (refs. 5 and 9). Interest in the magnetron was renewed when it was determined that the inherent noise levels could be reduced considerably when the filament was turned off after initial startup.

4. RADIATING ELEMENTS

The main thrusts in the radiating-element area were to investigate characteristics of a slotted-waveguide array, need for and characteristics of a separate receive aperture, and initial investigations into high-accuracy measurement techniques.

5. RECTENNA

The reference rectenna concept provides an extremely efficient means of receiving rf and converting it into dc for use by the utility grid. One of the disadvantages is the tremendous number of receive antennas/rectifiers required. Several studies were conducted to reduce the number of elements and to reduce the manufacturing costs of the large number of elements required (refs. 5 and 10). Problems of reradiation (both fundamental and harmonic) were also investigated (refs. 5 and 10).

E. SOLID-STATE CONFIGURATIONS

Because of the continued advancement of solid-state technology, application of this technology to SPS appears promising. As illustrated in figure II-1, there are two basic configurations for the solid-state application: a separate antenna similar to the reference concept and an integrated photovoltaic/antenna or sandwich approach.

Both of these concepts are characterized by larger antennas (due to device cooling requirements), greater satellite mass per kilowatt of delivered power, lower output to the utility grid, and smaller rectennas. They have the advantage of increased reliability and thus lower maintenance costs. Disadvantages include increased phase control system complexity,

13

lower voltage (higher loss) dc power distribution (for the separate antenna), larger parts count, and possible increased noise generation and EMI suscepti- bility.

F. CRITICAL SUPPORTING INVESTIGATIONS

Critical supporting investigations are special, generally experi- mental, investigations funded as part of the DOE/NASA SPS Concept Development and Evaluation Program. A better understanding of the hardware implications in the following areas was obtained through these studies.

1. Design and breadboard evaluation of the SPS reference phase con- trol system

2. SPS fiber optics link assessment

3. Six-element S-band active retrodirective array (ARA) phase error evaluation

4. SPS antenna element evaluation

5. SPS solid-state antenna power combiner

6. SPS solid-state amplifier development

7. SPS magnetron tube assessment

8. Microwave ionospheric interaction experiment

Details of these eight activities are discussed in Section IV of this report.

G. CONCLUSIONS AND REMAINING ISSUES

As a result of the activities performed during the DOE/NASA Concept Development and Evaluation Program, certain conclusions have been reached and certain remaining issues have been identified. These were presented and discussed as part of the system workshop held at JSC in January 1980. Over- all conclusions resulting from both experimental and analytical evaluations are (1) that transferring of gigawatt power levels between two points using microwaves is feasible and (2) that a 5-gigawatt SPS microwave PTAR system is probably technically feasible. Detailed conclusions and remaining issues for each subsystem area are discussed in Section III. The conclusions and remaining issues for the overall PTAR system are presented in Section V.

III. SYSTEM STUDIES

In this section, the activities accomplished in the area of microwave PTAR system studies are summarized. It contains a discussion of the major assessment activities for each subsystem (system performance, phase control, power amplifiers, radiating elements, and rectenna) plus a subsection on solid-state configurations. A technical summary and assessment is presented in each subsection together with conclusions reached and remaining issues identified. Also, each subsection contains a discussion of alternate approaches and changes to the reference configuration as applicable.

A. SYSTEM PERFORMANCE

The SPS microwave system, as defined in reference 1, has a 1-kilometer-diameter phased array antenna with a 10-decibel Gaussian taper illumination which focuses the beam at the center of the ground antenna/ rectifying system (rectenna). Approximately 88 percent of the power beam energy is contained within a 5-kilometer radius from the rectenna boresight, with a resultant beam width of 1.2 arc-minutes. Mechanical alinement of the 1-kilometer antenna is maintained within 1 arc-minute, whereas electronic alinement has an accuracy of 1.8 arc-seconds. The dc-rf power converters within the antenna are 70-kilowatt klystrons fed by 40-kilovolt powerlines from a series/parallel solar array configuration. The antenna is divided into 7220 mechanical subarrays, 10.4 by 10.4 meters on a side, having slotted waveguides as the radiating surface. Slotted waveguides were selected because of their high-power handling capabilities and low I^2R losses.

The klystrons are phase controlled at the individual tube level through the use of a retrodirective pilot-beam signal transmitted from the center of the rectenna and phase conjugated in receivers in each power module. An onboard phase reference signal is distributed through the antenna to provide the same reference in each conjugating receiver. The reference phase distribution system is implemented in the form of a four-level tree structure with electronic compensation for minimizing phase shifts due to unequal path lengths from the center of the transmit antenna to each phase control receiver. The uplink pilot-beam signal has a double-sideband, suppressed carrier with code modulation to provide link security and antijamming protection from radiofrequency interference.

The ground rectenna converts the rf energy to dc electricity using half-wave dipoles feeding Schottky barrier diodes. Coherence of the incoming phase front needs to be maintained only over the small area associated with those dipoles phased together. Physically, the current rectenna configuration is a series of serrated panels perpendicular to the incoming beam and covers approximately 75 square kilometers. A 75- to 80-percent optical transparency of the panels enables other use of the area beneath the rectenna if desired.

The SPS sizing of the 1-kilometer transmit antenna and 5 gigawatts of dc output power from the rectenna is based on a 23-kW/m^2 rf power density in the antenna (thermal dissipation limit) and a hypothetical 23-mW/cm^2 peak power density limit in the ionosphere to prevent nonlinear heating. System

15

sizing trade-offs given in Section III.A.4 indicate that the ionospheric limit is a critical design and costing parameter. This limit may be revised upward pending the completion of the Department of Energy environmental assessment studies on ionospheric heating.

The conclusions regarding SPS system performance are as follows.

1. System sizing

    a. Reduced power levels (<5 gigawatts) are feasible with a modest electricity cost increase.

    b. Antenna diameters for systems operating at 2.45 gigahertz should not be less than 1 kilometer.

2. Antenna illumination - A 10-decibel Gaussian taper maximizes rectenna collection efficiency and minimizes side-lobe levels while operating within antenna thermal requirements and ionospheric power density limitations.

3. Antenna/subarray mechanical requirements

    a. Alinement requirements are determined by grating-lobe peaks and scattered power levels.

    b. Antenna alinement requirement is 1 arc-minute or 3 arc-minutes depending on the phase control configuration.

    c. Subarray alinement requirement is 3 arc-minutes as determined by scattered power levels.

4. Startup/shutdown operations - Three possible startup/shutdown sequences provide satisfactory performance: random; incoherent phasing; and concentric rings, center to edge.

5. Scattered microwave power - System error parameters have been defined to minimize scattered power as shown in figure III-1.

6. Faraday rotation by the ionosphere is small.

7. Antenna construction techniques are projected to be within the state of the art to meet the stringent flatness/alinement tolerances if low coefficient of thermal expansion (CTE) materials are used.

16
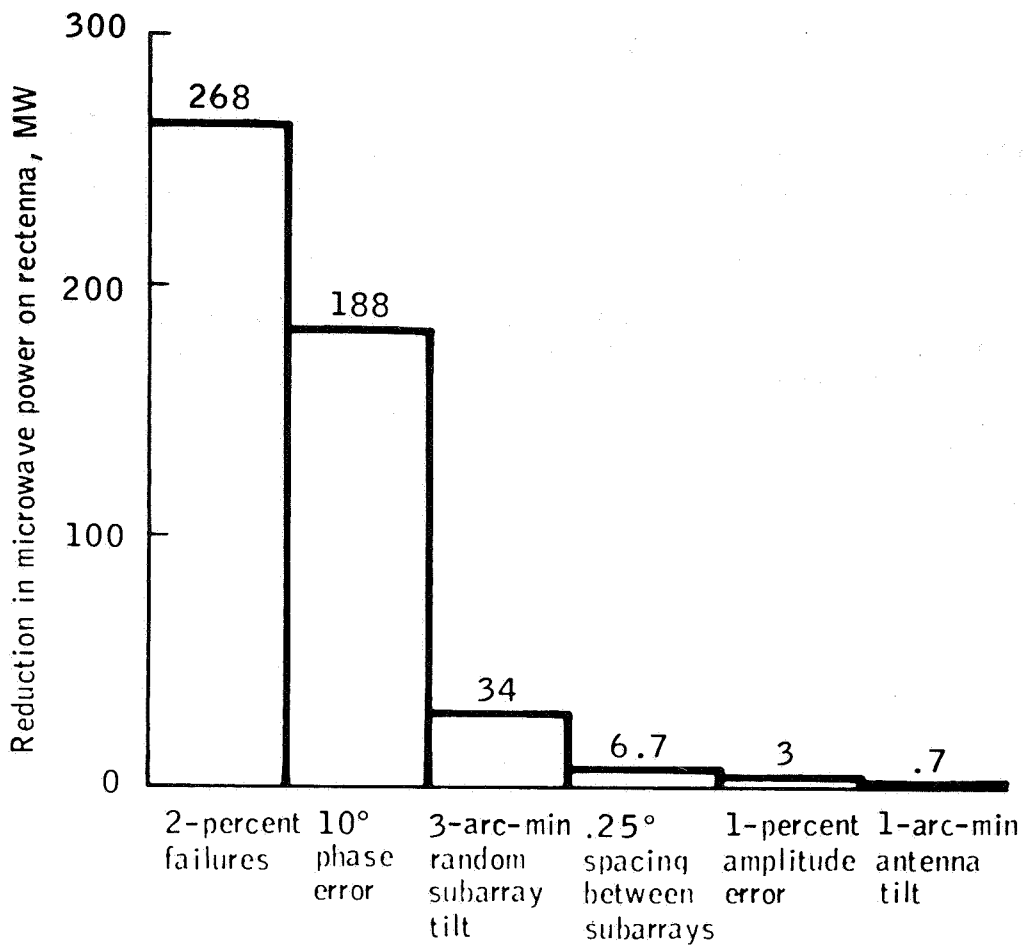
Figure III-1.- Reduction in microwave power due to electrical and mechanical errors (power-module-level phase control).

1. REFERENCE SYSTEM MODIFICATIONS

Several changes in the microwave system are recommended as a result of recent NASA and contractor studies. These modifications to the reference system documented in reference 1 include the following.

a. Phase Control to the Power Module (Tube) Level

It is recommended that phase conjugation be performed at each of the 101 552 power modules rather than at the 7220 subarrays. The advantages of phase control at the tube level are a reduction in the antenna and subarray mechanical tilt requirements (or a reduction in scattered microwave power if the same tilt requirements are maintained) and a reduction in the effects of distributed phase errors within the subarrays. The disadvantage is increased cost due to the 94 000 additional phase control receivers. At the DOE/NASA SPS Program Review held in Washington, D.C., in June 1979, it was reported that an overall cost savings could be achieved (i.e., the cost benefits of less scattered power were greater than the additional receiver costs) if the phase control receivers were less than $600 each. A later Boeing Aerospace Company study indicates that these receivers can be built for approximately $600 in high-volume quantities. There is also an environmental advantage in phase controlling at the power module level in that the grating lobes incident on the Earth are reduced in amplitude and in quantity. The locations and amplitudes of the grating lobes from a single 5-gigawatt SPS system with phase control to the power module level are shown in figures III-2 and III-3. Recent simulation results indicate that the off-axis grating lobes will be reduced by 2×10^{-4} (37 decibels down) from the data shown in the figures. Therefore, only the grating lobes on the principal axes (X and Y) are significant.

The location jitter, or the error in path length from the pilot beam transmitter to each radiating slot in the antenna, is reduced by going to the smaller antenna area associated with an individual tube rather than to the larger subarray. This location jitter, which appears as a phase error, scatters 6 megawatts of power at the tube level as compared to 87 megawatts at the subarray level. Another advantage of phase controlling to the tube level is that if a total failure of the phase control system occurs, the power density at the ground reduces to 0.0002 mW/cm^2, which is one-fourteenth the 0.003-mW/cm^2 value associated with phase controlling to the subarray level.

b. Allowable Amplitude Jitter

The reference SPS system has a ±1-decibel amplitude jitter across the surface of each subarray or power module. Analysis results indicate that power-transfer efficiency (88 percent for the reference system) is relatively insensitive to amplitude jitter. However, the voltage and amplitude regulations for the high-efficiency, high-gain klystron tubes have to be maintained to approximately 1 percent for satisfactory operation. Therefore, a ±1-percent amplitude tolerance is recommended for the antenna error parameter. This change will not affect the microwave transmission efficiency budget.

18
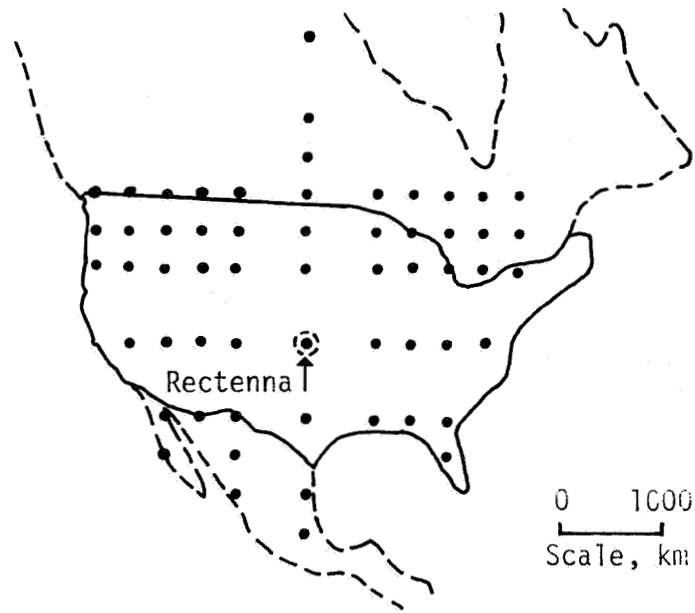
Figure III-2.- Grating locations for a single beam.
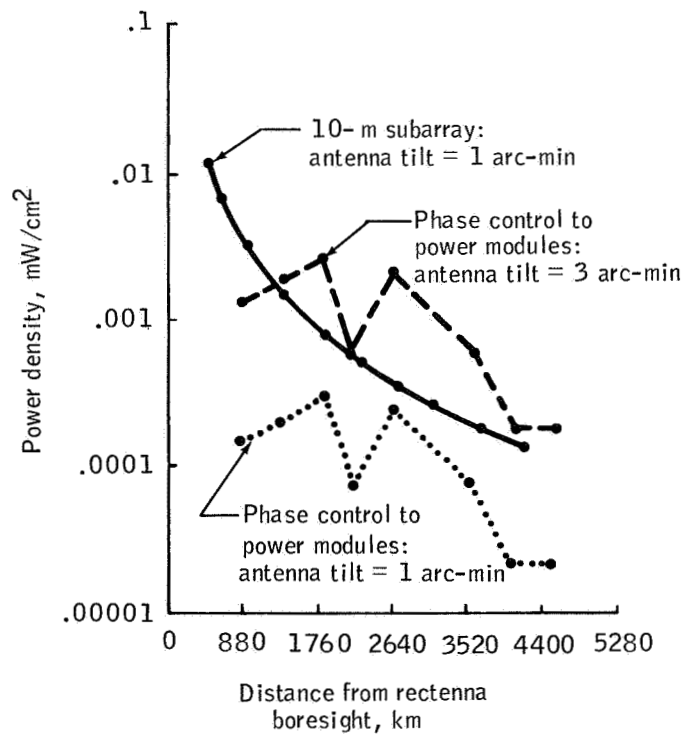
Figure III-3.- Grating-lobe peaks for 10-meter subarrays and phase control to power modules (tubes). Conditions: 10-decibel Gaussian taper, 10° phase error, ±1-decibel amplitude jitter, 2-percent failure rate, and no subarray tilt.

19

c.   Metal-Matrix Waveguides

The SPS reference system has aluminum for the subarray distribution and radiating waveguides. Because of thermal distortion problems, a graphite/aluminum metal-matrix composite is now being developed as a possible replacement for the aluminum.

The antenna structural members are composed of a high-temperature graphite plastic material for rigidity. The antenna primary structure has a 1040- by 1040- by 100-meter pentahedral truss configuration which supports a secondary structure. This secondary structure provides a base for mounting and alining the transmitter subarrays. Both primary and secondary structures must maintain a high degree of stability over wide operating-temperature fluctuations to preserve the 3-arc-minute flatness requirements; therefore, low-CTE materials are needed.

d.   Startup/Shutdown Procedure

The satellite will have to be shut down 87 times per year because of solar eclipses by the Earth. In addition, there will be eclipses by the Moon and other SPS's as well as scheduled shutdowns for maintenance. A number of possible sequences for energizing/deenergizing the microwave system were investigated (ref. 11). Three sequences provided satisfactory performance in that the resultant side-lobe levels during startup/shutdown were lower than the steady-state levels present during normal operations. These three sequences were random; incoherent phasing; and concentric rings, center to edge. Thus, no microwave radiation problems are anticipated during startup or shutdown operations, either scheduled or unscheduled.

The characteristics and error parameters of the updated microwave transmission system are summarized in table III-1. The relative importance of these electrical and mechanical tolerances on scattered microwave power (power not incident on the rectenna) is summarized in figure III-1.

2.   COST SENSITIVITIES FOR THE REFERENCE SYSTEM EFFICIENCY CHAIN

Changes in system efficiencies will have economic as well as environmental impacts on overall SPS performance. From a systems viewpoint, it is important to ascertain the benefits (or losses) derived from a small improvement (or degradation) in the performance of each subsystem. For example, is it economical to spend $50 million to improve the dc-rf conversion efficiency of the klystrons by 1 percent? The answer is yes, as will be shown.

The SPS efficiency chain from the solar array output in the satellite antenna to the utility grid busbar at the ground is shown in figure III-4 (ref. 1). In terms of economics, there are two types of degradations inherent in the system design.

a.   Type A - degradations leading to losses that can be compensated for by simply increasing the amount of power generated by the solar array

TABLE III-1.- CHARACTERISTICS AND ERROR PARAMETERS
OF MODIFIED MICROWAVE TRANSMISSION SYSTEM

Characteristic
  Transmit frequency, GHz 2.45
  Output power to power grid,[a] GW   5
  Transmit array diameter, km   1
  Power radiated from transmit
    array, GW 6.72
  Microwave system efficiency,[b]
    percent   63
  Array aperture illumination . . . .   10-step, truncated Gaussian
                                                 amplitude distribution with
                                                      10-dB edge taper

  Peak microwave density in
    ionosphere, mW/cm^2   23
  Phase control . . . .   To power module level
  Waveguide material . . . .   Metal-matrix composite

Error budget
  Total rms phase error per power
    module, deg   10
  Amplitude tolerance per power
    module, percent . . . .   ±1
  Failure rate of dc-rf power converter
    tubes, percent . . . .   [c]2
  Mechanical alinement, arc-min
    Antenna   1
    Subarray   3

[a]Direct current.
[b]dc/rf input to rf/dc output.
[c]Maximum failures at any one time.
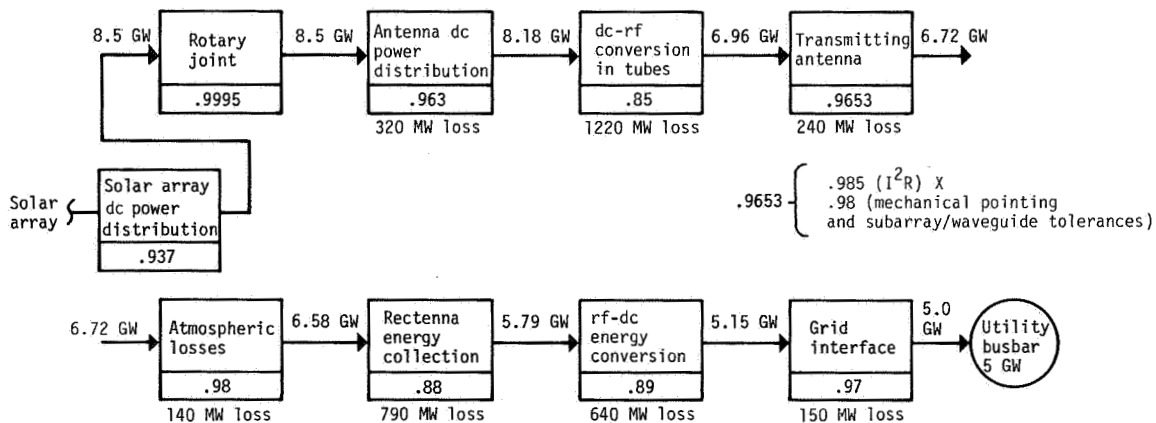
Figure III-4.- SPS efficiency chain.

21

b. Type B - degradations leading to losses that cannot be recovered by increasing the solar array size because of system limitations - An example is the dipole/diode rf-dc conversion loss in the rectenna when the system is operating at the maximum power density limit in the ionosphere.

The economic impact of a type A degradation is less than that of a type B loss as shown subsequently. The cost and mass statements for the reference satellite subsystems that are dependent on solar array power are shown in table III-2 (ref. 12). These costs may differ slightly from those given in reference 4; however, the relative impacts of changes in the various subsystem losses will remain essentially constant. These costs may be summarized into an overall SPS system cost. The overall cost per 5-gigawatt satellite is $12 432 million with a resulting electricity cost of 1.31¢/MJ (47 mills/kWh) (ref. 12). The differential cost per 1-percent increase in solar array power to compensate for losses in the microwave system is, to a first-order approximation, $56.4 million as obtained by summing the last column. This is the economic impact of a type A degradation. The corresponding increase in cost of electricity for a 1-percent increase in solar array power is 0.006¢/MJ (0.2 mill/kWh).

The type B degradations which result in a loss of electrical power to the utility grid are obtained by multiplying the electricity rate times the power delivered over the 30-year lifetime of the satellite.

Revenue loss = $0.047/kWh × 8760 hr/yr × 30 yr

× 50 000 kW (1 percent of 5 GW)

= $617 million

or an effective loss of 0.06¢/MJ (2.3 mills/kWh). In summarizing, the economic costs of a 1-percent reduction in power are: type A (compensated for by an increase in solar array output) - $56 million; type B (no compensation) - $617 million.

The relative importance of the microwave subsystem losses depends on the location in the efficiency chain at which they occur. That is, a 1-watt type A loss at the rectenna has a greater economic impact than a similar loss in the klystron tube. The microwave subsystem performance impact based on a 10-percent variation in each loss is as follows.

a. Klystron dc-rf Conversion Efficiency (85 Percent)

Although the antenna is operated at a peak power density of 23 kW/m^2, the thermal rejection system design can be improved to accommodate greater tube power and/or increased thermal losses (ref. 6). Therefore, the klystron dc-rf conversion efficiency (85 percent) is a type A loss (compensable). A 10-percent change in tube loss corresponds to an increase of 1.5 percent in conversion loss.

TABLE III-2.- COST AND MASS SUMMARY FOR REFERENCE
SATELLITE SUBSYSTEMS DEPENDENT ON SOLAR ARRAY POWER

Subsystem	Reference system		Differential impact for a 1-percent increase in solar array power	
	Mass, t	Cost, $	Mass, t	Capital cost, $
Solar array				
Structure	4 654	448×10^6	47	4.5×10^6
Solar cell blankets	21 145	1988	211	20
dc power distribution	1 246	150	12	1.5
Maintenance	621	274	6	2.7
Total	27 666	2860	276	28.7
Power transmission – klystrons and thermal control	7 007	477	70	4.8
Satellite total[a]	50 984	4946	346	33.5
Transportation				
EOTV[b]	--	652	--	6.5
PLV[c]	--	286	--	2.8
POTV[d]	--	14	--	.1
HLLV[e]	--	2167	--	10.5
Total	--	3119	--	19.9
Construction operations				
GEO[f]	--	648	--	1.5
LEO[g]	--	313	--	1.5
Total	--	961	--	3.0

[a]Includes rotary joint, antenna structure, waveguides, subarray structure, phase distribution, mechanical pointing, information management, altitude control, communications, and 22 percent mass growth not directly related to solar array output power.
[b]EOTV = electric orbital transfer vehicle.
[c]PLV = personnel launch vehicle.
[d]POTV = personnel orbital transfer vehicle.
[e]HLLV = heavy lift launch vehicle.
[f]GEO = geosynchronous orbit.
[g]LEO = low Earth orbit.

Klystron loss = $56 million per 1-percent increase in solar array output

   × 1/(dc power distribution efficiencies in solar array and antenn

   × increase in klystron loss)

= ($56 million/0.01) × 1/(0.937 × 0.963) × (0.85 - 0.835)

= $93 million

This $93-million cost figure should be independent of the size of the klystron. That is, if the klystron output were changed from 70 to 50 kilowatts, as has been suggested, the $93-million impact is still valid. The resultant cost impacts for the various subsystem losses are summarized in figure III-5.

   b.   Transmitting Antenna Efficiency (96.5 Percent)

      (1) <u>Losses from I^2R (0.985)</u> - The I^2R losses of 1.5 percent were calculated assuming an aluminum-plated composite waveguide (ref. 13). A 10-percent change in I^2R losses (type A losses) gives:

I^2R losses = ($56 million/0.01) × 1/(0.937 × 0.963 × 0.85)

   × (0.985 - 0.9835)

= $11 million

      (2) <u>Power module tolerances (0.98)</u> - Each power module consists of one klystron tube feeding a section of slotted-waveguide radiator. The waveguides or sticks and the feedguide have a standing-wave configuration. The sticks in the various sections of the antenna radiate at different power density levels because of the 10-decibel illumination taper. The power module tolerances (0.98) may be subdivided into the following type A losses.

         (a) Subarray surface: Antenna surface variations producing independent random errors with correlation intervals small in respect to the antenna diameter produce a 0.5-percent power loss. This loss corresponds to a ±0.127-centimeter (50 mil) root-mean-square (rms) surface error.

         (b) Power module tilt: Computer simulations indicate that a ±3-arc-minute random power module tilt scatters 28 megawatts of power, or a 0.4-percent power loss.

         (c) Mechanical gap between subarrays: The mechanical gap between the 10.4- by 10.4-meter subarrays is limited by the level of the allowable grating lobes rather than by a power loss in the main beam. A 0.64-centimeter (250 mil) gap is compatible with maintaining grating-lobe peaks below 0.01 mW/cm^2 while providing only a 0.13-percent power loss.

24
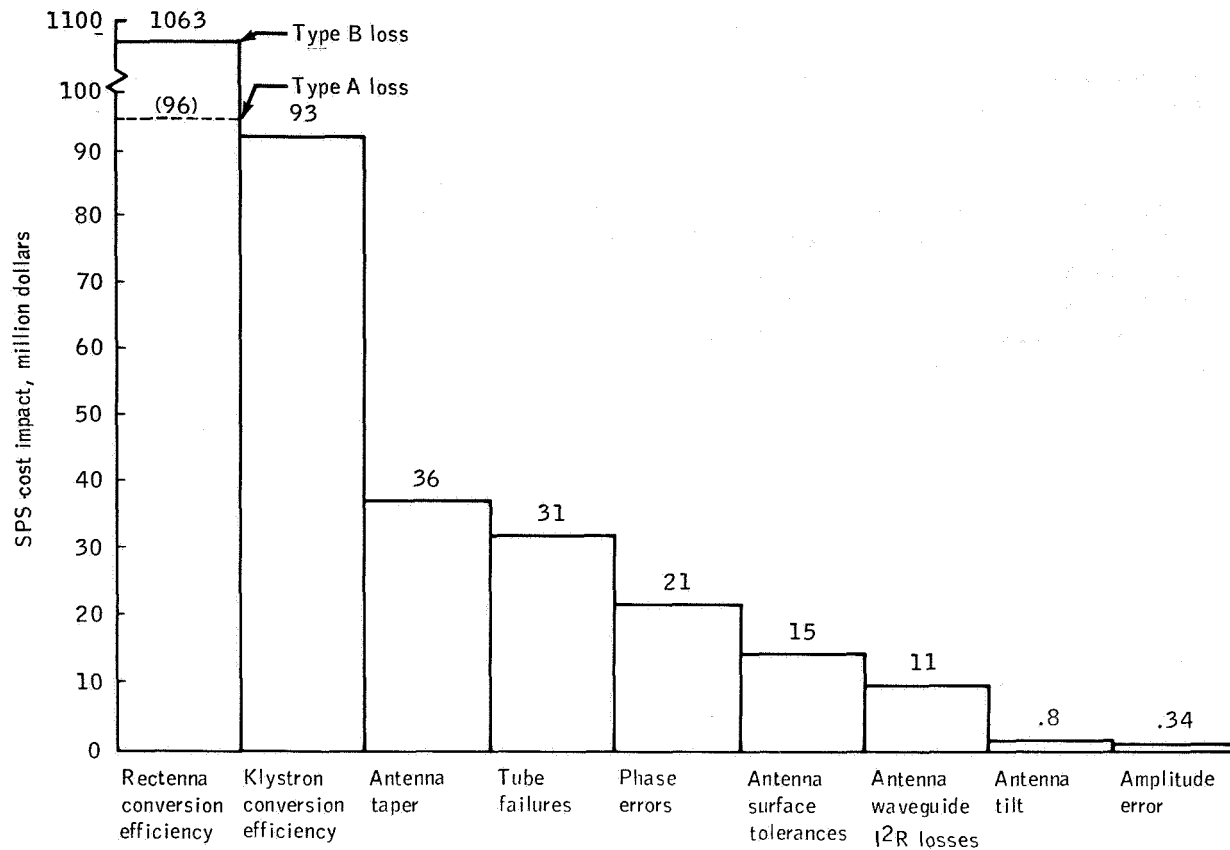
Figure III-5.- Summary of cost sensitivities for a 10-percent change in subsystem losses. Antenna tilt is doubled from 1 to 2 arc-minutes; all other subsystems have a 10-percent change.

(d) Radiating-stick tolerances: An analysis of the losses due to waveguide and feedguide dimensional variations has been made (ref. 14). The results are summarized in table III-3.

(e) Phase location errors: The uplink pilot-beam reference signal is received in each power module, and a single phase angle is conjugated in each receiver. For a 3-arc-minute power module tilt, the average phase error at the radiating slots due to the slight differences in range to the ground pilot-beam transmitter has been calculated to be 1.8°. The corresponding power loss for the entire antenna is 6 megawatts, or approximately 0.1 percent.

An additional 0.48-percent power loss should be added to the detailed losses in table III-3 to adjust the total upward to 2 percent as given in figure III-4. The economic impact for a 10-percent change in the transmitting antenna losses is

Antenna losses = ($56 million/0.01) × 1/(0.937 × 0.963 × 0.85 × 0.985)

× (0.98 - 0.978)

= $15 million

c. Rectenna Energy Collection Efficiency (88 Percent)

The rectenna energy collection efficiency (88 percent) is the percentage of energy transmitted by the antenna that is incident on a 10-kilometer-diameter rectenna. The amount of energy is dependent on the antenna illumination function and antenna error parameters such as phase error, amplitude error, failure rate, and antenna attitude control.

(1) Illumination taper effects - The reference configuration has a 10-decibel Gaussian illumination taper to maximize the rectenna collection efficiency and to minimize side-lobe peaks. For a perfect 1-kilometer-diameter antenna with no system errors, the collection efficiency for a 10-kilometer rectenna is 95.3 percent. Based on initial results, a 10-percent improvement (0.5 percent) in collection efficiency is a reasonable goal when using a better optimized antenna taper. Currently, there is no phase taper across the antenna surface; a relatively simple discrete-step phase taper might be used to modify the beam pattern. The economic factor for a 10-percent improvement in collection efficiency (0.47 percent) is

Taper improvement = ($56 million/0.01) × 1/(0.937 × 0.963 × 0.85

× 0.9653 × 0.98) × (0.9577 - 0.953)

= $36 million

TABLE III-3.- LOSSES DUE TO POWER MODULE TOLERANCES

Dimension	Tolerance		Effect	Main beam power degradation, percent
	Linear, mm (mil)	Angular, arc-min		
Power module surface	±1.27 (±50)[a]		Scattering from phase variance	0.50
Random tilt of power module		3	Power module pattern gain reduction	.40
Gap between mechanical subarrays	6.35 (250)		Grating-lobe enhancement	.13
Radiating stick Length Width	±.76 (±30) ±.08 (±3)		Mismatch loss Mismatch loss	.02 .12
Cross guide Length Width Coupling	±.76 (±30) ±.08 (±3)		Mismatch loss Mismatch loss Scattering from amplitude variance	.02 .03 .1
Slot offset	±.16 (±6)		Scattering from amplitude variance	.1
Phase location jitter		3	Gain reduction due to range errors	.1
Total				1.52

[a]Root mean square.

27

(2) Phase error – The existing error budget allows a
10° overall phase error for the phase control system in pointing and focusing
the beam. For a given phase error, approximately 10 percent of the power
loss is due to beam-pointing error and 90 percent is due to beam broadening
and random scatter. The total power loss is 188 megawatts, or 2.8 percent
of the radiated power. A 10-percent change in phase error has the following
impact.

Phase error = ($56 million/0.01) × 1/(0.937 × 0.963 × 0.85

× 0.9653 × 0.98) × (0.972 – 0.9692)

= $21 million

(3) Amplitude error – The beam pattern is relatively
insensitive to amplitude errors in the output of each power module. The
scattered power is only about 3 megawatts for a 1-percent amplitude error.
The economic factor for a 10-percent change in amplitude error is

Amplitude error = ($56 million/0.01) × 1/(0.937 × 0.963 × 0.85

× 0.9653 × 0.98) × (0.999 55 – 0.999 505)

= $0.34 million

(4) Tube failures – Tube failures have a significant in-
fluence on the power received by the rectenna. A single failure has a dou-
ble effect: the amount of transmitted power is decreased and the antenna
area is reduced and, thereby, the overall antenna gain is lowered. The ref-
erence error parameter budget has a 2-percent failure rate, which reduces
the power received by 268 megawatts, or 4 percent of the power. A 10-percent
change in failure rate produces a 0.4-percent change in received rectenna
power, with an economic factor of

Tube failures = ($56 million/0.01) × 1/(0.937 × 0.963 × 0.85

× 0.9653 × 0.98) × (0.96 – 0.956)

= $31 million

(5) Antenna tilt – The amount of allowable antenna tilt
is determined by the 0.01-mW/cm² power density constraint on grating-lobe
peaks. The effect of antenna tilt on the beam pattern and scattered power

is minimal. For a 1-arc-minute antenna tilt, the scattered power is 0.67 megawatt, or 0.01 percent of the total power. The economic impact of doubling the antenna tilt is

Antenna tilt = ($56 million/0.01) × 1/(0.937 × 0.963 × 0.85

$$\times\ 0.9653 \times 0.98) \times (0.0001)$$

$$=\ \$0.8\ \text{million}$$

The only type B degradation, other than aging and radiation damage to the satellite electronic components, is the rf-dc rectenna conversion efficiency. The current SPS system is sized to operate at the maximum ionospheric power density of 23 mW/cm^2. Although there are indications this density limit will be raised, future resizing of the SPS system will probably result in operation at the new ionospheric level because of increased transmitted power and/or larger satellite antennas. The 11-percent loss in conversion efficiency is due to impedance mismatch between the dipole/diode circuitry and the incident energy, losses in the half-wave rectifier, filter losses, etc. A 10-percent change in conversion efficiency has the following effect.

Rectenna conversion efficiency = ($617 million/0.01) × 1/(0.937 × 0.963

$$\times\ 0.85 \times 0.9653 \times 0.98 \times 0.88)$$

$$\times\ (0.89 - 0.879)$$

$$=\ \$1063\ \text{million}$$

The economic impacts due to subsystem losses are summarized in figure III-5. The rectenna conversion efficiency has the dominant impact because of the premise that the system is operating at the ionospheric limit. If the rectenna losses could be compensated for by increasing the transmit power, the economic impact would decrease by an order or magnitude as shown. Also, the importance of being able to predict the losses over the 30-year lifetime of the satellite is shown.

3. ENVIRONMENTAL CONSIDERATIONS

The SPS microwave power beam will affect the Earth's environment in three general areas: ionospheric heating, atmospheric interactions, and radiofrequency interference. These environmental factors are critical in determining the satellite size, the power transmission characteristics, and the electricity costs for the SPS. Work underway in assessing these environmental factors may be summarized as follows.

a. Ionosphere

There are two concerns regarding the ionosphere: heating of the ionosphere by the microwave power beam and phase perturbation of the SPS pilot-beam signal induced by the ionosphere. The 23-mW/cm^2 power density limit was a theoretical number derived early in the SPS program to ensure that no nonlinear ionospheric heating effects would occur (refs. 15 and 16). It was suspected that resistive (ohmic) heating effects by the power beam could produce nonlinear instabilities such as enhanced electron heating in the lower ionosphere (D- and E-regions) and thermal self-focusing effects in the upper ionosphere (F-region). The Department of Energy has subsequently sponsored a number of ionospheric studies. Theoretical and experimental analyses of the effects of underdense heating on ionospheric physics have been performed in part at the Arecibo, Puerto Rico, Observatory. This work is also funded by the National Science Foundation. Experimental studies have been performed by the Institute for Telecommunication Sciences (ITS) of Boulder, Colorado, into heated ionospheric effects on low-frequency communication and navigation systems (loran, OMEGA, National Bureau of Standards (NBS) standard-frequency station WWV, and amplitude-modulation broadcasting stations). This work is being performed by ITS using the Platteville, Colorado, heating facility. The results of the tests performed to date at Arecibo and Platteville show no evidence to support 23 mW/cm^2 as an upper limit. The electron temperature increases due to underdense heating are a factor of two or three, rather than the order of magnitude predicted in the early analyses (ref. 15). The theory is now being revised, and initial results predict a $1/f^3$ heating rather than $1/f^2$, where f is frequency, which would increase the power density limit. If scaling from low frequency to the SPS frequency follows $1/f^3$ and not $1/f^2$, then these tests were actually conducted at a higher scale power flux than previously thought. In addition, there are no indications of irregularities being formed in the lower ionosphere during underdense heating. Effects produced by simulated SPS heating are many times less than natural ionospheric disturbances as introduced by solar flares (ref. 17).

In addition to the DOE environmental studies, NASA is investigating system-level effects of errors introduced into the phase control system by a heated ionosphere. An experimental study is underway using differential Doppler techniques to measure electron density profiles through an ionosphere heated by the Platteville facility. A polar orbiting U.S. Navy navigation satellite (Navsat) transmits two coherent signals in the 150- to 450-megahertz frequency region from which the differential Doppler measurements are made. From the electron density profiles, a statistical model for phase perturbations of the 2.45-gigahertz pilot signal will be developed. Details of these tests are given in Section III.B.

30

Two of the most important issues in the entire SPS microwave system are determining an upper limit for the permissible power density through the ionosphere and the resulting pilot-beam phase errors induced by this heated ionosphere. The old theoretical number, 23 mW/cm^2, is not valid as shown by the heating tests at Platteville and Arecibo and also by new analytical work. This parameter for all practical purposes determines the size of the 2.45-gigahertz SPS system and has billions of dollars' impact on the electricity costs. From a system viewpoint, an ionospheric power density level of 55 to 60 mW/cm^2 might be reasonable and would accommodate the larger antenna/smaller rectenna systems proposed in Section III.A.4. However, more ionospheric experiments are needed with upgraded facilities at Platteville and Arecibo to produce the higher heating levels.

b. Atmosphere

The 2.45-gigahertz downlink power beam frequency is in the center of a 100-megahertz industrial, scientific, and medical (ISM) band. According to International Radio Regulations, "Radiocommunication services operating within these limits must accept any harmful interference that may be experienced from the operation of industrial, scientific, and medical equipment." This 2400- to 2500-megahertz band is not particularly affected by weather conditions; therefore, an SPS system should not encounter weather outages. The efficiency budget for the 2.45-gigahertz reference configuration has 98 percent transmission (2 percent loss) through the atmosphere. This signal attenuation is primarily due to rain and atmospheric absorption. The 2-percent attenuation, or 130-megawatt loss, represents a worst case condition (but not the worst possible, which occurs during wet hailstorms) for the 2.45-gigahertz frequency. Another ISM band (5800 ± 75 megahertz) is also available for possible SPS usage. However, an SPS operating in this frequency region may have to be shut down because of poor weather conditions. The 5.8-gigahertz frequency has approximately the same transmission efficiency as the 2.45-gigahertz frequency through a nonrainy atmosphere but is severely degraded under rainy conditions. The losses for two systems providing 5 gigawatts of ground grid power are summarized in table III-4 (ref. 18). The 2.45-gigahertz frequency has very minimal losses due to nonideal weather conditions; the 5.8-gigahertz frequency operates satisfactorily in the dry climates of the southwestern United States, but outages would occur in wetter regions.

The impact on a commercial utility grid of a 5.8-gigahertz microwave system which may have to be shut down on an unscheduled basis because of weather effects is not known. If a 5.8-gigahertz microwave system is to be seriously considered as an alternate to a 2.45-gigahertz system, an in-depth study of this area is required.

c. Radiofrequency Interference

Microwave interference with communication and navigation systems and radio astronomy will come primarily from four satellite sources: sideband radiation from the 2450-megahertz power beam, harmonics of 2450 megahertz generated by the klystrons, broadband noise outside the ISM frequency band (2450 ± 50 megahertz), and microwave noise generated by black-body

TABLE III-4.- ATTENUATION LOSSES FOR 5-GIGAWATT SYSTEMS

Medium	Power loss, W, at transmission frequency of -	
	2.45 GHz	5.8 GHz
Ionosphere	0.25×10^3	1×10^3
Neutral atmosphere at mid-U.S. latitude (water vapor and oxygen absorption)	90×10^6	100×10^6
Rain		
Heavy (15 mm/hr over 15-km path)[a]	148	1800
Moderate (5 mm/hr over 10-km path)[b]	34	405
Wet hail	2600	4990

[a]Occurrence: Central/Eastern United States, 9 hr/yr; Southern United States, 3 hr/yr; Western United States, 3 hr/yr.
[b]Occurrence: Central/Eastern United States, 45 hr/yr; Southern United States, 85 hr/yr; Western United States, 10 hr/yr.

radiation from the solar arrays. There will also be reradiations and re-
flections from the rectenna. In addition, the cases of mutual interference
between adjacent SPS satellites and an SPS satellite interfering with a
TDRSS (Tracking and Data Relay Satellite System) located in geosynchronous
orbit have been investigated.[1]

(1) Side-lobe radiation levels - The expected power levels
at the Earth's surface at the rectenna as a function of distance from bore-
sight for one SPS satellite under normal operating conditions are shown in fig-
ure III-6 for near side lobes and figure III-7 for far side lobes. The data
include the effects of random phase errors, amplitude errors, tube failures,
mechanical spacings between subarrays, antenna tilt, and random subarray tilt.
These antenna patterns have improved slightly since the reference system was
defined in October 1978 because of phase controlling to the power module level
(ref. 1). Although the energy in the side lobes of the 2450-megahertz main
beam is small, rejection filters may be needed in the front-end electronics of
sensitive receivers such as in radio astronomy systems to prevent overloading.
(This problem would be somewhat alleviated if 5.8 gigahertz was used as the
transmission frequency.) Grating-lobe peaks appear on the ground at intervals
of 848, 1272, 1696, 2120, and 2544 kilometers from the rectenna as determined
by the spacing of individual power modules (tubes) on the microwave array.

(2) Klystron (tube) noise - The probable level of noise
from the 101 552 klystron tubes in a single 5-gigawatt satellite is shown in
figure III-8 (ref. 19). This noise density curve was calculated using meas-
urement data from a Varian V-58 klystron, an "old" tube, combined with the
theoretical frequency response of a slotted-waveguide radiator. The perti-
nent radio astronomy requirements as given in the latest International Radio
Consultative Committee (CCIR) documentation, report 224-4, are as follows.

Frequency, MHz	Power flux spectral density, dBW/m^2-Hz
1400 to 1427	-255
2690 to 2700	-247
4990 to 5000	-241
10 640 to 10 740	-240

The noise data given in figure III-8 indicate that the CCIR requirements can
readily be achieved with regard to out-of-band tube noise, provided the tube
and waveguide characteristics are as assumed. Noise data for modern klystron
tubes are expected by Varian personnel to be better (lower) by about 40 deci-
bels from the -160-dBc/Hz noise level at frequencies greater than 100 megahertz

---

[1]G. D. Arndt and J. W. Seyl: RF Interference/Orbital Spacings for Solar
Power Satellites. Lyndon B. Johnson Space Center (Houston, Tex.), to be pub-
lished.
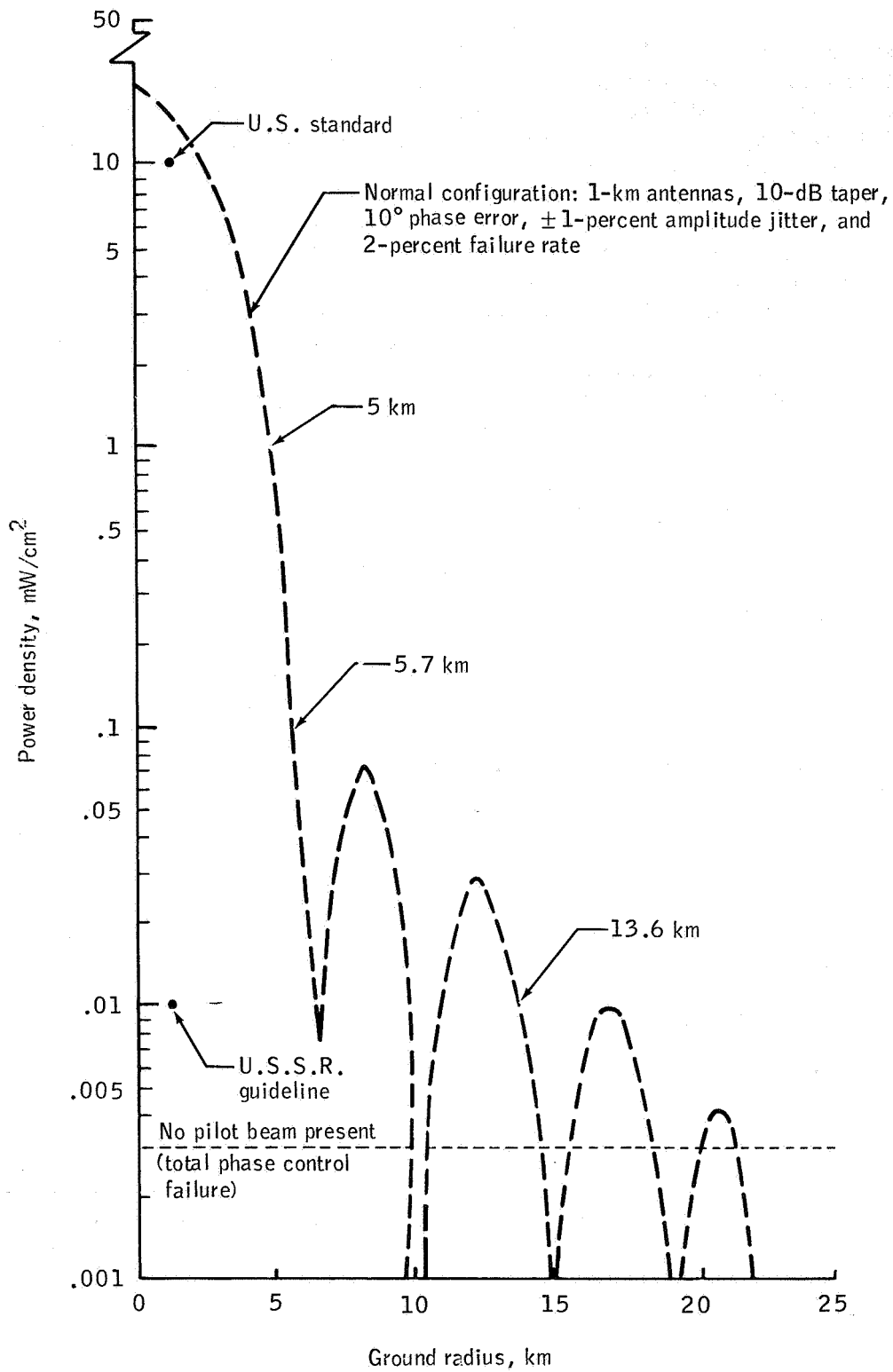
Figure III-6.- Power density at rectenna as a function of distance from boresight.
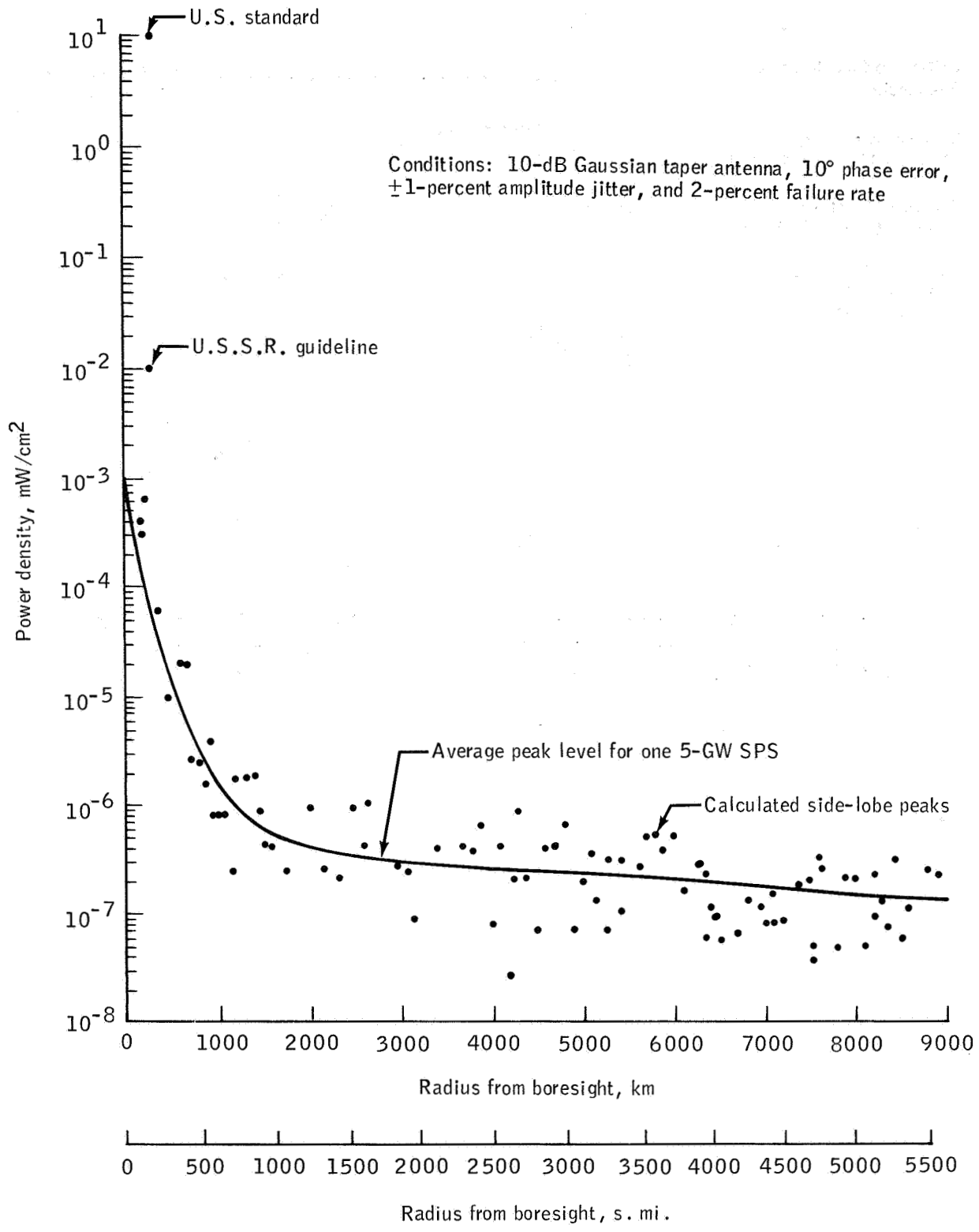
Figure III-7.- Peak power density levels as a function of range from rectenna.

Critical radio astronomy
frequencies:

Hydrogen resonance
 line - 1400 to 1427 MHz

Hydroxyl resonance
 line - 1660 to 1670 MHz

Astronomy bands -
 2690 to 2700 MHz
 4990 to 5000 MHz
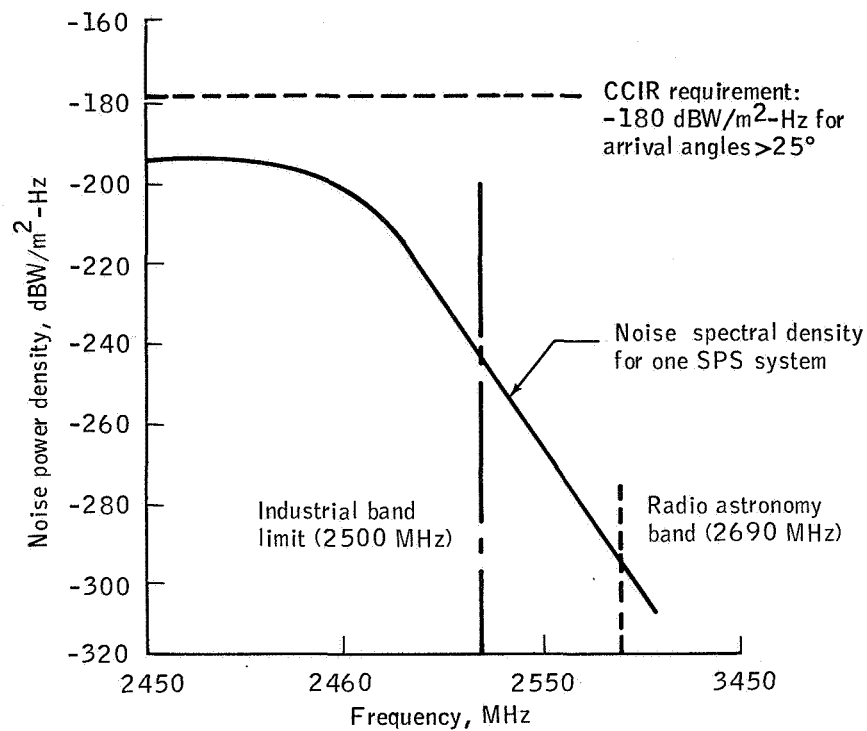
Figure III-8.- Noise power density at ground for a 1-kilometer-diameter, 5-gigawatt SPS antenna. The abscissa is a logarithmic scale, graduated from 1 to 1000 megahertz and normalized to 2450 megahertz.

from the carrier frequency used in the calculations. The filtering character-
istics for a small section of the slotted-waveguide radiators are being meas-
ured; however, the overall noise performance of a klystron-driven antenna is
still speculative and is an area for future work.

(3) Harmonic noise from the transmit antenna - The harmon-
ic powers generated by the klystron tubes are taken to be 53, 94, and 113 dec-
ibels down from the fundamental for the second, third, and fourth harmonics,
respectively (ref. 20). The harmonic antenna patterns have been measured for
an eight- by eight-slot slotted-waveguide subarray (ref. 21). The relative
gains with respect to the fundamental at small angles near boresight are -53
decibels for the third and fourth harmonics and -75 decibels for the second
and fifth harmonics. With these antenna and tube characteristics, the har-
monic noise spectral density at the ground is given by

$$
P_{H-gr} = \frac{P_H G_H}{4\pi R^2}
$$

$$
= \frac{(P_T - P_{LH})(G_A - G_{LH})}{4\pi R^2} \tag{1}
$$

where P_{H-gr} = harmonic power density at the ground

P_H = n-th harmonic power transmitted

P_T = fundamental (2.45 gigahertz) power transmitted

P_{LH} = harmonic power relative to fundamental

G_A = 1-kilometer-diameter antenna gain at 2.45 gigahertz

G_H = 1-kilometer-diameter antenna gain at n-th harmonic

G_{LH} = harmonic antenna gain relative to fundamental

R = range from satellite to ground

The power density at the ground for the second harmonic
(4.9 gigahertz), the third harmonic (7.35 gigahertz), and the fourth harmonic
(9.8 gigahertz) is calculated to be -104.4, -123.4, and -142.4 dBW/m^2, respec-
tively. If it is assumed that the broadband noise characteristics around the
harmonics are similar to those levels around the fundamental, then the overall
noise levels from a single 5-gigawatt satellite are as shown in figure III-9.

37
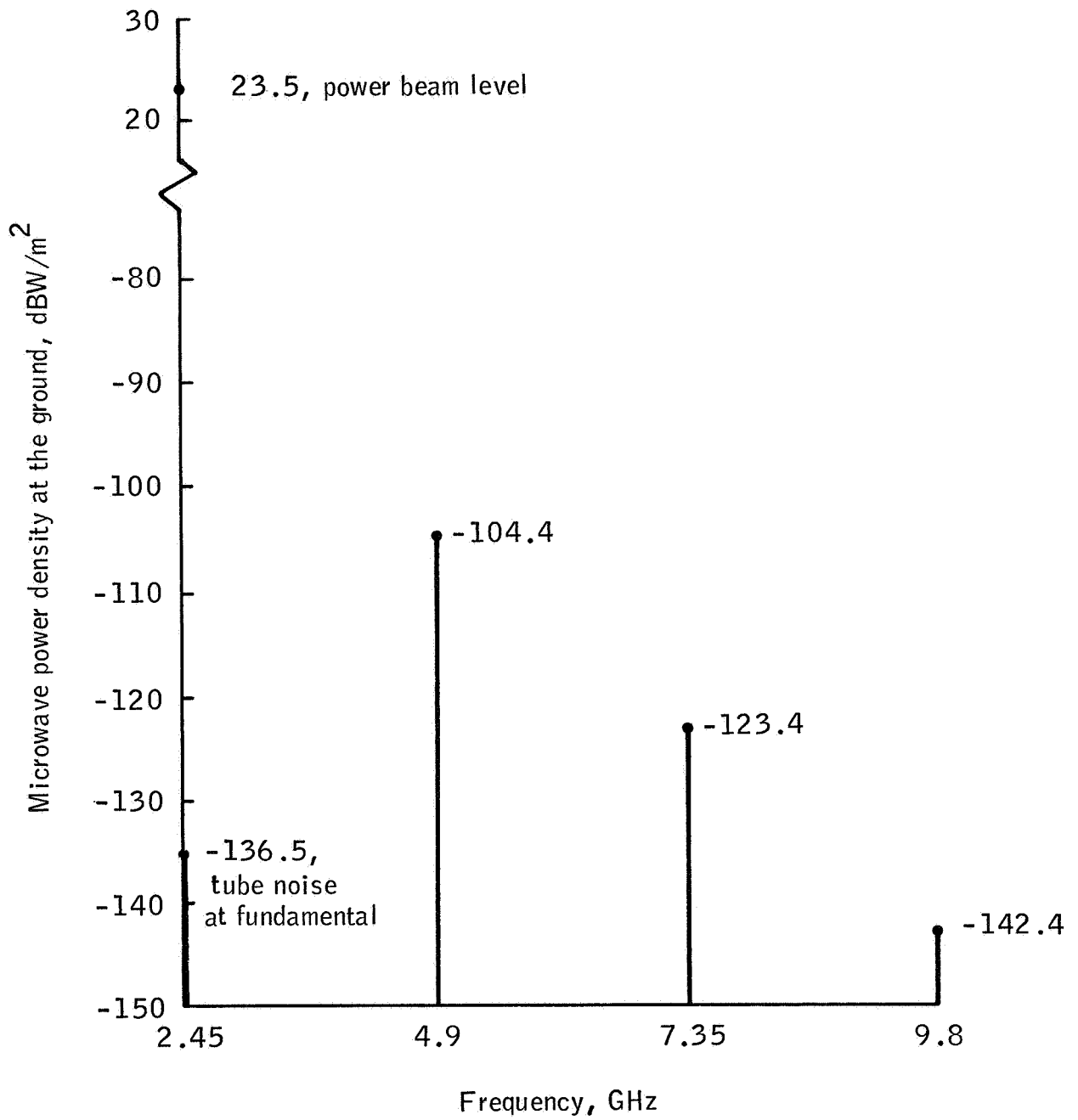
Figure III-9.- Harmonic noise power spectrum.

(4) <u>Thermal noise radiation from SPS solar arrays</u> - The solar array will act as a broadband noise radiator because of thermal emission from the hot solar cell blankets. Using a 310-K temperature for the reference silicon cells with a microwave emissivity of 0.95, the surface brightness for the solar blanket acting as an isotropic radiator will be

$$B = 8.13 \times 10^{-21} \ W/m^2/Hz/rad^2 \tag{2}$$

Viewed from the Earth, the 5.2- by 10.4-kilometer silicon array subtends a solid angle of 4.16×10^{-8} radian squared, and the resulting microwave power density as a function of wavelength at the ground is

$$P_D = \frac{3.38 \times 10^{-28} \ W/m^2/Hz}{\lambda^2}$$

$$= \frac{-274.7 \ dBW/m^2/Hz}{\lambda^2} \tag{3}$$

where λ is the microwave wavelength in meters. The resulting microwave noise power density as a function of frequency is shown in figure III-10, together with the CCIR requirements for the four astronomy bands of interest.

The data indicate that the SPS thermal noise radiation levels from a single satellite will approach but not exceed the radio astronomy emission requirements as defined in CCIR report 224-4. As more satellites are put into operation, these emission levels will eventually be exceeded. However, the SPS noise levels given in figure III-10 are for worst case conditions occurring at the observer's local midnight; as the position of the solar array changes while tracking the Sun, the thermal radiation cycles through two daily minimum levels when the array is oriented with the edge toward the observer. There will also be reductions in the noise levels as the declination of the satellite changes throughout the year.

(5) <u>Radiofrequency interference with adjacent satellites</u> - In addition to the rf interference with ground systems, the microwave beam from one solar satellite may interfere with nearby satellites. To investigate this problem, two possible interference conditions have been analyzed: (a) an SPS interfering with an adjacent SPS and (b) an SPS interfering with a TDRSS (Tracking and Data Relay Satellite System) located in geosynchronous orbit. These two particular systems were chosen for study because their microwave characteristics are well defined and the TDRSS is considered representative of existing communication satellites. Communication satellites in the year 2000 time frame of the SPS systems should have improved performance.
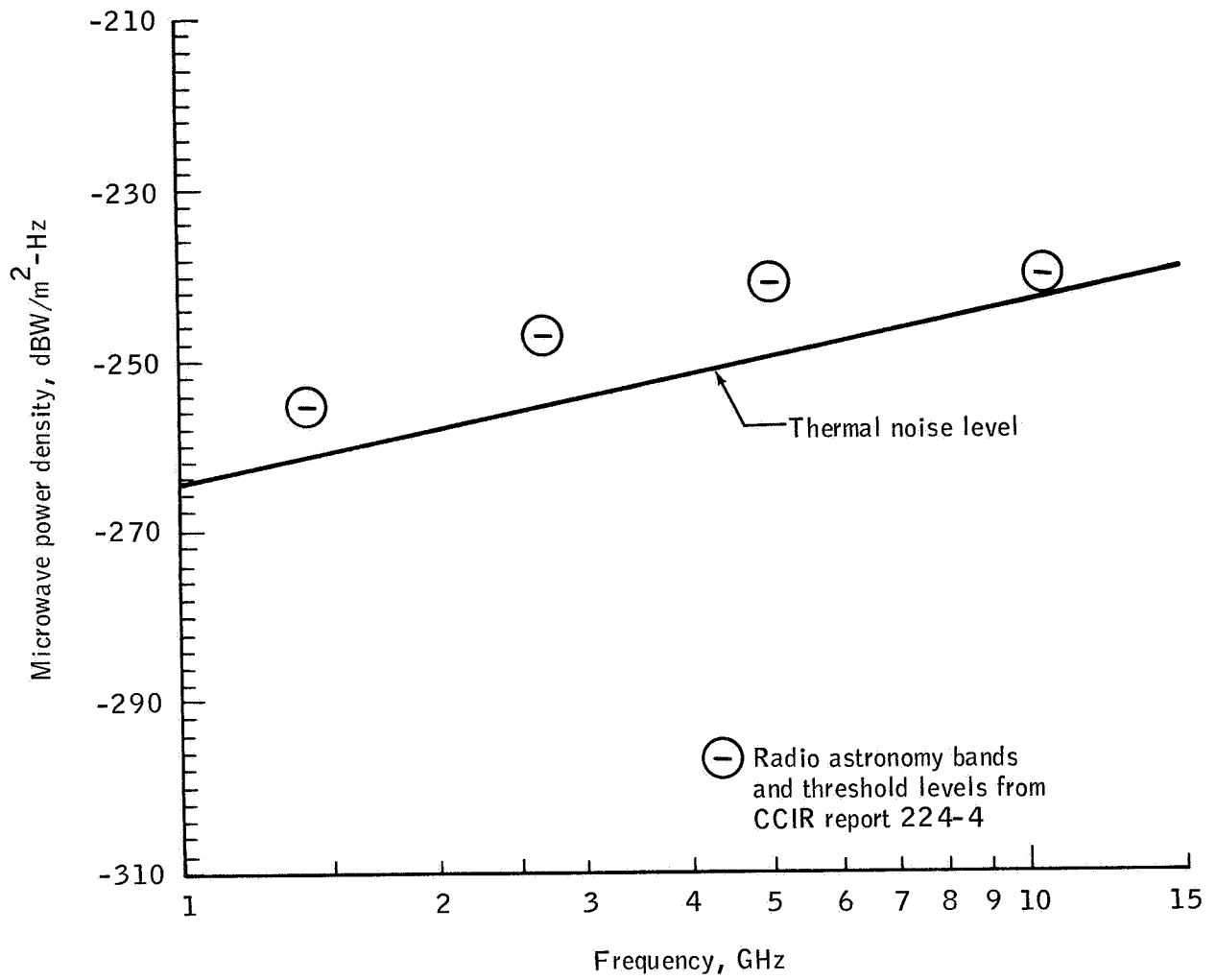
Figure III-10.- Microwave thermal noise levels for a single 5-gigawatt SPS silicon solar array.

The results of this study may be summarized as follows.

(a) SPS/TDRSS interference: The geosynchronous TDRSS acts as a repeater relay between low-Earth-orbit users (satellites, Space Shuttle, etc.) and the ground terminal at White Sands, New Mexico. There are three general relay classes: the single access (SA) relay, which has both S-band (SSA) and K-band (KSA) services on a high-gain antenna; the multiple access (MA) relay with 20 S-band links over an Earth-coverage phased array; and the satellite/ground links at S-band or K-band with tracking, telemetry, and command (TT&C) data. Although TDRSS's may be operated simultaneously, there are no communication links between the satellites. In addition, the communication antennas are constrained in their movements such that other geosynchronous satellites cannot be within their fields of view.

It is assumed that the TDRSS antenna gain with respect to an SPS will be 0 decibel. The TDRSS diplexer has a measured attenuation response of -80 decibels at 2450 megahertz (ref. 22). The block diagram of the input stages and associated signal levels for the TDRSS return links (user to satellite) is shown in figure III-11. The SPS interference level at a TDRSS with a 1° (700 kilometer) separation is shown in table III-5. Thus, it can be concluded that an SPS will not interfere with the TDRSS communication links. The degree of isolation provided by the TDRSS diplexer to out-of-band interference and the low gains of the communication link antennas relative to an adjacent SPS will reduce the SPS interference levels to 25 decibels below the TDRSS receiver noise level in a 100-megahertz bandwidth. Additional intermediate-frequency (i.f.) filtering is encountered as the channel bandwidth reduces, thereby maintaining acceptable signal-to-interference ratios.

(b) SPS/SPS interference: In considering the potential RFI problems of one SPS interfering with another SPS in adjacent geosynchronous orbital slots, it is apparent that a greater probability of interference occurs if one assumes a single SPS with multiple transmit antennas interfering with one another. In the limit, the worst case is that of a power module (70-kilowatt transmitter) interfering with its individual pilot receiver (self-interference). Four antenna spacings were considered in the analysis.

(1) 1° (700 kilometers) separation between satellites

(2) 20 kilometers separation between two antennas, one at each end of the satellite

(3) 5 kilometers separation between two antennas at opposite ends of the satellite

(4) Self-interference within a single power module by the klystron feeding energy back into its pilot signal receiver

The self-interference case (4) has by far the worst RFI conditions as detailed in table III-6. The pilot signal is to be received using a separate linearly polarized slot with opposite polarization to that of the transmitter waveguide

41
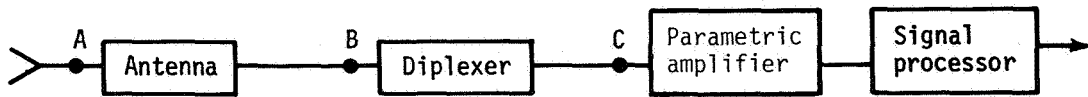
	Point A	Point B	Point C
SSA link	-117 dBm max.	-79.2 dBm max.	-80.2 dB max.
	-181 dBm min.	-102 dBm min. (RCVR noise)	-104.3 dBm min.
KSA link	-119 dBm max.	-64.7 dBm max.	-65.9 dBm max.
	-153 dBm min.	-87.3 dBm min. (RCVR noise)	-89.1 dBm min.
MA link	-120 dBm max.	-104 dBm max.	-104.3 dBm max.
	-170 dBm min.	-105 dBm min. (RCVR noise)	-106.6 dBm min.

Figure III-11.- Input stages and allowable power levels for the TDRSS return links.

TABLE III-5.- SPS INTERFERENCE LEVEL AT
TDRSS WITH 1° (700 KILOMETERS) SEPARATION

Parameter	Value
SPS radiated power (6.5 GW), dBm	128
SPS antenna gain at 90° from boresight, dB	-20
Space loss (700 km; 2.45 GHz), dB	-157.1
Satellite-to-satellite polarization loss, dB	-3.0
Input power to TDRSS antennas, dBm	-52.1
TDRSS antenna gain (SSA, KSA, or TT&C), dB	0
TDRSS diplexer filter attenuation at 2.45 GHz, dB	-80
Input power to TDRSS parametric amplifier, dBm	-132.1
Minimum TDRSS receiver noise level (100-MHz bandwidth), dBm	-106.6
Signal-to-interference margin (100-MHz bandwidth), dB	25.5

TABLE III-6.- SPS-TO-SPS RFI FOR FOUR SCENARIOS

Parameter	Scenario			
	Adjacent SPS, 1° (700 km) separation	2-antenna system, 20 km separation	4-antenna system, 5 km separation	Self-interference (power module)
Transmit power				
6.5 GW, dBm	[a]128	[a]128	[a]128	--
70 kW, dB	--	--	--	78.5
SPS transmit antenna gain (90°), dB	-20	-20	-20	[b]-20
SPS receiver antenna gain (90°), dB	0	0	0	0
Pilot transmit effective isotropic radiated power (ground antenna), dBm	126.4	126.4	126.4	126.4
Space loss, dB				
Interference I_R	-157.1	-126.3	-114.3	0
Pilot signal S_p	-191.4	-191.4	-191.4	-191.4
Receiver losses for I_R, dB				
Polarization[c]	-13.5	-13.5	-13.5	-13.5
rf filter	-60	-60	-60	-60
i.f. filter	-60	-60	-60	-60
Code processing gain	-70	-70	-70	-70
Receiver losses for S_p, dB				
Polarization	-3	-3	-3	-3
rf filter	-3	-3	-3	-3
i.f. filter	-1	-1	-1	-1
Figure of merit S_p/I_R, dB	180.6	149.8	137.8	73

[a]Transmitted power is for each antenna for the multiple-antenna SPS configuration scenarios.
[b]The self-interference is a result of mutual coupling of nearby radiating slots in the power module. The assumed total coupling coefficient was -20 decibels.
[c]The pilot receiver antenna is assumed to be vertically polarized omni and thus to provide a measure of isolation from the horizontally polarized power beam.

slots. The sum of the coupling coefficients for each transmitted waveguide slot to the receiver antenna is assumed to be -20 decibels total. The transmitted rf power component at 2450 megahertz, which represents the coherent interference term, contains essentially all of the 70-kilowatt klystron output power. The power is then coupled into the pilot receiver with the 20-decibel coupling loss. The resulting rf interference must be filtered and processed to effectively reduce the interference to an acceptable level. Figure III-12 is an SPS receiver functional block diagram with associated interference and pilot signal levels to illustrate the signal-to-interference ratio expected for this worst case self-interference condition.

The pilot signal received power level S_p is based on a 65-kilowatt transmitter using a ground antenna with 48.3 decibels gain. The total effective isotropic radiated power (EIRP) is then approximately +126.4 dBm (decibels referenced to 1 milliwatt). Assuming a geosynchronous range of 36 000 kilometers and a pilot-receiver vertically polarized slot of 0 decibel gain,

$$S_p = 126.4 \text{ dBm} - 191.4 \text{ dB} - 3 \text{ dB}$$

EIRP	Space loss	Polarization loss

$$= -68 \text{ dBm} \tag{4}$$

The coherent power beam signal power coupled into the pilot receiver antenna from all adjacent slots in the power module is

$$I_R = 78.5 \text{ dBm} - 20 \text{ dB} - 13.5 \text{ dB}$$

70-kW klystron output power	Total coupling coefficient	Polarization isolation (near field)

$$= +45 \text{ dBm} \tag{5}$$

Tracing the pilot signal power levels S_p and the continuous-wave (CW) interference levels I_R through the pilot receiver filtering and processing, the signal-to-interference ratio at the carrier synchronization loop input is

$$S_p/I_R = +73 \text{ dB}$$

Figure III-12.— SPS pilot receiver functional diagram. (Receiver gains not shown.)
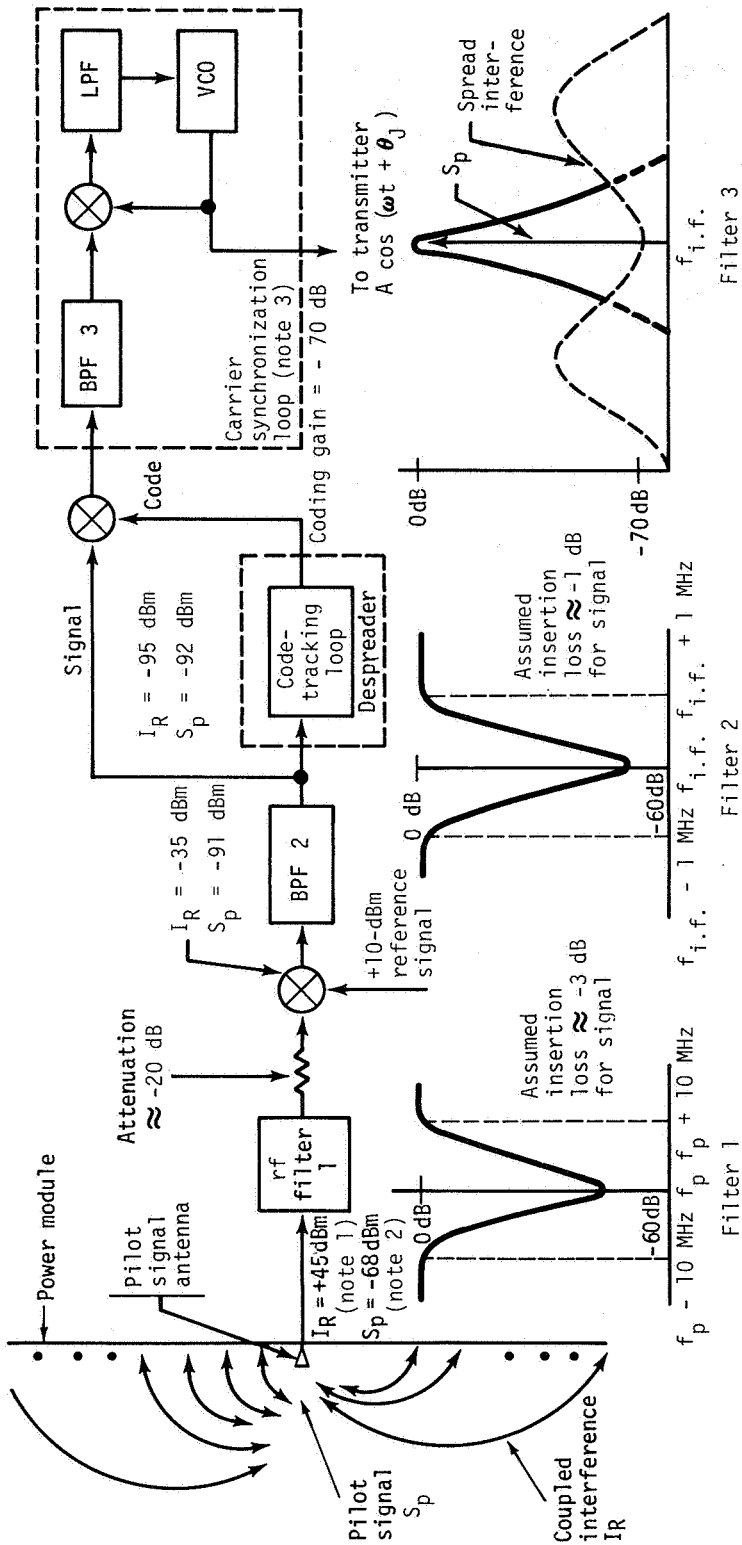
Notes: 1. $I_R = P_T - K_1 - L_p = 78.5$ dBm $- 20$ dB $- 13.5$ dB $= +45$ dBm
        $P_T =$ transmit power $= 70$ kW $= 78.5$ dBm
        $K_1 =$ interference coupling coefficient
             $= -20$ dB total (assumed)
        $L_p =$ polarization (near-field effects)
             $= -13.5$ dB (estimated)

        2. Pilot signal received power level $= -68$ dBm
            $S_p =$ EIRP - space loss - polarization loss $= +126.4$ dBm $- 191.4$ dB $- 3$ dB $= -68$ dBm

        3. Signal-to-interference ratio at the carrier synchronization loop
            input $= S_p/I_R = -92$ dBm $- (-165$ dBm$) = +73$ dB.
            Resulting phase jitter $\sigma_{GJ} = 0.1°$ rms.

BPF = band-pass filter
LPF = low-pass filter
VCO = voltage-controlled oscillator
  A = amplitude of pilot signal
  ω = downlink power frequency in radians per second
  t = time
  θ_J = phase jitter in radians

45

This signal-to-interference ratio is more than sufficient to maintain the recovered carrier phase jitter to values well within the allocated phase error tolerance for the pilot receiver. In general, the simulation perform-ance results indicated that for pilot signal effective radiated power levels equivalent to that used here (i.e., +126.4 dBm) and with similar receiver fil-ter characteristics, the carrier recovery loop phase jitter σ_{GJ} will be less than 0.1° rms for carrier loop bandwidths of 10 hertz or less (ref. 23).

One area of concern is achieving the needed isolation at the power signal frequency with an rf filter. To achieve sufficient level reduction before the first mixer, some additional attenuation may be needed between the rf filter and the first mixer. The amount of attenuation re-quired will depend on the amount of isolation achievable with the rf filter. In the figure III-12 example, an attenuation of -20 decibels was assumed. Higher pseudonoise (PN) spreading code rates and longer code lengths may be-come necessary if the desired rf filtering characteristics are unattainable. These trades are being studied, and a final design configuration will be de-termined as part of the LinCom Phase IV task (ref. 24). In any event, it ap-pears reasonable that the rf and i.f. filtering characteristics, code rates, code lengths, and loop bandwidth can be varied to achieve an acceptable level of jitter on the recovered pilot signal phase for the levels of interference postulated. Since the self-interference case has the worst RFI conditions, no problems are envisioned for adjacent geosynchronous orbit spacings of SPS's as far as mutual interference is concerned.

4. ALTERNATE SYSTEMS

The current SPS reference configuration has a 1-kilometer trans-mit antenna delivering 5 gigawatts of dc power out of a rectenna approximately 10 kilometers in diameter. The system uses high-power klystrons operating at 2.45 gigahertz. Several alternates to this reference system being studied in-clude the following.

a. Smaller systems configured with larger antennas, reduced output powers, and smaller rectennas

b. Systems operating at 5.8 gigahertz

c. Other power conversion devices including magnetrons, lasers, and solid state

The antenna sizing (1 kilometer) and maximum power transmission (5 gigawatts) were determined by two constraints: a 23-kW/m^2 rf power density limitation in the transmit antenna and a 23-mW/cm^2 maximum power density limit in the ionosphere. The differential costs in electricity for seven antenna/rectenna

configurations operating at 2.45 gigahertz and five satellite systems operating at 5.8 gigahertz have been determined and are described in detail in reference 6. The study results are summarized as follows.

a. Smaller System Sizing Trade-Offs

The advantages of smaller systems are twofold: (1) commercial utility companies may prefer to integrate lower power levels (less than 5 gigawatts) into their grids and (2) rectennas smaller than the 10-kilometer-diameter reference configuration may be preferred from the standpoint of land utilization and site location. In addition, smaller power blocks are desirable if the use of SPS systems were to be extended to foreign countries. The thermal limitation of 23 kW/m^2 at the center of the transmit antenna is due to the heat radiated by the dc-rf power converters (i.e., klystrons). The current configuration has 70-kilowatt klystron tubes operating at 85-percent conversion efficiency and cooled by passive heat-pipe radiators. This thermal limitation is a severe constraint on higher frequency (5.8 gigahertz) systems, which have lower efficiency klystrons (80 percent). An improved thermal design using graphite composite materials with high-emissivity coatings which provide a 33-percent increase in heat rejection is proposed in reference 6 and used in these calculations.

b. Optimized Microwave Systems - 2450 and 5800 Megahertz

To provide a smaller rectenna, the antenna size must be increased and the transmit power decreased if the 23-mW/cm^2 ionospheric limit is to be maintained. The microwave system was reoptimized with higher gain antennas and with various ionospheric and thermal power density limitations. One of the ground rules for the study was that the rectenna is sized for all configurations to receive 88 percent of the transmit power. Various Gaussian illumination tapers were investigated; however, as was true for the reference system, a 10-decibel taper provides maximum rectenna collection efficiency while minimizing side-lobe levels. The only constraint on side lobes is that the first side-lobe peak should have a power density of less than approximately 0.1 mW/cm^2. It is assumed that the antenna performance parameters are the same as those in the reference system. These include 10° rms phase error, ±1 percent amplitude error, 2 percent tube failure rate, 0.63 centimeter (0.25 inch) mechanical spacing between subarrays, ±1 arc-minute antenna tilt, and ±3 arc-minutes subarray tilt.

For the 2.45-gigahertz operating frequency, two constraints are considered: (1) retaining the 23-mW/cm^2 ionospheric limit by reducing transmitter power as the size of the satellite antenna increases and (2) allowing the ionospheric power density limit to increase by retaining the same transmit power as antenna size increases. The ionospheric limit is the critical parameter in system sizing for 2.45 gigahertz. The thermal limit on the antenna is not a constraint for the larger antenna/smaller rectenna systems operating at 2.45 gigahertz.

47

For operation in the 5.8-gigahertz ISM frequency band, a different set of constraints must be considered. Since the gain of an antenna is proportional to the frequency squared, antennas smaller than 1 kilometer diameter will result in smaller rectennas compared to 2.45 gigahertz. The antenna thermal limitation is the critical parameter for system sizing at 5.8 gigahertz. The ionospheric limit of 23 mW/cm^2 is no longer a factor because this threshold is also proportional to frequency squared. That is, the adjusted ionospheric limit for 5.8 gigahertz is

$$P_{D_{5.8GHz}} = P_{D_{2.45GHz}} \times \left(\frac{5.80}{2.45}\right)^2$$

$$= 23 \ mW/cm^2 \times 5.6$$

$$= 129 \ mW/cm^2 \tag{6}$$

Since the 5.8-gigahertz antenna will be smaller, or at least no larger, than 1 kilometer in diameter, the adjusted ionospheric limit of 129 mW/cm^2 will not be exceeded. Other factors influencing system sizing include lower efficiencies in several of the microwave subsystems operating at the higher 5.8-gigahertz frequency. The operating constraints at 5.8 gigahertz are

(1) Retaining the 23-kW/m^2 antenna power density limit by reducing transmit power as the size of the satellite antenna decreases

(2) Allowing the antenna thermal limit to increase as the antenna size decreases

(3) Reductions in subsystem efficiency including

(a) 80 percent rather than 85 percent dc-rf klystron conversion efficiency

(b) 97 percent rather than 98 percent for the normal atmospheric transmission

(c) 87 percent instead of 89 percent for the average rf-dc conversion efficiency in the ground rectenna

The relative antenna/rectenna sizes for 2.45- and 5.8-gigahertz operation are shown in figure III-13. Because of phase control and attitude control requirements for the antennas, the antenna diameters should probably be limited to 1 to 1.5 kilometers for 2.45-gigahertz operation and 0.75 to 1.0 kilometer for 5.8-gigahertz operation.

(1) _System cost trade-offs_ - A detailed analysis of subsystem costs and masses for the reference 5-gigawatt SPS with silicon solar
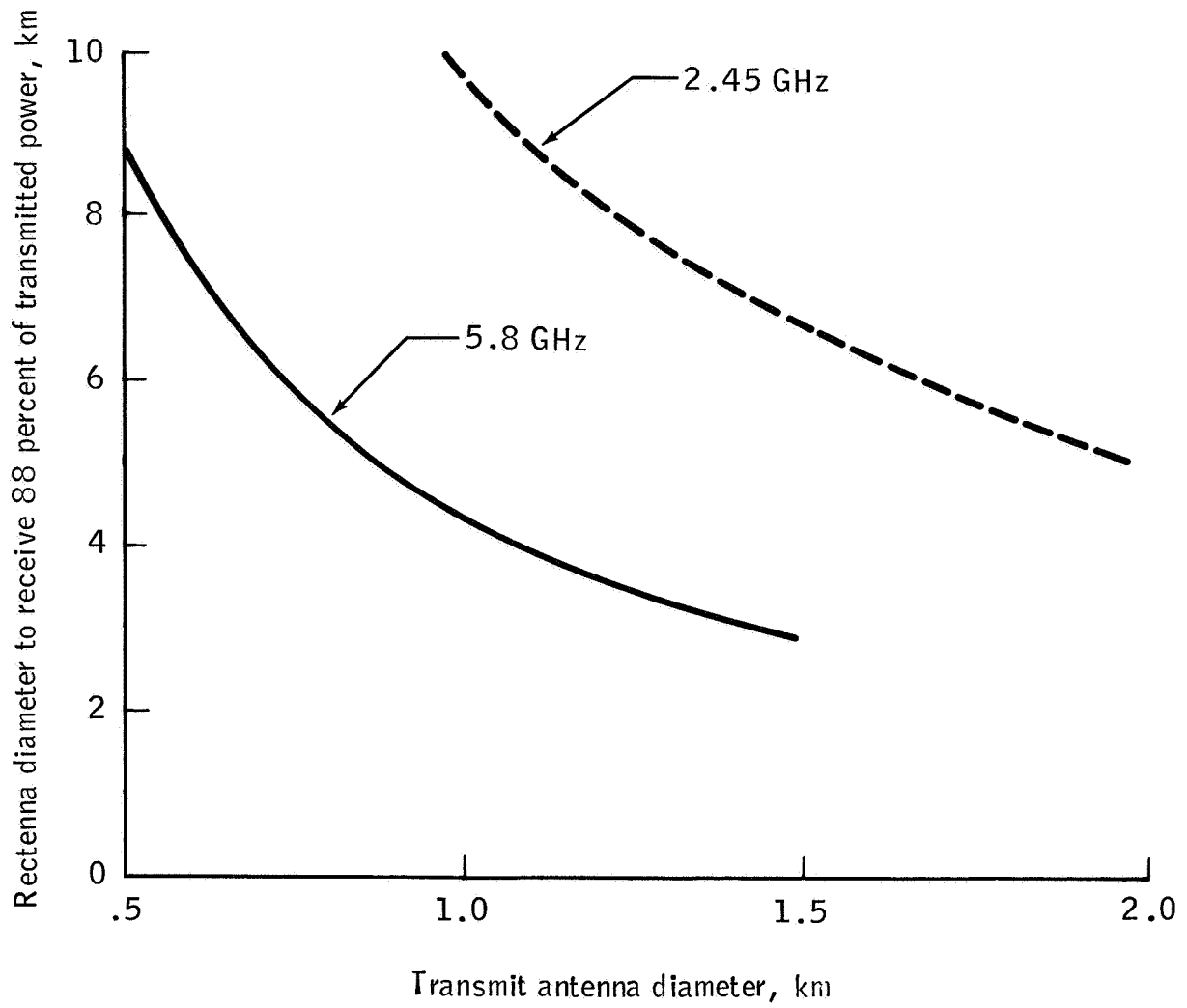
Figure III-13.- Antenna/rectenna sizing summary.

cells is given in reference 12. These values are used as a baseline for computing costs for the different antenna/rectenna configurations. The principal elements in the SPS recurring costs are satellite hardware, transportation (space and ground), space construction and support, rectenna, program management and integration, and cost allowance for mass growth. Some general costing assumptions include 30-year operating lifetime, 0.92 plant factor for 2.45-gigahertz operation, 0.90 plant factor for 5.8-gigahertz operation, 15 percent rate of return on investment capital, 22 percent mass growth factor to cover potential risks in solar array, and the following microwave system performance estimates: 17 percent of net SPS hardware cost factor to account for mass growth and 10 gigawatts per year additional power generation capacity.

The total mass and cost for the SPS system are taken to be 59 984 metric tons and \$12 432 million, respectively. The cost and mass statements for the individual satellite subsystem are divided into the following categories.

(a) Power collection: structure, solar cell blankets, power distribution, and maintenance

(b) Rotary joint

(c) Microwave antenna: structure, klystrons and thermal control, waveguides, subarray structure and control, power distribution (conductors, switchgears, dc/dc converters, and energy storage), phase control, maintenance systems, and antenna mechanical pointing

(d) Information management and attitude control: hardware and propellant

(e) Communications

(f) Transportation: electric orbital transfer vehicle, personnel launch vehicle, and heavy lift launch vehicle

(g) Construction operations: low Earth orbit and geosynchronous orbit

The cost and mass from each of these subsystems will vary according to total power, antenna size, frequency, etc., of the candidate antenna/rectenna systems. Since the calculations are quite lengthy, only the end results for 2.45- and 5.8-gigahertz operation are shown in tables III-7 and III-8, respectively. The details are given in reference 6, together with a complete sample calculation for one configuration. In table III-7 (2.45 gigahertz), the microwave system has been sized to conform with the 23-mW/cm^2 ionospheric limit for the first four antenna/rectenna configurations. Removal of this ionospheric constraint for the last three configurations results in a maximum of 91 mW/cm^2 for the 5-gigawatt, 2-kilometer-diameter antenna system.

TABLE III-7.- SPS SUMMARY COSTS FOR 2.45-GIGAHERTZ OPERATION

(a) Physical parameters

Parameter	23-mW/cm² ionospheric limit				Increased ionospheric limits		
Transmitter diameter, km	1	1.36	1.53	2	1.36	1.53	2
Transmit output power, GW	6.5	3.53	2.78	1.64	6.5	6.5	6.5
Power density at rectenna, mW/cm²	23	23	23	23	42	54	91
Rectenna diameter, km	10	7.6	6.8	5	7.6	6.8	5
Power delivered, GW	5	2.7	2.1	1.26	5	5.05	5.05

(b) Costs

Element	23-mW/cm² ionospheric limit				Increased ionospheric limits		
SPS hardware, million dollars	4946	4072	4120	5069	5898	6455	8112
Less amortization of investment, million dollars	473	257	202	119	473	473	473
Adjusted SPS hardware, million dollars	4473	3815	3918	4950	5425	5982	7639
Mission control, million dollars	10	10	10	10	10	10	10
Transportation, million dollars	3155	2735	2721	3186	3639	3918	4849
Construction operations, million dollars	961	1066	1170	1615	1233	1395	1933
Rectenna, million dollars	2578	1561	1293	835	1852	1646	1283
Program management and integration, million dollars	495	407	412	507	590	645	811
Cost allowance for mass growth, million dollars	760	649	666	841	922	1017	1299
Total cost, million dollars	12 432	10 243	10 190	11 944	13 671	14 613	17 824
Rate, ¢/MJ	1.31	1.99	2.52	5.00	1.44	1.53	1.86
Rate, mills/kWh	47	71.6	90.6	180.1	52	55	67.1
Increase in electricity costs over reference system, percent	0	52.4	92.7	283	10.6	17	42.7

TABLE III-8.- SPS SUMMARY COSTS FOR 5.8-GIGAHERTZ OPERATION

(a) Physical parameters

Parameter	Improved thermal design				Present thermal design
Transmitter diameter, km	0.5	0.75	1.0	1.5	0.75
Transmit output power, GW	1.68	3.78	6.5	2.88	2.84
Power density at rectenna, mW/cm^2	7.87	40	122	122	30
Rectenna diameter, km	8.75	5.8	4.3	2.8	5.8
Power delivered, GW	1.17	2.72	4.78	2.12	2.02

(b) Costs

Element	Improved thermal design				Present thermal design
SPS hardware, million dollars	1452	3038	5366	4777	2494
Less amortization of investment, million dollars	122	275	473	209	206
Adjusted SPS hardware, million dollars	1330	2763	4893	4568	2288
Mission control, million dollars	10	10	10	10	10
Transportation, million dollars	1288	2070	3120	2720	1794
Construction operations, million dollars	444	734	1057	1270	663
Rectenna, million dollars	4925	2672	2003	1063	2672
Program management and integration, million dollars	145	303	536	477	249
Cost allowance for mass growth, million dollars	226	470	832	777	389
Total cost, million dollars	8368	9022	12 451	10 885	8063
Rate, ¢/MJ	3.83	1.78	1.40	2.75	2.14
Rate, mills/kWh	138	64	50.3	99	77
Increase in electricity costs over reference system (2.45-GHz operation), percent	193	36	7	111	64

The electricity costs and the differential cost increase as compared to the 5-gigawatt, 1-kilometer antenna reference system are shown in figure III-14 for 2.45-gigahertz operation. The upper curve, constrained to an ionospheric limit of 23 mW/cm^2, shows a significant increase in electricity costs as the antenna size increases. Microwave power density in the ionosphere is directly proportional to transmit antenna area and total transmit power; therefore, if the antenna area is doubled, the power must be reduced by one-half to maintain the same power density. The electricity cost rates are determined by the total satellite costs divided by the delivered power. As seen from the cost summary in table III-7, the total satellite costs decrease at a much slower rate than does the delivered power as the antenna size increases. This cost disadvantage with larger antennas is removed if the total transmit power remains constant as the antenna size changes. However, the ionospheric power density increases accordingly.

The 5.8-gigahertz systems (table III-8) have thermal limitations in the transmit antenna rather than ionospheric limitations as the dominant constraint. The 5.8-gigahertz systems are inherently smaller (antenna sizing, transmit power, and rectenna sizing) as compared to the 2.45-gigahertz configurations because of the increased antenna gain at higher frequencies.

The electricity costs for the 5.8-gigahertz systems are compared to the reference 2.45-gigahertz system in figure III-15. The data indicate that a significant reduction in costs can be achieved with a modest improvement in thermal radiator design. Since the increase in differential cost is reduced from 64 to 36 percent for the 0.75-kilometer-diameter antenna by using a new thermal radiator configuration, improvements in thermal design are considered mandatory. Details of the thermal design estimates are given in reference 6.

In summarizing the costing results and the microwave system trade-offs, several options should be considered further.

2.45 GHz	Increase ionospheric limit to 54 mW/cm^2	1.53-km antenna; 6.8-km rectenna with 5 GW grid power; differential cost increase is 17 percent (to 1.53¢/MJ (55 mills/kWh))
2.45 GHz	Retain 23 mW/cm^2 as ionospheric limit	1.36-km antenna; 7.6-km rectenna with 2.7 GW grid power; differential cost increase is 50.2 percent (to 1.96¢/MJ (70.6 mills/kWh))
5.8 GHz	Increase antenna thermal limit by 33 percent	0.75-km antenna; 5.8-km rectenna with 2.72 GW grid power; differential cost increase is 36 percent (to 1.78¢/MJ (64 mills/kWh))
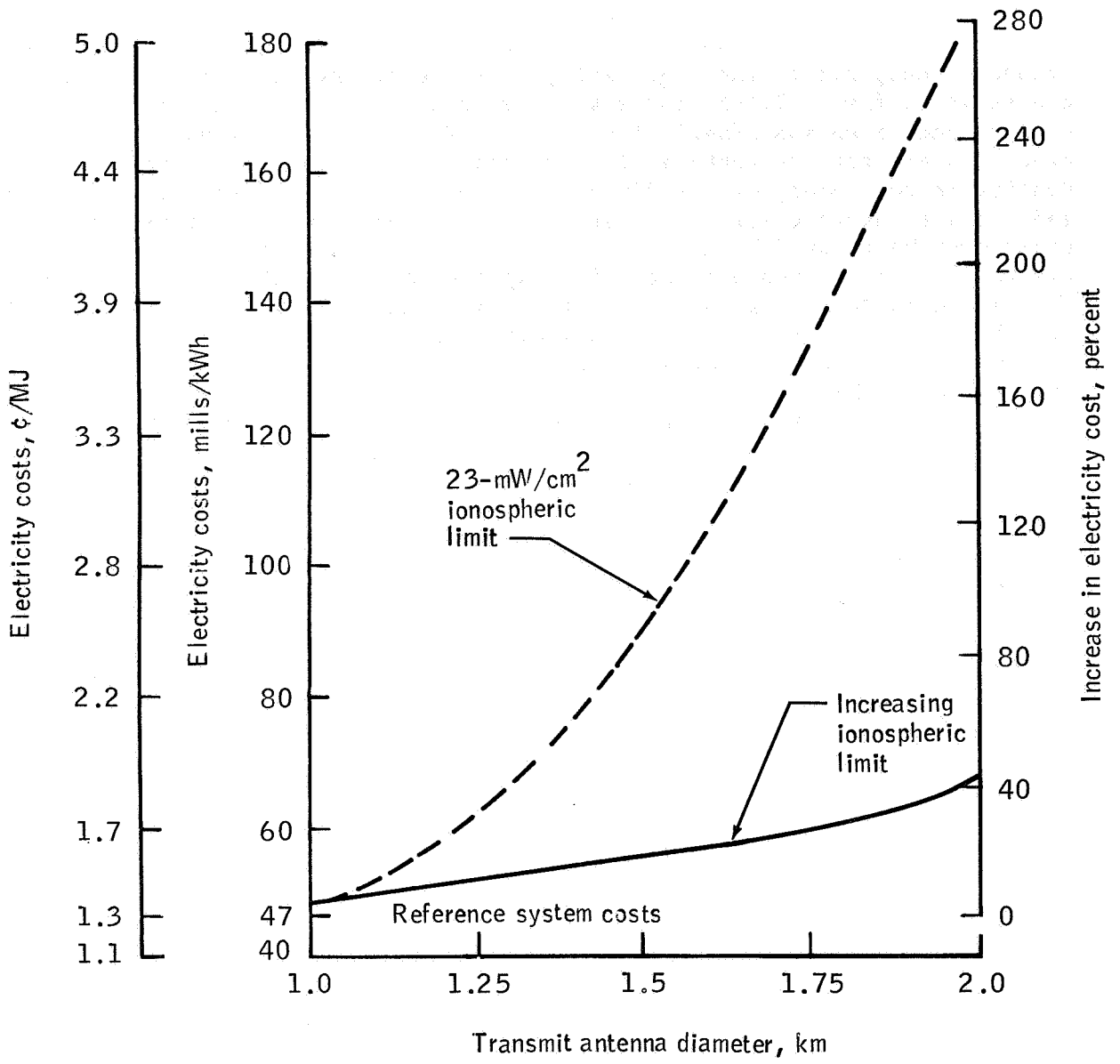
Figure III-14.- Electricity costs for 2.45-gigahertz systems.
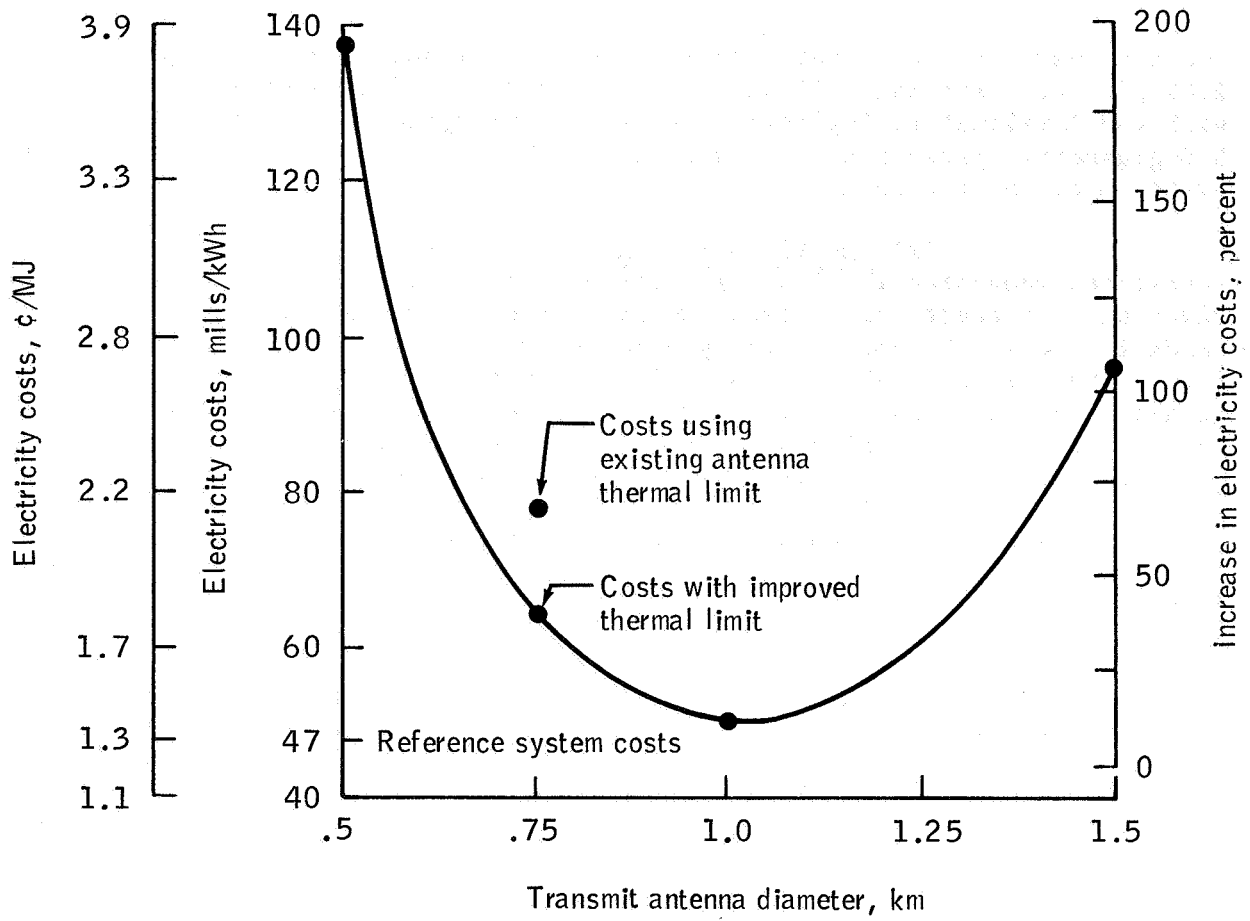
Figure III-15.- Electricity costs for 5.8-gigahertz systems.

The microwave radiation patterns for the 1.53-kilometer antenna operating at 2.45 gigahertz and the 0.75-kilometer antenna at 5.8 gigahertz are compared with the 1-kilometer, 5-gigawatt reference SPS system in figure III-16. The 5.8-gigahertz system has lower side lobes than the reference 2.45-gigahertz system near the rectenna.

        (2) <u>Multiple antennas</u> - The current SPS scenario has 60 satellites separated 1° (700 kilometers) in geosynchronous orbit, each delivering 5 gigawatts of rectenna dc grid power. Because of increased demands for geosynchronous slots by other users, it may become necessary to reduce the number of SPS's. Multiple antennas on one SPS are recommended. It has been shown that SPS antennas can operate in close promixity with negligible mutual interference. An example of a multiple-antenna system would be a 5- by 20-kilometer solar array (twice the size of the current solar array for one antenna) feeding two 5-gigawatt antennas, one at each end. It may be advantageous to have four or more antennas on a single satellite especially if a larger antenna/smaller rectenna configuration or a higher frequency (5.8 gigahertz) system is chosen. The relative sizes for a number of antenna/rectenna configurations are shown in figure III-17.

        (3) <u>Summary</u> - The satellite and associated microwave system have been reoptimized with larger antennas (at 2.45 gigahertz), reduced output powers, and smaller rectennas. Four constraints were considered: (a) the 23-mW/cm^2 ionospheric limit, (b) a higher (54 mW/cm^2) ionospheric limit, (c) the 23-kW/m^2 antenna power density limit (thermal), and (d) an improved thermal design allowing 33 percent additional waste heat. The differential costs in electricity for seven antenna/rectenna configurations operating at 2.45 gigahertz and five satellite systems operating at 5.8 gigahertz have been calculated. The conclusions are as follows.

        (a)   Larger antenna/smaller rectenna configurations are economically feasible under certain conditions.

        (b)   Transmit antenna diameters should be limited to 1 to 1.5 kilometers for 2.45-gigahertz operation and 0.75 to 1.0 kilometer for 5.8-gigahertz operation.

        (c)   Two 2.45-gigahertz configurations (table III-7) are selected, dependent on the ionospheric power density limit.
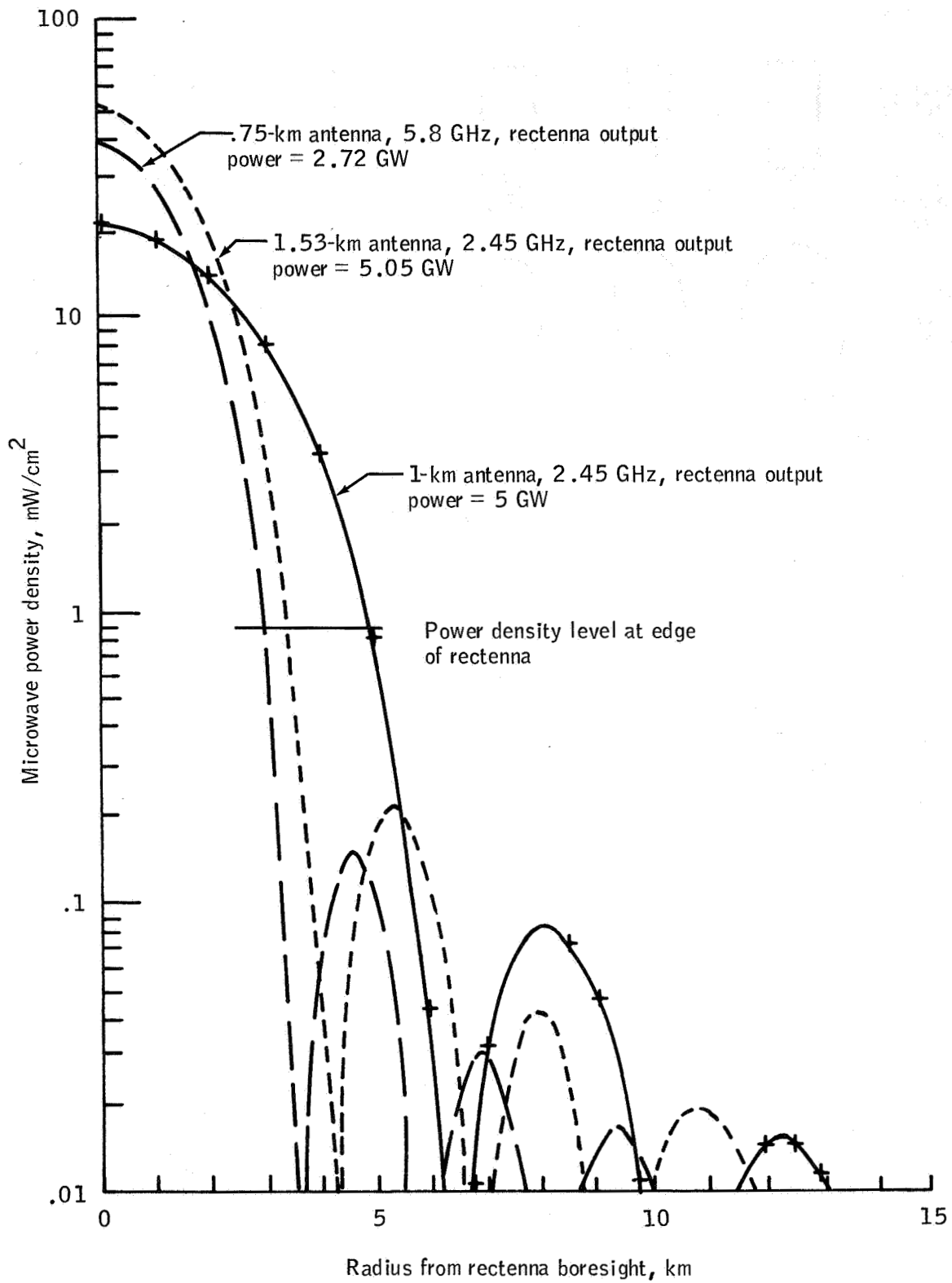
Figure III-16.- Antenna patterns for three SPS configurations.

The plot shows Microwave power density, mW/cm^2 (vertical axis, logarithmic from .01 to 100) versus Radius from rectenna boresight, km (horizontal axis, 0 to 15).

.75-km antenna, 5.8 GHz, rectenna output power = 2.72 GW

1.53-km antenna, 2.45 GHz, rectenna output power = 5.05 GW

1-km antenna, 2.45 GHz, rectenna output power = 5 GW

Power density level at edge of rectenna

57

Frequency   2.45 GHz   5.8 GHz

Relative satellite size

Transmit antenna diameter   1 km   1.36 km   1.53 km   .75 km   1 km   1.5 km

Relative rectenna size

10 by 13 km   7.6 by 9.9 km   6.8 by 8.8 km   5.8 by 7.5 km   4.3 by 5.6 km   2.8 by 3.6 km

Ground power output   5 GW   2.7 GW   5.05 GW   2.72 GW   4.78 GW   2.12 GW

(a)   Single-antenna configurations.

Two -
5-GW,
1-km-diam
systems at
2.45 GHZ

Four -
5.05-GW,
1.53-km-diam
systems at 2.45
GHz

Four -
2.72-GW,
.75-km-diam
systems at 5.8
GHz

10 by 13 km   6.8 by 8.8 km   5.8 by 7.5 km

(b)   Multiple-antenna configurations.

Figure III-17.- Relative antenna/rectenna sizing configurations.

58

	23-mW/cm^2 limit	54-mW/cm^2 limit
Antenna diameter, km	1.36	1.53
Rectenna dc grid power, GW	2.76	5.05
Rectenna diameter, km	7.6	6.8
Relative rectenna area, percent . . .	56	46
Electricity cost increase, percent . .	50	17
Electricity cost, ¢/MJ (mills/kWh) . .	1.96 (70.6)	1.53 (55)

Note: The rectenna areas and electricity costs are in comparison to those for the reference SPS system.

> (d) The existing ionospheric limit of 23 mW/cm^2 is too low and should be raised after the ionospheric heating tests and studies are completed. For SPS cost considerations, it is very important to ascertain the true upper limit.
>
> (e) The 5.8-gigahertz configurations (table III-8) are constrained by antenna thermal limitations rather than ionospheric limits. A reasonable configuration based on a 33-percent improvement in waste heat rejection is

Antenna diameter, km	0.75
Rectenna dc grid power, GW	2.72
Rectenna diameter, km	5.8
Relative rectenna area, percent . . .	33
Electricity cost increase, percent . .	36
Electricity cost, ¢/MJ (mills/kWh) . .	1.78 (64)

> (f) The impact on commercial utility grids of a 5.8-gigahertz system which has to be shut down on an unscheduled basis due to localized weather conditions is not known.
>
> (g) Multiple (two to four) antennas on a single SPS are definitely recommended regardless of the particular antenna/rectenna configuration chosen. This is a means for maintaining the same amount of power supplied to the ground while reducing the geosynchronous slots (spacings) required for the satellites.

    c. Magnetron, Laser, and Solid-State Configurations

Several alternate microwave systems are being studied in which the klystron tubes are replaced with medium-power magnetrons or low-power solid-state amplifiers. Laser transmission offers the possibility of

replacing the entire microwave system. Results of preliminary studies into these alternatives may be summarized as follows.

(1) Magnetrons - The use of an injection-locked magnetron is being studied by W. C. Brown of the Raytheon Company. Two configurations have been proposed: (a) a magnetron connected with a three-port ferrite circulator and (b) two matched magnetrons connected to a four-port "magic T." Although the magnetron and the amplitron are both crossed-field amplifiers, the magnetron has a higher gain (20 to 30 decibels as compared to 10 decibels for the amplitron) and superior noise performance characteristics. The possible use of magnetrons gained impetus from the discovery that these tubes have an extremely high signal-to-noise ratio (S/N) when the filament power is turned off. Subsequent studies indicate that random noise from the tube is not an inherent property of the basic energy conversion process but is associated with one or more extraneous mechanisms not currently understood (ref. 25). Not all tubes exhibited the large reduction in noise when the filament was turned off, although the reason was not known.

A microwave antenna implemented with magnetrons would be considerably different from a klystron antenna. A single magnetron would be used to provide the rf drive into the circulators or the magic T's for 50 to 100 magnetron tubes. The output of each tube would be sampled, and an error signal would operate an rf phase shifter at the tube input to maintain proper phasing. Since this phase shifter operates between the output of the driver magnetron and the input to the second magnetron, the device has relatively high power in comparison to the phase controller for the klystron tube system. The reason for the difference in the phase control systems for the magnetrons and the klystrons is the difference in the gains of the tubes (50 decibels for klystrons and 20 to 30 decibels for magnetrons). The phase shifter for the magnetrons may be a mechanical device.

In summary, the magnetron shows promise of achieving high efficiency with long operating lifetimes. The noise performance when operating these tubes at high-strength magnetic fields to obtain the desired efficiency and at high voltage-to-current ratios to achieve long lifetimes is being investigated.

(2) Lasers - An SPS system using lasers would employ many smaller power transmission links to ground receivers with diameters on the order of 100 meters; therefore, the use of lasers would greatly reduce any rectenna siting problems. However, lasers do incur a number of problems that must be solved. These include low conversion efficiencies (i.e., existing systems typically have 10-percent efficiencies), technology status, beam pointing, thermal limitations, reliability, and weather effects. Since several government agencies have substantial basic research programs in the area of high-power, high-efficiency laser systems, these problems are being studied.

System studies by the Boeing Aerospace Company indicate that a laser power transmission satellite would probably employ a number

of lasers in the 1- to 10-megawatt power range (ref. 3). The most promising laser options include the following.

(a) Gas electric discharge laser – The gas electric discharge laser (EDL) has potential for high power and fair efficiency. The carbon monoxide (CO) and carbon dioxide (CO_2) lasers were investigated in some detail. Mass comparisons in terms of mass in space per unit ground grid power (kg/kW) indicate that the subsonic CO_2 system is approximately six times as heavy as the reference microwave system. The supersonic CO laser system is seven times heavier than the microwave system.

(b) Indirect optically pumped gas laser – In this system, the solar array is eliminated since the solar energy is concentrated on a cavity for heating a lasant gas such as CO or CO_2. A Brayton cycle turbine power system processes the heated gas through a laser cavity, where the energy is extracted via a laser beam. This system has potential for marked improvement with technology advances and is less massive than the EDL systems.

(c) Free electron laser – The free electron laser (FEL) has potential for high power and good efficiency, but technology is still in the embryonic stage. In this system, coherent light is emitted by interaction of an electron beam with an alternating magnetic field. Three types of accelerator configurations were studied, with the single-pass storage ring system chosen as the most promising. An overall accelerator efficiency of 40 percent from the electricity input from the solar arrays to laser power output is considered a reasonable goal. The total system efficiency from sunlight onto the solar array to electricity at the ground is 4 percent as compared to 7 percent for the microwave reference system. The FEL system is also the least massive of the laser options if the efficiency estimates are valid.

An optical rectenna for converting the laser energy at the ground into electricity was also studied. This ground system uses simple parabolic concentrators and pulsed laser operation for generating high power intensities for efficient light-to-electricity conversion. A conversion efficiency of 80 percent is projected.

In summary, lasers with sufficient technology advancement can provide small (less than 100 megawatts) blocks of power with modest increases in electricity costs as compared to the reference 5-gigawatt microwave system. Operational availability is better than ground solar but

not as good as the microwave system. The most promising areas for research include the free electron laser and the optical rectenna.

(3) Solid state - The major advantage of solid-state devices is the increased reliability compared to tubes. Solid-state microwave transmission concepts would have a major impact on the reference SPS design. The solid-state transmitter will have a lower power density of microwave energy in the center of the antenna because of temperature limitations. The transmitting antenna will be larger than 1 kilometer in diameter in order to transmit several gigawatts of power and, consequently, the rectenna will be smaller.

Two configurations are being studied: (a) a dedicated antenna with solid-state devices replacing the klystron tubes and (b) a "sandwich" concept, in which solid-state amplifiers and solar cells are combined. Details of these configurations and trade-off considerations are given in Section III.F.

B. PHASE CONTROL

1. SYSTEM REQUIREMENTS AND CONCEPTS

The forming, steering, and control of the SPS microwave beam are of major concern not only because of power-transfer efficiency considerations but also from a safety and environmental viewpoint. At the heart of the microwave power beam is the phase control system. This system, in essence, must adjust the phase of each radiating element, automatically accounting for element location, antenna-pointing error, surface roughness (mechanical alinement of subarrays), and phase distribution system delays.

Significant efforts have been underway to define the phase control system functional requirements and to establish acceptable performance limits. Major system studies conducted by Boeing Aerospace Company and Rockwell International have helped to define the functional requirements of the phase control system. Early work accomplished by the Raytheon Company, the NASA Jet Propulsion Laboratory (JPL), and the LinCom Corporation resulted in the retrodirective beam-steering system concept presently employed as the basis of the SPS phase control system. Other sources have offered several alternate approaches and some with refinements to the retrodirective approach. For example, Novar Electronics Corporation has outlined a ground-based phase control technique using interferometry techniques; others (e.g., Raytheon) suggested pattern-synthesis techniques for phase control. LinCom Corporation has recently conducted an initial analytical evaluation of a potential ground-based phase control concept resulting from the Novar initiative with modifications and refinements suggested by JSC.

a. System Requirements

As pointed out in the introduction, the phase control system must accomplish three major functions: power beam forming, power beam pointing, and power beam safing (control). The generic or functional requirements in each of these major areas are fairly obvious. First, a highly

62

directional microwave signal must be generated. In the SPS, the signal is generated by properly phasing each spacetenna radiating power module (or subarray) to produce a broadside radiation pattern equivalent to the array beam shape.

Once a properly formed beam is achieved, the center of the beam must be precisely pointed at the Earth-based rectenna to transfer power efficiently. Since the mechanical pointing accuracy of the spacetenna and of the individual subarrays within the spacetenna is expected to be on the order of 1 and 3 arc-minutes, respectively (ref. 26), the potential miss distance on the Earth's surface from geosynchronous altitude would be on the order of 10 to 30 kilometers, which would result in completely missing the 10-kilometer-diameter rectenna site. To compensate for this pointing inaccuracy, the SPS phase control system must be capable of properly adjusting the phase of each radiating-element power module to shift the power beam center without degrading the beam shape. The accuracy that must be achieved dictates development of new and highly sophisticated phase control techniques, which are discussed later.

The final function which must be provided by the phase control system is that of power beam safing. This aspect is inherent in the phase control process since the power beam intensity is greatly diffused if loss of phasing occurs, because of the excessive element-to-element phase errors. For example, if the phase error across the spacetenna exceeds 90° rms at the rf beam frequency, the array pattern has diffused to that of a single transmitting element (power module) and the total energy is spread over an extremely large area. Although the power density at a given location far removed from the rectenna site may increase when dephasing occurs, it will remain well below the U.S. and U.S.S.R. standards for S-band radiation exposure (10 and 0.01 mW/cm^2, respectively), as shown previously in figure III-7. Thus, complete loss of phasing results in automatic safing as far as power density requirements are concerned. The other aspect of phasing loss which must be considered is that of partial dephasing or covert (jamming) dephasing. To protect against an intentional dephasing attempt or an attempt to redirect (rob) power, a method of coding each SPS pilot signal is included in the existing baseline system. To protect against the possibility of beam wander due to excessive phase errors during system startup or shutdown, some type of ground sensor network may be required in the vicinity of the rectenna sites. Thus, by using the concept of a retrodirective phase array system incorporating a coded (secure) pilot signal and ground sensors for additional safing considerations, the baseline SPS phase control system meets the general functional requirements discussed previously.

b. System Concepts

Achieving the phase accuracy necessary to meet the design goal power-transfer efficiency (≈90 percent) will require advanced concepts and implementation techniques for the SPS phase control system. Two broad categories of phase control concepts have been investigated. First, techniques which employ phase corrections introduced at the transmitting array by way of ground system command links were considered. Several approaches to

obtaining the phase estimate required for control of each transmit element's phase have been investigated. These include the following.

(1) Element phase estimation based on power beam pattern synthesis in the vicinity of the rectenna site (refs. 16 and 27)

(2) Multiple transmit frequencies for each radiating element to achieve phase estimation from traveling-wave interferometer measurements (ref. 8)

(3) Direct phase measurement of signals transmitted from individual elements by sequential comparison of a coded (modulated) element's signal with the averaged phase of all other element signals at the rectenna center (ref. 16)[2]

None of the ground-based phase control techniques have been thoroughly evaluated. However, NASA is actively investigating techniques involving sequential comparison of element signal phases using multiple tones to isolate the phase of the wanted signal from that of the power signal and the interferometer-based technique for phase estimation.

c. Conclusions and Remaining Issues

As a result of the analytical, simulation, and test activities conducted to date, the following conclusions have been drawn with respect to the SPS phase control system.

(1) <u>Performance conclusions</u> - The following conclusions can be stated with respect to performance.

(a) Beam misalinement (pointing error) is not critical when 10° rms phase error is achieved providing antenna/subarray mechanical alinement requirements are maintained.

(b) Upward bound on phase error is determined by acceptable economic losses in scattered power rather than beam-pointing errors or environmental factors.

(c) Based on the reference system configuration, for 10° rms phase error, the power lost from the main beam is less than 3 percent and the beam-pointing error is less than ±250 meters with 99 percent probability.

---

[2]J. C. Vanelli: Scheme for Phase Control of Spacetenna Elements. Lockheed Electronics Company interdepartmental communication LEC-79-17-769-01.

(d) Phase control to the smallest transmitter area (power module for the reference system) reduces the grating-lobe peaks and relaxes subarray mechanical alinement and antenna positioning constraints.

(e) Phase control to the power module level is environmentally justified and economically sound on the basis of cost trade-offs between phase control electronics and main beam power losses.

(2) <u>Retrodirective phase control conclusions</u> - The following conclusions can be stated with respect to retrodirective phase control.

(a) Implementation/performance appears feasible based on analytical simulations and experimental (laboratory) evaluations.

(b) Secure operation can be achieved (coded pilot signal in reference system).

(c) Doppler effects are not a problem.

(d) Biases in distribution system constitute a potentially serious calibration problem.

(e) Ionospheric effects on phase control are uncertain and could affect system concepts.

(f) Retrodirective phase control features fast response automatic phase tracking/adjustment.

(g) Retrodirective phase control features automatic/rapid fail-safe operation. Dephasing occurs in milliseconds and diffuses power beam to 0.003-mW/cm^2 density levels.

(h) Retrodirective phase distribution system is complex, and its performance is critical to efficient power transmission (distributed and centralized techniques).

(3) <u>Ground-based phase control conclusions</u> - The following conclusions can be stated with respect to ground-based phase control.

(a) Implementation/performance appears feasible, based on analytical studies.

(b) Secure operations can be provided with coded command channel.

65

(c) Ionospheric effects on phase control performance are uncertain and could affect system concepts.

(d) Biases in distribution system can be adjusted out during normal operations (part of the phase control loop).

(e) Ground-based phase control features closed-loop phasing (measures phase at ground and commands phase adjustments by way of communication link).

(f) Ground-based phase control has slower responses than retrodirective (0.25-second delay due to geosynchronous transmit time).

(g) Dephasing process of ground-based phase control is slower than retrodirective and may require additional beam-safing measures.

(4) Hybrid phase control conclusions - The following conclusions can be stated with respect to hybrid (retrodirective and ground based) phase control.

(a) Hybrid phase control combines the best features of each concept.

(b) System implementation concepts/feasibility have not been studied in sufficient detail for comparison with individual concepts (i.e., retrodirective and ground based).

(5) Remaining issues - The remaining issues relating to the phase control system which must be addressed before selection of an SPS phase control system design concept are as follows.

(a) Phase error buildup in distribution system

(b) Array topology for distribution system (phase error buildup compared to reliability)

(c) Cable compared to fiber optics distribution techniques

(d) Power signal interference on pilot signal receiver

(e) Phase conjugation accuracy

(f) Effects of ionospheric/atmospheric disturbances

(g) Alternate concepts to retrodirective approach

(h) Accuracy of beam formation and pointing

(i) Failure effects on beam forming and pointing

(j) RFI of power module due to phase-lock loop around
     power amplifier (PA)

2. REFERENCE PHASE CONTROL SYSTEM

At the present time, none of the ground-based phase control
techniques have been thoroughly analyzed; however, NASA is actively investi-
gating two ground-based techniques referred to in subsection 1b. Since the
performance criteria using ground-based phase control concepts have not been
fully developed, the baseline SPS phase control system incorporates onboard
phase reference distribution and retrodirective phasing for beam forming and
steering (pointing). The concepts of retrodirective arrays are not new; how-
ever, application of these concepts to such large arrays as required for the
SPS system has presented many new and unique problems, such as the distribu-
tion of highly accurate reference phase information over 500-meter distances.
Several investigations of the applicability of retrodirective techniques to
the SPS phasing problems have been conducted. The JSC, MSFC, and JPL have
conducted in-depth in-house studies as well as awarding study contracts to in-
dustry. As a result of these study activities, a baseline phase control sys-
tem has been established using the results of the LinCom study (refs. 1, 28,
and 29) as a basis for system analysis and performance evaluation. The base-
line phase control system incorporates the basic concepts of reference phase
distribution and retrodirective beam steering.

a. Reference System Description

The phase control system has been divided into two major
levels. The first level is the phase distribution system consisting of a ref-
erence phase distribution network or tree which electronically compensates
for path-length variations to maintain a constant-phase reference at each of
101 552 radiating elements. The second level is the beam-steering and micro-
wave amplifier control system consisting of the phase conjugating and pilot
receiving equipment which receives a uniquely designed pilot signal and al-
lows carrier reconstruction and phase conjugation at the power beam frequency.
This concept avoids the problems of beam deflection due to frequency offsets
between pilot and power beam signals. The second level also provides the
phase control necessary to maintain an equal and constant phase independent-
ly through each of the microwave power amplifiers. A generic block diagram
of the overall phase control system, incorporating the master slave return-
able timing system (MSRTS), is shown in figure III-18.

The phase distribution portion of the system includes the
distribution "cables" and phase control electronics, which transfer a con-
stant phase throughout the network. To maintain the precise phase/timing ac-
curacy required over the 1-kilometer aperture of the SPS, some method of ac-
tive phase control is necessary within the phase distribution system. In the
baseline system, this control is accomplished using a technique referred to as

67
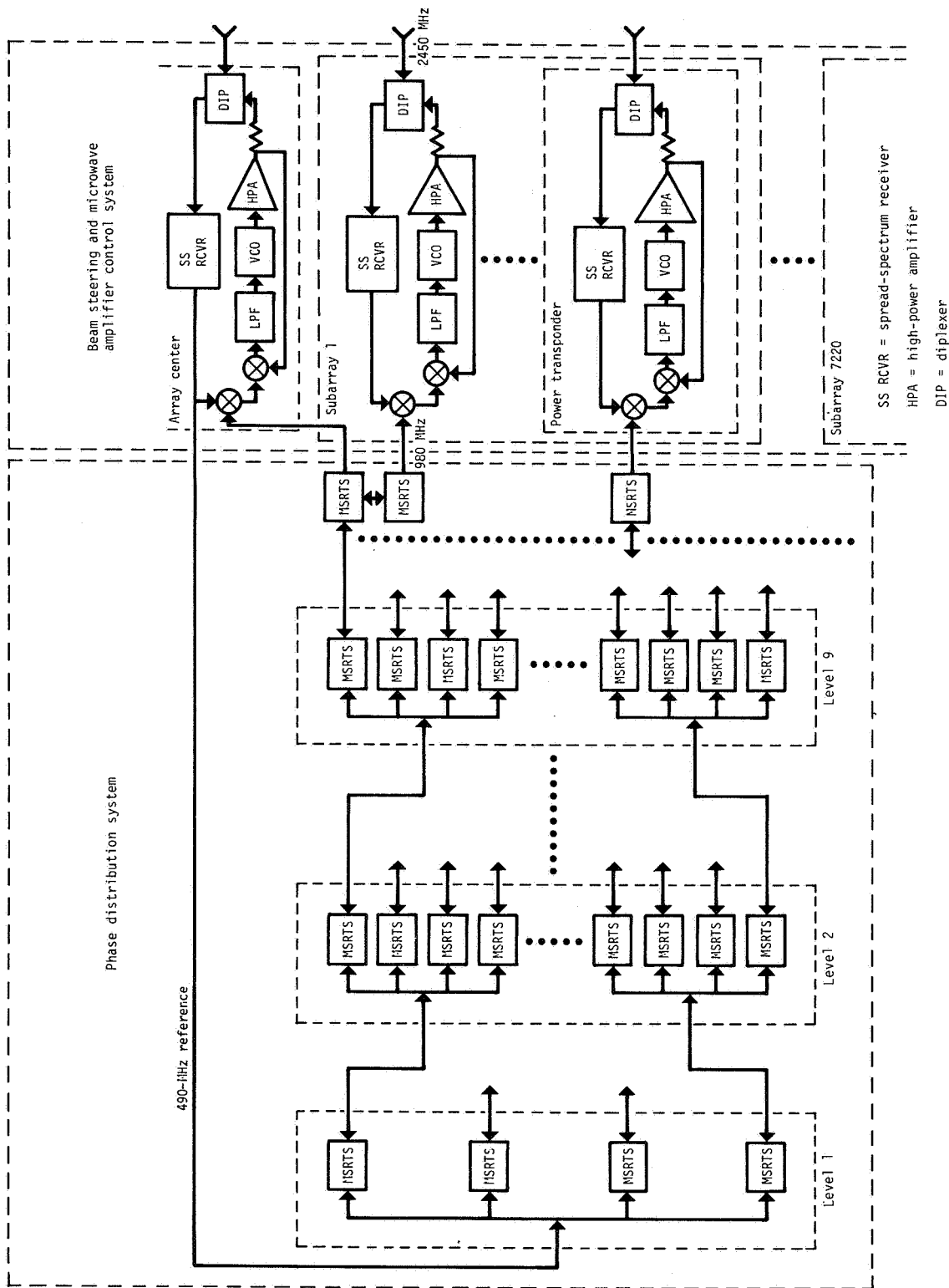
Figure III-18.- Solar power satellite phase control system. The master slave returnable timing system (MSRTS) provides cable delay compensation.

68

returnable timing (ref. 28) illustrated in figure III-19. A portion of the reference signal at the received location is amplified and coupled back into the distribution cable by way of a circulator. This returned signal sample is then used for phase locking to the original reference input of the phase control center (PCC). Since the same frequency is transmitted in both directions over the distribution cable, phase errors due to frequency dispersion of the cable are eliminated. When phase lock occurs, the resultant signal at point B in figure III-19 is driven to, and maintained at, the same phase as the reference signal at point A, even if the path length varies. Providing the distribution signal frequency is an even submultiple of the reference signal frequency required for conjugation, the phase can be distributed accurately over various lengths of cable without ambiguity.

The method for distributing the phase reference signal over the large area of the SPS array is illustrated in figure III-20. The system is referred to as the master slave technique (ref. 28) and consists of a master or reference signal source derived from the pilot signal receiver located at the center of the SPS array. The phase of this signal is then distributed (using the returnable timing delay compensation technique described previously) to a group of secondary or slave oscillators and serves as the phase reference signal for the phase control centers at the next level of the distribution network. These secondary or slave oscillators then serve as the master oscillators for the second group of oscillators (slaves) by providing the same reference phase as the original reference (master oscillator). The phase of the master is thus promulgated throughout the distribution network or tree to each of the 101 552 radiating power modules of the SPS system. The exact configuration for the distribution tree is not completely defined; however, the configuration recommended in the Boeing Aerospace Company SPS definition study (ref. 29) has been incorporated as the existing baseline to establish performance characteristics for various amounts of phase error buildup in each branch of the tree. This distribution tree incorporates a 20-way power division at the first level and a 19-way power division at levels 2 and 3, with a variable degree of power division at the fourth or final level to match the network to the number of power modules in each subarray.

Once a constant reference phase is distributed to each radiating power module, a method for recovery and conjugation of the received pilot signal's phase must be employed. Figure III-21 is a block diagram of the power transponder, which includes the pilot signal receiver, the phase conjugation electronics, and the power amplifier with its phase control loop. As mentioned previously, a uniquely coded pilot signal has been developed. The signal design consists of nonreturn-to-zero command data (optional), modulo two added with a split-phase, direct-sequence pseudonoise code, which then biphase modulates the rf pilot carrier signal of 2450 megahertz.

The one-sided power spectral density of the modulated pilot signal is shown in figure III-22. The split-phase format of the PN sequence results in a spectral distribution of energy which peaks either side of the carrier at approximately $3R/4$, where R is the PN code chip rate. Proper selection of R will thus enable rf filtering at the power transponder receiver to provide isolation between the desired pilot signal and the unwanted power signal present at the pilot carrier frequency f_p of 2450 megahertz.
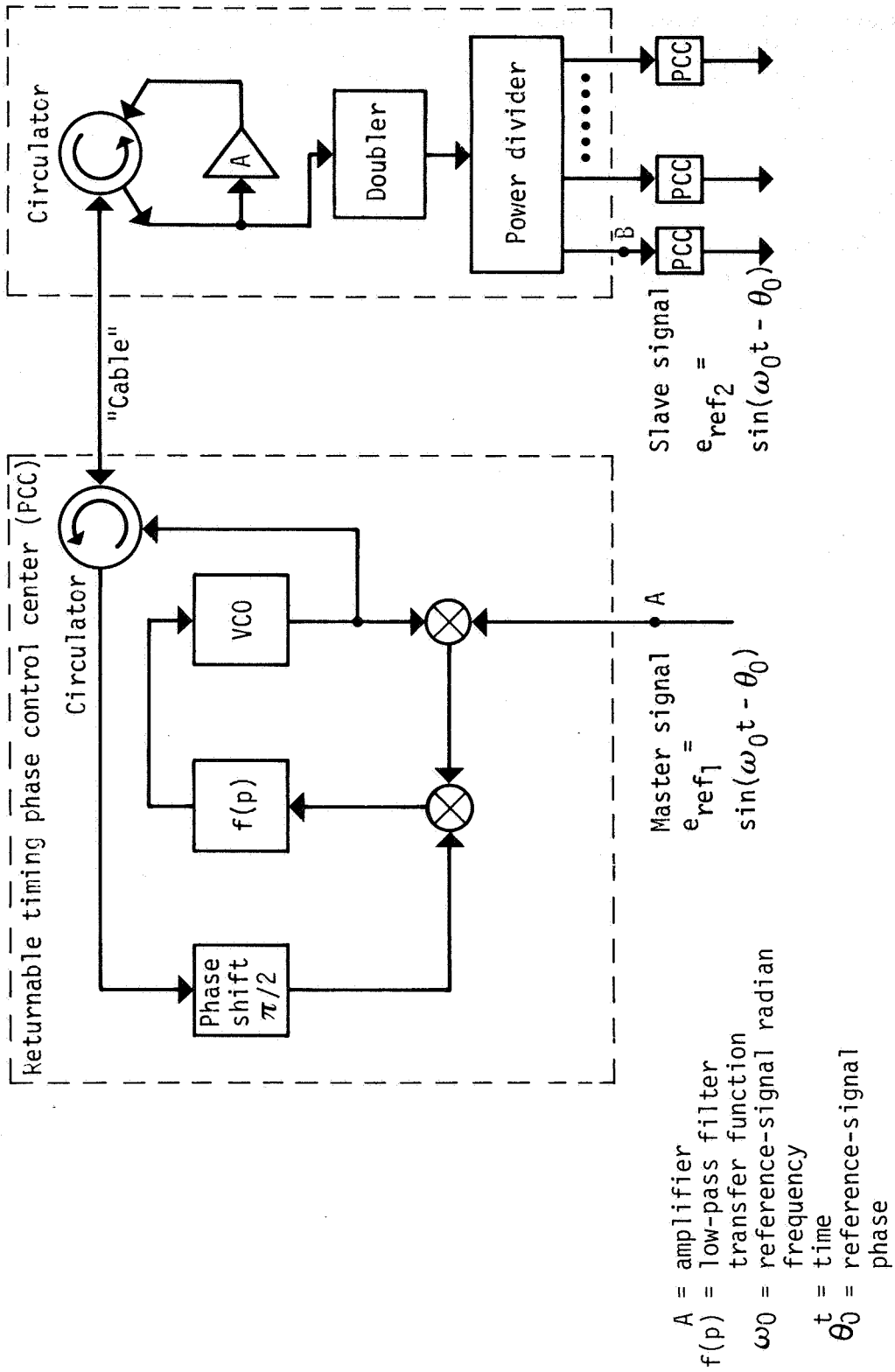
Figure III-19.- Master slave returnable timing system.

Master signal
$e_{ref_1} =$
$\sin(\omega_0 t - \theta_0)$

Slave signal
$e_{ref_2} =$
$\sin(\omega_0 t - \theta_0)$

A   = amplifier
f(p) = low-pass filter
       transfer function
ω_0 = reference-signal radian
       frequency
t   = time
θ_0 = reference-signal
       phase
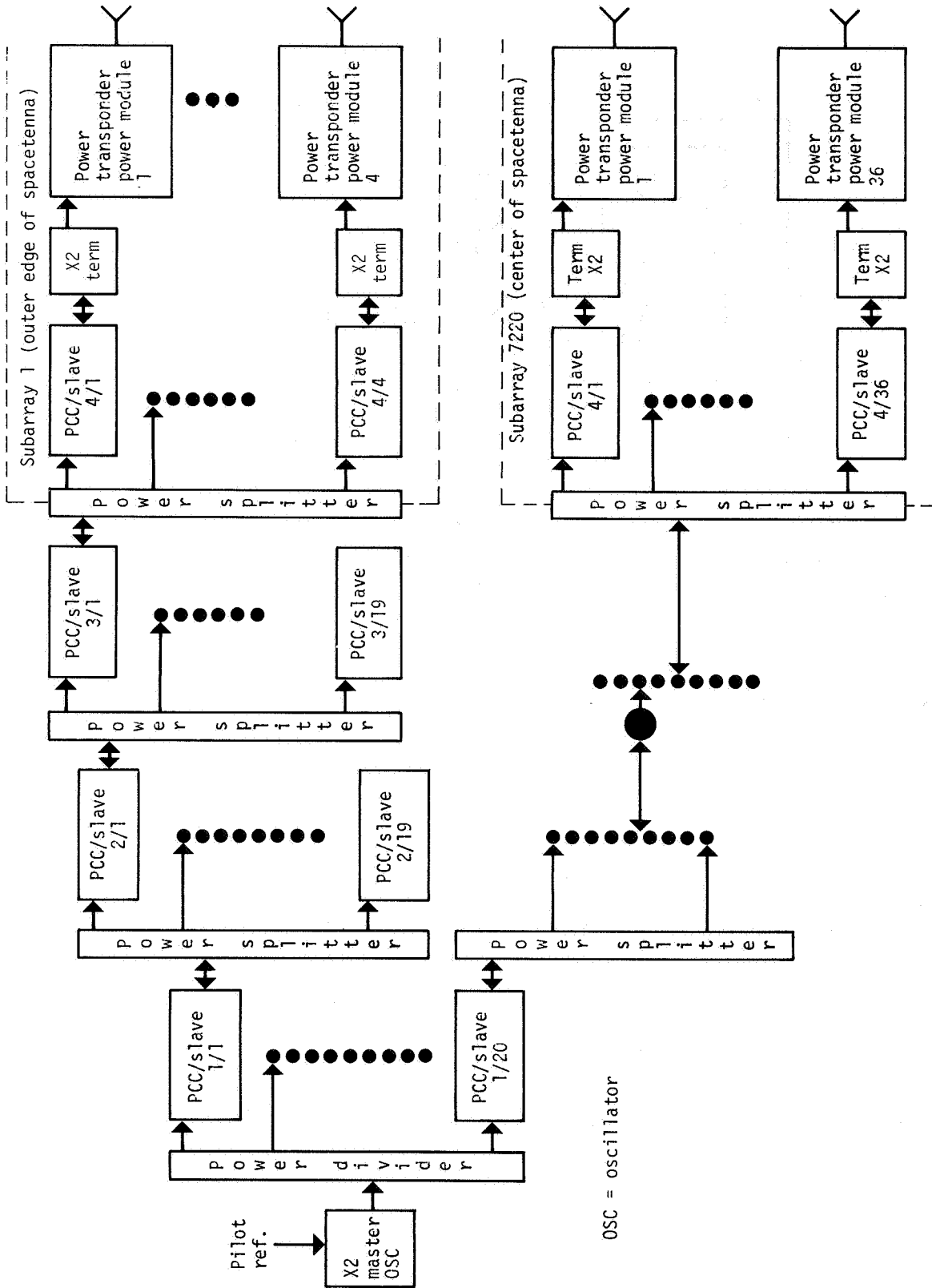
Figure III-20.— MSRTS distribution network.

71
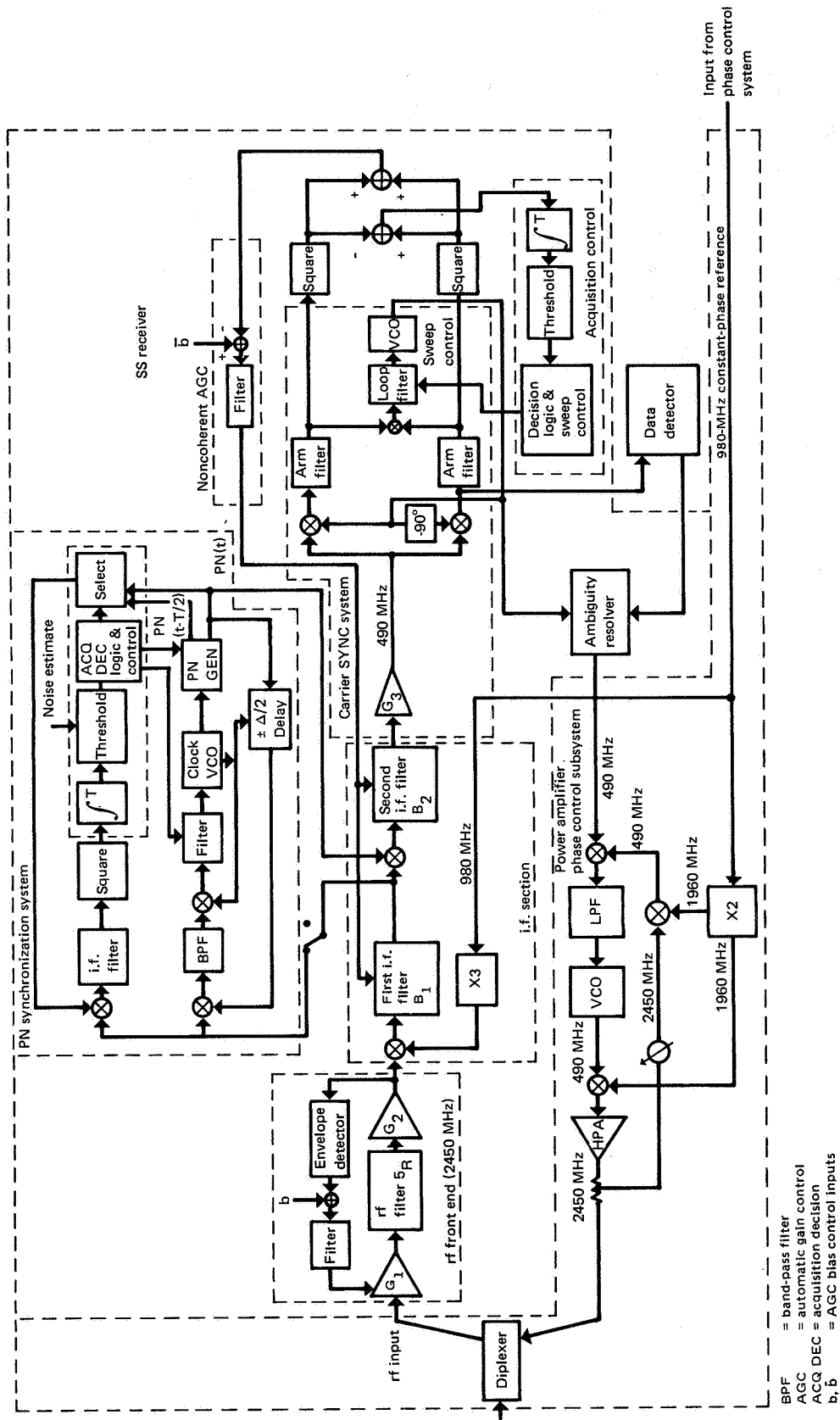
Figure III-21.- SPS transponder functional block diagram.
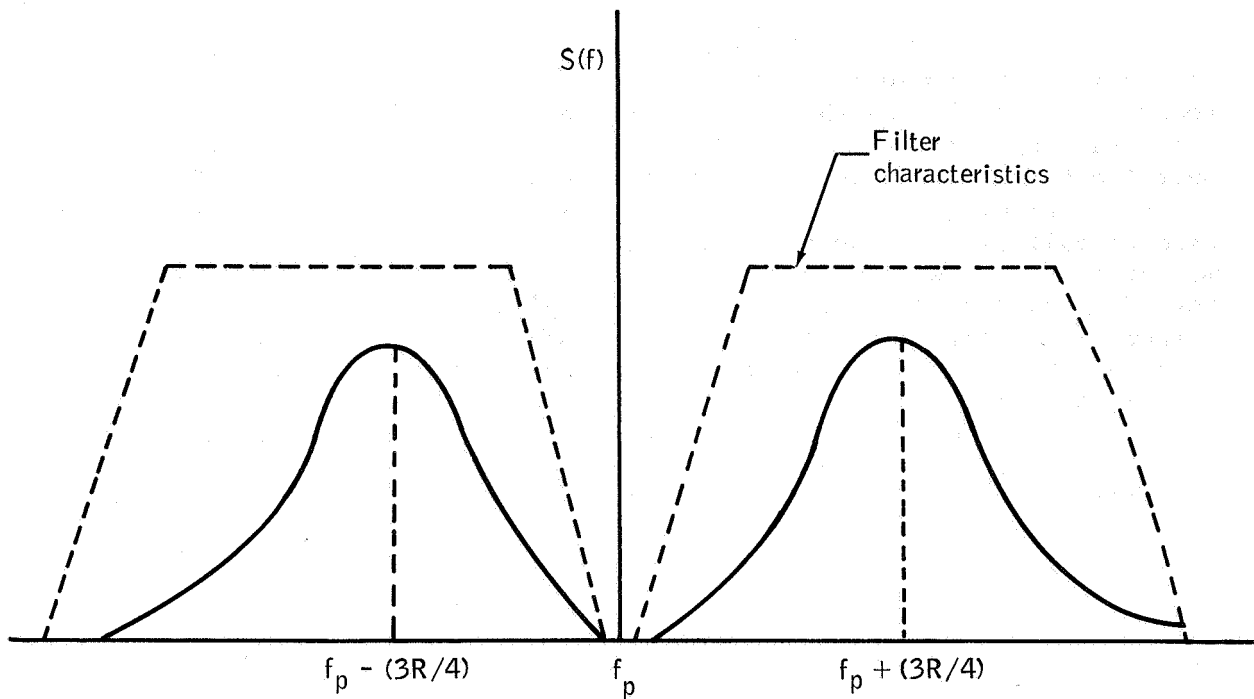
S(f) = power spectrum

Figure III-22.- One-sided pilot-signal power spectrum.

Within the power transponder, the PN spread signal is converted to an intermediate frequency, and the PN code is acquired and tracked (noncoherently) by the PN synchronization system (PNSS) using a tau-dither code-tracking loop with a microprocessor-controlled acquisition algorithm. Once the PN code is acquired, the local code generator in the PNSS begins accurately tracking the pilot signal's code phase. This local code is then used to multiply the incoming modulated i.f. pilot signal, effectively removing the PN code modulation or despreading the pilot signal. After despreading occurs, the pilot signal is coupled to the carrier synchronization system. The carrier synchronization is achieved by reconstruction of the phantom carrier (assuming command data are phase-shift keying the pilot carrier signal) using a Costas loop. The carrier loop voltage-controlled oscillator (VCO) is multiplied and serves as the first local oscillator signal resulting in a long-loop phase-modulation receiver configuration. The carrier loop acquisition will be automatic, and the potential phase ambiguity associated with the Costas loop detection process will be resolved by establishing a required polarity for the command data format. Once the correct unambiguous phase has been established, the carrier loop VCO signal is mixed with the reference signal provided by the phase distribution system. In the mixing process, the lower sideband term is used to convert the sign of the reconstructed pilot signal's phase. This process is referred to as conjugation of the pilot phase and, after multiplication by the appropriate factor, serves as the input signal phase reference to the power amplifier phase control subsystem.

The power amplifier phase control loop is used to compensate for phase-delay variations between power tubes and to ensure that the signal at the farthest monitorable output point is kept in phase with the conjugated pilot signal. This control is accomplished by using a sample of the PA rf output for phase locking of the power amplifier source oscillator to the pilot signal conjugated phase reference provided by the carrier synchronization system. The PA output is then coupled through the rf filter into the slotted-waveguide antenna feed sticks. From this point on within the waveguide sticks of the slotted array power module, there is no active phase control. The spacing of each slot and the surface accuracy of the power module radiating elements must be maintained mechanically by ensuring a rigid structure which will not deform appreciably with environmental variables.

The required and projected performance of this baseline phase control system, relating to effects of phase errors resulting from the various subsystem elements, is discussed in the following subsection.

b. Reference System Performance Evaluation

From the system engineering viewpoint, the SPS transmission system which incorporates retrodirectivity is depicted in figure III-23. As seen from the figure, the system consists of three major subsystem elements.

(1) The reference phase distribution system (MSRTS)

74

Solar power

```
              Solar power
              to electrical
           power conversion
                system
```

Phased-array
spacetenna

Phase conjugation
reference signal

dc power

```
  Reference phase          Beam-forming and
   distribution            microwave power-
     system                generating system
```

Microwave
power

"Pilot"
signal

Phase control system
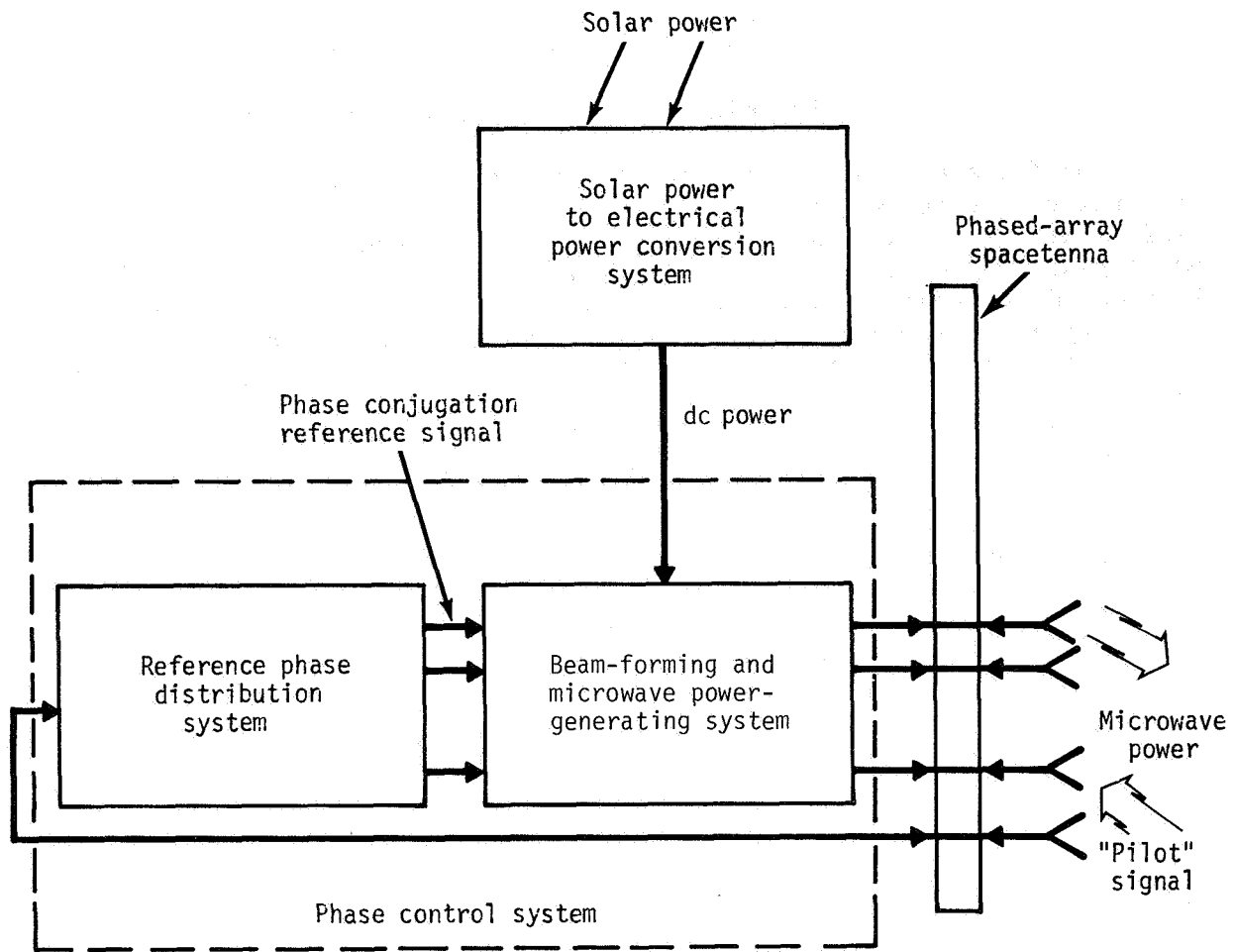
Figure III-23.- SPS transmission system (phase conjugation).

(2) The beam-forming and microwave power-generating system

(3) The solar power to electrical power conversion system

In the performance evaluation task, the phase distribution system is modeled
in terms of its phase error buildup and randomness due to both electrical im-
perfections in the system and mechanical misalinement and jitter of the power
module/subarray configurations. The beam-forming and power-generating system
is modeled in terms of interference and ionospheric effects on the received
pilot signal, transponder phase errors (jitter), and PA phase variations and
phase noise characteristics. The solar power to electrical power conversion
system only enters into the microwave performance evaluation in terms of the
dc power provided to the PA's and the random error introduced by the power
distribution system across the 1-kilometer spacetenna array.

(1) Reference phase distribution system – The reference
phase distribution system has been implemented on a four-level tree structure
using the MSRTS technique to electronically compensate for phase shifts due
to path-length variations from the spacetenna center to each power module.
The detailed mathematical model and analysis is provided in reference 23.

(2) Power transponder and pilot signal design assessment –
In addition to distributing the constant-phase reference signal over the
spacetenna, a method for recovering the phase of the received pilot signal
is required. The functional diagram of the SPS power transponder was shown
previously in figure III-21. The power transponder includes the pilot signal
receiver, phase conjugation electronics, and the high-power amplifier phase
control system.

In the mechanization of the SPS power transponders,
two receiver "types" will be required; however, most of the hardware will be
common between two receivers. One receiver, the pilot spread-spectrum (SS)
receiver, is located at the center of the spacetenna or the reference sub-
array. It serves two major functions.

(a) Acquires the SS code and the rf carrier and
demodulates the command signal

(b) Provides the main input signal to the reference
phase distribution system

The second receiver type is located at each power mod-
ule. Its main purpose is to phase conjugate the received pilot signal and
transpond power by way of the j-th spacetenna element, where $j = 1, 2, \ldots,$
101 552. In the case that data transmitting capability is not implemented
for the pilot signal, the Costas loop can be replaced by a CW loop to avoid
the need for provisions to resolve the associated Costas-loop-induced phase
ambiguity.

One of the key technical problem areas concerning the
design and specification for the SPS power transponder is RFI. The inter-
ferences are generated by different mechanisms.

76

(a) Self-jamming due to pre-power-beam package from
     the diplexer/circulator

(b) Mutual coupling from adjacent transponders

(c) Thermal noise

(d) Interference from adjacent SPS's

        The signal and interference spectrum at the input to
the SPS transponder is depicted in figure III-24. In general, the combined
phase noise interference from the power beams consists of a coherent and a
noncoherent term. Depending on the mechanization of the antenna structure
and pilot antenna characteristics, these terms are associated with gains K_1
and K_2. Note that the phase noise interferences are concentrated around the
carrier frequency f_o (2450 megahertz). Conversely, the uplink pilot signal
has little or no power around this frequency. Its power spectrum peaks at
$f_o \pm 0.75R_c$, with a value directly proportional to the product of the received
power P_r and the PN chip rate R_c and inversely proportional to the PN code
length M. The parameters R_c and M are related to the processing gain of
the PN spread signal and determine its interference-suppression capability.
The rf filter characteristic is estimated on the basis of theoretical wave-
guide antenna bandwidths ranging from 15 to 45 megahertz. The goal is to
optimally select (a) the pilot signal so that it passes the rf filter with
negligible distortions and (b) a practical notch filter that rejects most of
the phase noise interference. When this procedure is followed, one can be
assured that the reconstructed pilot signal phase after the synchronization
loops is within a tolerable error for the retrodirective scheme.

        Analytical models developed for the SPS transponder
tracking loop system include the following.

(a) The PN despreader loop

(b) The pilot phase tracking (Costas) loop

(c) The PA phase control loop

        The model also includes the noise processes introduced
by the phase reference receiver that feeds the phase distribution system and
various other sources of potential phase noise interference which affect the
performance of the individual loops. In particular, a model of the phase
noise profile of the klystron amplifier is introduced to evaluate important
implications on the PA noise control loop design.

        Using the analytical model for evaluating the overall
performance of the SPS transponder, the phase fluctuations at the output of
the transponder have been shown to be directly related to the various noise
processes through the closed-loop transfer functions of the tracking loops.
These noise processes are either generated externally to the transponder cir-
cuitry, such as ionospheric disturbances and transmit frequency instability,

77
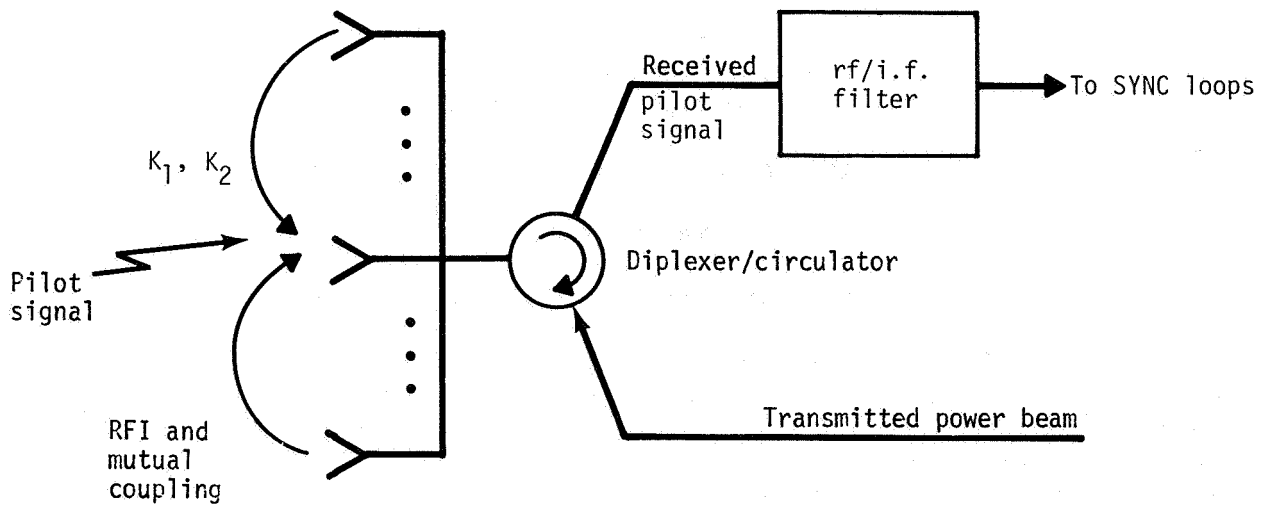
(a) SPS power transponder front end (conceptual).
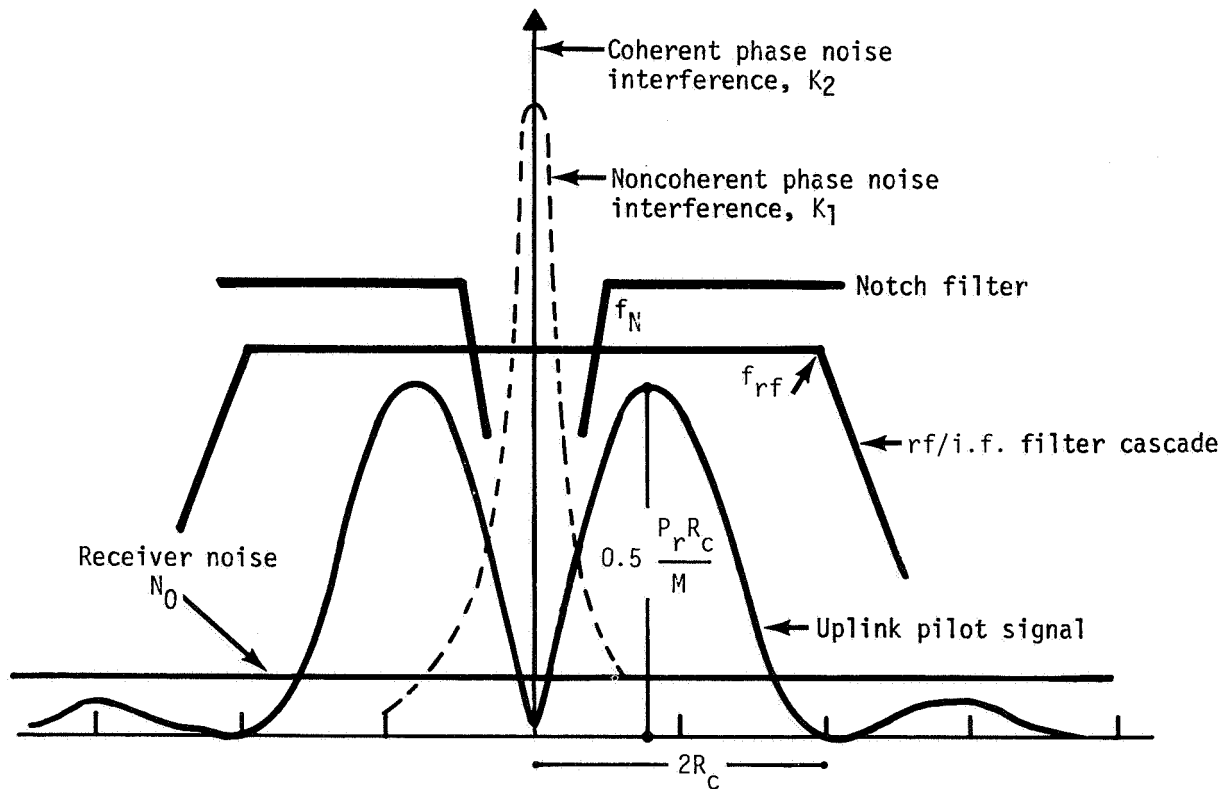
(b) Signal and noise spectrum.

Figure III-24.- Signal and interference spectrum into SPS transponder.

or generated internally, such as receiver thermal noise, power beam interference, data distortions, VCO/mixer phase noise, and phase variations introduced by the reference distribution tree.

The preliminary specifications for the pilot signal and transponder design parameters can be summarized as follows.

(a) EIRP - 93.3 decibels referenced to 1 watt

(b) PN chip rate - 10 megahertz

(c) rf filter 3-decibel cutoff frequency - 20 megahertz

(d) Notch filter 3-decibel cutoff frequency - 1 megahertz

(e) Notch filter dc attenuation - 60 decibels

(f) PN code period - 1 millisecond

(g) Costas loop phase jitter - $0.1°$ for 10-hertz loop bandwidth

(h) Channel Doppler - negligible

(i) Klystron phase control loop bandwidth - 10 kilohertz

The preliminary results are generated using a tentative model of RFI with coupling coefficients $K_1 = K_2 = 20$ decibels. Explicitly, it was assumed that the transponder input encounters a CW interference with power equal to 0.65 kilowatt and a phase noise ($1/f$ type) interference at about 20 watts. Of course, when these values are changed significantly, the predictions have to be modified. For this reason, the development and verification of an acceptable model for the effects of mutual coupling on the phased-array antenna based on the "near field" theory is extremely important and essential in the near future.

A maximum-length linear-feedback shift-register sequence (i.e., m sequences generated by a 12-stage shift register with a period equal to 4095) is recommended as the spread-spectrum code. In the code-division multiple-access situation, the theoretical optimal solution is to use the set of 64 bent-function sequences of period 4095, enabling as many as 4095 simultaneous satellite operations of the SPS network. The bent sequences are guaranteed to be balanced, have long linear span, and are easy to initialize. However, depending on the code partial correlation requirement and the number of satellites in the network, the set of maximum-length sequences of period 4095, although suboptimal, may suffice.

Currently, results indicate that it is feasible to hold the antenna array phase error to less than $1°$ per power module for the

79

type of disturbances modeled. However, some irreducible error sources are not considered herein and their effects remain to be seen. They include reference phase distribution errors and differential delays in the rf path.

c. End-to-End System Performance Evaluation

Because of the complicated nature of the problem of evaluating performance of the SPS phase control system and because of the multiplicity and interaction of the parameters as they relate to subsystem interfaces, the methods of analysis and computer simulation (analytical simulation) have been combined to yield a performance evaluation of the SPS system. The result is "SOLARSIM," a computer simulation program package developed by LinCom Corporation that enables a parametric evaluation of critical performance issues. The current capabilities of SOLARSIM are highlighted in table III-9. The SOLARSIM program and its various subroutines have been exercised in great detail to provide system engineering trade-offs and design data for the reference system. For example, a typical power pattern is depicted in figure III-25. The following discussion is focused on the key results obtained thus far.

(1) Definition of power-transfer efficiency - Power-transfer efficiency is defined as power received by the 10-kilometer-diameter rectenna divided by total power radiated by the spacetenna. The idea is clarified in figure III-26. The power-transfer efficiency can be redefined as power output at terminals A and B divided by power output at terminals C and D. This definition is convenient because the multiplying constants due to the propagation through the medium cancel out from the numerator and denominator. The total radiated power term (denominator) needs special attention since the average power pattern includes an "isotropic" term which is computationally difficult to account for if the individual (transponder) radiation phasors are not perfectly alined in phase as a result of system jitters and imperfections. The current analytical approach alleviates this problem and is superior to the widely used Monte Carlo technique in this respect.

(2) Effects of system jitters and imperfections on power-transfer efficiency - The system jitters and imperfections can be grouped into two main classes: (a) jitters due to spacetenna electrical components (which include such effects as the amplitude jitter of the feed currents to the radiating elements of the spacetenna and the phase jitters of the feed currents originated from the phase control system) and (b) jitters due to the mechanical imperfections of the spacetenna (which include subarray tilt (mechanical pointing error), tilt jitters, and location jitters). The location jitters include the transmitting and receiving elements and arise from the displacement of the radiating elements. The basis for modeling these mechanical imperfections is illustrated in figure III-27.

(3) Effects of system imperfections on SPS efficiency - The effects of the various system imperfections on the SPS power-transfer efficiency obtained through SOLARSIM are summarized in figures III-28 to III-30. In figure III-28, the power-transfer efficiency is plotted against the total phase error produced by the SPS phase control system. For a mechanically perfect system with no location jitters and no mechanical pointing

80

TABLE III-9.- SOLARSIM SUBROUTINE PACKAGE CAPABILITIES

Subroutine name	Purpose
Pointing error	Evaluation of the effect of phase error introduced by the phase distribution tree on pointing error
VARSUM	Evaluation of the effects of subarray tilts, location jitters, and phase distribution system error on spacetenna gain
Power pattern	Evaluation of the power pattern as a function of subarray tilts, current-amplitude jitter, phase jitters, and location jitters
Power-transfer efficiency	Evaluation of power-transfer efficiency or power pattern as a function of subarray tilts, current-amplitude jitter, phase jitters, and location jitters
SIDR	Evaluation of the reconstructed pilot phase error (rms) as a function of pilot signal design parameters, link budget, rf/notch filter characteristics, and Costas loop bandwidth
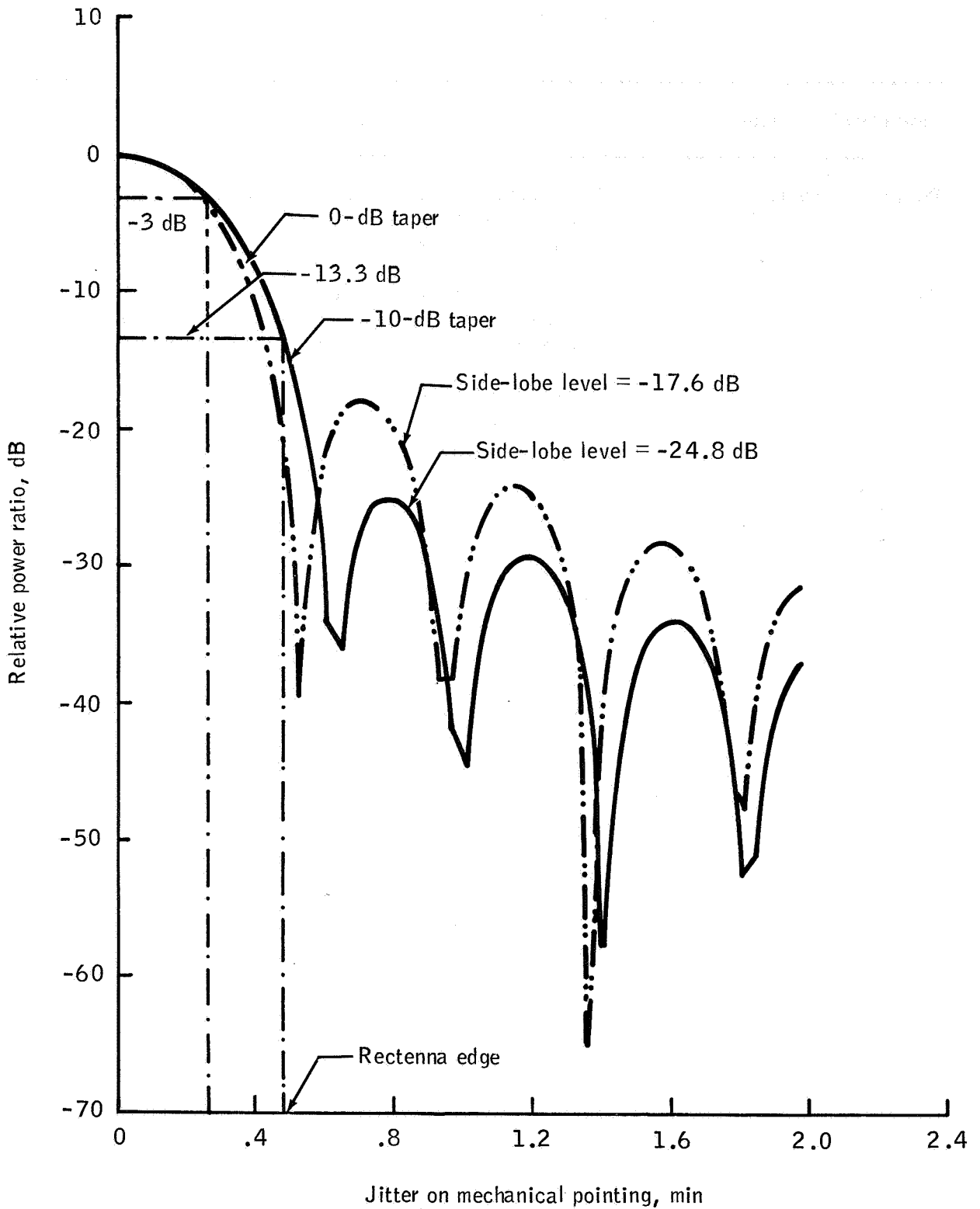
Figure III-25.- Power pattern for 5° rms equivalent rf phase error in each level of the four-level phase distribution tree.
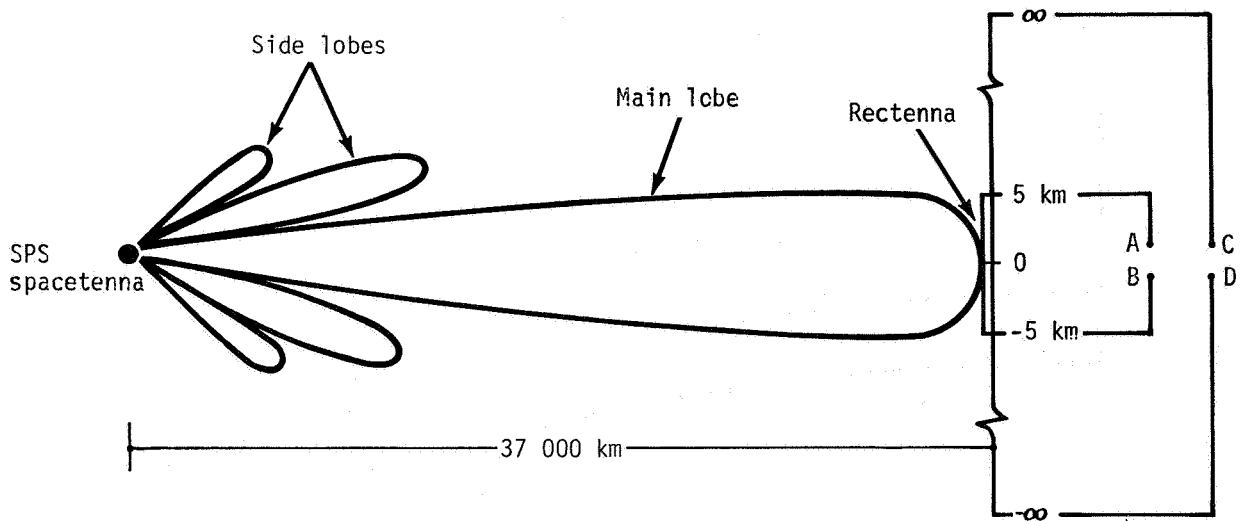
Figure III-26.- Geometry of the power pattern.
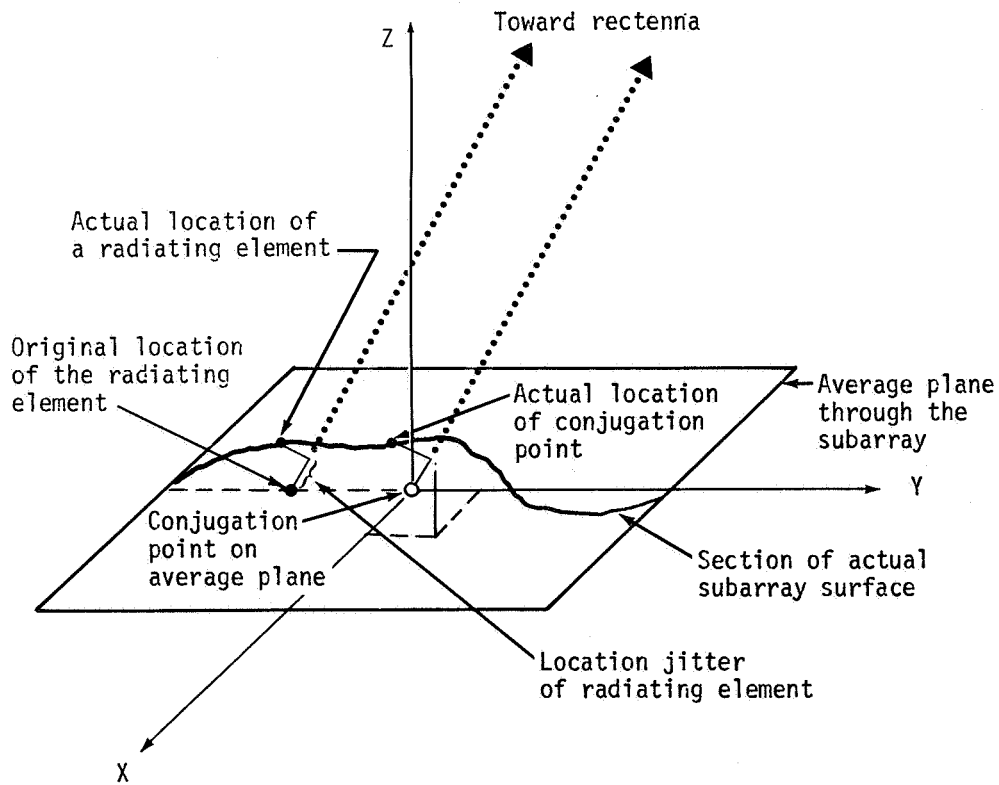
Figure III-27.- Location jitters of radiating and receiving elements.

83
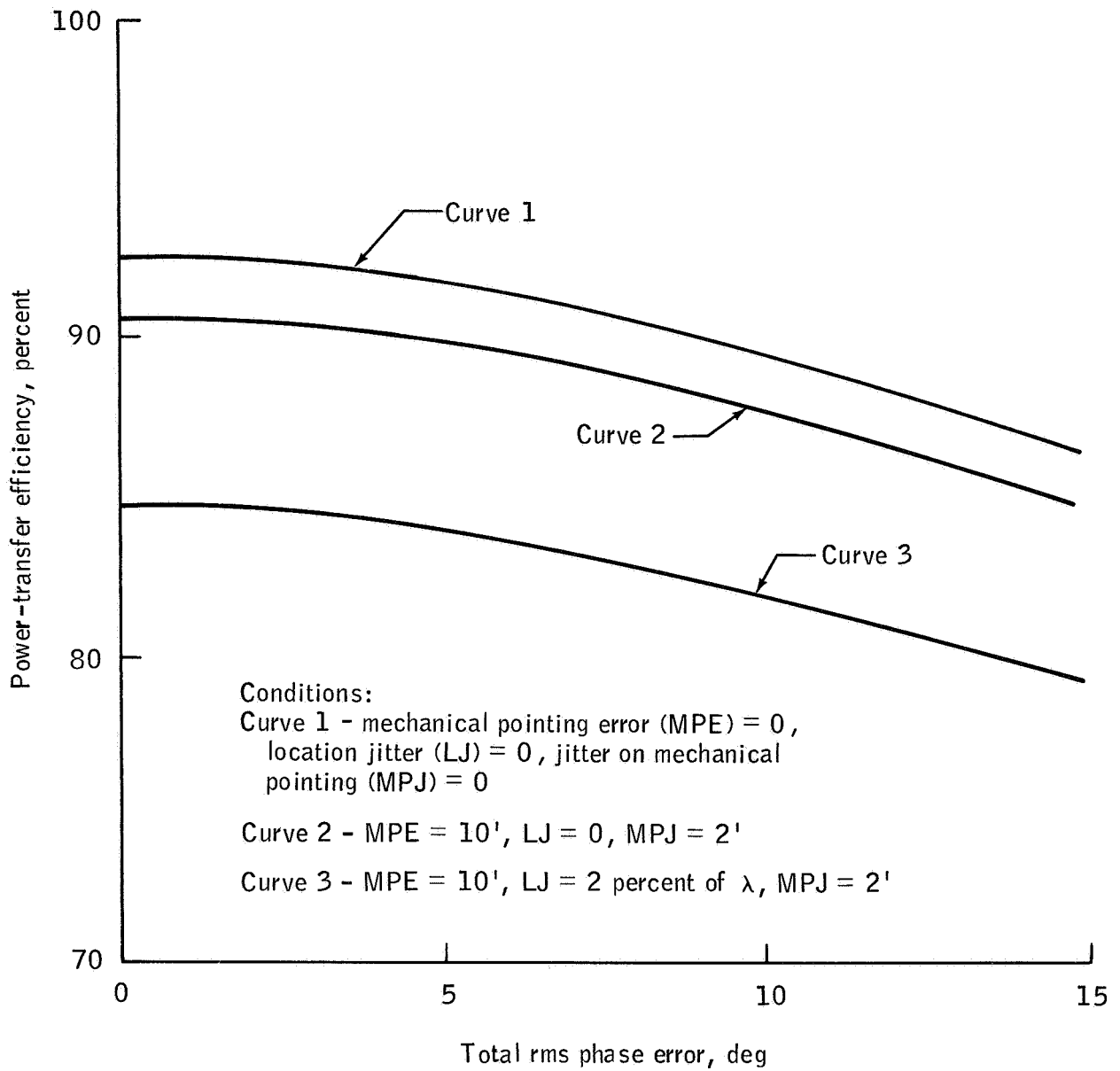
Figure III-28.- Curves of power-transfer efficiency as a function of total rms phase error for 10-kilometer-diameter rectenna with current taper of 10 decibels.
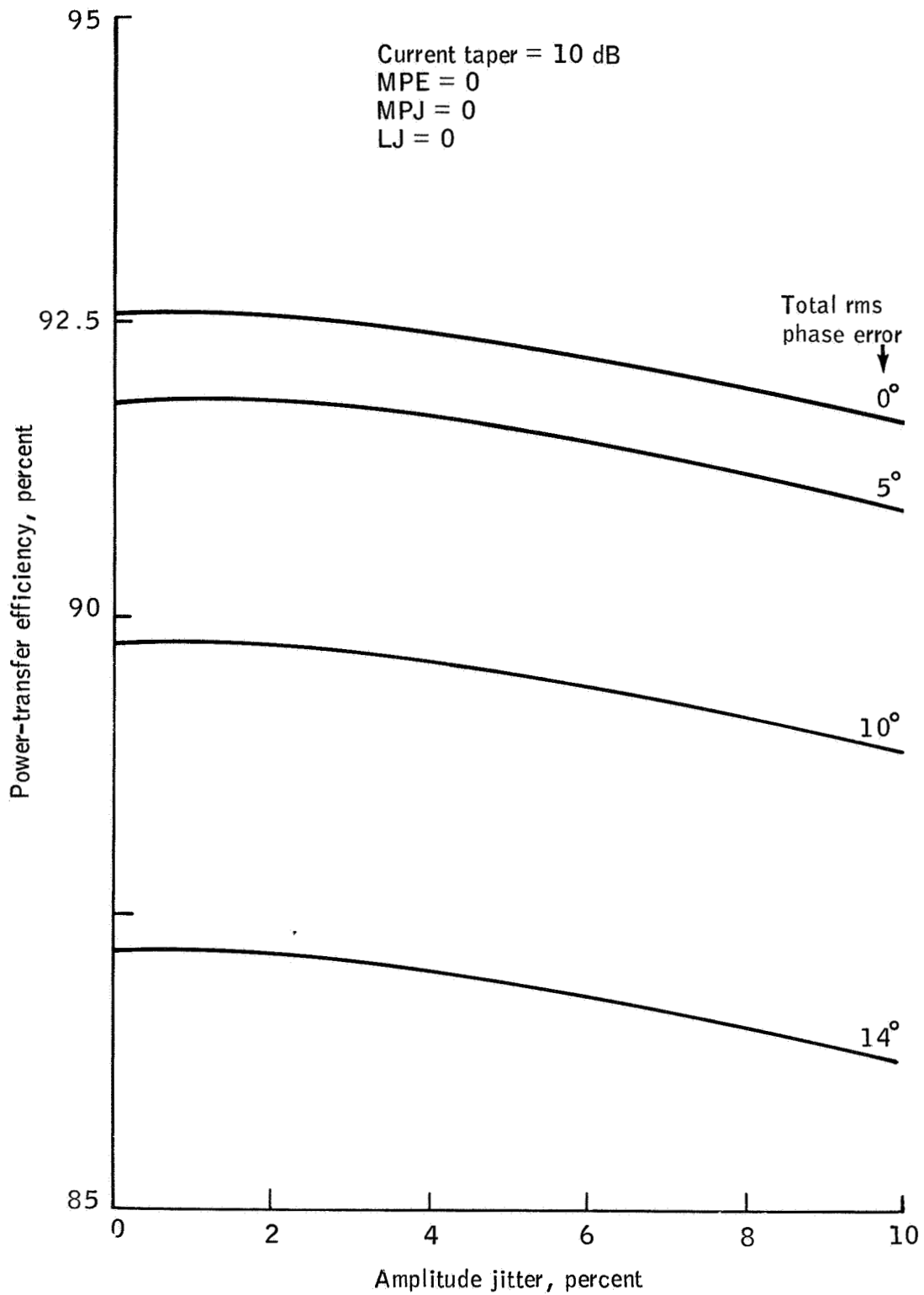
Figure III-29.- Effect of amplitude jitter on SPS power-transfer efficiency (10-kilometer-diameter rectenna).
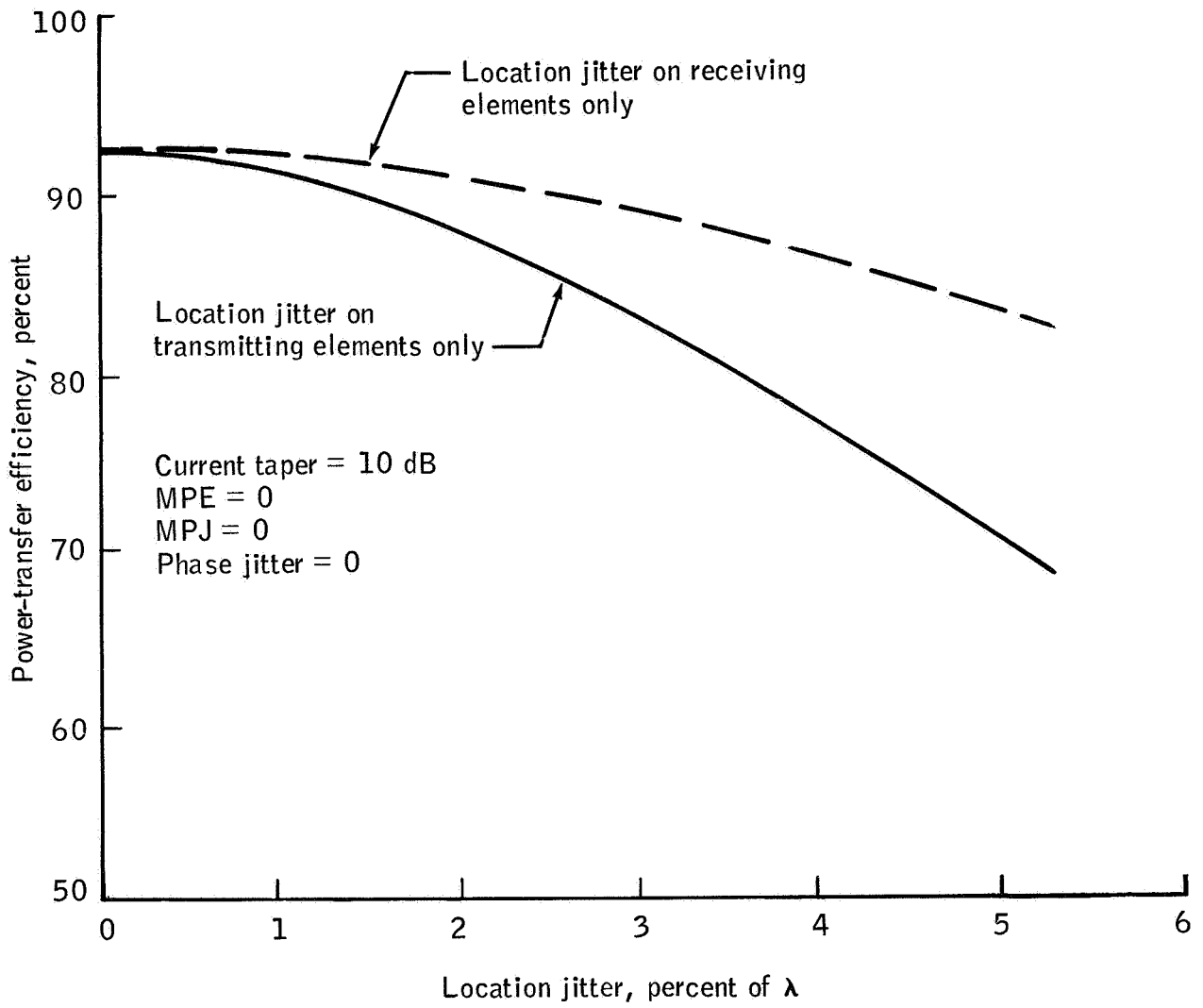
Figure III-30.- Effect of location jitters on the otherwise perfect SPS (10-kilometer-diameter rectenna).

errors or jitters (curve 1), the total rms phase error is restricted to less than 10° at rf to yield greater than 90 percent efficiency. Curve 2 depicts the influence of the mechanical pointing error (assumed to be 10' with a jitter of 2') when the location jitters are absent. As can be seen from the figure, for a total phase error of 10°, the power-transfer efficiency of the spacetenna decreases to 87.3 percent. When the location jitter of 2 percent of λ, where $\lambda = 360°$, is added for the transmitting and receiving elements, the power-transfer efficiency decreases to 82.0 percent. (See curve 3.) In order to achieve the efficiency required for economical operation (while maintaining hardware within reasonable state-of-the-art technology), it is expected that the SPS system will operate in the region between curves 1 and 2. In this case, the power-transfer efficiency will be less than 90 percent for a typical rms phase error of 10°.

The effect of the current-amplitude jitter is shown in figure III-29 for a mechanically perfect system. As can be seen from the figure, for an amplitude jitter of 5 percent, the power-transfer efficiency of the mechanically perfect spacetenna with the current-phase jitter of 0° is 92.3 percent. This value drops to 91.63 percent for the total phase error of 5° and to 89.57 percent for a total phase error of 10°. One can conclude that the power-transfer efficiency is relatively insensitive to amplitude jitters.

The effects of location jitters on the power-transfer efficiency of an otherwise perfect SPS are illustrated in figure III-30. As can be seen from the figure, the degradation of efficiency is severe; for a location jitter on each radiating element of 2 percent of λ, the power-transfer efficiency drops to 88.3 percent. As a comparison, curve 1 in figure III-28 reveals that for an rms phase error of 7° (2 percent of $\lambda = 7.2°$), the efficiency decreases to 91.2 percent. Thus, the effect produced by location jitters on the receiving (conjugating) elements is comparable to the effect produced by the phase error because both these effects enter into the transmission system at the same physical point; i.e., the center of the subarray. On the other hand, power-transfer efficiency is rather sensitive to the location jitter on the radiating elements.

3. ALTERNATE PHASE CONTROL CONCEPTS

As noted, several alternate concepts have been briefly evaluated. Two approaches for ground-based phase control systems are still under active investigation. These systems are the Novar interferometer-based phase control technique and the LinCom coherent multiple-tone (CMT) technique. Each of these approaches is briefly reviewed in this section. Detailed information concerning the system characteristics and expected performance can be found in references 7 and 8.

a. Interferometer-Based Phase Control System

Novar Electronics Corporation has evaluated an interferometer-based phase control system (ref. 8). This approach, which is called interferometric phase control (IPC), has three significant characteristics that differentiate it from the reference system retrodirective approach.

(1) Interferometric phase control is a ground-based closed-loop system - Unlike the retrodirective approach, the phase correction information is obtained on Earth by measuring the transmission of the spacetenna power modules and comparing them against a reference.

(2) The spacetenna's power modules are calibrated sequentially - A signal from a reference transmitter near the center of the spacetenna is phase compared with a sequential calibration transmission from each of the power modules.

(3) During normal power transmission, the frequency of each power module is shifted slightly for phase calibration - Maintenance of a properly focused and pointed power beam can be accomplished concurrently with the normal transmission of power from the SPS by using frequencies for calibration that are different from the power beam frequency. A description of the system and its operating features follows.

On or near the rectenna site, a phase-measurement antenna receives the transmission from the spacetenna reference transmitter and the particular power module being phase tuned (calibrated). Analysis of these signals provides sufficient information to generate a phase error correction term, which is transmitted to the onboard phase control circuitry (shown in fig. III-31) of the power module undergoing calibration.

Simultaneously with the transmission of the power beam, coherent signals at three different frequencies are transmitted from the spacetenna. Two of these signals are transmitted from the reference transmitter, which is located near the center of the spacetenna, and one is transmitted from the power module being phase tuned, as shown in figure III-32. The two signals transmitted from the reference transmitter are s_1 and s_{r1}, and the signal transmitted by the power module being phase tuned is s_2. The frequency of s_1 is midway between that of s_{r1} and s_2 so that the beat frequency of s_1 and s_2 is the same as that of s_1 and s_{r1}.

At the rectenna, simple mixing and filtering circuitry detects two different frequency signals. One signal is due to s_1 and s_2. The other, which is a phase reference signal, is due to s_1 and s_{r1}. These two beat-frequency signals are then phase compared to determine the phase difference that results from z-axis deformations (deformations in a direction toward or away from the rectenna) in the power module being phase tuned plus biases in the SPS phase feed network. Certain components of the phase difference change with a change in frequency; others do not. Since the power module being phase tuned is transmitting at a frequency different from the power beam frequency, it is necessary to distinguish between these frequency-dependent and frequency-independent components to determine the phase adjustment that will be correct at the power beam frequency. This distinction is made by shifting s_{r1} and s_2 to a different set of frequencies, according

88
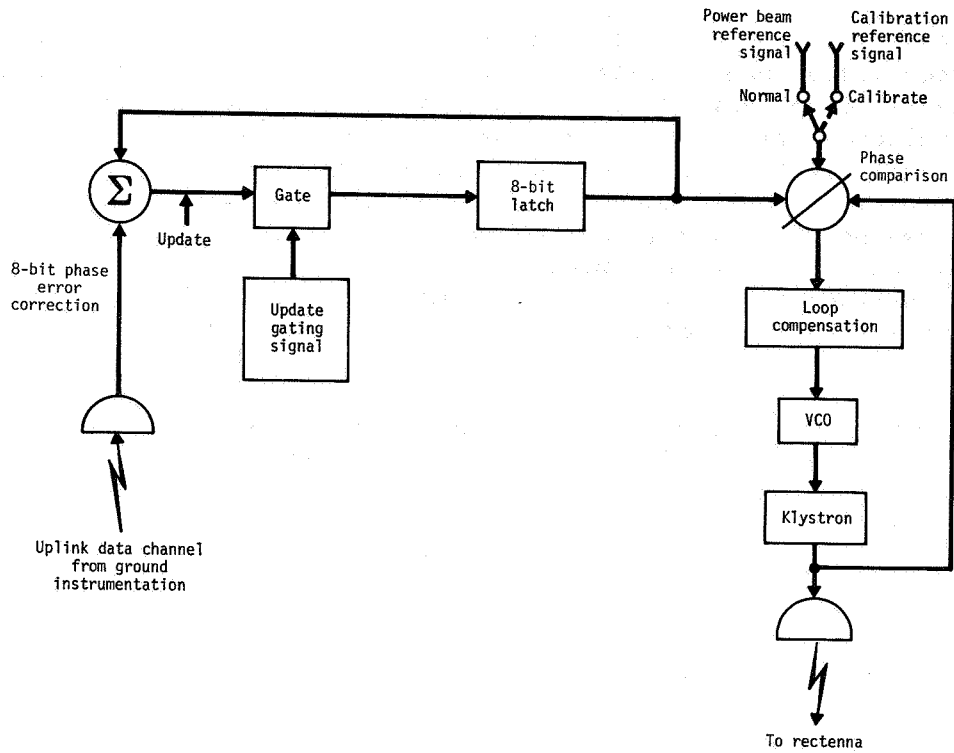
Figure III-31.- Power module phase control circuitry.
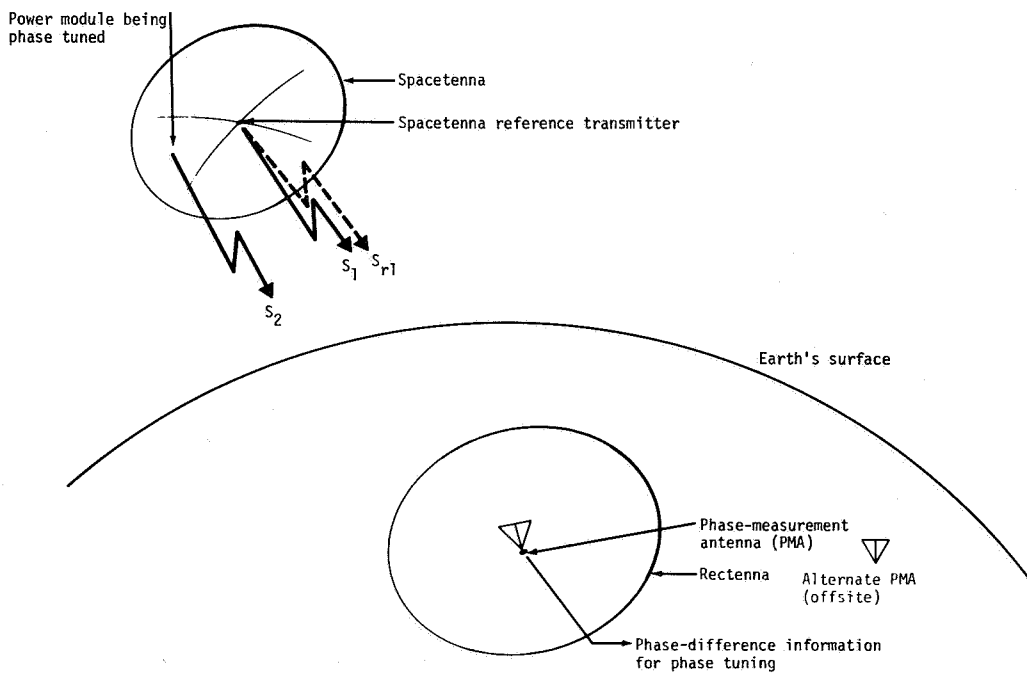
Figure III-32.- Interferometric phase control.

89

to a phase-ambiguity error-avoidance criterion, and making a second phase-difference measurement. These two phase-difference measurements are numerically adjusted by -2π, 0, or $+2\pi$ according to a second phase-ambiguity error-avoidance criterion. These two numerically adjusted phase differences provide sufficient information to calculate the phase error correction transmitted back to the SPS power module being phase tuned. This phase error correction can be made with an 8-bit binary word sent to the SPS by way of a data channel. An 8-bit accuracy produces a phase resolution of $360° \div 2^8 = 1.4°$, which is sufficient to give a power-beam-pointing resolution better than 140 meters at the rectenna.

A trade-off exists between satellite bandwidth requirements and the power module updating rate, which is limited by filter settling times. It is anticipated that the frequency separation among s_1, s_2, s_{rl}, and the power beam will be on the order of 1 megahertz. At these frequency separations, the update interval for an entire spacetenna could be on the order of a few seconds, which may be fast enough to correct for any changes that will occur at the spacetenna because of deformations, thermal effects, etc.

With the ground-based closed-loop interferometer phase control approach, ionospheric effects are limited to phase errors introduced into the space-to-Earth transmission path only. Although the phase-measurement antenna is shown to be at the center of the rectenna, it is not necessary that it be located there or even within the rectenna site. Offsite measurement has the advantage that the signals being phase tuned do not have to pass through an ionosphere that may be subjected to undetermined heating effects by the power beam.

An important advantage of interferometric phase control is its inherent capability to make use of statistical error reduction techniques to minimize any ionospheric effects. This capability includes time averaging and/or spatial averaging using several onsite and offsite phase-measurement antennas.

Although interferometric phase control was originally developed as a closed-loop, ground control approach for focusing and steering the power beam because of Novar's concern over possible ionospheric effects on the retrodirective pilot beam, it could provide a useful adjunct to the retrodirective system in mitigating phase biasing problems and in providing a backup system for use if atmospheric/ionospheric conditions preclude use of a retrodirective system. Pending completion of definitive studies of atmospheric/ionospheric effects on the retrodirective system, the simultaneous development of power beam control techniques using both the retrodirective approach and interferometric phase control should be pursued.

b. Coherent Multiple-Tone Ground-Based Phase Control System

The CMT ground-based phase control concept has been under study at LinCom as an alternative approach to the reference SPS phase control system. The details of the ground-based phase control system study are documented in reference 7.

The ground-based phase control system achieves beam forming by adjusting the phases of the individual transmitters onboard the SPS. The phase adjustments are controlled by ground commands. To specify the correct adjustment, the phases of the power beams from each individual transmitter arriving at the rectenna center must be measured and the appropriate corrections must be determined (to ensure that all power beams arrive at the same phase) and relayed to the SPS. The proposed scheme to be considered is sequential; i.e., the phase measurement is performed one at a time for each individual transmitter at approximately 1-second intervals. (Measurement time allocated is 10 microseconds for each transmitter.) The phase corrections are updated once every second. A 10-bit phase quantization for the corrections giving 0.35° resolution is envisioned. The uplink command data rate is on the order of 10 megabits/sec. The functional operation of the ground-based phase control concept is summarized in figure III-33. As evident from the figure, the key issues that need to be addressed are

(1) Measurement waveform design and selection

(2) Phase-measurement pilot reference design and selection

(3) Uplink-phase-correction command link format and design

(4) System synchronization techniques

In the basic two-tone measurement scheme, two side tones at $f_o \pm \Delta f$ are transmitted from the satellite to the ground receiver. A phantom carrier can be reconstructed from the side tones by passing the signal through a squaring circuit. The output will then have a CW component with frequency $2f_o$ and a phase component equal to $(\phi_1 + \phi_2)$, where ϕ_1 and ϕ_2 are the channel-induced phase shifts at $f_o + \Delta f$ and $f_o - \Delta f$, respectively. This phase shift is very close to double the one that would have occurred if the downlink signal were a single sinusoid at frequency f_o. If the $2f_o$ component is divided by 2, the average phase $(\phi_1 + \phi_2)/2$ is obtained. Unfortunately, the divide-by-2 circuit results in a 0°-180° phase ambiguity.

A four-tone measurement scheme, which is a simple modification of the two-tone scheme, has been developed. Basically, frequencies at $f_o \pm 2\Delta f$ are used for phase error measurement, which introduces ambiguity. Then, frequencies at $f_o \pm \Delta f$ are used for ambiguity resolution. A detailed discussion of the ambiguity-resolving process is given in reference 7.

The implementation of the ground-based phase control concept is determined by the phase control waveform design employed. Based on the four-tone waveform selection, functional subsystems to implement the ground-based phase control concept have been identified and are shown in block diagram form in figure III-34.

The ground-based system envisioned employs satellite-based frequency/timing reference with an i.f. of 490 megahertz. A four-tone measurement scheme using frequencies at 2450 ± 9.57 and 2450 ± 19.14 megahertz is
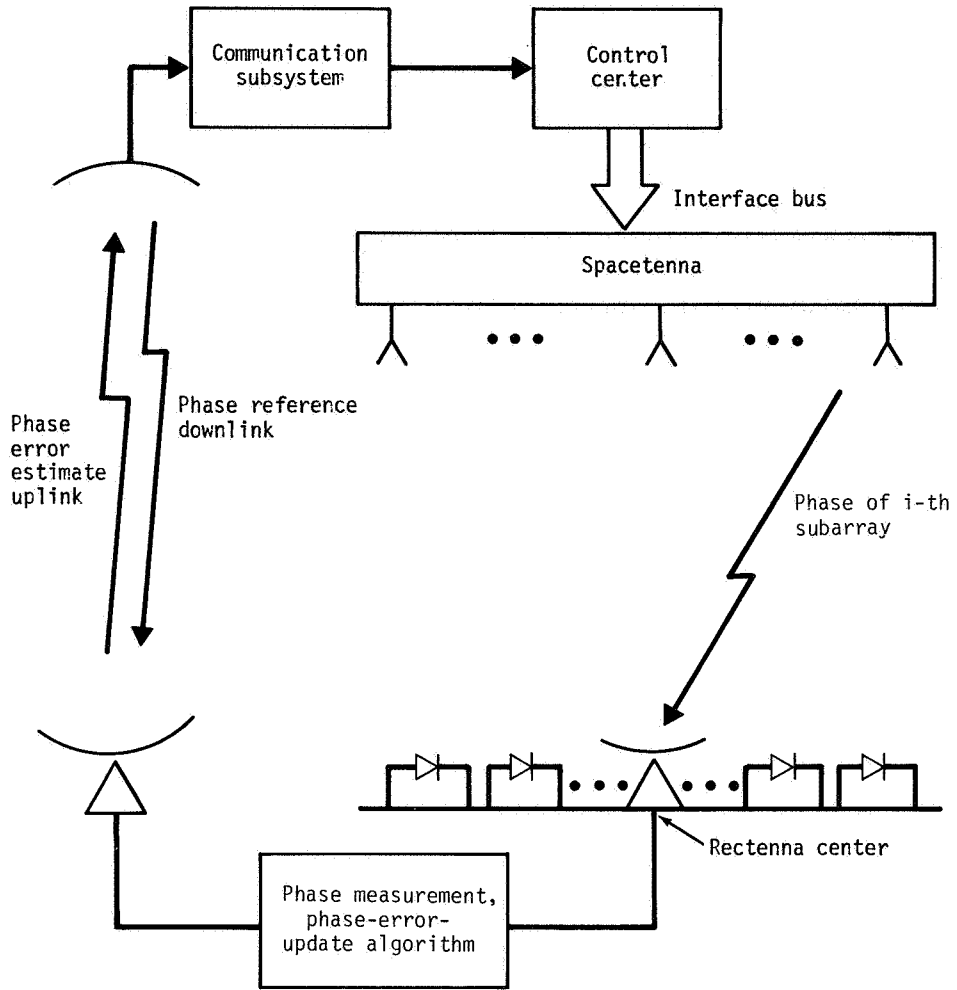
Figure III-33.- Ground-based phase control system concept with major functional blocks.
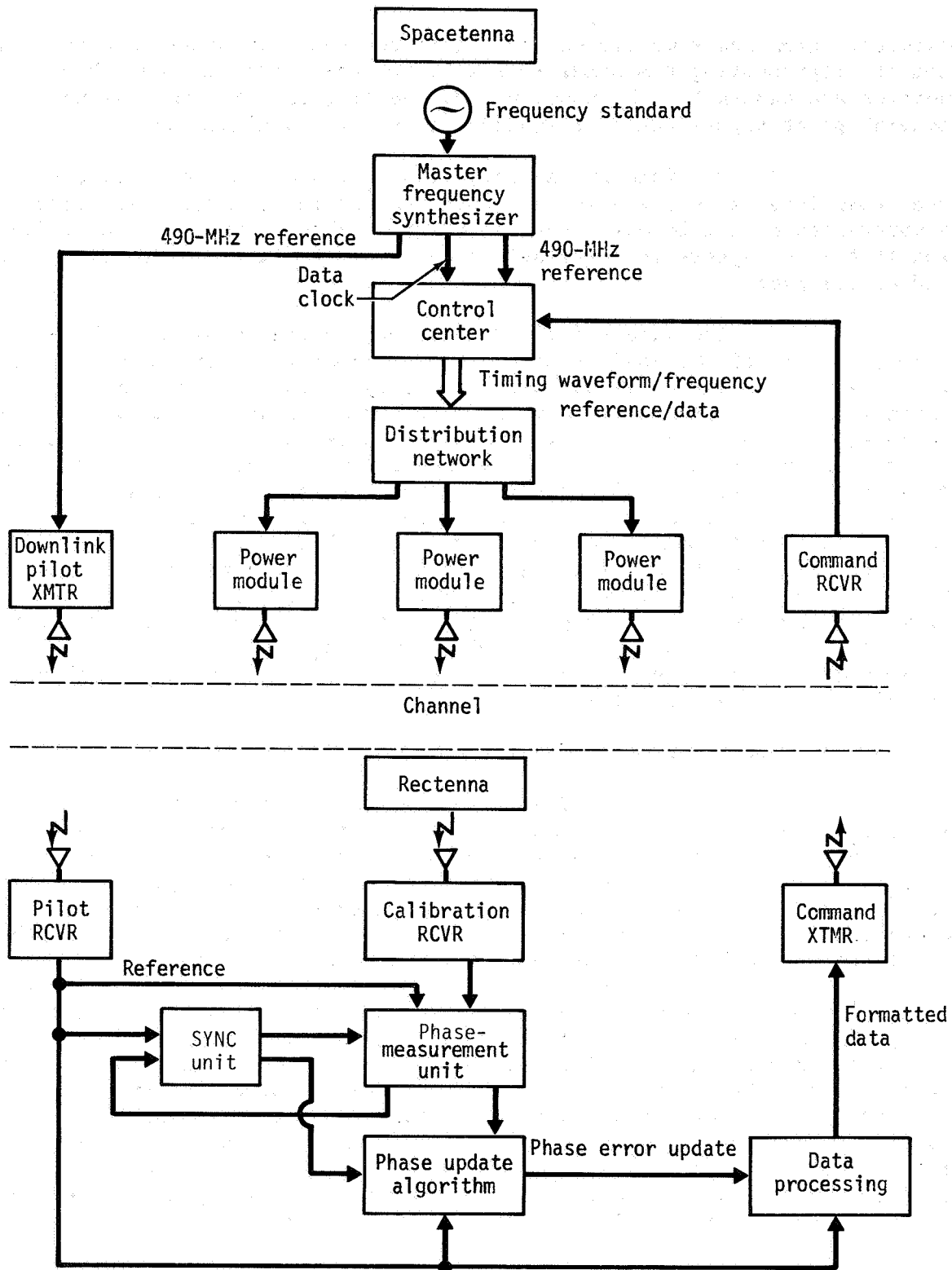
Figure III-34.- SPS ground-based phase control functional block diagram showing system timing hierarchy.

selected. Each power module devotes 10 microseconds to phase correction meas-
urement, representing a minimal loss in total power transmitted. Two fre-
quencies are chosen for the downlink and one frequency for the uplink; the
downlink pilot signal center frequency is set at 4.9 gigahertz.

Preliminary investigation indicates that the effects of
power beam interference and thermal noise on the phase-measurement error can
be controlled to a tolerable level. The ground-based system can also func-
tion if the ionosphere is nonturbulent and the satellite's tilt rate is lim-
ited to 0.5'/sec.

The feasibility of the ground-based phase control concept
becomes unclear if the conditions for the ionosphere and the satellite motion
are not met. The ground-based system can only correct for random phase fluc-
tuations having a correlation time that is large compared with 1.25 seconds.
The noise components that are faster than 1.25 seconds are uncorrected and
result in degradation of transmission efficiency. Unfortunately, measured
ionospheric data suitable for the SPS system are not readily available. (Most
data are concerned with spatial correlations rather than temporal correla-
tions. Also, most data are measured from low-orbit satellites rather than
geostationary satellites which significantly alters the geometric effects.)
The other limiting factor is the statistical behavior of the random pointing
error exhibited by the spacetenna. Again, the fast component of this error
is not corrected and contributes to efficiency degradation. Currently, the
development and specification of models for ionospheric phase disturbance and
satellite motion is considered to be essential.

4. IONOSPHERIC/ATMOSPHERIC CONSIDERATIONS

As noted in the discussions of the two ground-based phase con-
trol system concepts, a major concern is the potential effect of the iono-
sphere on microwave signal phases. No ionospheric model is available to
quantitatively predict the phase errors resulting from ionospheric disturb-
ances. When the SPS heats the ionosphere, an additional unknown factor is
encountered. Early efforts have been made to determine the effects on the
ionosphere of SPS heating; however, data taken did not allow modeling of the
ionosphere's spatial and temporal phase perturbation functions. The first
in a series of experiments recommended by JSC to obtain the needed data for
ionospheric modeling was conducted in April 1980, and a preliminary model
was developed for initial SPS phase control system performance assessments.
Future experiments are also planned to enable updating and refinement of the
ionospheric model developed. Some early consideration has been given to the
possible effects of an unstable ionosphere on the baseline retrodirective
control system. On the assumption that these effects are intolerable, a
potential method for mitigation of these effects has been proposed by Rock-
well International (refs. 30 and 31) and is discussed in this section.

a. Ionospheric Effects on Single-Tone Pilot Beam

An important feature of the retrodirective array is that
the downcoming beam is phase coherent when it arrives at the ground pilot
source. This statement is rigorously correct only if the propagation medium

94

is nondispersive, spatially homogeneous, and temporally stable. In the iono-spheric case, one or more of the preceding conditions are violated. Under certain conditions, beam-pointing error can occur and phase coherence at the source can be lost.

Consider the situation shown in figure III-35. Assume the uplink and downlink frequencies are given by f_u and f_D, respectively ($f_u \neq f_D$). The phase shift (path dependent) at f_u on one particular radio link can be written as

$$\phi(f_u) = \frac{2\pi f_u L}{C} - \frac{b}{2\pi f_u C} \int_0^L N \, d\ell \qquad (7)$$

where $b = e^2/(2\varepsilon_0 m) = 1.6 \times 10^3$ $C^2/(F/m\text{-}kg)$, e = electron charge, m = elec-tron mass, ε_0 = free-space permittivity, L is the physical path length in-volved, C is the speed of light in a vacuum, and the integral term is the integrated electron density along the path under consideration ($\approx 10^{17}$ to 10^{19}). Note that the second quantity on the right-hand side of equation (7) accounts for ionospheric effects on a CW tone. On using appropriate constants, one can write

$$\phi(f_u) = \frac{2\pi f_u L}{C} - 40.5 \times \frac{2\pi}{f_u C} \int_0^L N \, d\ell$$

$$= \frac{2\pi f_u L}{C} - \frac{K_u}{f_u} \qquad (8)$$

where K_u represents ionospheric effects on the uplink signal. Since one is interested in knowing the phase shift at f_D, a reasonable estimate of the phase can be obtained by multiplying $\phi(f_u)$ by f_D/f_u. (This estimate be-comes increasingly accurate as $f_u \rightarrow f_D$.) Thus,

$$\phi(f_D) = \frac{f_D}{f_u} \times \phi(f_u)$$

$$= \frac{2\pi f_D L}{C} - \frac{K_u}{f_u^2} \cdot f_D \qquad (9)$$
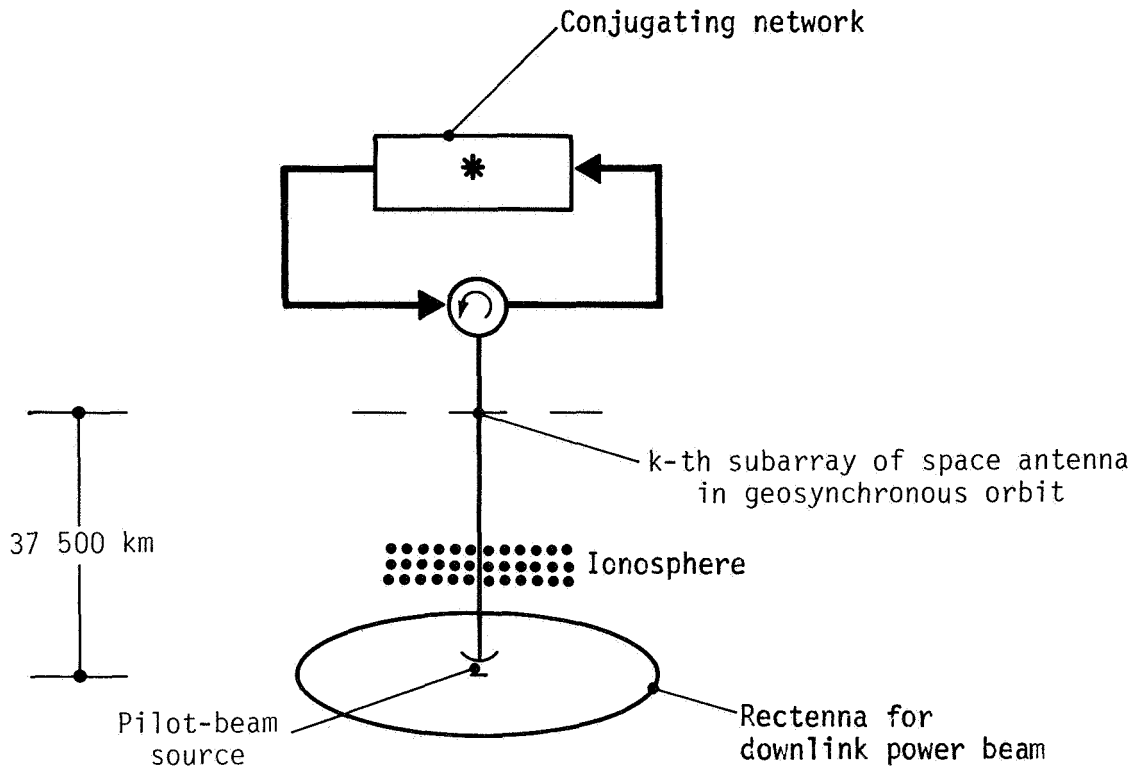
Figure III-35.- Diagram showing effects of ionosphere on single-tone
pilot beam.

On conjugating this phase, one obtains

$$\phi^*(f_D) = -\frac{2\pi f_D L}{C} + K_u \frac{f_D}{f_u^2} \tag{10}$$

The downlink signal at the transmitting end can be written as

$$s_{down}^T(t) = \cos\left(\omega_D t + 2\pi f_D \frac{L}{C} - K_u \frac{f_D}{f_u^2}\right) \tag{11}$$

where t is time and ω is angular frequency. The downlink signal at the receiving end is given by

$$s_{down}^R(t) = \cos\left[\omega_D t - \left(K_u \frac{f_D}{f_u^2} - \frac{K_D}{f_D}\right)\right] \tag{12}$$

For a temporally stable ionosphere and ignoring second-order effects, one can set $K_u = K_D$ in equation (12) and obtain

$$s_{down}^R(t) = \cos\left[\omega_D t - K_u \left(\frac{f_D}{f_u^2} - \frac{1}{f_D}\right)\right] \tag{13}$$

If, in addition, the propagation medium is assumed to be nondispersive, then the second term on the right-hand side of equation (13) involving K_u could be equated to zero. In the current situation, this kind of assumption is highly unrealistic. Note that in equation (13), K_u applies to a particular radio path and will, in general, be different on different paths because of ionospheric inhomogeneity. A consequence of this fact is that the phase coherence (at source) property of the downlink signal mentioned earlier is no longer valid. Furthermore, if a coherent phase perturbation occurs because of some ionospheric large-scale feature (such as a wedge), then even a beam-pointing error is possible. The magnitude of these effects needs to be evaluated for worst case ionospheric conditions.

> b.   Three-Tone Pilot-Beam System for Mitigating Ionospheric Effects

In the following discussion, a three-tone approach is used to resolve the ambiguity problem commonly associated with the two-tone averaging schemes. It is based on a direct measurement of $N\, d\ell$ along the paths

of interest and subsequent use of this information to estimate the path-related phase shift at the downlink frequency f_D.

Consider a frequency-amplitude pattern as shown in figure III-36, where the three uplink tones f_1, f_2, and f_3 are coherent at ground. Indeed, the three tones can be generated by a low-deviation phase-modulated transmitter. For three frequencies f_1, f_2, and f_3, one can write

$$\delta\phi_A = \phi_2 - \phi_1$$

$$= \frac{2\pi}{C} (f_2 - f_1) L - 40.5 \times \int N \, d\ell \times \left(\frac{1}{f_2} - \frac{1}{f_1}\right) \tag{14}$$

and

$$\delta\phi_B = \phi_1 - \phi_3$$

$$= \frac{2\pi}{C} (f_1 - f_3) L - 40.5 \times \int N \, d\ell \times \left(\frac{1}{f_1} - \frac{1}{f_3}\right) \tag{15}$$

The second difference of phase shift is given by

$$\delta_2\phi = \delta\phi_A - \delta\phi_B$$

$$= \frac{2\pi}{C} \times 40.5 \times \int N \, d\ell \times \left(\frac{2}{f_1} - \frac{1}{f_3} - \frac{1}{f_2}\right) \tag{16}$$

For suitably chosen Δf, one obtains

$$\delta_2\phi \simeq -\frac{2\pi}{C} \times 40.5 \times \int N \, d\ell \times \frac{2 \, \Delta f^2}{f_1^3} \tag{17}$$

Suppose one needs to avoid a 360° ambiguity in $\delta_2\phi$ for values of $N \, d\ell$ less than 10^{19}. From equation (17), one easily finds

$$\Delta f^2 \simeq -\delta_2\phi \times f_1^3 / \left[(2\pi/C) \times 40.5 \times 2 \times \int N \, d\ell\right] \tag{18}$$

98
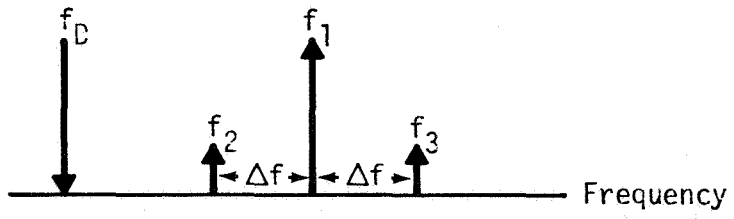
Figure III-36.- Diagram of frequency-amplitude pattern.

Let

$$f_1 = 2.45 + 0.153\ 125$$

$$= 2.603\ 125\ \text{GHz} \tag{19}$$

Then

$$\Delta f^2 \simeq (2\pi) \times (2.6 \times 10^9)^3 \times C/(2\pi \times 81 \times 10^{19})$$

$$= 0.651 \times 10^{16} \tag{20}$$

or $\Delta f \simeq 80.6$ megahertz. Thus, with $\Delta f \leq 80.6$ megahertz and assuming that $\delta_2\phi$ can be measured, then $N\ d\ell$ can be calculated rather easily from equation (17). An implementation that is capable of measuring $\delta_2\phi$ with relative ease is shown in figure III-37. Reordering equation (17), one easily obtains

$$N = \text{computed value of } \int N\ d\ell$$

$$= \frac{f_1^3}{2\ \Delta f^2} \times \frac{C}{2\pi} \times \frac{1}{40.5} \times (-\delta_2\phi)$$

$$= \alpha \cdot (-\delta_2\phi) \tag{21}$$

where $(-\delta_2\phi)$ is measured. For $f_1 = 2.603$ gigahertz and $\Delta f = 80.0$ megahertz, one can compute $\alpha = 1.6 \times 10^{18}$. Based on signal-to-noise ratio considerations, the accuracy of the N computation in equation (21) is determined by the accuracy of $\delta_2\phi$ measurement and is given by

$$a_N = a \cdot \sigma_{\delta_2\phi} \tag{22}$$

On the basis of limited available data and geometry considerations (the proximity of the ionosphere to the rectenna), it appears unlikely that any compensation for ionospheric effects would be necessary. However, to make a definite conclusion, more data on wedge structure are desirable. In addition, this problem needs examination in the light of ionospheric heating effects due to the downlink power beam.
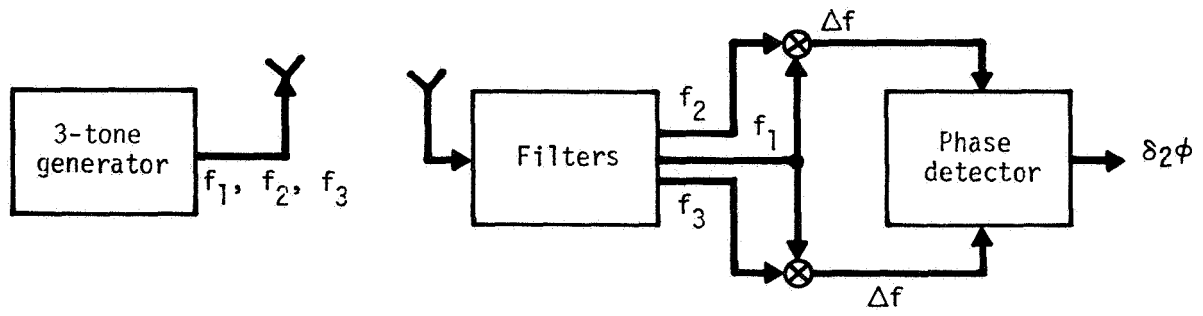
Figure III-37.- Measurement of $\delta_2\phi$.

C. POWER AMPLIFIERS

1. INTRODUCTION

In-depth studies performed on the microwave system include investigation of the amplitron (crossed-field amplifier) and the klystron (linear beam amplifier). The amplitron was characterized by high efficiency and low gain, whereas the klystron was characterized by high gain, low noise levels, and high efficiency. The amplitron study was accomplished before the joint DOE/NASA SPS Concept Development and Evaluation Program. Trade-offs were performed on amplitron compared to klystron tube parameters as well as on integration into the microwave system. The study resulted in the conclusion that either 5-kilowatt amplitrons in series or 50-kilowatt klystrons in parallel could be used. In the MSFC study, concluded in November 1976, the amplitron was selected for initial study because of the possible efficiency and lifetime advantage.

In the JSC studies, concluded in August 1976, both the amplitron and the klystron were investigated. Traveling-wave tubes (TWT's) and solid-state amplifiers were also investigated. It was concluded that both the amplitron and the klystron had the best potential for use on the SPS, with the edge being given to the klystron because of system implementation considerations. The major advantages of the klystron were (a) much higher tube power, which simplified initial assembly and installation operations and ameliorated maintainability requirements; (b) higher operating voltage, which reduced power distribution system weights; (c) much lower phase control drive power; and (d) lower rf noise characteristics.

In the Boeing studies, the klystron was chosen as the amplifier to investigate further, and an in-depth, comprehensive study of klystron configurations, integration into the microwave system, maintenance scenarios, manufacturability, cost, weight, etc., was performed. The results of the study demonstrated that a klystron can be integrated into an overall SPS and that it does have certain advantages.

a. Conclusions

(1) Power amplifier/microwave system trade-offs - Based on current assumptions of microwave system requirements and projected performance of various microwave power amplifiers, the klystron offers a feasible approach for SPS microwave power generation, the amplitron appears to be less suitable, and investigation of the magnetron should be continued to better understand its performance characteristics relative to SPS applications. Based on SPS microwave system applications, it is desirable to have maximum power output and gain consistent with other microwave system parameters.

(2) Klystron - The klystron power amplifier has the attractive features of high gain (40 to 50 decibels), low drive power required from the phase control system, high power (50 to 70 kilowatts), low noise characteristics, and fewer tubes per antenna requiring phase control. Cathode lifetime and its maintenance implications are major concerns for the SPS. Efficiencies of 75 percent at S-band and a power output of 50 kilowatts have already been

recorded. The application of depressed collectors has increased tube efficiencies. It appears likely that an efficiency of 85 percent can be achieved. A heat-pipe cooling system is required for heat rejection.

(3) Amplitron - Projected performance of amplitrons is less attractive for SPS applications because of low power (5 kilowatts), low gain (7 decibels), higher noise levels, higher drive power required from the phase control system, and more tubes per antenna requiring phase control. The amplitron is less complex, and passive cooling techniques appear to be within the state of the art.

(4) Magnetron - Because of recent projections in performance characteristics (low noise, high efficiency, and moderate gain), magnetrons warrant continued investigation. The magnetron is also less complex and hence the maintenance implications appear to make it more attractive.

b. Power Amplifier Remaining Issues

Power amplifier remaining issues are as follows.

(1) High rf-dc conversion efficiency ($\geq$85 percent)

(2) Reliability

(3) Amplifier RFI (noise, harmonics, filtering requirements)

(4) Other operating parameters (temperature, gain)

(5) Proof of thermal cooling concept

(6) Specific weight

(7) High-volume manufacturing techniques

(8) Precision manufacturing

(9) Design for ease of maintenance

(10) Design of power supply/power amplifier for stable operation

(11) Depressed collectors (klystrons)

(12) Investigation of circuit protection devices

(13) Launch/transportation packaging considerations

(14) Metals/materials research (magnets, cathodes)

2. KLYSTRONS

a. Reference Description

An rf transmitter configuration of 101 552 70-kilowatt CW klystron amplifiers operating at 42 kilovolts with 45 to 50 decibels gain using a compact, efficient (82 to 85 percent) solenoid wound-on-body design approach with conservative design parameters (0.15 A/cm^2 cathode loading) to achieve long life is currently used in the reference system. Proposed multiple-tube development programs and assessment of high-voltage operation in space will provide the final answer to the transmitter selection. The layout of the basic klystron building-block module, including the various elements, is shown in figure III-38. The six-cavity design, with a second-harmonic-bunching cavity for short length and high efficiency, features a dual-output waveguide with 35 kilowatts in each arm. The thermal control system used to cool the output gap, the depressed collector, and the solenoid consists of heat pipes with passive radiators and has design temperatures of 573 K (300° C) maximum on the body and 773 K (500° C) on the collector. The driver for the klystron power amplifier will require an output of about 3 watts CW for a 45-decibel output amplifier saturated gain. This power level is compatible with several off-the-shelf, reliable, low-noise amplifiers which can be driven directly from phase-regeneration circuitry. The driver could be either a low-noise, high-gain TWT or a multistage transistor ampli-fier with as much as 10 decibels gain per stage. The phase-regeneration cir-cuitry will be operated at power levels below 1 milliwatt. In arriving at the reference configuration, high-power klystrons and crossed-field ampli-fiers were considered to the same depth in the rf transmitter approach. This statement does not imply that the reference klystron design is the preferred solution, merely that such a transmitter can be integrated into the overall antenna array design and that it does have certain desirable features. The ultimate choice will have to be made on the basis of demonstrated performance assessment of both types of devices, particularly in terms of life, efficiency, spurious radiation, ease of integration and replacement, and specific weight.

The reference design approach for the klystron had as its objective high efficiency (85 percent) at a reasonable voltage (>40 kilo-volts); discussions with various tube manufacturers have led to a design with the parameters given in table III-10. These parameters do not result in a klystron with the lowest specific weight and cost but provide a baseline on which to establish a reference design.

(1) <u>Element mass</u> - The klystron mass per tube is estimated to be 0.8 kg/kW at 70 kilowatts, decreasing to less than 0.4 kg/kW at 500 kil-owatts CW (ref. 32).

(2) <u>Element cost</u> - The mature industry mass production cost per 70-kilowatt CW klystron has been estimated at $2800 (ref. 32) (depending on mass production rate).
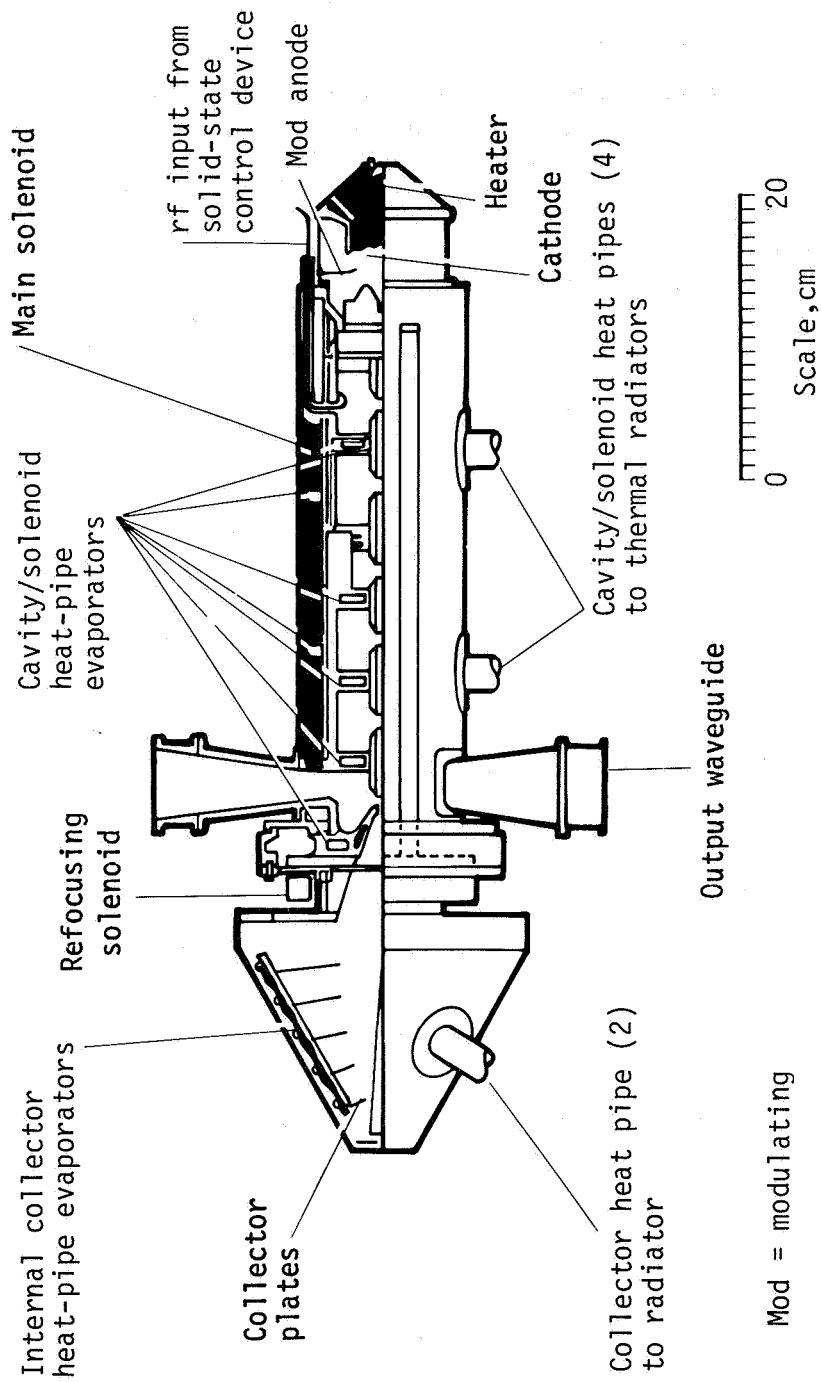
Figure III-38.— 70-kilowatt klystron.

Mod = modulating

TABLE III-10.- REFERENCE 70.6-KILOWATT[a] KLYSTRON DESIGN CRITERIA

Component	Type	Remarks
Collector	5-segment depressed	Based on experimental results on collector recovery of $\approx$50 percent, obtained by using a small refocusing coil in collector section
rf design	Single second-harmonic-bunching, 6-cavity	Results in high basic efficiency in a compact drift-tube configuration. Purpose: to obtain a gain of about 40 dB, resulting in solid-state driver feasibility and low-power phase-shift requirements (<10 W)
Focusing	Solenoid (ref.) PM/PPM[b] (future)	Purpose: to obtain high efficiency with low-risk approach. If in the process of SPS development, a high-power samarium-cobalt PM/PPM design can be proven with good efficiency, it should be considered.
Thermal design	Heat pipe with passive radiators	Purpose: to obtain the desired CW level with conservative heat dissipation ratings
Auxiliary protection	Modulating anode	Purpose: to provide rapid protection shutoff capability at the individual tube level and thereby to eliminate the need for resistive load shifting
Cathode	Coated powder or metal-matrix medium convergence	Purpose: to obtain a cathode emission of <200 mA/cm^2 for longer life (30 yr to emission wearout)
Power extraction	2-port output	Results in rating of 35 kW CW per each waveguide output; capable of operating in vacuum with radiative cooling only at a temperature below 473 K (200° C)

[a]Based on a perveance of $S = 0.25 \times 10^{-6} = I_o/V_o^{3/2}$ as determined to maintain high efficiency at maximum potential of 42.1 kilovolts.
[b]PM/PPM = permanent magnet/periodic permanent magnet.

b. High-Efficiency Klystron Design Assessment

Considerable data have been accumulated on the feasibility of an 80- to 85-percent-efficient high-power klystron design from previous studies and discussions with General Electric Power Tube Department, Schenectady; Thomson-CSF Electron Tubes; and NASA Lewis Research Center. The most likely configuration to realize both high efficiency and high gain ($\sim$40 decibels) is a six-cavity design with one second-harmonic-bunching cavity focused by an electromagnet as described by E. Lien of Varian Associates. A refocusing section will probably be required for efficient depressed-collector operation. An outline of the klystron configuration is given in figure III-38. The preliminary power output is dictated by the desire to keep the operating voltage low. The 70-kilowatt CW output level resulted from a maximum selected voltage of $\sim$40 kilovolts. If this voltage limitation can be relaxed, even higher power options become of interest. The basic klystron efficiency will probably not exceed 70 to 75 percent without collector depression. Although impressive gains have been achieved in raising the basic efficiency from 54 to approximately 70 percent with a 10-stage depressed collector, the estimated efficiency gain resulting from 5-stage collector depression indicated in figure III-39 at the 75-percent level is only about 8 percent, resulting in an overall efficiency of about 83 percent. These are best estimates only and will have to be verified by experiment, since the velocity distribution of the spent electron beam entering the collector is not precisely known. An alternate way to determine the efficiency estimate is to trace the energy flow through the klystron, as is done in table III-11 on the basis of best design values obtained from Varian Associates. In this case, slightly different values of collector recovery potentials were used (40 percent for three-segment and 60 percent for five-segment collector) to assess the differential benefit between the designs.

(1) Depressed-collector design – One of the uncertainties in the design is the velocity distribution of electrons in the output gap, particularly for a tube having high basic efficiency. There are few guidelines short of experimental verification that will enable the selection of proper depressed voltages at each collecting electrode. Varian has reported that about 10 percent of the electrons develop twice the dc beam voltage in a 50-percent-efficient tube. It is estimated that this value will be reduced to perhaps 2 percent for an 80- to 85-percent-efficient tube. To obtain initial specifications for the collector supply, an estimate was made of the possible voltage ratios required, as indicated in figure III-40. The postulated collector currents associated with these ratios are also indicated, the criteria being a reasonable distribution based on extrapolated experience and an energy balance resulting in the expected efficiencies. These ratios were used in establishing the supply requirements; the supplies themselves need not be regulated since a 10-percent fluctuation in them is not expected to affect the operation of the klystron bunching region.

(2) Voltage regulation – The klystron drift-tube interaction depends entirely on the modulation anode electron velocity, which is dependent on the cathode-to-anode voltage and the anode-to-body voltage; these voltages are in series with each other. The amount of current intercepted at
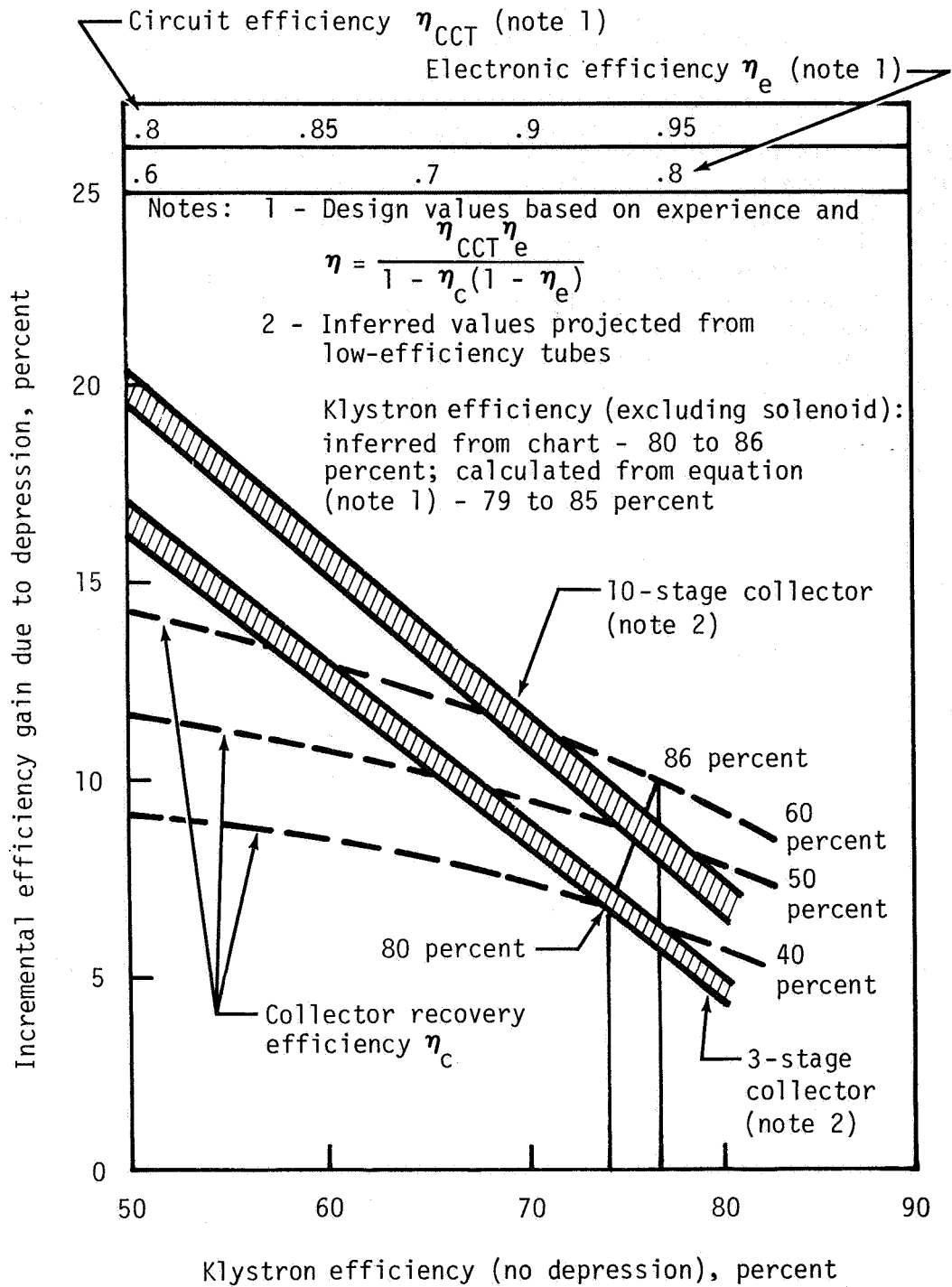
Figure III-39.- Estimated effect of collector depression.

TABLE III-11.- ENERGY BALANCE IN REFERENCE FIVE-SEGMENT-COLLECTOR
KLYSTRON DESIGN

Variable	Value
Beam power, kW	92.62
rf loss in driver cavities, kW	0.40
rf power output,[a] kW	70.67
Output cavity rf loss, kW	2.19
Output interception loss,[b] kW	1.62
Power entering collector, kW	17.75
Collector recovery at 60 percent, kW	10.65
Thermal loss in collector, kW	7.1
Net beam power, kW	81.97
Efficiency excluding solenoid, percent	86.2
Net efficiency,[c] percent	84.6

[a]Electronic efficiency (0.79) times output circuit efficiency (0.97)
times remaining power (92.22 kilowatts).

[b]Based on 4-percent interception at $V_{o}/3$ (33 percent) and $2V_{o}/3$
(67 percent); i.e., $0.0178V_{o}I_{o}$.

[c]Includes 1.5 kilowatts for solenoid and heater power.

Estimated current and voltage distributions

Collector configuration	3-segment			5-segment		
	V/V_0	I/I_0	P/P_0	V/V_0	I/I_0	P/P_0
Mod anode supply	.5	.04	.040	.5	.04	.040
Body supply in series	.5	-	-	.5	-	-
Spike electrode 0	0	.02	-	0	.02	-
Collector 1	.6	.02	.012	.5	.02	.010
Collector 2	.9	.04	.036	.6	.04	.024
Collector 3	.95	.88	.836	.7	.07	.049
Collector 4	-	-	-	.9	.15	.135
Collector 5	-	-	-	.95	.66	.627
Total		1.0	.924		1.0	.885
Efficiency improvement			1.08			1.13
Estim. efficiency, excl. solenoid (76.3% nominal undepressed)			32.4%			36.2%

V = voltage
I = current
P = power
@ = at
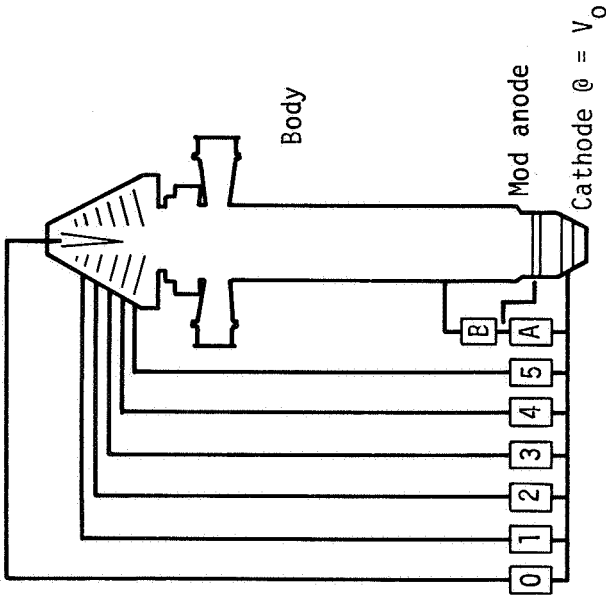
Cathode @ = V_0

Figure III-40.- Reference klystron depressed-collector design.

110

these electrodes is roughly 4 percent, which, at the full cathode-anode volt-
age, corresponds to 4 percent of the beam power. The remaining beam current
is collected in the collector and does not require regulation; it is adequate
if it rises and falls with the beam voltage. The only requirement on the col-
lector voltages is to avoid returning some of the electrons into the interac-
tion regions; this requirement is aided by the presence of the refocusing
coil. It is estimated that if the collector voltages are within ±5 percent
of their nominal values, efficiency will not be degraded.

(3) <u>Electron beam focusing design</u> – The focusing options
for the klystron indicated in figure III-41 include (a) straightforward sole-
noid electromagnetic (EM) focusing based on confined-flow experience, (b)
multiple-pole EM focusing with periodic field reversals, introducing the
possibility of permanent magnet (PM) implementation, (c) periodic permanent
magnet (PPM) focusing used successfully in low- and medium-power tubes
(mostly TWT's), and (d) combined PM/PPM focusing wherein the PM section at
the output is used to retain good efficiency as well as best collimation in
the high-power rf region. The low-risk EM solenoid approach was adopted to
achieve highest efficiency, but research and development efforts in a com-
bined PM/PPM approach should be investigated for possible later incorporation.

It is anticipated that the solenoid will consist of a
copper sheet with glasslike insulation between layers, wound directly on the
tube body. With factory-adjusted cavity tuning, there will be no protruding
tuners. It is possible that the solenoid may be used for baking out the tube
in space.

c. Life and Reliability Assessment

A stated ground rule for the SPS is an operational life of
30 years. Major transmitter elements which contribute to length of life are
summarized as follows.

(1) Beam formation

(a) Cathode manufacturing material processing

(b) Emission suppression from surfaces

(c) Cathode base material purity-poisoning mechanism

(d) Evaporation rails from impregnated cathodes

(e) Heater warmup

(f) Burn-in period – avoidance of premature failure

(2) Beam focusing

(a) Solenoid design/materials – space bakeout feasi-
bility and control

111
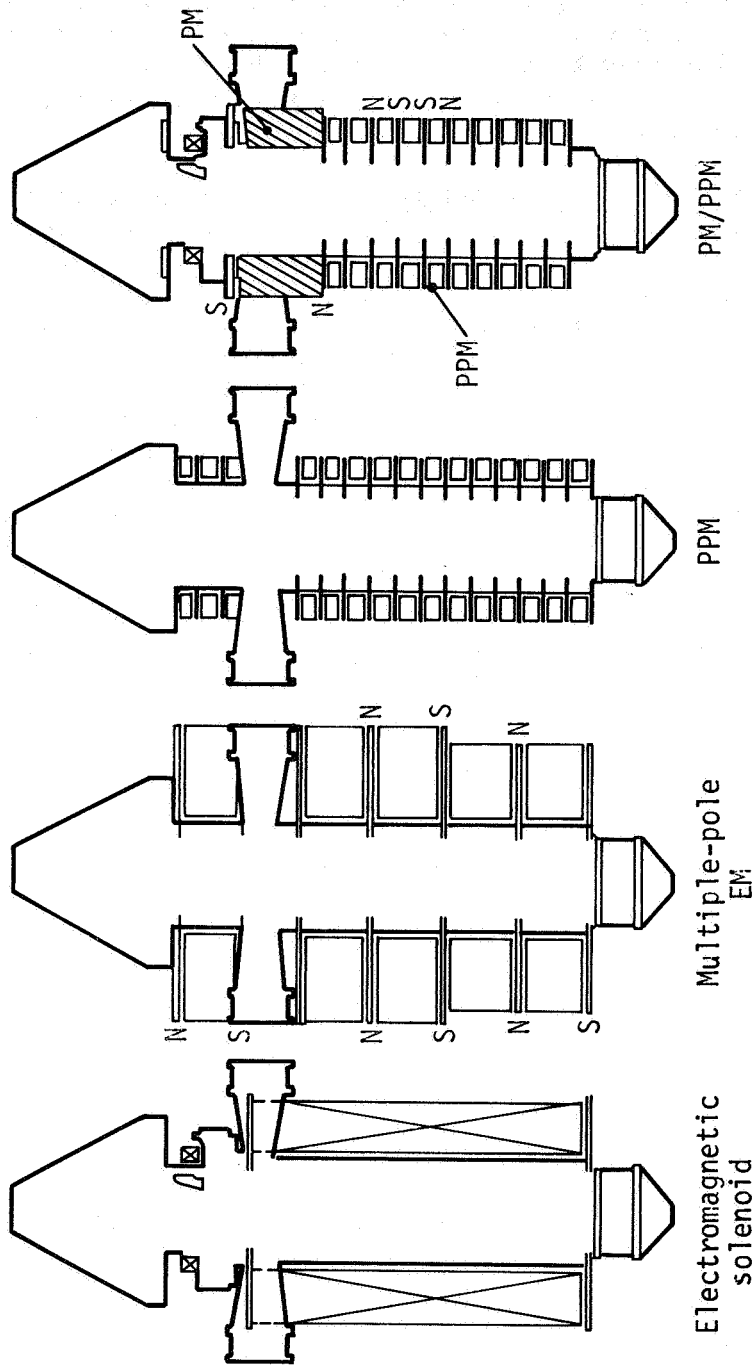
Figure III-41.- Methods of focusing klystron beam.

       (b)   Magnetic circuit material selection – samarium-
             cobalt (Sm-Co), Alnico, flux conductors

   (3) rf circuit

       (a)   Copper alternatives for cavities

       (b)   Properties of lossy internal ceramics

       (c)   Output window power limits – beryllium oxide,
             aluminum pentoxide

   (4) Body and collector

       (a)   Leakage of insulators due to high voltages

       (b)   Suppression of secondary emission

   (5) External – lead and connector compatibility

Leakage of insulators due to high voltages and high cathode current per unit area are two of the more critical factors affecting transmitter tube life. Experience with operational klystrons lends credibility to the projected 30-year life. For example, the best 10 high-power klystrons installed in the ballistic missile early warning system have seen approximately 10 years of service and are still operational. Current space-based TWT's are being qualified for 7 years of life, with proper burn-in procedures. More than 100 such tubes currently in space have been operational for well over 3 years.

It is anticipated that with the reference design tube, partial or full bakeout in space will be feasible and the need to perform costly burn-in on the ground can be avoided. Also, with mass production, automated manufacture, good quality control, and maintenance, premature failure can be minimized.

With roughly $N = 100\,000$ tubes, if a maximum of 2 percent of all klystrons are allowed to fail at scheduled SPS shutdown (every 6 months), the required tube mean time between failures (MTBF) would be approximately

$$\frac{(0.02N)\ (\text{tube MTBF})}{N} = 6 \text{ months, or } 0.5 \text{ year}$$

$$\text{MTBF} = (50)\ (0.5 \text{ year})$$

$$= 25 \text{ years}$$

This value is compatible with the reference klystron design; however, development of a more refined reliability model, of which the exponential failure

mode is but one case corresponding to a constant failure rate, is needed. With proper burn-in procedures, and as better understanding of failure modes is developed, the SPS klystron may require a much lower MTBF to meet the preceding criteria.

    d. High-Power Klystron Trade Studies

    The following trade studies were made on the klystron.

    (1) Specific weight comparison - To arrive at some reliable estimates of specific weights, an investigation of various manufacturer's catalogs was made, augmented by verbal discussions of projected advances, primarily for airborne transmitter applications. The projected advances rely primarily on advanced solenoid designs or usage of lightweight permanent magnets, neither of which has been reduced to practice in quantity production. The total tube weights at 2.5 gigahertz as a function of CW power level are estimated in figure III-42(a); the advantage of CFA's at lower power levels is indicated. When the tube weights are replotted on a normalized basis (fig. III-42(b)), the specific weights of klystrons and CFA's become roughly equal at power levels on the order of 200 kilowatts or above.

    (2) Thermal and X-ray comparison - The klystron may have a slight thermal advantage over a CFA since it will not be limited by the operating temperature of samarium-cobalt magnets ($\sim$520 K ($\sim$250° C)) and its collector may operate at much higher temperatures (773 to 973 K (500° to 700° C)). However, the X-ray level will be several orders of magnitude greater. In any case, the results were of sufficient interest to consider further a higher power klystron design, particularly from the tube MTBF point of view. There are no compelling reasons to expect a high-power tube to have a significantly lower MTBF than a low-power tube. Thus, a significant advantage may accrue in the overall transmitter comparison.

    3. MAGNETRONS

    The source of all data on magnetrons discussed herein is William C. Brown, Raytheon Company, New Products Center, Waltham, Massachusetts. In 1975, R. M. Dickinson of JPL proposed that because of its high production volume and low cost, the microwave oven magnetron be incorporated into a directional amplifier package and considered for SPS ground tests. These tests were planned to evaluate the phase control. While subsequently investigating this approach, two important discoveries were made: (a) the microwave oven magnetron, when operated with a ripple-free dc power source and with no externally applied filament power, has a much higher signal-to-noise ratio than the conventionally operated magnetron, and (b) under these conditions, the carburized thoriated-tungsten cathode can be operated at such low temperatures that a potential life of more than 50 years is indicated under the high-vacuum and highly controlled operating conditions in space.

    The magnetron directional amplifier has been further evaluated under an NASA (MSFC) contract. This investigation involved an extension of
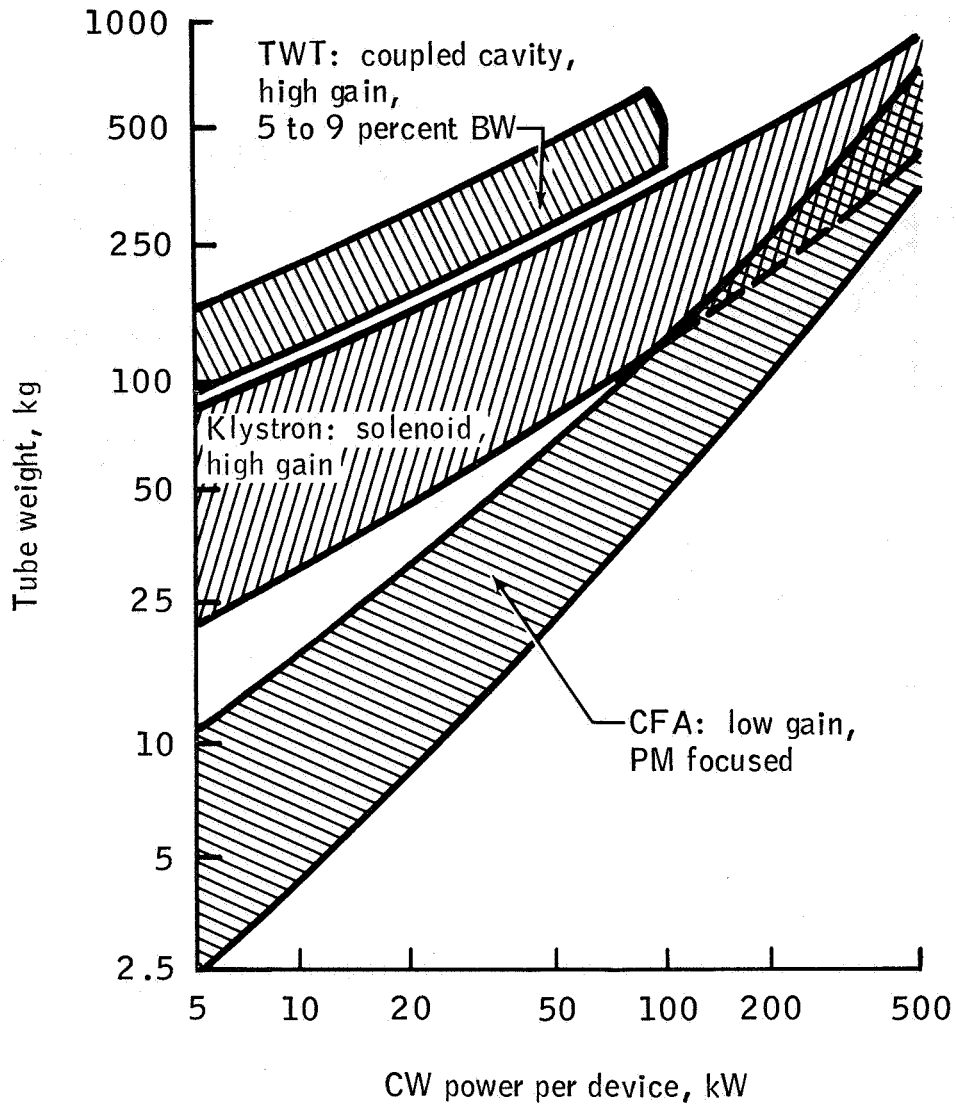
BW = bandwidth

(a) Tube weight.

Figure III-42.- Weight comparison of high-power CW transmitters operating
at a frequency of 2.5 gigahertz.
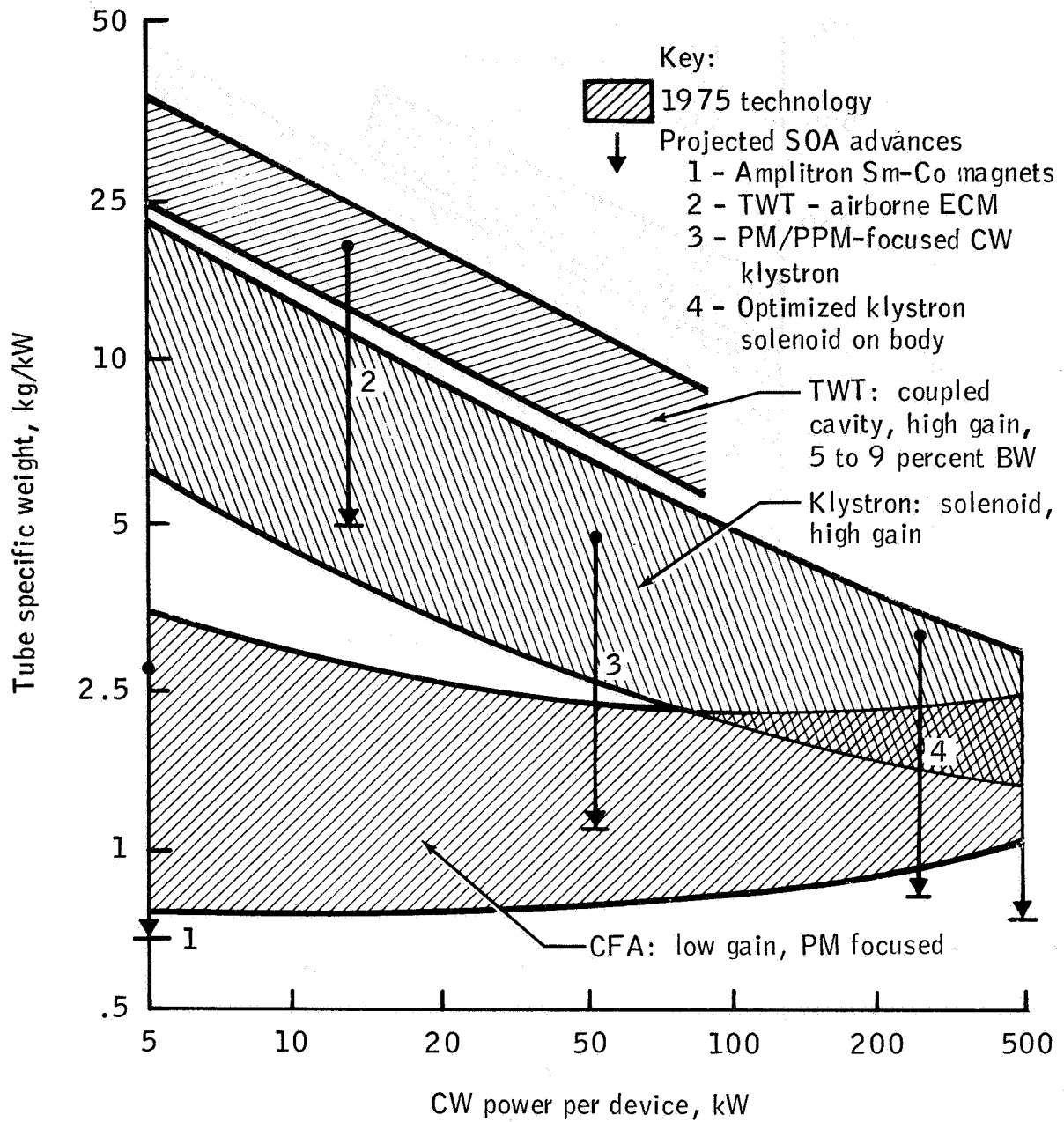
(b) Tube specific weight.

Figure III-42.- Concluded.

the laboratory data base on the magnetron directional amplifier using the microwave oven magnetron. These data, when combined with information obtained from other sources, will make it possible to accurately define the projected characteristics of a higher powered version of the magnetron directional amplifier for SPS use and to define a program of technology development that would result in the development of such an amplifier.

a. Desirable Features of the Crossed-Field Microwave Generator

Desirable features of the crossed-field microwave generator are high efficiency, high signal-to-noise ratio, life of 50 years or more, favorable ratio of mass to microwave power output, advantageous system power-conditioning requirements, and simplicity of construction.

(1) High efficiency - Overall efficiencies in excess of 85 percent have been demonstrated in an off-the-shelf magnetron used for industrial microwave heating. An efficiency in excess of 80 percent at power levels of 3 kilowatts (low enough to use passive cooling) has also been obtained.

(2) High signal-to-noise ratio - In experiments conducted by Raytheon, measurements have been made of random noise levels in a 1-megahertz band which are down 0.100 decibel or more at frequencies above and below carrier frequency by more than 10 megahertz.

(3) Life of 50 years or more - Long life is made possible by operating at low emission-current densities and thereby at low temperatures. At these low temperatures, carburized thoriated-tungsten cathodes have been operated for extremely long periods (ref. 25).

(4) Ratio of mass to microwave power output - The current mass-to-power ratio estimate by Raytheon is 0.4 kilogram per kilowatt of microwave power at the tube output. This ratio includes the weight of the passive radiator but excludes the buck-boost coils, which are considered a power-conditioning function.

(5) System power-conditioning requirements - The buck-boost coils necessary for output amplitude control of the magnetron can take on the added function of adjusting the input of the microwave system to operate at the optimum output voltage for the solar array.

(6) Simplicity of construction - Construction of the crossed-field device, particularly in its magnetron form, is very simple. More than two million magnetrons that closely resemble the tube required for the SPS are manufactured annually for microwave ovens. This simplicity of construction and experience in mass production should lead to low cost. (See fig. III-43.)

117
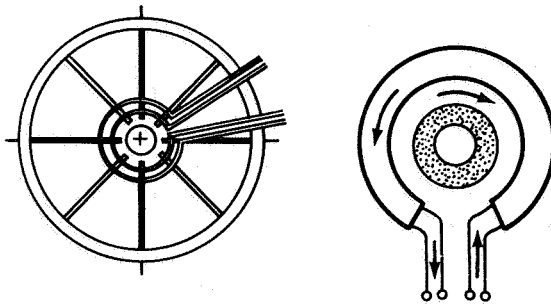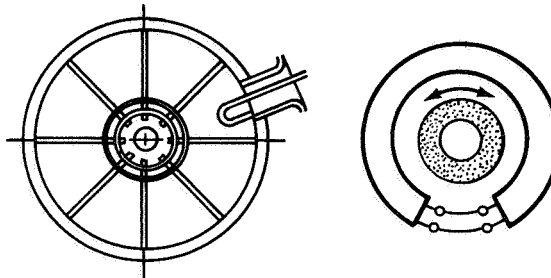
(a) Amplitron.

(b) Magnetron.

Figure III-43.– Diagram illustrating the basic differences of construction
and operation between the amplitron and the magnetron.

b. Integration Into the Antenna Subarray

The concept shown in figure III-44 involves the following problems.

(1) The microwave generators must dispose of their heat directly to space by operating at temperatures in the 473- to 573-K ($200°$ to $300°$ C) range. This problem is solved by designing the generators to radiate heat in only one direction.

(2) Phase and amplitude sensors, phase and amplitude references, and electronic components associated with the control loops for phase and amplitude control must be incorporated. In the subarray concept, the phase and amplitude references are fed from the backbone of the subarray through flat ducts welded to the surface of the slotted-waveguide arrays.

(3) Interface with the microwave drive source – In figure III-44, the microwave drive source is not shown, but it is derived from another magnetron directional amplifier identical to the ones directly attached to the waveguide radiators. At a gain level of 20 decibels, 1 magnetron directional amplifier can drive between 50 and 100 other magnetron directional amplifiers. The microwave drive for any one subsection is delivered to the intended tube through a waveguide, which runs the length of the subsection and serves all the tubes. The energy may be tapped by a number of different techniques including directional couplers and the standing-wave techniques used in the design of the slotted-waveguide radiators.

(4) Sources of auxiliary power – Auxiliary power may be obtained by tapping off a portion of the microwave power from the magnetron directional amplifier that drives the subsection array, then performing the desired impedance transformations at microwave frequency and rectifying the output with the highly efficient type of rectifier used in the rectenna. The auxiliary power is then distributed to the individual magnetron directional amplifiers in the subsection array through the flat conduits located on the slotted-waveguide array surface.

c. Phase and Amplitude Tracking

The output phase of any microwave generator in the SPS must be maintained to within $1°$ to $2°$ accuracy. Open-ended control is not feasible. The control must use a low-level phase reference at the output, a comparator circuit to compare the phase of the generator output with the reference
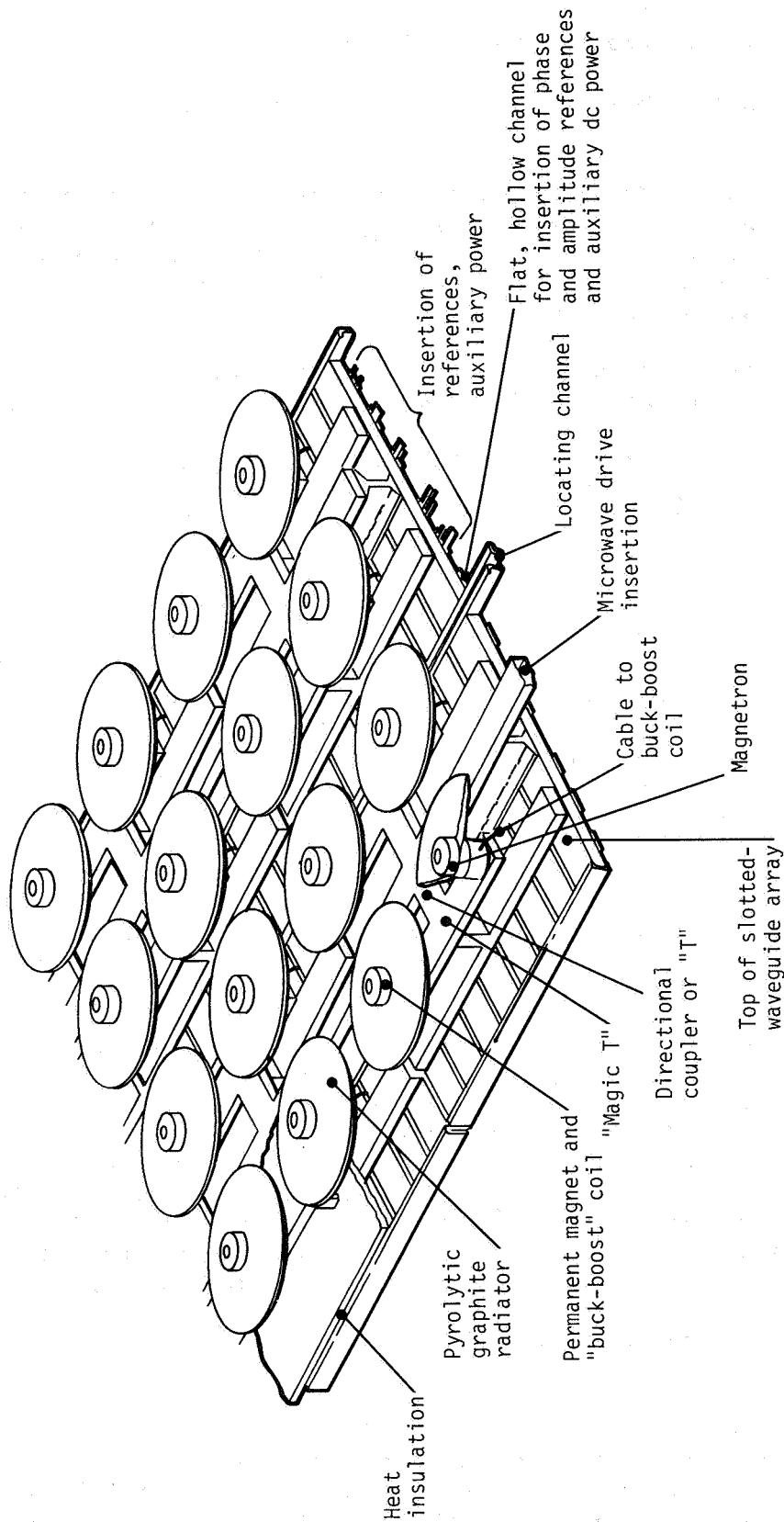
Figure III-44.– Assembly architecture for the magnetron directional amplifier in the antenna subarray. Two subsections are shown. Microwave drive and all references and auxiliary power are inserted from the "backbone" of the subarray. The array has two distinct temperature zones. The top is used to radiate heat. The bottom is used for mounting solid-state components.

Insertion of references, auxiliary power

Flat, hollow channel for insertion of phase and amplitude references and auxiliary dc power

Locating channel

Microwave drive insertion

Cable to buck-boost coil

Magnetron

Directional coupler or "T"

Top of slotted-waveguide array

Permanent magnet and "buck-boost" coil "Magic T"

Pyrolytic graphite radiator

Heat insulation

phase and to generate an error signal, and a feedback loop to make a compensating phase adjustment at the input.

The control of the output amplitude in the face of many factors that tend to change that amplitude is also essential for generating an efficient microwave beam. The output amplitude can be controlled to a predetermined value by another control loop which makes use of small electromagnets to boost or buck the residual field provided by permanent magnets.

The overall schematic for the combined phase and amplitude control of the magnetron directional amplifier is shown in figure III-45. Also shown is the manner in which this control can be related to the overall power absorption by the solar cell array. A central computer establishes the most efficient operating point (maximum power output) of the solar cell array and then adjusts the reference power output of the banks of magnetron directional amplifiers.

The phase and amplitude tracking system requires a set of references and a set of sensors. These references and sensors are located at the front face of the slotted-waveguide array, where the most accurate sensing of the phase and amplitude can be made and where the solid-state sensing and control devices are exposed to a tolerable temperature environment.

The amplitude reference is a dc voltage the value of which can be remotely controlled from a central source. The amplitude sensor is a crystal detector coupled to the slotted-waveguide array that provides a dc voltage for comparison with the reference dc voltage. The error voltage, after suitable gain, establishes a current in the buck-boost coils that changes the magnetic field; the magnetic field, in turn, changes the magnetron current and thereby the power output of the magnetron in a direction that minimizes the error voltage.

The phase control system makes use of a phase-controlled signal from a central source, a sample of the output power, and a balanced detector which compares their phases. The error signal can be used to operate a number of different types of phase shifters positioned in the input side of the magnetron directional amplifier.

A test bed (fig. III-46) has been constructed to check out the proposed control system. For most laboratory measurements, a resistive microwave load is substituted for the slotted waveguide. The sensors are located in the waveguide approach to the load. Although evaluation of the control system is not complete, the initial information indicates predicted behavior.

d. Noise Emission Properties

The lack of historic data on the noise performance of CW crossed-field devices and the consequent inability to predict CFA behavior in the SPS application, where the noise level of the transmitter is a highly

Figure III-45.- Schematic diagram of phase and amplitude control of magnetron directional amplifier output (ref. 25). The proposed packaged unit is enclosed by dashed line. Relationship to SPS overall system is indicated outside dashed line.

Figure III-46.- Test bed for the phase and amplitude tracking investigation, shown with slotted-waveguide load as an option.

122

critical issue, became a major factor in the preliminary selection of a generator approach in the reference design. Many measurements of signal-to-noise ratio over frequency ranges of as much as ±1000 megahertz either side of the carrier have been made on magnetron directional amplifiers (fig. III-47). The data were obtained both with normal external power applied to the filament and with no external power applied. Note the very high signal-to-noise ratio that is obtained over a frequency sweep of 200 megahertz with no external power applied. The signal-to-noise ratio is 100 decibels for a 1-megahertz band of noise. This value corresponds to a signal-to-noise ratio of 130 decibels per 1 kilohertz noise, which is comparable with a klystron.

Because the measurements are still limited by equipment sensitivity, it is possible that the signal-to-noise level is substantially better than 100 dB/MHz. The sensitivity is being increased by 20 decibels so that signal-to-noise ratios of as great as 120 dB/MHz can be measured.

Although these noise measurements were made with a device gain of approximately 20 decibels, the noise behavior remains independent of gain at high gain levels. At high gain levels, the drive source appears as a small reflection factor (0.1 for a gain of 20 decibels), which has a negligible impact on the behavior of the tube.

These low-noise measurements have been observed on magnetrons made by different manufacturers and in different time periods, but not on all magnetrons that have been randomly selected. However, no statistical studies have been made and none probably should be made until more sensitive measuring equipment is available. In addition, it may be more effective to devote any limited future effort to better understanding the sources of noise in the magnetron.

Measurements of near-field phase-modulation noise added by the magnetron directional amplifier were also made when it was operating with a gain of approximately 20 decibels. These measurements indicated a carrier-to-noise level that was typically 115 decibels for a 1-kilohertz band of noise in the range of 10 to 100 kilohertz removed from the carrier frequency.

A method of making harmonic measurements in a small coaxial line and water load attached adjacent to the magnetron output, with normal loaded impedance matching, was employed. By this means, the problem of multiple-mode propagation is avoided. Measurements made on two representative tubes, designated as numbers 11 and 12, are given in table III-12. The findings are somewhat better than had been anticipated. The unexpected presence of significant energy at the fifth harmonic is an indication of the difficulty in predicting the more complicated characteristics of any microwave generator.

e. Cathode Life of 50 Years

It is well known from the theory and experience associated with properly carburized thoriated-tungsten cathodes that such cathodes can have extremely long life if they are operated at low temperatures in an effective vacuum. Investigations not only have indicated that very long life can

123
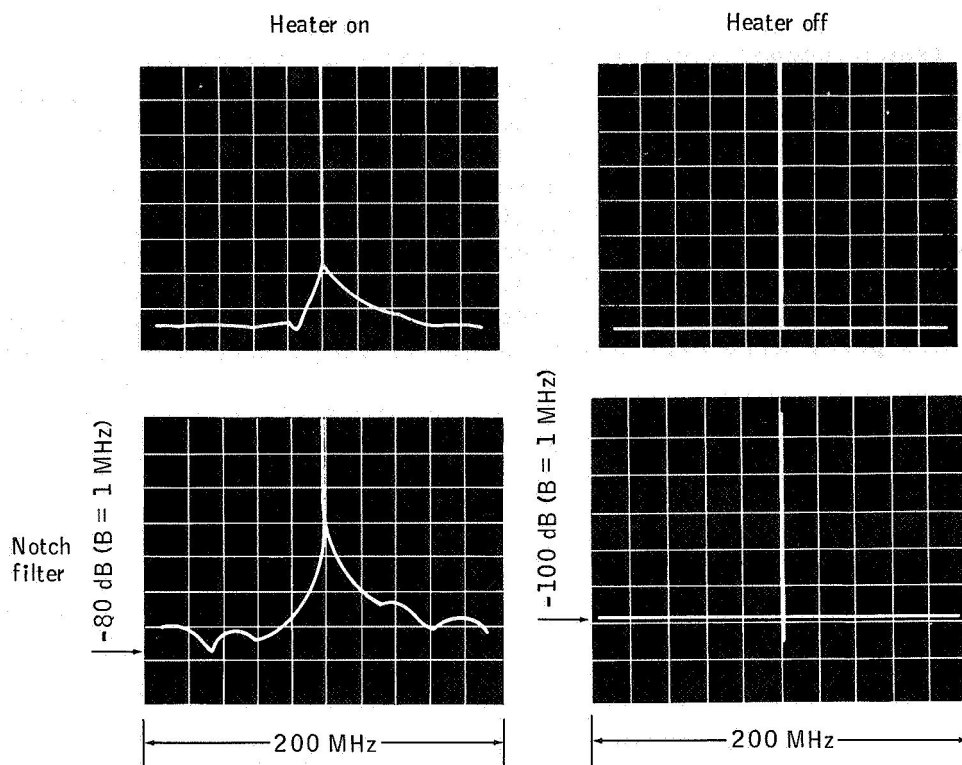
Figure III-47.- Spectrum of locked magnetron.

TABLE III-12.- HARMONIC MEASUREMENTS ON
REPRESENTATIVE TUBES

Frequency	Harmonic level, dBc,[a] for tube no. -	
	11	12
f_o	0	0
$2f_o$	-71	-69
$3f_o$	<-97	-85
$4f_o$	-86	-93
$5f_o$	-62	-64

[a]dBc = decibels below carrier level.

124

be achieved but also have led to the discovery of an apparently overlooked feedback mechanism in the magnetron by which the emitting surface of the cathode is maintained at a temperature just sufficient to supply the needed current that flows from the cathode to the anode. This mechanism ensures that the lifetime of the tube is independent of external circumstances with the exception of compromised high vacuum and demand for increased anode current beyond the design value.

It has been established from life test evaluations that the life of a carburized tungsten cathode is a very steep function of the operating temperature. The difference between lifetimes at 2000 and 1900 K is a factor of 10.

The conclusion is that a good argument can be made for extremely long cathode life in the proposed SPS magnetron. The argument is based on observations of low operating cathode temperatures in operating magnetrons, an internal mechanism that will automatically keep the cathode temperature as low as possible over closely controlled operating conditions in the SPS, a body of experience and information on the carburized thoriated-tungsten cathode that is documented in published papers and books, and the correlation of the long life of the Machlett tubes with predicted life. A lot of 12 tubes was manufactured by Machlett Labs Inc. for use in the WWV transmitter. The filament wire was 0.089 centimeter (0.035 inch) in diameter and 20 percent carburized, and the tubes were operated at 1950 K. The 12 tubes had a total running time of 850 000 hours, and no failures had occurred when the equipment was retired from service. These tubes were also high-power and high-voltage tubes, similar to the projected SPS magnetron.

4. SOLID-STATE POWER AMPLIFIERS

System studies on the solid-state concept (Section III.F) indicate that efficiencies, power handling capabilities, and the 373- to 398-K (100° to 125° C) operating temperatures required for long life will limit power densities at the center of the SPS antenna to levels significantly lower than those of existing tube designs. However, the study results are encouraging and additional work is underway in the solid-state area.

During an applied science workshop held at JSC, it was recognized that the high voltages associated with the operation of the SPS power tubes in the reference configuration may lead to large plasma leakage currents and/or arcing. Solid-state devices, operating at much lower voltages, represent a potential solution to this arcing problem. In addition, solid-state devices would be more compact than the tubes and would possibly permit economies in delivery of antenna systems to orbit through higher density launch payloads. Finally, as solid-state devices have supplanted tubes in a wide variety of commercial and military applications, their high reliability and long-life operation have become well known; these characteristics are of prime importance in SPS design considerations. Thus, high-power solid-state devices appear to be an attractive alternative to the high-voltage power tubes.

In reviewing candidate solid-state devices for SPS applications, attention was limited to those devices capable of generating or amplifying appreciable amounts of microwave power: outputs in excess of 1 watt with efficiencies greater than 25 percent. The devices falling into this category were impact avalanche transit time (IMPATT) and trapped plasma avalanche triggered transit (TRAPATT) diodes and bipolar and field-effect transistors. A summary of the characteristics of the four devices investigated can be seen in table III-13 and figure III-48. It was concluded that FET's appeared to be the best choice in terms of their relative high gain and high efficiency. In addition, the manufacturing process associated with FET's make them easier and cheaper to manufacture in large quantities. The following characteristics of microwave field-effect transistors appeared feasible as reasonable goals for future solid-state work.

Characteristic	Value
Efficiency, percent	80 to 85
Power output, W	1 to 3
Frequency, GHz	2.45
Temperature, K ($^{\circ}$C)	398 to 423 (125 to 150)
Noise temperature, K	60
Weight, g/amplifier	0.1
Reliability, yr mean time to failure	100

a. Device Technology for SPS During 1978 and 1979

The JSC sponsored a study, "Analysis of S-Band Solid-State Transmitters for the Solar Power Satellite" (ref. 9), based on the assumption that a high-efficiency, solid-state SPS transmitter may be feasible. The study was performed by RCA Laboratories.

During the first phase of the study, the feasibility of replacing the microwave transmitting tubes with clusters of solid-state elements was assessed. This assessment was followed by an alternate approach in which a solar cell "blanket" is used to provide dc power to a distributed array of solid-state amplifiers having output power combined in space, still maintaining constraints of the reference system. The RCA conclusions were that the direct replacement entails an unacceptable weight penalty due to (1) the thermal control system required for the solid-state device substrate; (2) the low-voltage/high-current power distribution and conditioning system; and (3) the degradation of efficiency due to microwave power combiners required for high-power modules.

In addition, an experimental amplifier was built by RCA using a commercial FET. A maximum power-added efficiency of 58.5 percent with an output power of 3.05 watts and a gain of 6.8 decibels was achieved, as shown in figure III-49. The device was operated in class AB with the bias voltage optimized for maximum efficiency. Some improvement in power-added efficiency may be achieved by increasing the gain of the device. Further testing of this amplifier is planned as an in-house JSC activity.

126

TABLE III-13.- CHARACTERISTICS OF FOUR SOLID-STATE
DEVICES INVESTIGATED

Amplifier	Efficiency range, percent	Power output, W	Frequency range, GHz	Temperature, K (°C)
IMPATT diode[a]	20 to 37	3	3 to 300	473 (200)
TRAPATT diode	20	3	0.4 to 12	(b)
Bipolar transistor	40	40	3 to 4	373 to 398 (100 to 125)
Field-effect transistor[c]	68	.261	4	373 (100)

[a]Mean time to failure = 10^7 hours.
[b]Room temperature.
[c]Mean time to failure = 100 years.
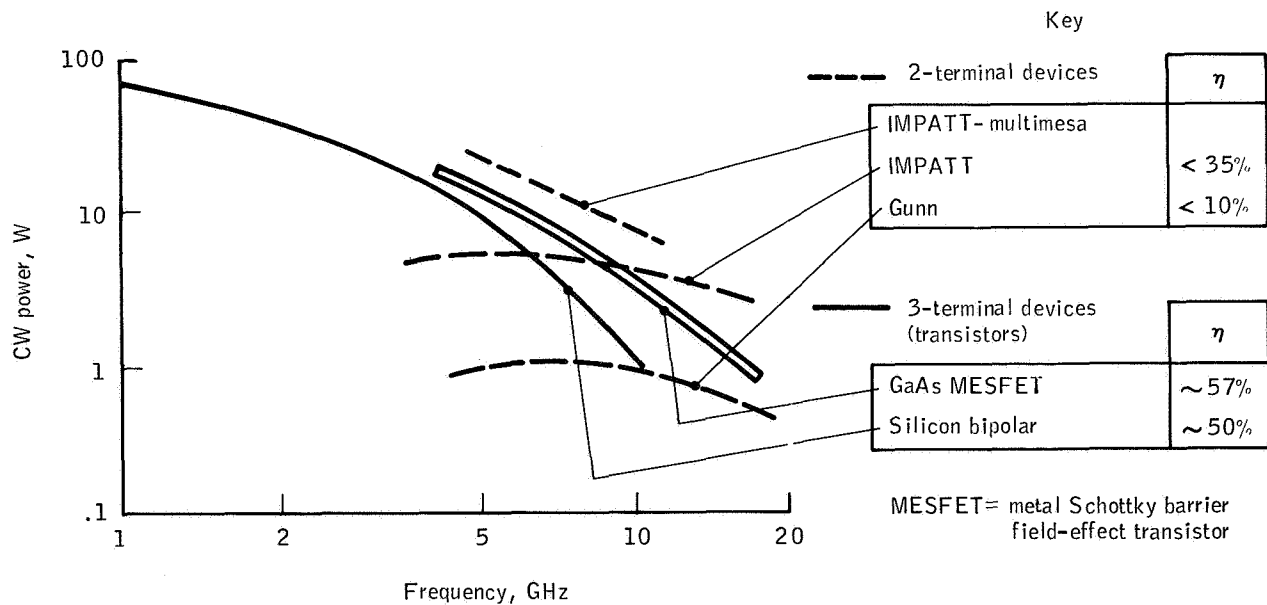
Figure III-48.- Solid-state CW power status for single packaged devices in 1978.
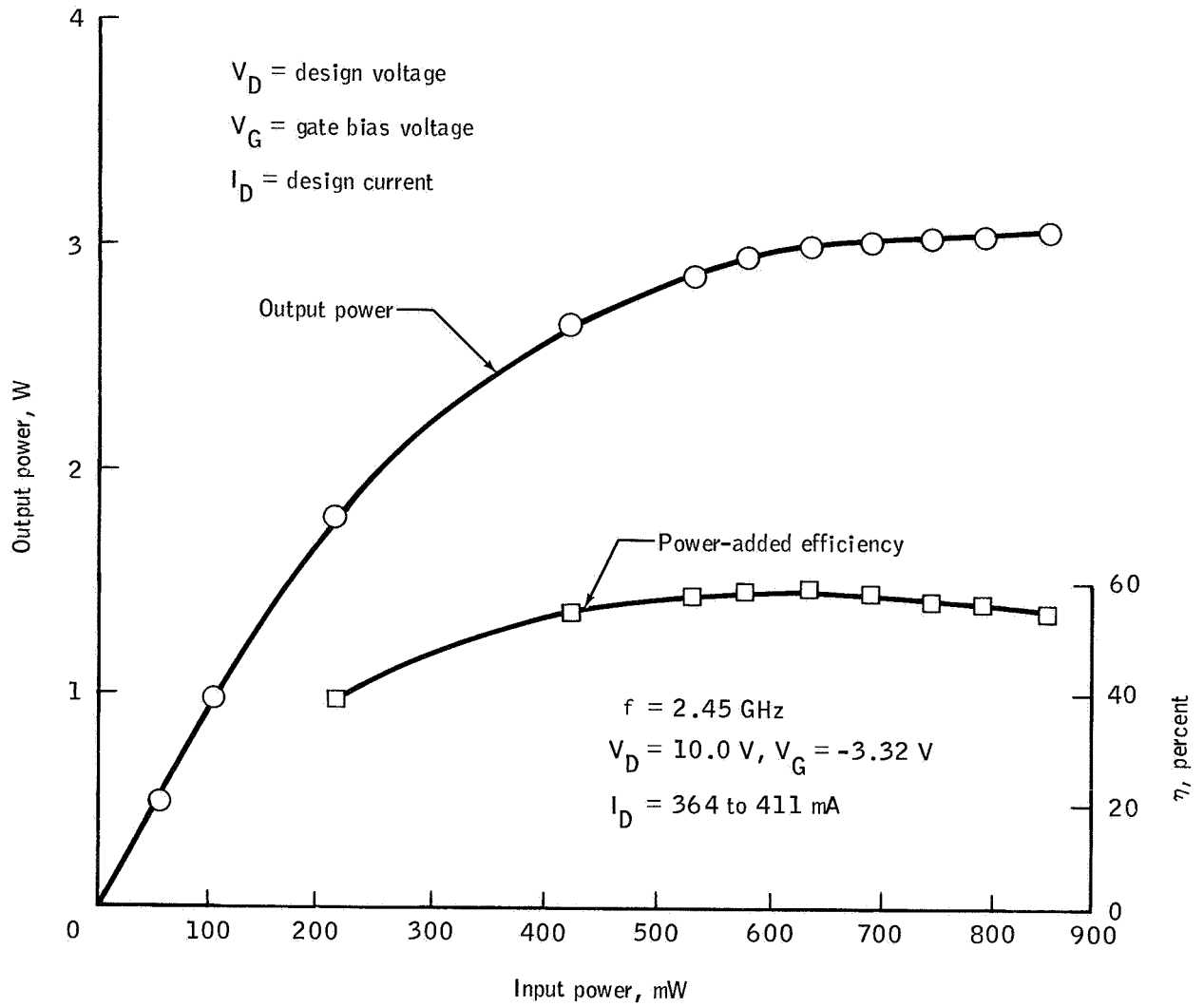
Figure III-49.- Output power and power-added efficiency η as a function of input power.

One of the important recommendations of this part of the study was the undertaking of a follow-on experimental and theoretical program to ascertain the factors contributing to high-efficiency operation of microwave FET's. Previous experience with specialized large-signal computerized equipment pointed to the benefits of using this equipment for the recommended follow-on program.

(1) <u>Antenna system investigations</u> - The reference system served as a basis for the first phase of the antenna system investigation. If an attempt is made simply to replace the thermionic devices contemplated in the reference system by clusters of solid-state devices the power of which is combined to form equivalent transmitting elements, penalties in voltage-distribution losses, power-combining losses, and thermal problems must be seriously considered. From detailed analyses performed during the study, it soon became apparent that a solid-state replacement program of this nature, although possibly contributory toward the overall reliability of the system, would fall short in terms of the operational parameters, particularly in terms of a factor of merit measured in watts per kilogram.

Emphasis was placed on a concept that incorporated direct conversion of sunlight into microwave power-generating modules and thereby obviated the need for voltage distribution altogether and essentially solved the potential thermal problem. Some specific problem areas peculiar to this approach were addressed in the study; e.g., the relative orientations of the solar array and the microwave antenna, the spacing of the antenna elements, and, most importantly, the near-field properties of such an antenna.

It was concluded that this type of system may be lighter than the reference system and that a tubular beam can indeed be created. Computer simulations of this type of antenna beam were performed at the conclusion of the study. Recommendations for adapting this approach, after further study, were made.

(2) <u>Module investigations</u> - The module study yielded the notion that the efficiency of the power module is the most important design parameter, since it directly affects the overall SPS cost in terms of dollars per watt of output power. Here again, power-combining losses and primary power-distribution problems pointed toward the concept of a system design in which low-power amplifier modules are directly powered by elements of the solar cell array. In such a system, the efficiency and weight penalties of a dc distribution system are not incurred. An analysis of the practical power limits placed the module power output somewhere between 0.5 and 30 watts, with the power-efficiency trade-off indicating an optimum value of 1.5 to 3 watts and an efficiency of 80 percent.

Two design concepts were developed in which modules were placed on a 1.3λ by 1.3λ grid, with 16-module clusters controlled by a single receiver module and providing 50 watts of transmitter power per cluster. As was the case with the device designs, both module designs (a "high Q" version and a "patch resonator" approach) were meant to represent the approach rather than to be specific. (See fig. III-50.)

129
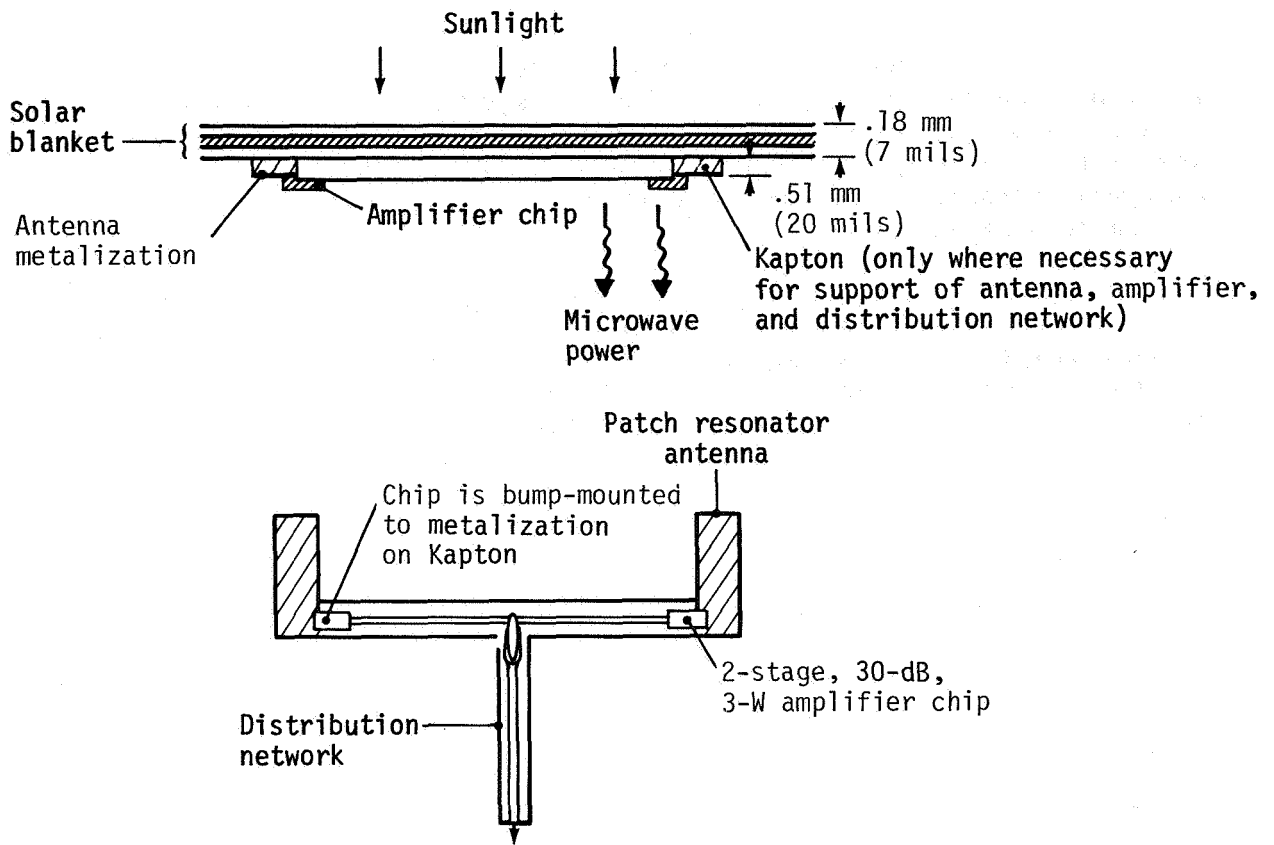
Figure III-50.- Patch resonator design.

130

(3) <u>Conclusions and recommendations</u> - The RCA study (ref. 9) yielded the following conclusions.

(a) It does not appear prudent to simply replace the klystrons in the reference system with equivalent clusters of solid-state devices.

(b) Real benefits can be obtained if the system architecture is designed for maximum compatibility with the operating parameters of solid-state microwave devices. This objective leads to a concept of direct use of the solar-panel-generated power by low-power microwave amplifiers, known as the sandwich concept.

(c) The postulated 80-percent power-added efficiency of the microwave amplifiers appears ultimately achievable. Gallium arsenide FET's are the logical device candidates for this service.

(d) Devices providing 4 watts at greater than 80 percent power-added efficiencies were considered feasible.

(e) The undertaking of a follow-on experimental and theoretical program to ascertain the factors contributing to high-efficiency operation of microwave FET's was recommended.

b. Amplifier Development Program

The NASA MSFC, through Rockwell International, sponsored the "SPS Solid-State Amplifier Development Program" (ref. 33), which was an extension of the effort performed as part of the JSC study; its main purpose was to gain a better understanding of the factors contributing to the high-efficiency performance of GaAs FET's. Large-signal waveform analysis techniques were a major investigative tool in the program.

The program consisted of the demonstration of an amplifier having an output power of 10 watts, a gain of 10 decibels, and a power-added efficiency of 65 percent. To date, a survey of available devices from a total of six domestic and foreign manufacturers of GaAs FET's has been made, and circuits using various devices are being built and analyzed as the transistors are received. Although "class E" operation is of interest for the SPS application because of its potential for very high efficiency, it is by no means certain that such a mode of operation can be obtained at microwave frequencies and the work under the program is not restricted to multipole operation of the FET's.

As previously mentioned, computer-aided analysis techniques are used extensively in the program, not only in the normal small-signal device characterization mode but also to define the available trade-offs under

131

large-signal operating conditions. Examples of such techniques are the automatic plotting of circles of constant efficiency, constant gain, constant power output, and constant intermodulation distortion on special instrumentation at RCA Laboratories. In addition, a technique has been demonstrated for synthesizing current and voltage waveforms under FET amplifier full operating power. This approach is also a powerful analytic tool in the investigation.

Although the effort is still in progress and any attempts at projections of final results are considered premature, some very significant findings have already been made. When optimized for maximum efficiency at the SPS frequency, a power amplifier stage using a transistor designed for 12-gigahertz operation yielded 71 percent power-added efficiency. This result was obtained at a power output of approximately 1 watt and a gain in excess of 11 decibels. The mode of operation can be described as an inverted class AB, since the drain current is highest at low rf drive and lowest at full rf drive: the rf voltage deactivates the device during a substantial fraction of the rf cycle; hence, the high efficiency. However, when the same type of operation was attempted with a transistor from the same manufacturer (but rated at somewhat lower power output at 12 gigahertz), low efficiency was observed at 2.45 gigahertz but power output was much closer to the rated value. These results are under investigation. The current and voltage waveform analyses are expected to clarify the hitherto unexplained aspects of this type of FET performance.

Power-combining circuits will be used in the final amplifier configuration. A study of such circuits is included in the program.

c. Technology Forecast

Solid-state technology is in a period of rapid growth in both the microwave and the signal-processing areas. Specific applications of this technology in a variety of spaceborne systems occur with increasing frequency and effectiveness. Interest in solid-state devices, components, and integrated circuits has been demonstrated, on the one hand, by the commercial computer industry for integrated-circuit logic components and, on the other, by the military systems for microwave solid-state devices. This trend is quite independent of the SPS concept. Thus, the solid-state SPS concept will derive benefits from the very large investments made in this technology.

The directions of technology research pertinent to the SPS concept span all fields familiar to the solid-state industry: materials, devices, circuits, processing methods, and automated test procedures. In the semiconductor materials area, gallium arsenide currently is the most important compound for microwave applications. The silicon-on-sapphire technology probably will provide an excellent base for selecting the SPS solid-state antenna substrate materials.

New device concepts in addition to the FET, which appears to be the best candidate for amplifiers at the SPS frequency, are the vertical FET and the power metal-oxide semiconductor (MOS) transistor, both of which are in advanced stages of exploration. The most important area in circuit development is the return to the concept of microwave lumped-circuit

132

design. Lumped circuits designed for operation at 2.45 gigahertz permit extreme miniaturization of the amplifiers and make large distributed antenna arrays feasible.

Finally, modern processing methods (e.g., ion-beam milling and plasma etching) should extend the techniques of the integrated-circuit chips to microwave circuits. Furthermore, the selective implantation of impurities by means of ion-implantation and laser-annealing techniques may enable the fabrication of monolithic components directly on semi-insulating gallium arsenide.

D. RADIATING ELEMENTS

The function of the radiating element is to couple rf energy from the power amplifier into a radiation field in space with a minimum of loss. Although the radiated power density across the total antenna is tapered to obtain appropriate beam forming, the individual radiating elements are required to launch a radiation field of uniform power density and phase. The antenna elements have been investigated only to the depth necessary to estimate weight and performance in support of system studies. Judicious judgments have been made, and various calculations and estimates have been performed. However, serious "design optimizations" have not been attempted.

1. CONCLUSIONS AND REMAINING ISSUES

The following conclusions have been reached.

a. Low-CTE materials are required to hold mechanical tolerances to the levels required for an efficiency of 96 percent. An aluminum-graphite metal matrix is a leading candidate.

b. A phased array using slotted-waveguide techniques is the most efficient radiator for large power blocks.

c. High-voltage breakdown in radiating slots and distribution waveguides is not expected to be a problem at geosynchronous altitude. However, study should be continued to determine the extent to which the SPS produces an atmosphere.

d. Linear polarization is preferred for simplicity, and analyses show that Faraday rotation does not produce a significant loss.

e. Improved techniques (for measuring absolute radiated power), equipment, and analysis will be required to verify system performance.

The significant issues remaining to be resolved for the radiating element are as follows.

a. Determining a practical design goal for efficiency considering mass production techniques and their inherent tolerances

b. Developing suitable low-CTE material capable of maintaining the required tolerances in an operational environment

c. Developing receiving techniques for the pilot signal to provide adequate isolation and acceptable transmit loss

d. Developing rf measurement technology capable of evaluating ultra-high-efficiency components economically

2. REFERENCE DESIGN DESCRIPTION

The subarrays are the basic power-radiating elements of the transmitter (ref. 34). There are 10 types of subarrays corresponding to the 10 power intensity levels of the illumination taper. These 10 types use the same equipment, but the arrangement and numbers of equipment elements vary with the number of klystrons. (See fig. III-51.)

The radiating waveguide, at the subarray level, is composed of 120 waveguide sticks that are 10.43 meters (60 guide wavelengths λ_g) long. The method of attaining various numbers of module units per subarray is to install internal short circuits (conducting walls) within the sticks and to distribute rf power, from each klystron, with the distribution waveguides to the desired number of waveguide sticks. In this manner, it is possible to obtain 10 types of subarrays, ranging from 36 to 4 klystrons per subarray to achieve the desired power taper. The integral radiating waveguide forms a subarray unit 10.43 meters square, which remains unchanged throughout the array and is based on realizable mechanical tolerances and acceptable error plateau levels.

The distribution waveguides feed power from the klystron output waveguide to the radiating waveguide. The distribution-waveguide sticks are arranged in pairs, each one distributing half of the rf power from a given klystron module. The arrangement of klystrons and rf power-distribution waveguides was selected to minimize continuous stick length subject to the constraint that the length of each stick must be an integral number of wavelengths. Short circuits within the sticks establish the length of each radiating element. Minimizing stick length provides three advantages: reduced sensitivity to temperature; greater slot offset, which reduces scattering-loss sensitivity to tolerances in slot offset; and reduced rf I^2R losses. The geometries of the subarray types are illustrated in figure III-51. All subarray types except type 6 employ a split klystron output to minimize active stick length. The active stick length must be an even multiple of guide wavelengths. The total stick length for a subarray is 60 guide wavelengths, which is not evenly divisible by 8. Therefore, the type 6 subarray, which contains four klystrons along the stick runs, may not use power splitting at the klystron output port. This type subarray will contain single

134
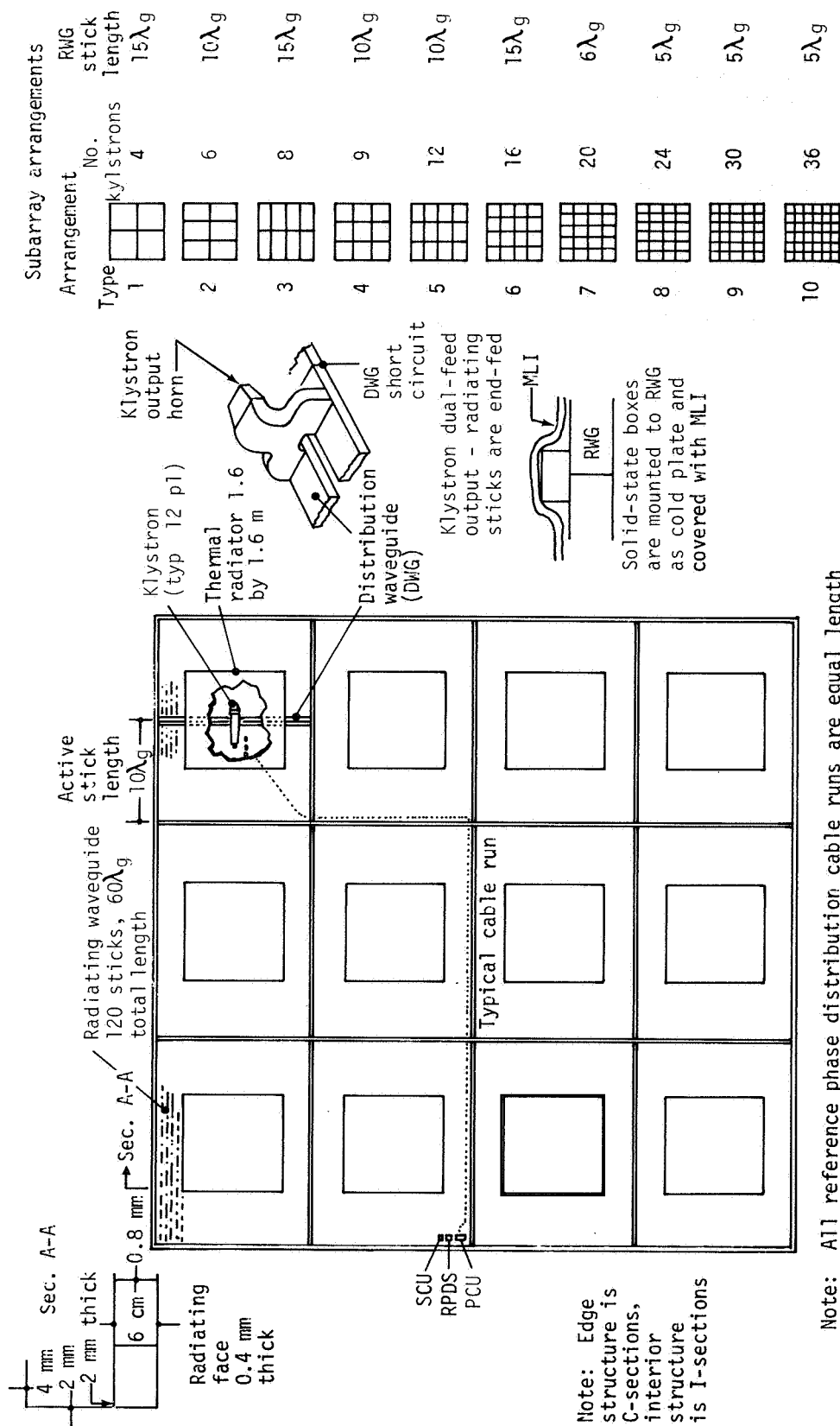
Figure III-51.— Diagram of reference design subarray (type 5).

Subarray arrangements

Arrangement Type	No. kylstrons	RWG stick length
1	4	$15\lambda_g$
2	6	$10\lambda_g$
3	8	$15\lambda_g$
4	9	$10\lambda_g$
5	12	$10\lambda_g$
6	16	$15\lambda_g$
7	20	$6\lambda_g$
8	24	$5\lambda_g$
9	30	$5\lambda_g$
10	36	$5\lambda_g$

Note: Type 6 uses single-feed output

Klystron output horn

Klystron (typ 12 pl)

Thermal radiator 1.6 by 1.6 m

Distribution waveguide (DWG)

DWG short circuit

Klystron dual-feed output – radiating sticks are end-fed

MLI

RWG

Solid-state boxes are mounted to RWG as cold plate and covered with MLI

Radiating waveguide 120 sticks, $60\lambda_g$ total length

Active stick length $10\lambda_g$

Typical cable run

Sec. A-A

0.8 mm

SCU
RPDS
PCU

Sec. A-A

4 mm
2 mm
2 mm thick

6 cm

Radiating face 0.4 mm thick

Note: Edge structure is C-sections, interior structure is I-sections

Note: All reference phase distribution cable runs are equal length

SCU = signal-conditioning unit
RPDS = reference phase distribution system
PCU = power control unit
RWG = radiating waveguide
MLI = multilayer insulation

135

klystron outputs feeding 15 guide wavelength sticks, each containing 30 slots. The radiating-waveguide faces are 0.4 millimeter thick, the stick dividers are 0.6 millimeter thick, and the distribution waveguide is 0.8 millimeter thick.

The subarray distribution and radiating waveguides are assumed to be fabricated from graphite/aluminum metal-matrix composites. The structure members are a high-temperature graphite plastic-matrix composite. Solid-state components are mounted on the radiating-waveguide assembly under multilayer insulation so that the radiating waveguide serves as a cold plate. In addition, thermal insulation is used to force the klystron heat-rejection system to radiate only out the backface of the antenna; by this means, the thermal environment for the solid-state components is also improved.

3. WAVEGUIDE PARAMETERS AND PERFORMANCE

An analysis of efficiency factors as a function of mechanical tolerances was conducted for a reference system configuration which consisted of radiating-waveguide lengths between $10\lambda_g$ (1.65 meters) and $30\lambda_g$ (4.96 meters), for which the weighted average length was $16.7\lambda_g$ (2.76 meters) (ref. 14). Thus, the guide length used for the analysis was the $16.7\lambda_g$ (2.76 meter) unit. For most cases, this was an iterative process in which a reasonable mechanical tolerance was selected and the resultant loss calculated. Tolerance and loss were then adjusted as considered appropriate. The efficiency factors thus developed are listed in table III-14 and discussed briefly in the following paragraphs. This tolerance budget includes both manufacturing and operating errors and has led to the conclusion that low-CTE materials will be required to meet SPS design goals.

a. Subarray Tolerances

The mechanical tolerances for each subarray which contribute to systems losses are surface flatness, subarray average tilt, and gaps between subarrays. Errors in surface flatness and gaps between subarrays produce scattering into the side-lobe area. Subarray tilt produces a decrease in gain for the subarray in the direction of the target.

(1) Subarray surface - A power loss of 0.5 percent was budgeted for subarray surface flatness. Using the theory of Ruze, this loss requires an rms surface error of 0.127 centimeter.

(2) Subarray tilt - A power loss of 0.4 percent was budgeted for subarray tilt. This loss translates into an edge-to-edge offset of 0.254 centimeter.

(3) Gap between subarrays - The vast size of the SPS antenna and the overall flatness requirement, together with thermal and steering stresses, require some form of stress relief (i.e., gaps) between the subarrays. The gaps represent "unfilled" aperture and thus contribute to gain loss in the main beam and scattering of the lost energy into the side-lobe areas. A gap of 0.64 centimeter between the subarrays was budgeted. This gap produces an efficiency loss of 0.13 percent.

136

TABLE III-14.- SPS SUBARRAY LOSSES AND DIMENSIONAL TOLERANCES

Dimension	Tolerance, mm	Efficiency loss,[a] percent
Subarray surface	±1.27	0.50
Subarray tilt	2.54	.40
Gap between subarrays	6.35	.13
Radiating guide		
Length	±.76	.02
Width	±.08	.12
Slot offset	±.16	.10
Feedguide		
Length	±.76	.02
Width	±.08	.03
Coupling	(b)	.10

[a]Total loss = 1.42 percent.
[b]Not available.

b. Radiating-Element Tolerances

The losses in the radiating element consist of I^2R losses and mismatch and scattering losses. An attempt has been made to minimize the primary variable associated with I^2R losses: the path length between the power tube and the radiating slots. Scattering and mismatch losses result from mechanical errors in waveguide length and width and errors in slot placement.

(1) Waveguide length and slot spacing - Errors in slot position relative to the standing wave in the radiating "stick" produce an impedance mismatch at the slot and hence contribute to voltage standing-wave ratio (VSWR) loss at the feedpoint. Errors in slot placement within an ideal radiator would tend to vary slightly about the desired location and thus contribute an insignificant amount to system losses. However, an error in the length of the radiating guide would tend to produce the effect of offsetting all slots in the same direction. Thus, the slot mismatch would be accumulative at the feedpoint. A 0.76-millimeter tolerance for the guide length is calculated to produce a loss of 0.02 percent.

(2) Waveguide width - A change in waveguide width produces a change in the propagation factor within the waveguide. Thus, an error in waveguide width produces an apparent error in waveguide length; the loss consists of reflected power at the feedpoint. An allowable tolerance of 0.08 millimeter contributes a loss of 0.12 percent.

(3) Slot coupling - The reference design consists of longitudinal slots for which the coupling is controlled by the offset of the slot from the guide centerline. Errors in the slot offset will produce a variation in the power radiated by the slot. The resultant amplitude variation over the antenna produces a scattering loss. A 0.16-millimeter tolerance is projected to produce a 0.1-percent efficiency loss for the antenna.

(4) Feedguide tolerances - The loss due to coupling variation in the feedguide slots was not estimated. This effect would be similar to the variation in radiating-slot coupling which produces scattering due to amplitude variation. A loss factor for this effect equal to that of the radiating-slot coupling error is included in table III-14. The corresponding tolerance for feedguide slot configuration is not available.

(5) Thermal distortions - Thermal environment varies radially over the antenna because of the radiated power taper and also because of the 24-hour antenna rotation, seasonal variations, and eclipses. Thermal expansion will produce changes in both guide length and guide width. These distortions then produce losses in the same manner as that allowed for mechanical tolerance. An aluminum waveguide with no tolerance errors would have an efficiency loss of 1.4 percent when elevated in temperature by 55 K (55° C). A similar waveguide with a low-CTE material would drop only 0.2 percent in efficiency for the same conditions.

(6) <u>Losses from I^2R</u> - Boeing has measured the I^2R losses for a $10\lambda_g$ radiating element by closing off the slots and evaluating the reflected power at the input terminal. The implied I^2R loss was 1.2 percent (ref. 35). Raytheon also evaluated I^2R losses for a $4\lambda_g$ radiator by means of measuring the actual thermal losses (ref. 36). Their result was 1 ± 0.1 percent for this unit.

Methods available for calculating the I^2R losses in a resonant waveguide radiator should be implemented when possible. These losses are obviously larger than the standard waveguide transmission losses and would tend to increase with larger antenna element size. However, a 2-percent loss budget is considered to be a reasonable estimate for this efficiency factor. Refinements in the antenna design are probably required to attain this performance level.

c. Receiving-Technique Evaluation

The receiving antenna receives a pilot signal from Earth with phase information to keep all modules in phase (ref. 37). For symmetry, the pilot signal should originate from the center of the SPS Earth rectenna. Because of ionospheric phase shift and Faraday rotation, the pilot signal should be centered on the SPS power frequency with the phase information in symmetrically disposed sidebands. The purposes of the receiving-technique evaluation by Boeing were as follows.

(1) To compare shared antennas with separate receiving antennas to determine feasible pilot-beam budget and receiving-antenna constraints due to power module efficiency, bandwidth, and isolation consideration

(2) To design and select a pilot-beam receiving-antenna technique compatible with a power beam array configured for simultaneous transmission of the S-band power beam and reception of the pilot-beam spread-spectrum signal

The pilot-beam link analysis established that very small, low-gain pilot receiving-antenna elements embedded in the transmitting array are significantly superior to any scheme of diplexing, because (1) the total system power losses are two orders of magnitude lower with a separate antenna than with any state-of-the-art diplexing device; (2) the small antenna, because of its inherent broad bandwidth, is fully compatible with a spread-spectrum signal, whereas the transmit array is not; and (3) the small, low-gain antenna represents a much lower development risk compared to a diplexing device.

Also from the pilot-beam link analysis, formulations were developed from which to determine values of pilot-transmitter power and antenna aperture as well as pilot receiving-antenna aperture. The transmitter power and aperture depend primarily on the requisite pilot-link effective radiated power (ERP). The ERP, in turn, depends on the signal-to-noise requirement of the pilot-link receiver and, hence, the noise environment in

139

which the receiving system must operate. Consequently, the ERP requirements were found to be extremely sensitive to the cutoff frequency of a required receiver i.f. notch filter.

The relationship between pilot-transmitting-antenna diameter and system power loss (efficiency) is not monotonic, because an increase in the antenna diameter produces two opposing effects: the amount of pilot-transmitter power required to produce the requisite ERP is reduced while, simultaneously, the degree of rectenna blockage is increased. At low diameters, the transmitter-power effect dominates and the loss decreases with increasing diameter, whereas at larger diameters, rectenna blockage becomes most important and the system loss increases with increasing diameter. Thus, for a particular ERP, there is a rather limited set of pilot-transmitter power/aperture combinations that give minimum system loss.

For small apertures, an increase in aperture reduces system losses due to a decrease in the required ERP. At large apertures, the system losses increase with increasing aperture, because of receiving-antenna blockage of the spacetenna. The specific nature of this relationship depends on the required signal-to-noise ratio in the pilot receiver and also on the bandwidth of the intermediate-frequency notch filter. As S/N is increased, the pilot ERP must increase and so also must the system losses. As bandwidth is increased, more of the power transmitter noise spectrum is passed by the receiver i.f. This increase in noise must be overcome by an increase in pilot-link transmitter power.

The optimum receiving aperture, under any foreseeable conditions, is quite small. Consequently, the pilot-link receiving-antenna requirement can be satisfied by a simple dipole or slot antenna. These antennas may be dimensioned to be either resonant or nonresonant. The aperture of the resonant structure is larger but so also is the effect on the impedance of the neighboring transmitting-antenna radiating slots. To the extent that the lower aperture can be tolerated, the nonresonant structure is preferred.

An important consideration in the pilot-link design is the isolation of the pilot receiver from noise inherent to the high-power downlink beam. With the dipole, isolation can be improved by rotating the receiving antenna so that it is cross polarized with respect to the power transmitting antenna. These are separated by $\lambda_0/4$, where λ_0 is free-space wavelength, and can therefore be connected to pass, as would a directional coupler, radiation coming from the Earth while rejecting local radiation.

One of the candidate receiving antennas, the slot, or "credit card" receiving antenna, has been built and sweep-tested. It consists of a 4.44- by 0.16-centimeter Teflon-glass microcircuit board short-circuited around three edges to form a low-impedance waveguide cavity. Radiation patterns were measured for this configuration mounted in a laboratory model of a 10- by 20-slot waveguide antenna (10 waveguide radiators, 20 slots per guide). Scalloping of the receiving-antenna pattern indicated considerable mutual coupling between that antenna element and the waveguide slots. Isolation measurements are not available. The evaluation of a cross-polarized receiving antenna should be implemented in any program continuation.

140

4. VARIATIONS ON WAVEGUIDE TECHNIQUES

The reference design described is rather conservative in "assumed" construction techniques and possibly also in materials weight. Certainly, this "design" can be improved by judicious iterations of waveguide cross section, feedguide cross section, slot placement, and possibly a higher degree of aperture sectioning.

The resonant cavity radiator (RCR) concept developed by Rockwell is a potential technique for reducing losses, and Raytheon has developed a promising waveguide fabrication concept. These two subjects are discussed in more detail in the following paragraphs.

a. Resonant Cavity Radiator

The RCR has been investigated by Rockwell as a potential radiating element for the SPS (ref. 38). This concept has the potential for improving antenna efficiency and reducing antenna weight. However, the realization of this potential remains to be demonstrated.

(1) Basic principle – Conventional waveguide designs such as the transverse electric TE_{10} mode waveguide slotted array make tube installation fairly complex. To solve the resultant temperature interface problem and possibly increase the rf efficiency of the radiator, Rockwell developed the resonant cavity box excited with the TE_{mo} mode, where m can be varied between 1 and approximately 10. Physically, the RCR is a conventional standing waveguide radiator with the common walls removed. The RCR has three significant potentials: improvement in efficiency; lighter weight; and simpler structure, which enables integration of the RCR with the rf tube to alleviate the thermal interface problem.

(2) Theoretical attenuation estimates – The loss mechanisms of the RCR can be best explained by comparison to conventional arrays. The typical flat-plate antenna array is formed by side-by-side placement of several rectangular waveguide sections, as shown in figure III-52.

The mode that propagates down each waveguide is the dominant TE_{10}. The currents that flow in adjacent sidewalls are flowing in the opposite direction, and, because the system is symmetrical, they are of equal magnitude. If the sidewalls are removed as in the RCR, these two equal and opposite currents cancel. Since conduction losses are simply I^2R losses, any reduction in surface currents will make the antenna array more efficient.
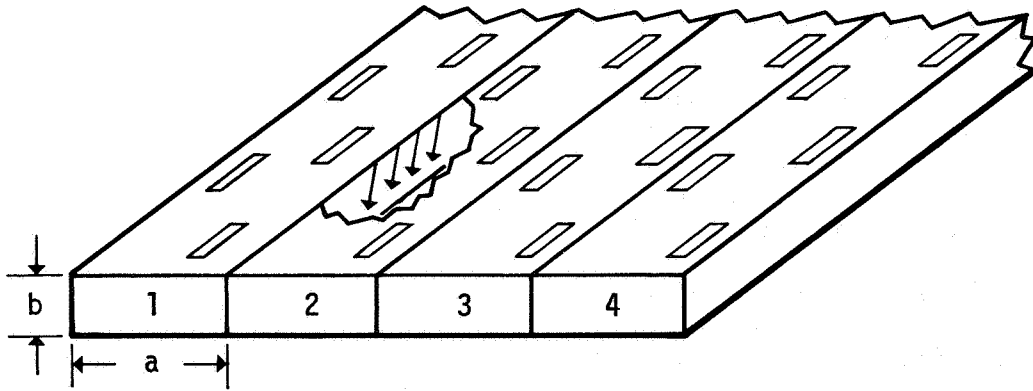
Figure III-52.- Typical TE_{10} slotted-waveguide array.

The closed-form analytical expression for conduction losses (decibels per meter) for a silver-plated RCR supporting the TE_{mo} modes is given as:

$$\alpha_c = \frac{2.8738 \times 10^{-2}}{b\sqrt{1 - \frac{m\lambda_o^2}{2a}}} \left(1 + \frac{2b}{a}\frac{m\lambda_o^2}{2a}\right) \tag{23}$$

For an a dimension of 11.319 centimeters (4.450 inches) and a b dimension of 5.40 centimeters (2.130 inches), the losses have been calculated from equation (23). For a typical array length of 2.5 meters, a TE_{70} RCR has the potential of saving 4.3×10^6 watts of power in a 5-gigawatt system. Antenna weight saving is achieved by two design features: (a) the RCR is designed with no sidewalls with the exception of the cavity walls and (b) the RCR can be designed to be structurally integrated with a magnetron or klystron heat dissipator because of the simplicity of the structure.

(3) Measurement results – One of the primary uncertainties with the RCR is the suppression of higher order modes. One of the easiest ways of detecting the existence of higher order modes is by observing radiation patterns. Higher order modes will collimate in off-boresight locations and cause null filling and higher side lobes. Rockwell developed special feed techniques which led to the reduction of higher order modes. To prove that the technique does suppress higher order modes, scaled tests were conducted. A TE_{70} RCR was fabricated and tested. The RCR was uniformly excited for a -13-decibel peak side-lobe level. Measured side-lobe levels in the E and H planes were -13 decibels for good correlation. Off-axis patterns also were taken at predicted higher order mode locations. No existence of higher order mode propagation was found. These tests were performed on a limited scale; however, that the RCR has a potential for improving array efficiency was definitely proved.

b. Thin-Wall Slotted-Waveguide Array Fabrication

The method for forming thin-walled slotted-waveguide arrays described herein grew out of a necessity to narrow the broad range of estimated cost for slotted-waveguide arrays in ground-based arrays (ref. 39). In most items that are designed for automated production, the cost of the material is the dominant element of cost. Therefore, the use of thin material is attractive because of the large reduction in material cost. Then, if a rapid, inexpensive method of fabrication can be devised, the cost of the slotted-waveguide arrays will be low and can be accurately estimated.

Such a fabrication method has been devised in principle by Raytheon. Working models of the design were built as part of a contract with JPL for the improvement of microwave beamed power technology, using a slight modification of their electrical design for such an array.

143

The working models that were made from 0.51-millimeter (0.020 inch) material were mechanically strong and the fabrication technique was well adapted to even thinner material. The potential for a slotted-waveguide array made from 0.13-millimeter (0.005 inch) or even thinner material for the SPS applications is very good.

The slotted-waveguide array consists basically of a folded top plate the corrugations of which contribute the three sides of the waveguide and a bottom plate into which the radiating slots are punched (fig. III-53). The two sections then flow together and are joined either by resistance spotwelding or by laser-beam welding to form the finished assembly (fig. III-54).

The holes punched into the material are spaced accurately and serve to accurately locate the material in the bending fixture, which is also accurately machined and ground. The holes also are used to aline the top and bottom halves for accurate assembly.

It is possible that the broad faces of the waveguide members, both top and bottom, may need some stiffening to avoid bending and "oil canning." The thin, flat channels that are proposed to house the phase and amplitude references and auxiliary powerlines stiffen the slotted surface. The unslotted surfaces could be embossed for stiffening.

The individual slotted waveguides in the array are fed from a feed waveguide. Transfer of energy is made through diagonal slots between the feed waveguide and radiating waveguides. The feed waveguide is attached to the array by means of pop rivets.

Pattern measurements conducted by JPL indicate little scattering of power into the side-lobe areas, although the measured gain was somewhat low and indicated an efficiency in the 80- to 90-percent area. Raytheon subsequently measured the thermal dissipation within a similarly constructed four-slot array quite accurately. This test implied an I^2R loss of 1 ± 0.1 percent, which is consistent with budgeted losses for this area.

The JPL/Raytheon data are in the same general area as those obtained by Boeing for a larger (10 by 20 slot) test model. The raw data for the Boeing test indicated an efficiency of slightly less than 90 percent for measured gain compared to physical area. The Raytheon/JPL fabrication concept is considered a promising technique.

5. HIGH-ACCURACY MEASUREMENT TECHNIQUES

An excellent example of state-of-the-art antenna measurement techniques is the improved calibration of the NASA/JPL Deep Space Network S-band antennas (ref. 40). This calibration was performed by JPL and the National Bureau of Standards. In the course of the program, NBS calibrated standard-gain horns using a "modified three-horn technique." This calibration was accomplished to an accuracy uncertainty of ±0.036 decibel. Then, JPL was able to perform a "gain comparison" measurement between the NBS-calibrated horn and a similar "working horn" with an uncertainty of ±0.025

144
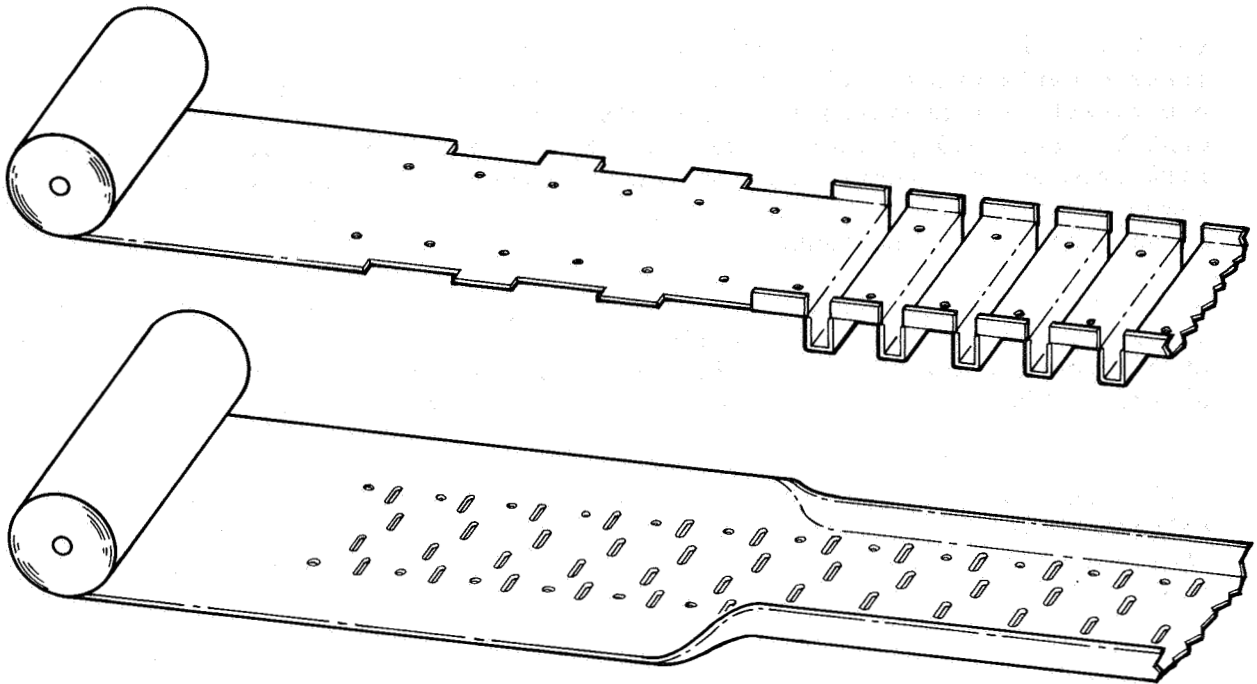
Figure III-53.- Thin-wall waveguide array fabrication concept.

Pointwelds
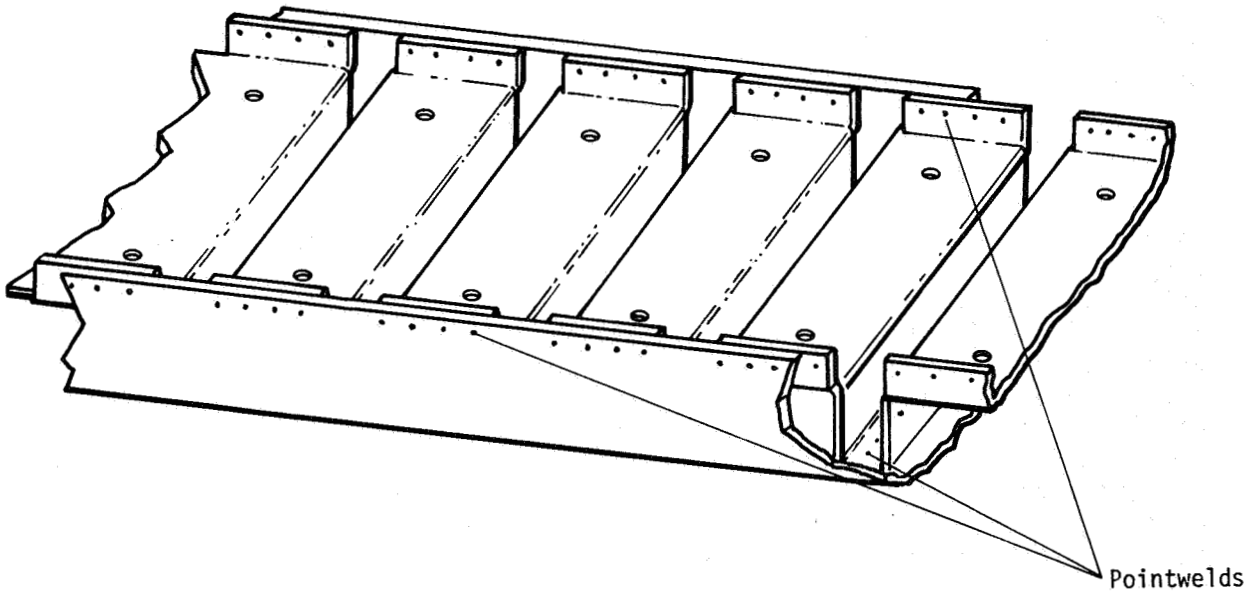
Figure III-54.- Thin-wall waveguide array assembly concept.

decibel. The end accuracy was taken conservatively as the simple sum of these uncertainties, 0.061 decibel. In terms of percentages, these numbers are direct gain measurement by NBS, ±0.7 percent; and gain transfer measurement by JPL, ±0.5 percent. These are by no means routine tests and cannot be performed on the average antenna range. However, it appears reasonable to assume that selected samples of SPS radiating elements can be evaluated to an accuracy of 0.5 percent.

Georgia Institute of Technology has studied the problem of measuring the performance of a 10- by 10-meter SPS subarray to an accuracy of 1 percent (ref. 41). Both far-field and near-field techniques were considered. The error budgets used are given in tables III-15 to III-17.

This set of error budgets implies development of improved precision attenuators, gain standards, stable oscillators, and computer normalization for a far-field measurement. Near-field measurements require development of precision scanner mechanisms, calibrated field probes, and computational techniques.

Because of the large electrical size of the SPS subarray and the requirement for high-accuracy measurements, specialized measurement facilities are required. Most critical measurement error sources have been identified for both conventional far-field and near-field techniques. Although the adopted error budget requires state-of-the-art advances in microwave instrumentation, the requirements appear feasible based on extrapolation from current technology. Additional performance and cost trade-offs need to be completed before the choice of the preferred measurement technique is finalized.

E. RECTENNA

The function of the rectenna in the SPS system is to convert the downcoming microwave power beam to electrical grid power. Because of its large physical size (i.e., a typical rectenna site is a 10- by 14-kilometer ellipse) and element composition (many repetitive components), the projected cost savings of automatic mass production are of prime importance. The fundamental processes at the rectenna consist of rectifying the incident rf field into dc using Schottky barrier diodes, filtering the rectified output, and combining and processing the output to higher voltages for distribution. Hierarchical combination and processing of currents is done several times to integrate the relatively low power per diode to electrical grid power magnitudes. Provisions for power control for equipment protection and load management exist at each step in the hierarchy (ref. 42).

The reference configuration described in Section III.E.1 is based on the rectenna element design developed by Raytheon and NASA over the past several years. This concept has been proved capable of achieving the high efficiency required for an SPS. However, the projected rectenna cost is an important factor in the SPS economics, and investigation of alternate concepts should be continued in the interest of reducing cost.

TABLE III-15.- MEASUREMENT ERROR BUDGET

Error source	Components	Allowable value,[a] dB	Comments
Antenna range	Field uniformity Quadratic phase error Extraneous reflections Standard-gain antenna uncertainty Atmospheric effects	0.036	Adequate gain standard not yet identified Reference receiver must be normalized for effects of atmosphere
	Axial ratio		
Structural/environmental	SPS antenna rigidity/stability Positioner error Wind loading/thermal	.01	Wind loading/thermal variation can be controlled by radome over test antenna
Transmitter	Amplitude stability Frequency stability	.01	Phase-locked techniques and temperature stabilization must yield amplitude stability of 0.007 dB
Receiver	Precision attenuator uncertainty Reference input phase/amplitude errors Signal-to-noise (S/N) ratio Frequency stability Dynamic range Detector linearity VSWR	.01	Attenuator calibrated to 0.005 dB S/N ratio must exceed 40 db Detector calibration can exceed 0.005 dB VSWR kept below 1.05 dB

[a]Total root-sum-square error = 0.04 decibel.

147

TABLE III-16.- ANTENNA RANGE MEASUREMENT
ERROR SUBBUDGET

Error component	Allowable value,[a] dB	Comments
Field uniformity	0.015	Maximum amplitude taper at edge of SPS subarray ≈ 0.04 dB
Quadratic phase error	.010	Requires range greater than [b]$6D^2/\lambda$
Standard-gain antenna uncertainty	.020	Development of gain standard needed
Atmospheric effects	.005	Atmospheric effects canceled by reference
VSWR	.005	VSWR loss canceled by calibration
Extraneous reflections	.025	Extraneous reflections below -57 dB

[a]Root-sum-square error subtotal = 0.037 decibel.
[b]D = antenna diameter.

TABLE III-17.- ERROR SUBBUDGET FOR RECEIVER ELECTRONICS

(a) Allowable SPS errors

Error source	SPS error budget,[a] dB	Comments
Linearity	0.005	Microcomputer calibration required
i.f. amplifier drift	.002	Temperature stabilization and microcomputer calibration required
Cable losses	.002	Precision amplitude reference will normalize cable loss variations
Crosstalk	.003	Microcomputer compensation required
Amplitude resolution	.001	17-bit parallel binary code decimal receiver outputs required for 0.001-dB resolution
S/N ratio	.005	Narrow i.f. bandwidth required to extend dynamic range
Line voltage variation	.001	Voltage regulation and microcomputer compensation required
Precision i.f./rf attenuators	.005	Microcomputer compensation may be required
VSWR	.002	All VSWR's maintained below 1.05 dB and/or canceled by calibration

(b) State-of-the-art performance[b]

Error source	Performance
Linearity, dB per 10 dB	0.05
i.f. amplifier drift, dB/K	0.05
Cable losses, percent/K	0.2
Crosstalk, dB for 40-db difference between channels	0.1
Amplitude resolution, dB over 80-dB dynamic range[c]	0.1
S/N ratio, dB for S/N = 60 dB	0.01
Line voltage variation, dB for 1-percent change in line voltage	0.02
Precision i.f./rf attenuators, dB for 10-dB steps	±0.2
VSWR, dB for VSWR = 1.3:1	0.15

[a]Total root-sum-square error = 0.01 decibel.
[b]Data based on Scientific Atlanta (S/A) 1711 and 1770 receivers.
[c]Data based on S/A 1832A amplitude display unit.

The following conclusions have been reached regarding the SPS rectenna.

1. The rectenna concept (individual antenna elements feeding directly into a rectifying circuit) has been shown by analysis and research to be the most technically effective and economically feasible rf-to-dc power converter for providing electrical power.

2. Analysis of rectenna collection techniques indicates that parallel and series combining inefficiencies are nearly identical.

3. It is preferable, from the standpoint of combining inefficiencies, to combine rectenna power in concentric rings rather than in continuous rows.

4. High power output at a long range with high combined collection/conversion efficiency has been demonstrated with a rectenna design that is tolerant to angle of incidence, temperature, polarization, flux density levels, and load resistance magnitude changes.

Remaining issues which must be resolved in the SPS rectenna development are

1. Maintaining an acceptable level of reradiation at fundamental and harmonic frequencies during normal operation and failure modes

2. Developing a mass production technique which maintains the required efficiency at an acceptable cost

3. Developing required environmental protection designs which do not degrade performance beyond acceptable limits

4. Developing appropriate rectenna topology with acceptable losses

5. Developing rf measurement techniques and equipment with required accuracies

1. REFERENCE CONFIGURATION AND PERFORMANCE

The reference configuration consists of half-wave dipoles with a capture area of 70 square centimeters (typical) providing between 1 and 2 watts per diode at the center of the rectenna (ref. 42). Dipole arrays that are more directional must be used toward the rectenna edge to limit power density to $\simeq 1$ mW/cm^2; for instance, a four- by four-dipole array would again provide 1 watt per diode. Care must be exercised to avoid selecting an excessively large array, which would pose problems of directional reception and increased losses in the rf collection lines. In the reference design, the dipoles and their associated power and microwave circuitry are integrated

inside an aluminum environmental shield and support structure, which is amenable to mass production methods (figs. III-55 and III-56).

A representative rectenna design at 35° latitude is described, characterized by a Gaussian tapered beam with a peak incident microwave power density of 23 mW/cm^2. Power is collected out to the point at which the interception efficiency is 95 percent. The basic receiving element is a dipole above a ground plane. The dipole assembly also contains a filtering and matching circuit to match the dipoles to the incoming wave with a reflection coefficient of better than -20 decibels. It is assumed that all dipoles are identical throughout the rectenna. The number of dipoles in the rectenna is approximately 1.3×10^{10}. These dipoles are mounted in a 7.9-centimeter (0.64λ) triangular array format.

Component designs for the rectenna are varied to most effectively match the incident power flux in 10 rings. Basically, all microwave system components of a given type are similar within a ring. However, power busing and control segmentation at the 5- to 10-megawatt power level and above extends across ring boundaries. Local dc voltages on the panels are designed to not exceed ±3.25 kilovolts. The geometry of the ring layout is illustrated in figure III-57.

Because of the power density variation over the rectenna aperture, a single type of radiating element or a single type of rectifier will not provide optimum conversion efficiency. Either a number of radiating-element types or a number of diode types must be provided. Currently, one type of diode operated with four different types of antenna elements is assumed. Besides the dipole element just described, antenna elements are formed by using the basic dipoles in arrays containing two, four, or eight dipoles. The corresponding assemblies are called types 1, 2, 3, and 4 receiving arrays. There are approximately 7.654×10^9 receiving arrays (diode assemblies) in the overall rectenna.

The receiving arrays are combined into panels, which are the smallest assembly units from the fabrication point of view. The panel area selected was 10 square meters, with a north-south (N-S) plane dimension of 3 meters and an east-west (E-W) plane dimension of 3.33 meters. It is assumed that all panel sizes are identical; therefore, 7 060 224 panels are required in the rectenna. There are four different types of panels, corresponding to the four different types of receiving arrays. Although the dipoles and the diodes are identical for all panels, the combining-matching-filtering circuits and the diode wiring are of four types. These panel types are illustrated schematically in figure III-58.

Units are combined from panels in such a manner that nominally 1000 panels are in one unit and the N-S dimension of a unit is always $32 \times 3.662 = 117.18$ meters. The number of panel rows in the N-S plane is always 32, which allows a standardization of the unit layouts to a minimum of 7 types. The N-S dimension of the units is standardized to 117.18 meters everywhere within the rectenna, and only the E-W dimension of the units varies from ring to ring (ref. 42). The wiring layout for the seven unit types is shown in figure III-59.
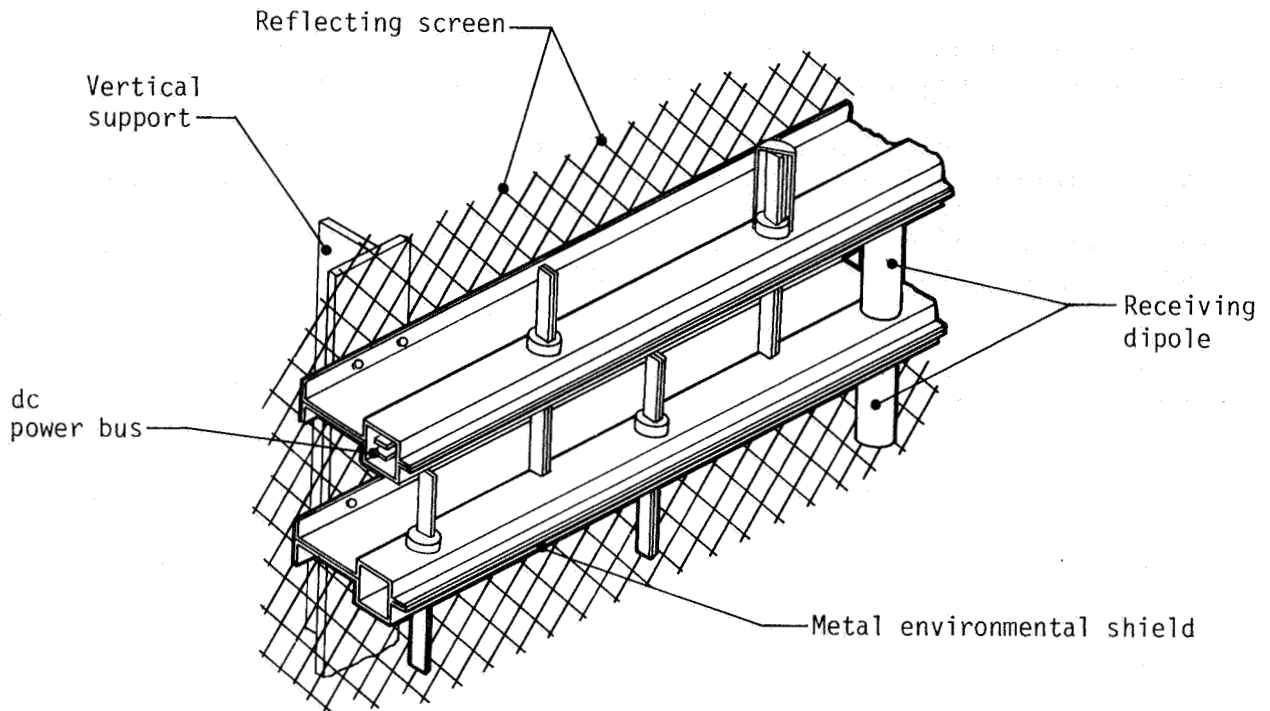
Figure III-55.- Drawing of the two-plane rectenna construction format consisting of a reflecting screen or ground plane and the foreplane, which contains a dipole antenna, wave filters, diode rectifiers, and busbars, all protected from the environment by a metal shield.
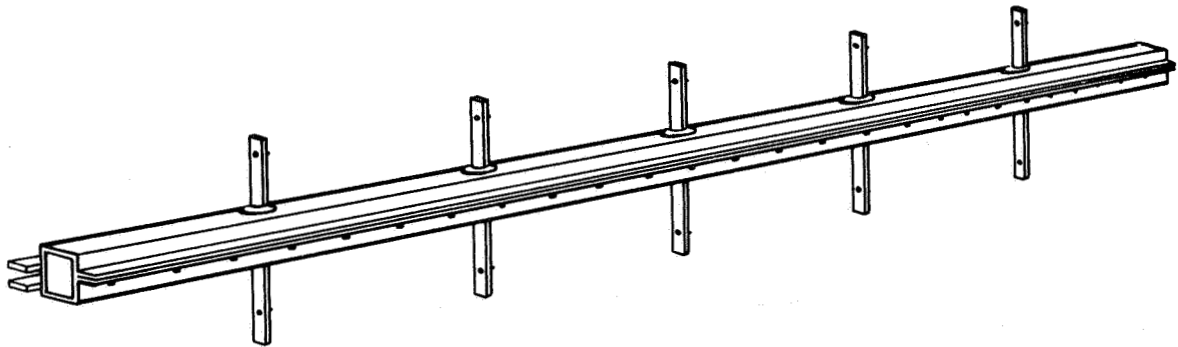
Figure III-56.- Completed rectenna foreplane assembly consisting of a metallic shield and the core assembly of five rectenna elements. This section has been substituted for a section of the three-level construction in a rectenna and found to perform as well.
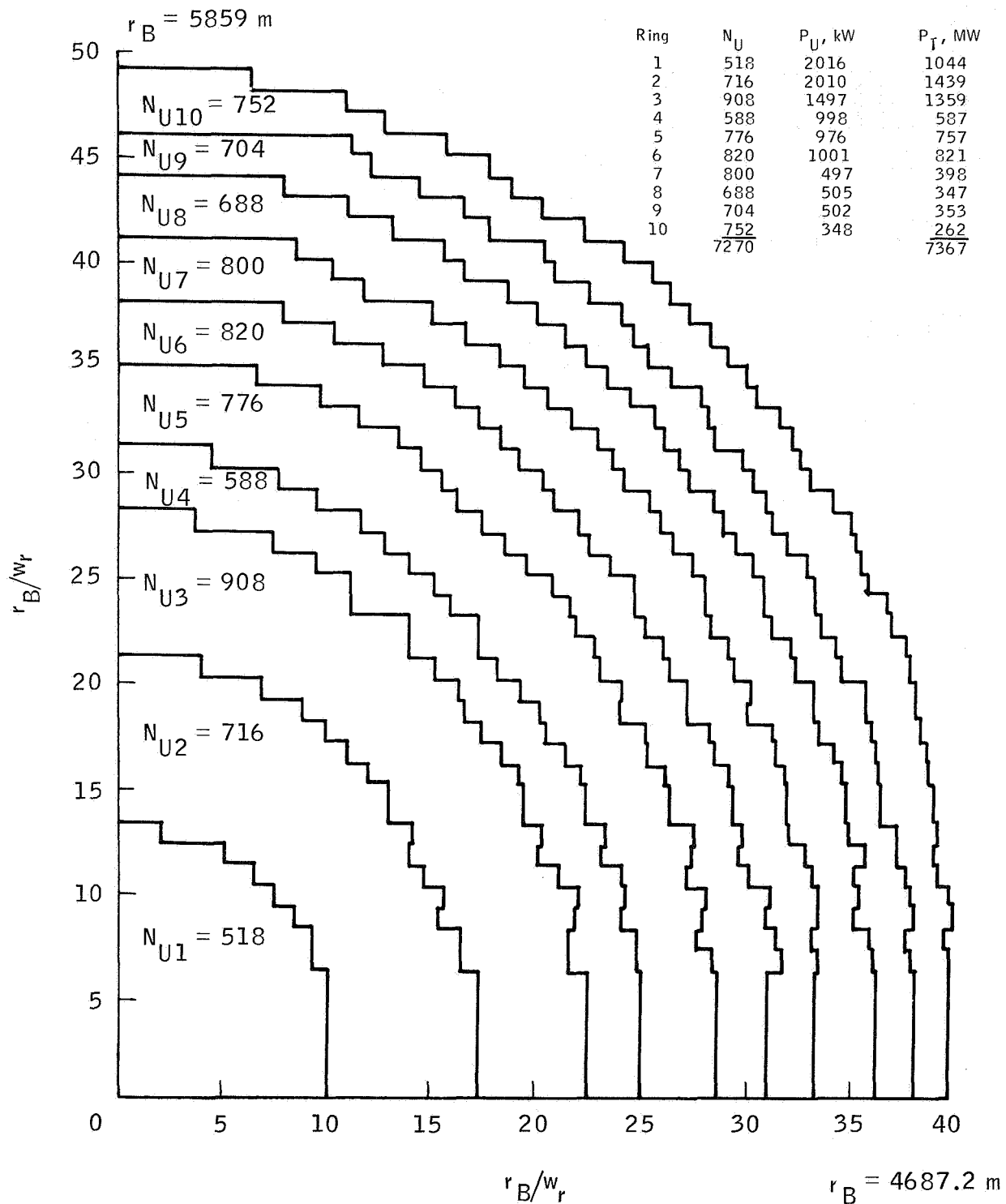
Figure III-57.- Geometrical layout of unit boundaries in the rectenna. (Within each of the 10 rings of units, different unit power levels are used.) Symbols are as follows: N_U = number of units, P_U = unit power, P_T = total power, r_B = boresight radius, and w_r = ring width (117.18 meters).

153
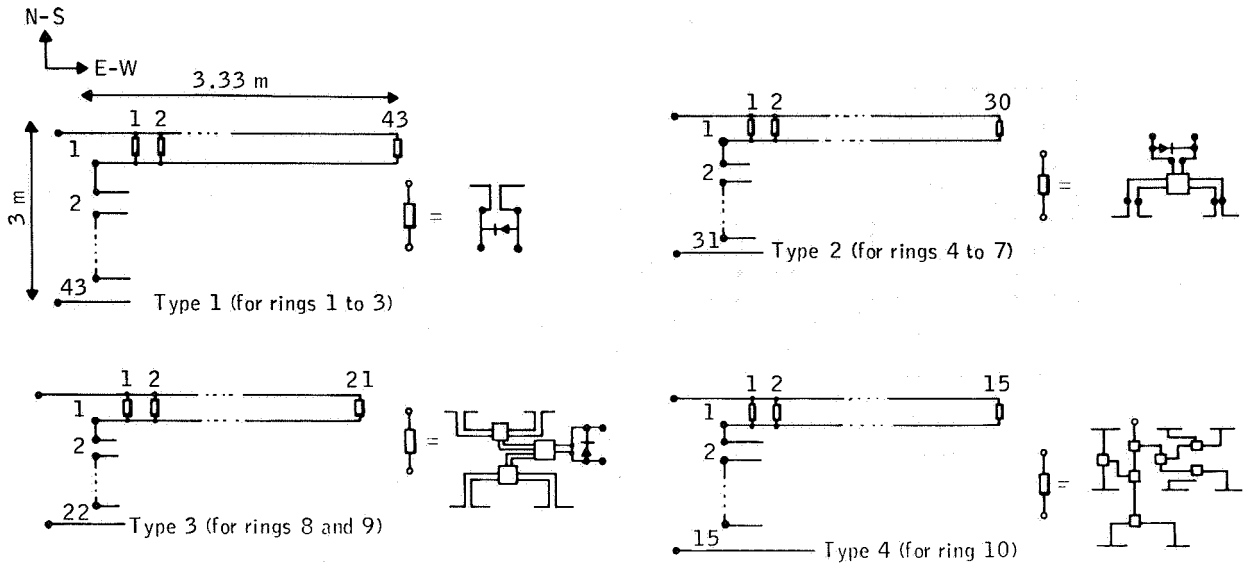
Figure III-58.- Wiring layout of the four different panel designs used
in the rectenna.

154

Figure III-59.- Wiring layout of the seven different unit designs used in the rectenna for the low-voltage configuration.

155

The last assembly formed at dc is called a "group" as illustrated in figure III-60. This assembly brings the power output into the 5- to 10-megawatt range. To keep the voltage levels relatively low, groups are formed from the units by parallel connections only. Unit outputs are brought to the group centers, where the dc-to-ac inverters are located, by relatively long transmission lines that are connected in parallel at the group centers. Alternating-current (ac) processing begins with 40-megawatt dc-to-ac inverter blocks. These blocks receive their inputs from several dc groups.

Layout for the rectenna ac system depends on the location and the power levels of the dc/ac converters as well as on the needs of the bulk power transmission system. The 40-megawatt converter station output is transmitted by underground cable to a 200-megawatt transformer station, where the voltage is increased to 230 kilovolts, then collected in 1000-megawatt groups and transformed to 500 kilovolts for interface with the bulk transmission system. The selection of the voltage level for the ultimate bulk power transmission interface with the utility grid, as well as the possibility of interconnecting two or more of the 1000-megawatt switching stations, should be optimized on the basis of detailed information about the connecting utility system.

Availability calculations for the reference rectenna design show that 80 percent of the rated satellite power is available 96.8 percent of the time and that scheduled no-power periods total only 208 hours per year. To define the requirements for a given specific situation, load flow and system stability studies are required. It is likely, however, that the SPS power system would be far more stable than a conventional powerplant of the same rating and, consequently, that the transmission distances could be increased for a given line loading without need for as much series compensation as in conventional powerplants.

a. Scattering and Radiofrequency Interference

The microwave transmission link must meet a stringent standard of electromagnetic cleanliness which states that out-of-band power must be more than 150 decibels down from the link power. There are enough scattering mechanisms for producing diode rectifier harmonics to make achievement of this requirement questionable. Some of the approaches to reducing reradiation are summarized in the Raytheon data of table III-18.

In the reference design, two low-pass filter sections which attenuate the second and higher order harmonics by more than 25 decibels isolate the rectifier. More filter sections add approximately 14 decibels more suppression, each at a cost of approximately 1 percent efficiency loss. Other alternatives, also with an efficiency penalty, are to use stubline filters or full-wave rectification. All these approaches have mechanical configuration problems that, although solvable, will increase rectenna diode array assembly cost. Given these difficulties, it may become necessary to seek SPS-assigned bands at the first few harmonic frequencies.

156
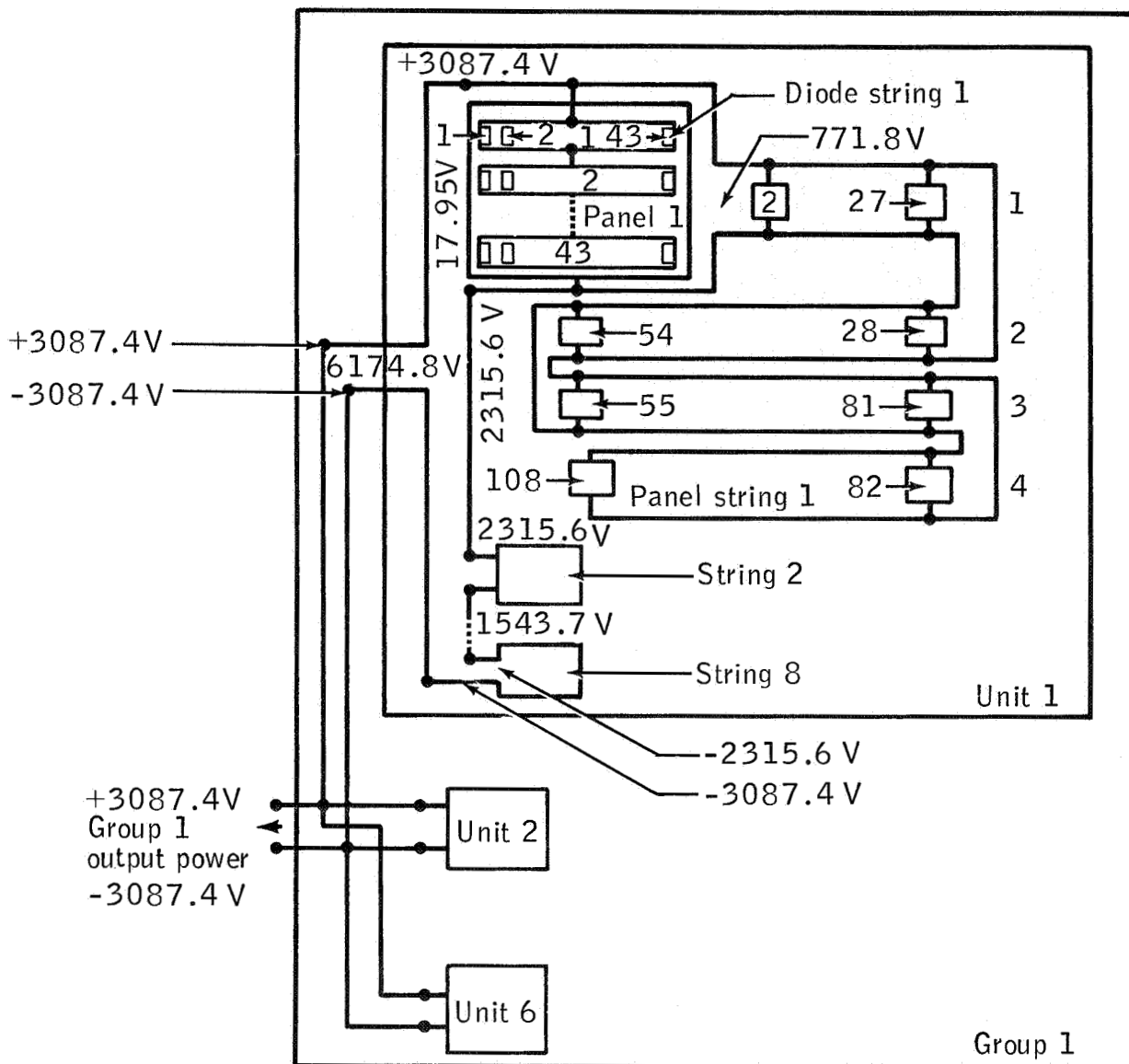
Figure III-60.- Block diagram of a typical group for the low-voltage con-
figuration. Example shows a group within the inner ring (circle) of the
rectenna aperture.

157

TABLE III-18.- APPROACHES FOR DECREASING RECTENNA HARMONIC RADIATION

Approach	Expected improvement in 2nd, 3rd, and 4th harmonics, dB	Implications
More filter sections of existing design	$^a \approx 14$	Results in crowding and 1-percent efficiency loss for each section
Stublines to short circuit higher harmonics at dipole terminals	≈ 30	Mechanical tolerance problem 2nd-harmonic reduction easily added 3rd and higher harmonics require added width to core section Less than 1 percent decrease in circuit efficiency Could degrade electronic efficiency
Incorporate stublines as part of filter sections	≈ 60 to 80	Mechanical tolerance problem Requires additional width of core section Some circuit efficiency degradation Could degrade electronic efficiency
Full-wave rectification	≈ 15	Increases number of diodes Greatly complicates electrical circuit and mechanical construction

^{a}per section.

Another type of scattering which affects system design is Fresnel edge diffraction from the rectenna panel edges. A slight overlapping of panels can reduce these losses but will increase total panel area and cost. The expected capture loss and resultant efficiency loss is estimated at between 1 and 2 percent.

b. Rectenna System Optimization

Optimization of a rectenna system design to minimize costs can be performed at several levels (ref. 42). It is desirable from the cost per unit power standpoint to transmit as much power through the transmission link as the ionospheric medium and beam pattern constraints will allow. The rectenna should be sized so that the incremental rate of return from sales of the intercepted power is marginal.

Much of the cost of the rectenna is in the material required to support the structure against wind and snow loads. Different types of rectenna panels have been considered. The reference design is intermediate between the inexpensive but high-load flat panels and the more expensive, low-load panels, which have circuit topology problems. The current rectenna panel support structure evolved from stiff edge-supported panels to a more centrally supported frame as illustrated in figures III-55 and III-61.

c. Rectenna Construction

Construction of the rectenna is, by necessity, highly automated. Starting with prefabricated dipole assembly components, a dipole machine manufactures completed dipole/diode assemblies at a high rate. These assemblies are combined with other prefabricated parts to manufacture receiving-element sticks. The sticks, the metal frame, and the ground plane are then tackwelded together to form panels.

The completed panels are taken to the rectenna site, where specialized equipment prepares the site through the emplacement of panel support arches. The panels are then lowered on the support arches, fastened, and connected electrically. There must, of necessity, be some rather conventional construction operations at the rectenna for the grid power system and the pilot-beam transmitters, but these constitute only a small fraction of the construction cost.

d. Direct-Current Power Combining

In the rectenna, numerous rectifier circuits share a common dc load to achieve useful power levels (ref. 43). The rectifier outputs can be combined in series and/or parallel to enhance the voltage and/or current level, respectively.

A fundamental question in this receiving, rectification, and power-combining process is caused by the power taper of the incident microwave beam. The incident power density can vary by 10 decibels over the rectenna area, since a high percentage of the transmitted microwave power

159
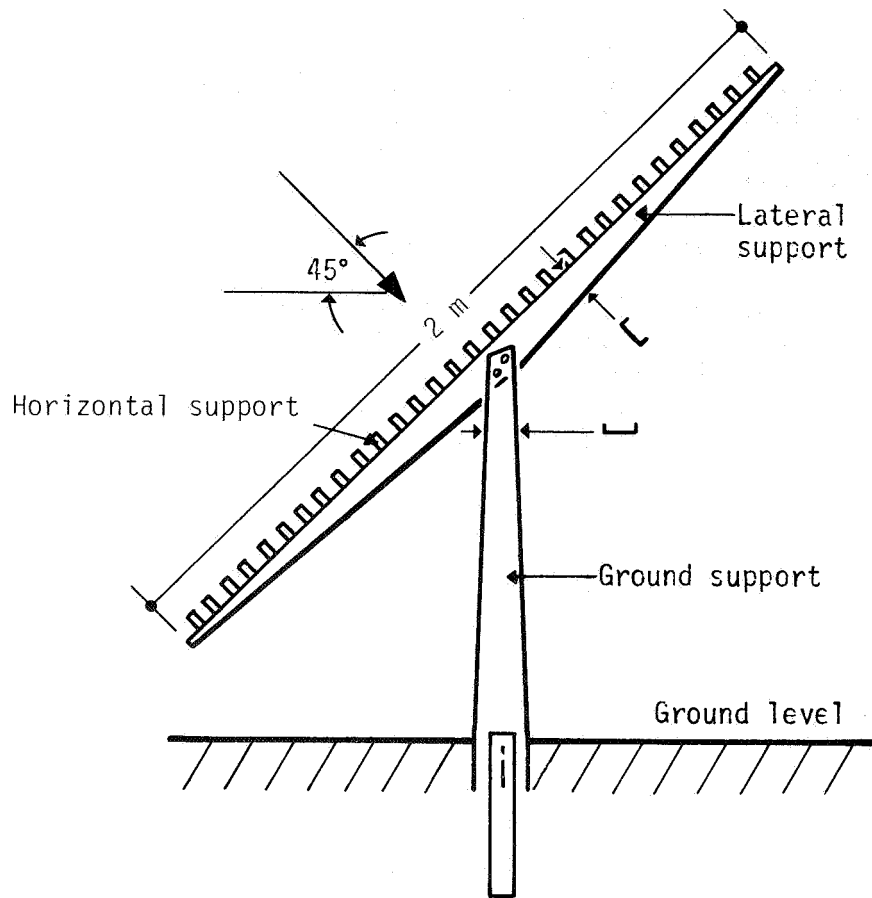
Figure III-61.- Rectenna rf baseline.

needs to be collected. Since the output (dc terminal) characteristics of the rectifier are power dependent, rectifiers at different power levels that share a common dc load cannot be operated at optimum conditions. With individual rectifiers operating near 90 percent maximum efficiency, the resultant efficiency degradation could be significant. The efficiency degradation that results when an array of microwave power rectifiers shares a common dc load has been assessed as described in the following paragraphs.

To evaluate the power-combining inefficiency, an accurate output-equivalent circuit model of the conversion circuitry is needed. This model was obtained using two independent approaches. First, an approximate closed-form circuit model of the rectifier was developed assuming an ideal diode and lossless circuit elements. Then, the output loadline was obtained analytically. Second, a more precise computer simulation model was used, and the output-equivalent circuit was obtained by varying the dc load resistance and plotting the resultant output loadline.

When using these models and various assumed power density variations, it was found that parallel combining is marginally better than series combining and that the closed-form analytical model results in only slight underestimation of the power-combining inefficiency compared to the computer simulation results. Assuming a uniform power density distribution, the power-combining inefficiency is 1.0 percent when the ratio of maximum to minimum power density is 2.0 to 1.0. The inefficiency is reduced to 0.3 percent if the ratio is 1.4 to 1.0. This result has an important effect on the design of the rectenna dc power-combining network; ring combining rather than row combining is favored, particularly near the rectenna edge.

e. Measured Rectenna Array Performance

High-efficiency (greater than 50 percent) rectenna array characteristics were demonstrated by Raytheon and JPL for the condition of highest collection-conversion efficiency performance associated with a laboratory demonstration of overall system end-to-end dc transfer efficiency (ref. 21). The array consisted of 199 half-wave gallium arsenide Schottky barrier diodes connected to half-wave dipoles through a two-section low-pass filter projecting through a flat solid ground plane. The elements were arranged in a triangular lattice the outline configuration of which was a hexagon. The collecting area per element was about 52 square centimeters. The incident flux density ranged downward from 203 mW/cm^2 in a Gaussian distribution over the aperture of the array (a 19-decibel taper); dc load collection consisted of 21 separate concentric rings of adjustable resistances tailored to the ring radius. A one-tenth-wavelength dipole probe in front of the array measured an on-axis VSWR of about 1.11 to 1 under matched conditions.

The peak collection-conversion efficiency of an individual element was measured as 87 ± 1.5 percent, whereas the average efficiency of the entire array at approximately 0.5 kilowatt output dc power was 82.7 percent of the available rf power incident on the array (not counting the estimated 4 percent spillover energy). The array transfer efficiency decreased less than 2 percent for a 16.7-percent decrease in rf input power level.

161

A larger rectenna array tested at Goldstone, California, consisted of 4590 elements arranged in 17 subarrays of 270 elements each arranged in a triangular grid pattern. The subarrays were grouped in a three-column arrangement with the top-center subarray absent. The measured performance was, in general, accurately predicted from general transmission-line reflection-coefficient theory with regard to the load variations, and the polarization and angle-of-incidence performance followed array theory. Computer models for the diode and associated rf circuitry produced predictions of the element performance as a function of the input rf amplitude; however, the array performance was poorer than predicted, in most cases by a few percent. This difference may be due to the effect of array mutual coupling, which is not modeled in a single-element analysis. Nevertheless, over a 10-decibel range of input power density, the rectenna array performance may be adequately predicted within a few percent, on the basis of measured diode assembly characteristics.

f. Lightning Protection

The large size of the SPS rectenna and the very high lightning flash density in many parts of the United States will require the incorporation of a lightning protection system within the rectenna design (ref. 44). Individually, the microwave diodes are self-protecting with respect to "average" lightning and those near the center of the rectenna are safe from extreme lightning. However, the series connection of the diodes to form high-voltage strings creates a protection requirement for the string. Standard surge-protection practices will satisfy this requirement.

A distributed lightning protection system concept studied by Rice University will protect the rectenna components from direct lightning strike damage and will, in addition, provide reduced induced-lightning effects in the power and control circuits. This system could be incorporated as a structural member of the rectenna support system. Such a concept would add little, if any, additional materials to the rectenna and thus would minimize cost for lightning protection. Electric power industries usually attribute 10 percent of the cost of power transmission equipment to lightning protection requirements.

It is felt that the efficiency reduction in the rectenna due to the lightning protection system could be quite small. However, this opinion has not been quantified and demonstrated.

2. ALTERNATE CONCEPTS

The reference system described previously is based on a design concept that has been proved capable of the high conversion efficiency required for SPS application. Some concepts advanced appear to be quite amenable to mass production techniques, but the projected costs are quite high and environmental protection requirements have not been completely evaluated in terms of cost or efficiency degradation. Therefore, several other concepts have been considered to some degree and their evaluation should be continued.

162

a. Medium-Gain Elements

Medium-gain antenna elements with a gain on the order of 10 decibels could reduce the parts count of rectenna elements significantly. The pointing loss would not be drastically reduced nor would installation difficulty be increased severely. Consideration of this type of antenna as a competitor against the reference configuration should be continued.

(1) Dipole arrays - The reference system includes dipole arrays for the rectenna outer areas, where the power density is low. This measure is required to produce a power level at the rectifier which can be converted efficiently to dc. If this technique can be shown to be cost effective (i.e., maintaining an acceptable efficiency while reducing the fabrication cost), it should be extended to the higher power regions of the rectenna.

(2) Yagi elements - Since the transmitted rf power is linearly polarized, a yagi antenna is a good candidate for a medium-gain element. Compared to individual dipoles, yagis would lower the parts count of both antenna elements and rectifiers. Conceptually, yagi fabrication could be accomplished rather simply. However, it remains to be shown that a yagi rectenna can maintain the required efficiency and, if so, the extent of reduction in parts count and cost. An attractive possibility for the yagi implementation is the elimination of the "ground plane screen," which contributes considerable design problems because of wind loading, icing, and snow accumulation. Experimental verification would be required to determine the parts-count reduction, efficiency level, and leakage for a yagi system with no ground screen.

(3) Stripline implementation - An analysis was performed to assess the possibility of implementing the reference concept in stripline. Stripline is usually a good candidate for high-volume, low-cost fabrication. The required harmonic filter, however, reduces the potential efficiency by 2 to 4 percent when implemented in stripline. The potential cost savings were estimated to be very small, if any, and not nearly enough to offset the efficiency loss.

b. High-Gain Elements

High-gain antenna elements have two distinct disadvantages: active cooling of the rectifier and pointing of the element. (This is not to say that the reference system and others do not have their own shortcomings.) Considerable research is in order to establish the crossover point in lifetime cost between high-count, simple low-gain elements and lower count, more complex high-gain elements.

c. Hogline Elements

The hogline concept (an infinitely wide variation of the familiar "hog horn" antenna) has been given only preliminary evaluation to date. This design consists of a parabolic cylinder reflector which concentrates the incident rf energy into a relatively narrow receiving area. In

163

its ideal form, the rf energy could be received by a linear "feed" but would probably use a line of high-power dipole-diode rectennas. This ideal situation would, in effect, produce a receiving antenna with a very broad pattern in the horizontal plane (essentially equal to a dipole over a ground plane) and a relatively narrow pattern in the vertical plane. In actuality, an array of dipoles (or equivalent elements) would be used in the vertical plane to match the incident waves. This concept requires a singularly curved reflecting surface as opposed to the flat reflecting surface of the reference configuration. This configuration also requires very accurate pointing of the large reflector during initial installation and possibly "pointing correction" during the lifetime of the rectenna.

The large reflector-type rectenna has unique requirements relative to the reference design. However, the lifetime cost of this type of antenna has not been adequately investigated to the point at which an intelligent trade-off can be made against the reference system. Effort should be expended to determine whether there is an advantage to this concept; i.e., smaller "parts count" with its implied increase in installation complexity and possibly operational complexity.

d. Waveguide Techniques

Waveguide techniques are included in the SPS transmitting system, and the projected efficiency is 96 percent. This value is somewhat lower than the efficiency represented by the estimated 1- to 2-percent loss in the dipole itself. However, waveguide techniques are quite versatile and compatible with environmental protection. Some degree of harmonic suppression is also inherent in the waveguide antenna technique. Wind-loading and support requirements appear to be substantial. The basic concept is worthy of consideration; however, material requirements and their cost impact can be expected to be very substantial.

e. Offshore Rectenna

An offshore rectenna evaluation has been conducted. It has been established that such a rectenna is technically feasible; however, the economic feasibility has not been confirmed. The reference design is not compatible with an offshore rectenna for several reasons. Thus, a rectenna design concept must be developed in conjunction with economic evaluation of an offshore rectenna.

F. SOLID-STATE CONFIGURATIONS

The current SPS configuration has high-power klystron tubes for the dc to rf power converters in the antenna. A possible alternative is to replace the klystrons with low-power solid-state devices. The major advantage of solid-state devices is the increased reliability over tubes; a disadvantage is lower conversion efficiency.

Solid-state microwave transmission concepts are considerably different from the current NASA/DOE reference system. The solid-state transmitter will have a lower power density of microwave energy in the center of

the space antenna because of temperature limitations. The transmitting antenna will be larger than 1 kilometer in diameter in order to transmit several gigawatts of power; consequently, the rectenna will be smaller in area. If the limitation of 23 mW/cm^2 for power density through the ionosphere must be maintained, improved techniques for beam shaping may be considered to possibly yield a flatter peak of microwave energy received at the rectenna.

Two solid-state designs have been proposed and have been studied in some detail. The first system is a simple replacement of the reference klystron antenna with a solid-state antenna. The second configuration is a "sandwich" concept in which the solid-state amplifiers and solar cells are combined; that is, the back surface is covered with GaAs solar cells operating under a high concentration ratio, whereas the front side (toward the Earth) is a conventional microwave antenna. A complex arrangement of mirrors is used to maintain sunlight on the back of the microwave elements (i.e., the solar cells) while the microwave array is continually pointed toward the Earth. The proposed advantage of the sandwich concept is elimination of the low-voltage dc processing; the solar cell outputs are fed directly into the solid-state rf devices.

Both of these concepts are characterized by larger antennas (because of thermal limitations), smaller rectennas (because of the larger, higher gain antennas), and greater satellite mass per kilowatt of delivered power. They have the advantage of increased reliability and thus lower satellite maintenance problems and costs. Disadvantages include increased phase control system complexity compared to the conventional klystron antenna, low-voltage (higher loss) dc power distribution for the separate antenna configuration, and increased noise generation.

1. CONCLUSIONS

As a result of the program studies and experiments on solid-state devices, several conclusions have been reached.

    a. Solid-state SPS concepts have not had the same depth of systems definition as the reference concept; however, preliminary results indicate the following.

        (1) The system sizing parameters are optimized such that lower power is delivered to the utility grid.

        (2) The transmit antenna is larger primarily because of the thermal limitations.

        (3) The rectenna land requirement is smaller.

        (4) Weight per delivered kilowatt is projected to be more.

        (5) Maintenance cost projections are less because of the higher reliability.

b. Type of power amplifier - Based on studies to date, the GaAs FET is the preferred solid-state power amplifier.

c. Antenna unit costs - Solid-state antennas will have high parts count similar to the solar array; therefore, unit costs are critical.

d. Mitigating designs - Conceptual designs have to some degree mitigated the issues of thermal and low-voltage power distribution.

e. Items of concern - Techniques of phase distribution (possibly to more points on the array) and power distribution (i.e., on the end-mounted configuration, more dc-to-dc converters are required) are major items of concern in the solid-state concept.

f. Technology - Associated technology development is more likely for solid state because of the advancing technology base.

2. REMAINING ISSUES

Based on current findings, continued investigation of solid-state concepts and issues is warranted. Remaining issues include the following.

a. Efficiency ($\geq$80 percent)

b. Operating temperature

c. Low-voltage distribution

d. Harmonic noise suppression

e. Power combining

f. Subarray size

g. Monolithic technology

h. Lifetime

i. Mutual coupling

j. Amplifier gain and power output

k. Input-to-output isolation

l. Charged-particle and ultraviolet radiation effects

m. Reliability/temperature trade-offs

166

n. Phase stability and control

o. Unit costs

3. NOISE GENERATION

One of the main problems with solid-state power transmission is the amount of rf noise generated by the system. Normally, a solid-state amplifier is considered to be a low-noise device. However, to obtain a dc/rf conversion efficiency in excess of 80 percent, the amplifiers may have to be configured for "switch mode" operation (class D, E, or F). In the switch mode of operation, the devices are switched on and off at rates perhaps 10 times that of the rf period. These waveforms have high-frequency components, only part of which will be attenuated by the 2.45-gigahertz resonant-frequency output circuits that transform the switched waveform into a sine wave. The broadband noise associated with the switched solid-state amplifiers will not have the same degree of filtering provided by a multicavity klystron feeding slotted-waveguide radiators as in the reference SPS system. The spectral and amplitude distributions of the broadband noise are not known currently but are considered a major problem area.

Several power amplifier/antenna radiator configurations have been proposed for the separate antenna system. For the high-power-density areas at the center of the transmit array, the configuration having four solid-state amplifiers directly coupled to a single resonant output cavity shown in figure III-62 is applicable. Since the power density at the outer areas of the antenna is one-tenth the density at the center, a single amplifier feeding a simple half-wave dipole antenna as shown in figure III-63 should be sufficient. Both antenna modules are relatively low-gain devices; the four-amplifier/cavity scheme has a measured 7-decibel boresight gain, and the single amplifier/dipole should have approximately a 3-decibel gain. These gains are small compared to the 38-decibel gain associated with 70-kilowatt klystron power modules. Thus, the coherent noise footprint will be spread over a larger area on the Earth for the solid-state antenna. The relative improvement (decrease) in peak noise density at boresight on the Earth's surface for a solid-state antenna as compared to a klystron antenna may be calculated as follows.

$$\frac{\text{Solid-state noise power density}}{\text{Klystron noise power density}} = \frac{P_{T-SS(N)}}{P_{T-K(N)}} \frac{G_{SS}}{G_K}$$

$$= \frac{P_{T-SS(N)}}{P_{T-K(N)}} \times (-33 \text{ dB})$$

$$= \frac{P_{T-SS(N)}}{P_{T-K(N)}} \left(\frac{1}{2000}\right) \qquad (24)$$

167

Metalized ground plane

Metalized radiating element

Microstrip antenna/power combiner (outside view)

Metalized border for cavity attachment

Microstrip antenna/power combiner (underside view)

Metalized antenna exciting element

Cutouts for feed-line entries

Dielectric substrate

Metal cavity

(a) Breakaway view.

Antenna ground plane

Slotline field

Substrate dielectric

Radiating element

Antenna exciter (cavity side)

Microstrip feedline

Radiating slot

Antenna ground plane

(b) Electric-field profile.

Figure III-62.- Power-combining microstrip slotline antenna.

168

1-mm (40 mil) ceramic radiation shield

GaAs IC's

.25-mm (10 mil) Al dipole

1-mm (40 mil) dielectric plugs

.25-mm (10 mil) outer conductor

B⁺

Adhesive-backed flat-tape power pigtail

Fiber optic cable

.25-mm (10 mil) Al ground plane

IC = integrated circuit
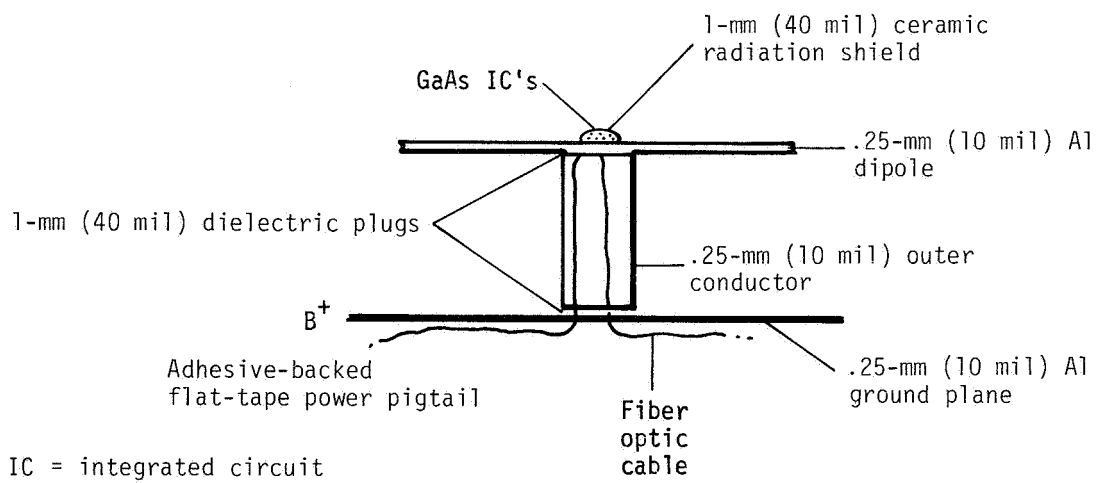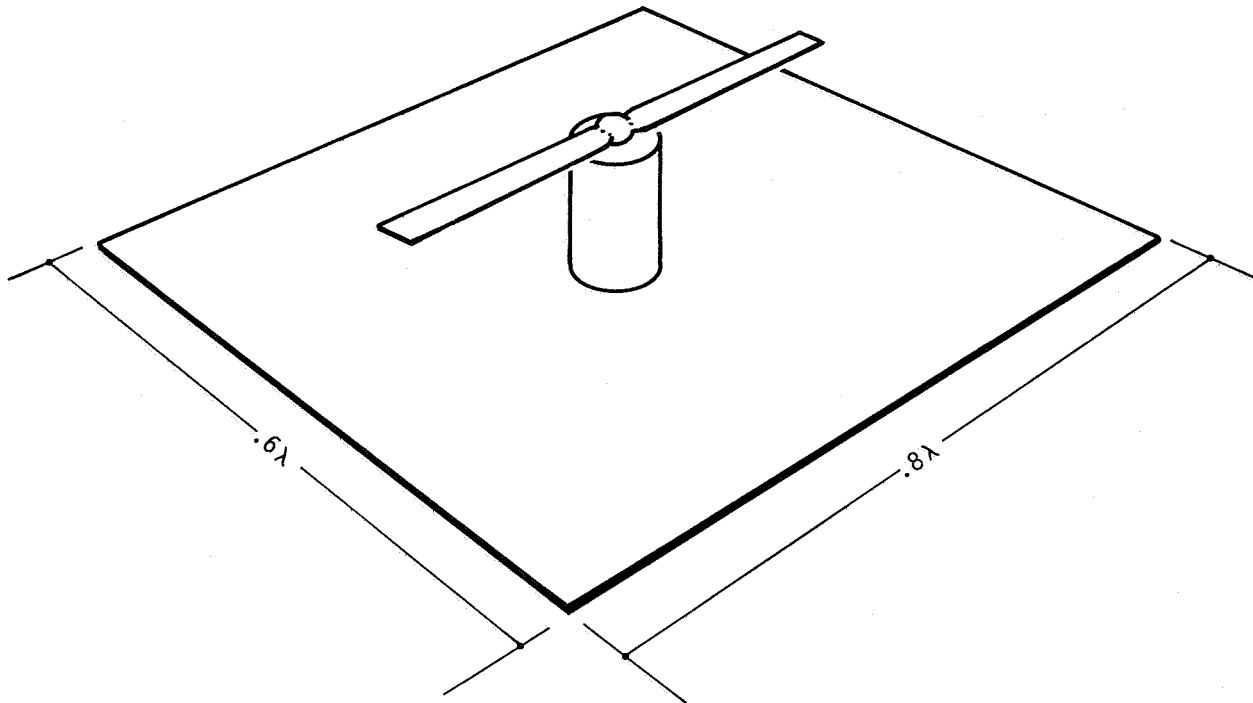
Figure III-63.- Solid-state dipole radiator module.

where $P_{T-SS(N)}$ = transmitted noise power from a solid-state antenna

$P_{T-K(N)}$ = transmitted noise power from a klystron antenna

G_{SS} = antenna gain of an average solid-state power module (5 decibels)

G_K = antenna gain of an average klystron power module (38 decibels)

Thus, for equal transmitted noise power from the two antennas, the solid-state system will have one two-thousandth (-33 decibels) the peak noise density of the klystron system at the ground rectenna but the total noise power will be spread over a much larger area. As a reference for comparison, the expected noise spectral density at the ground from a 5-gigawatt, 1-kilometer klystron antenna system is shown in figure III-8. The solid-state antenna system must have similar characteristics to meet the CCIR (International Radio Consultative Committee) and radio astronomy requirements. Filtering of the noise and signal harmonics will be required in each of the solid-state power devices, both for the separate antenna system and the sandwich configuration.

4. SEPARATE ANTENNA SYSTEM

The current configuration for the separate solid-state antenna system is an end-mounted array having a diameter of 1.42 kilometers as shown in figure III-64 (ref. 45). The dc power delivered to the solid-state devices in the antenna is approximately 4.3 gigawatts and results in 2.5 gigawatts at the output of the ground rectenna. This larger antenna, lower power (1.42 kilometers, 2.5 gigawatts) system is sized differently from the reference klystron system (1 kilometer, 5 gigawatts) because of thermal considerations in the solid-state antenna.

The overall efficiency for the separate antenna system from the dc power output of the solar array to the collected dc power output of the rectenna is given in figure III-65. The chain includes a 0.975 efficiency for operating the solar cell strings at reduced power levels compared to the maximum point on the voltage/current (V/I) curve. This solar array mismatch must be considered when operating at lower voltages compatible with the solid-state amplifiers.

The 10-step 10-decibel baseline SPS Gaussian taper has been adapted to the solid-state transmitting antenna. The peak rf power density in the center of the array is limited to 5.5 kW/m^2 (as compared to 23 kW/m^2 for the reference klystron antenna) because of thermal limitations. Assuming a single device power output of 7.5 watts, 11 devices per λ^2 are needed to provide the 5.5 kW/m^2. Low-loss rf combining of individual devices is needed to achieve this peak power density.

The Boeing Aerospace Company has developed a low-loss four-amplifier power combiner which feeds two half-wavelength slotline antennas coupled together by way of an aluminum cavity structure. The efficiency of

1.42 km

5340 m

7342.5 m

Perspective
sketch of SPS
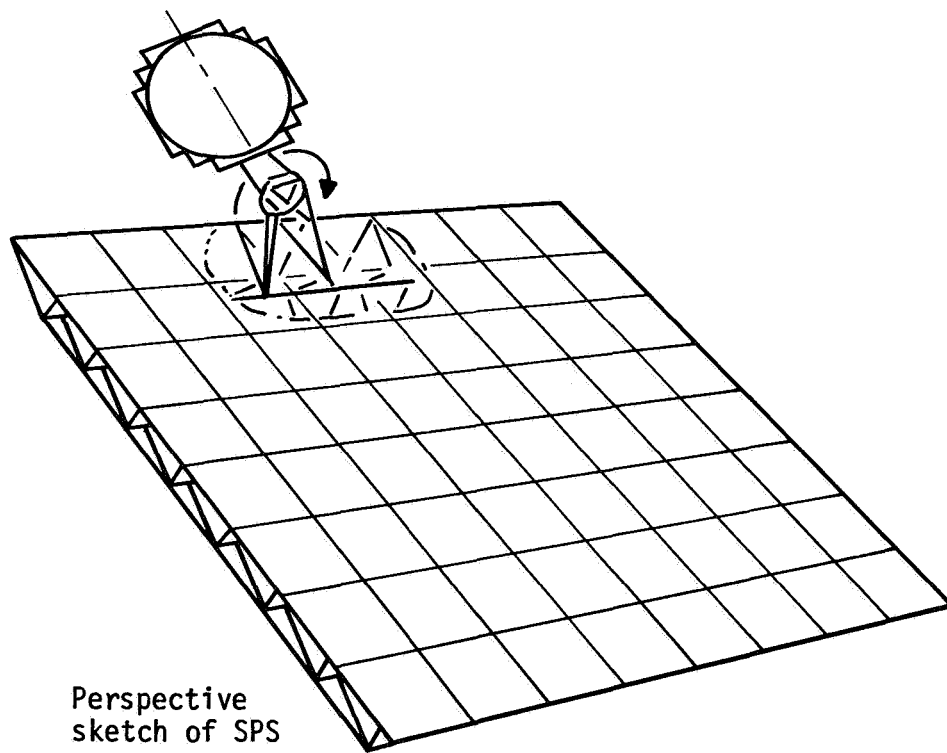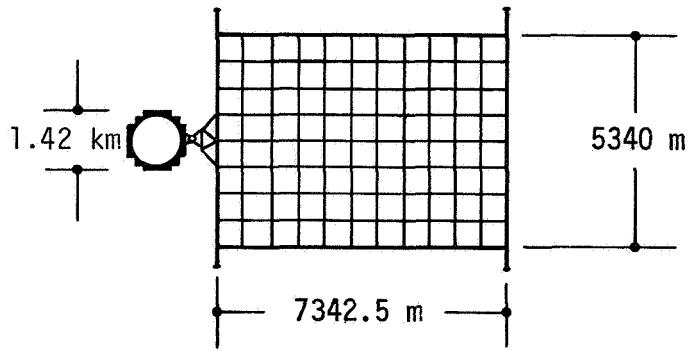
Figure III-64.- 2.5-gigawatt solid-state SPS configuration.

171

Figure III-65.- SPS efficiency chain for solid-state separate antenna system.
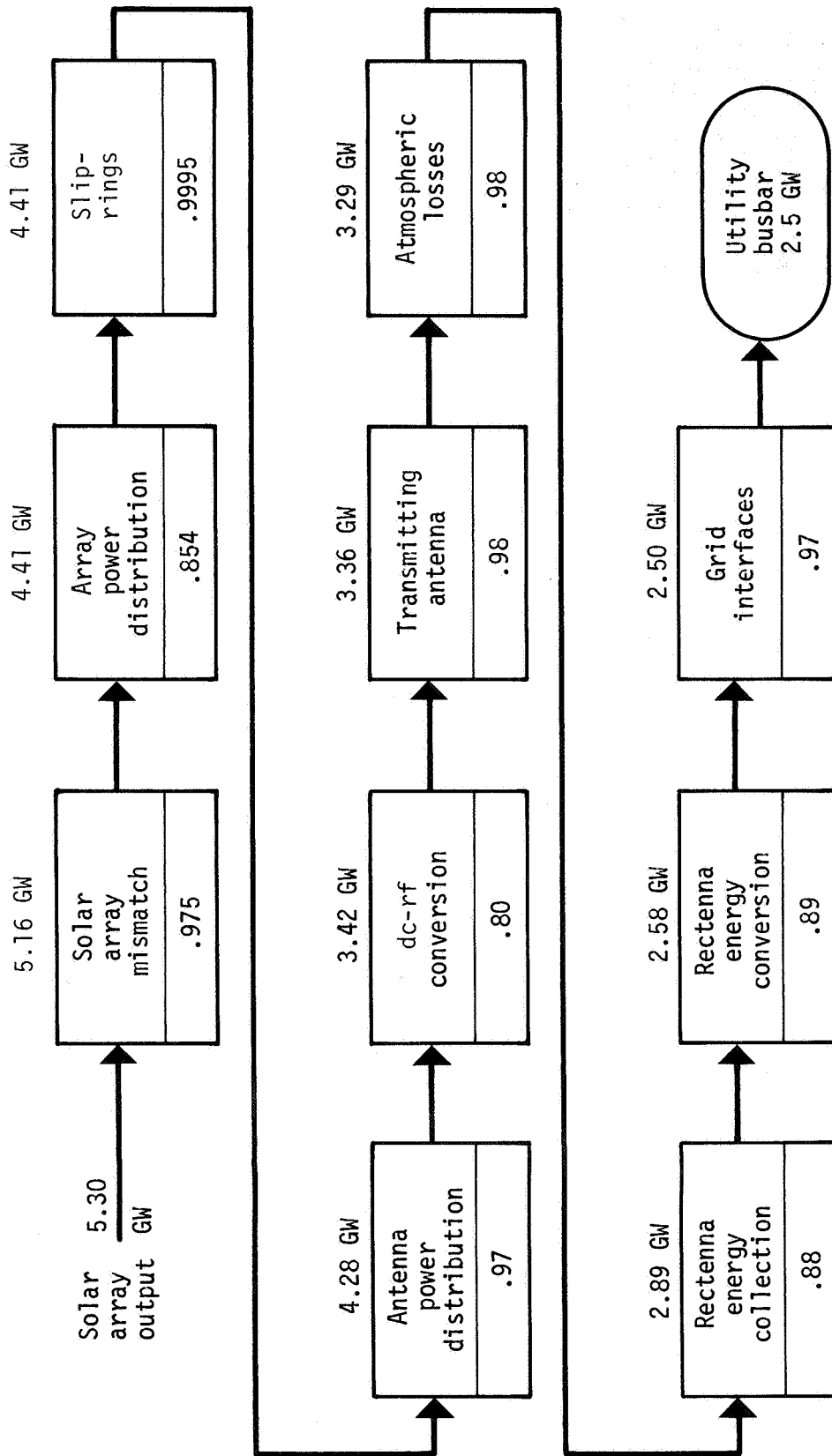
MPTS efficiency = 60.1 percent

the power-combining antenna as fed with four silicon bipolar transistor amplifiers yielding 0.5 watt output has recently been measured by Boeing to be approximately 100 percent; i.e., no discernible loss as limited by their measurement capability. However, the efficiency chain in figure III-65 provides a 2-percent loss for rf power combining. Additional measurements indicate a 7.0-decibel antenna gain with close-in side lobes 22 decibels down. The four power amplifiers yield a gain of 8.2 decibels each and a relative insertion phase error of $\pm1°$ at an output power level of 132 milliwatts each. Figure III-62 contains several views of the power-combining microstrip antenna.

Within the 10-step antenna taper, there are 5 different types of rf power modules (high-power, 4-FET cavity radiator; reduced-power, 4-FET cavity radiator; 2-FET cavity radiator; 2-FET dipole; and 1-FET dipole). At the center is the previously discussed high-power, four-FET cavity radiator, which provides 5.5 kW/m^2 power density. Near the periphery of the antenna, the lower power per unit area allows the use of simple, less massive dipole radiator modules as shown in figure III-63. The mass per unit area of these devices is approximately 30 percent of that of the cavity radiators in the center of the antenna.

The radiation pattern for the 10-decibel Gaussian taper, 1.42-kilometer array with specified error parameters of $\sigma = 10°$ rms phase error, ±1 percent amplitude error, and 2 percent random failures is shown in figure III-66. The peak power densities are 22.5 mW/cm^2 at the rectenna boresight, 1.0 mW/cm^2 at the edge of the rectenna, and 0.08 mW/cm^2 for the first side lobe. A 6.8-kilometer-diameter rectenna is needed to receive 88 percent of the transmitted energy from the satellite. Thus, the larger solid-state antenna enables reduction of the rectenna area to 46 percent of the reference 10-kilometer-diameter rectenna area.

Mechanically, the antenna consists of 10.4- by 10.4-meter subarrays made up of solid-state rf amplifier modules. These subarrays are supported by a pentahedral truss structure, which is relatively simple to construct and provides good access for maintenance equipment. The current concept has 64 solid-state combiner modules as the basic layout panel as shown in figure III-67. The 10.4- by 10.4-meter subarray has 324 panels containing 20 736 modules as shown in figure III-68.

The phase control system is the same as for the reference klystron SPS antenna in that the active, retrodirective array has a pilot-beam reference for forming a single coherent beam at the ground rectenna. Each subarray has four phasing receivers which process the uplink pilot-beam reference to provide phase conjugation. There are 58 112 phase control receivers, one for each 5- by 5-meter subsection of the subarray (ref. 12). The phase conjugated signal is distributed from each receiver by way of a closed-loop distribution system to the panel level. The phase information is then distributed over a microstrip feedline to each solid-state combiner/amplifier. Details of the phase distribution system from the receiver to the amplifiers have not been studied. In general, the phase control system for the solid-state antenna is more complex than for the high-power klystron reference antenna. This complexity results from the need for distributing
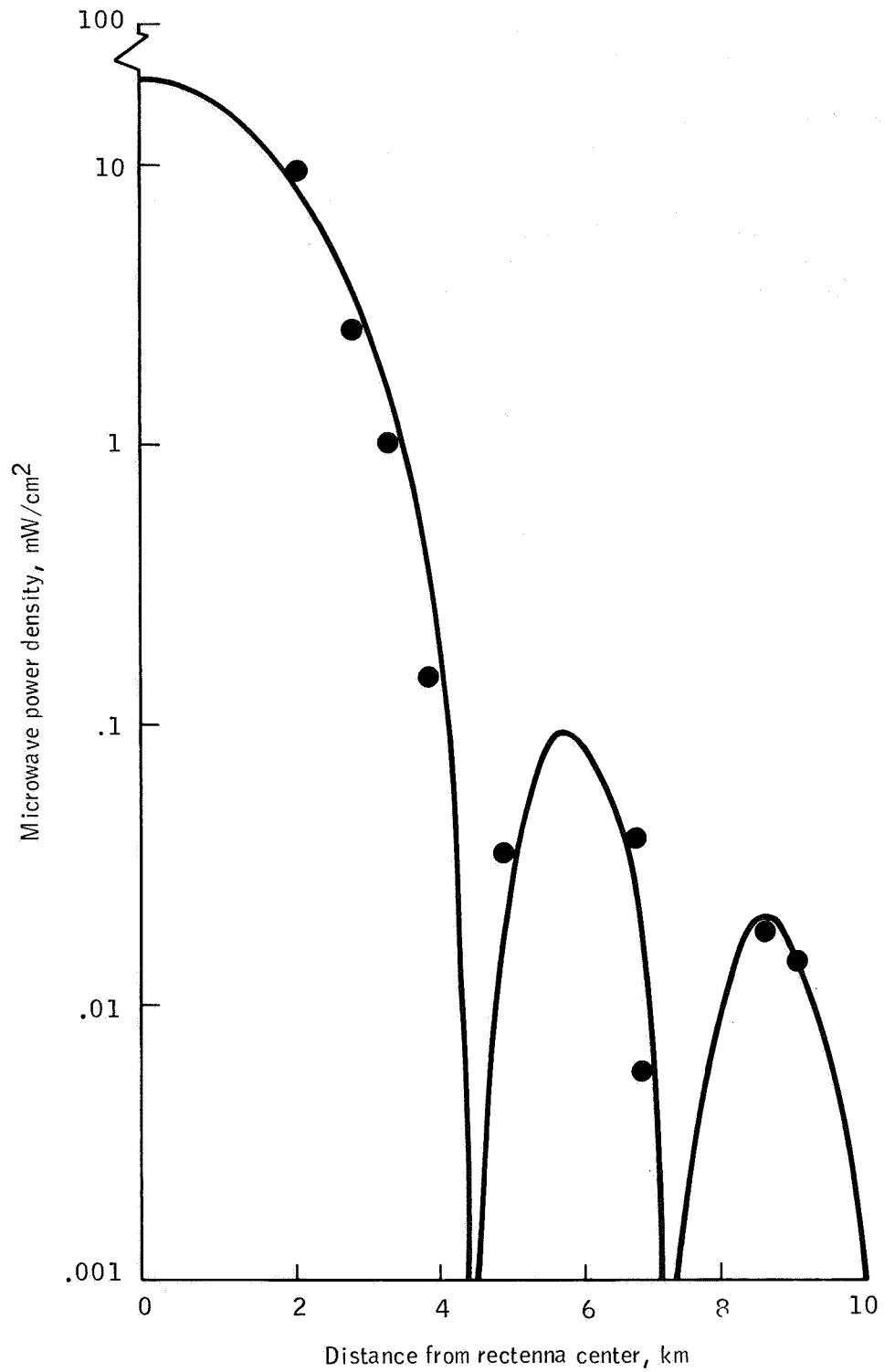
Figure III-66.- Microwave power density as a function of distance from rectenna boresight for the 2.5-gigawatt, 1.42-kilometer antenna diameter, solid-state system.

174
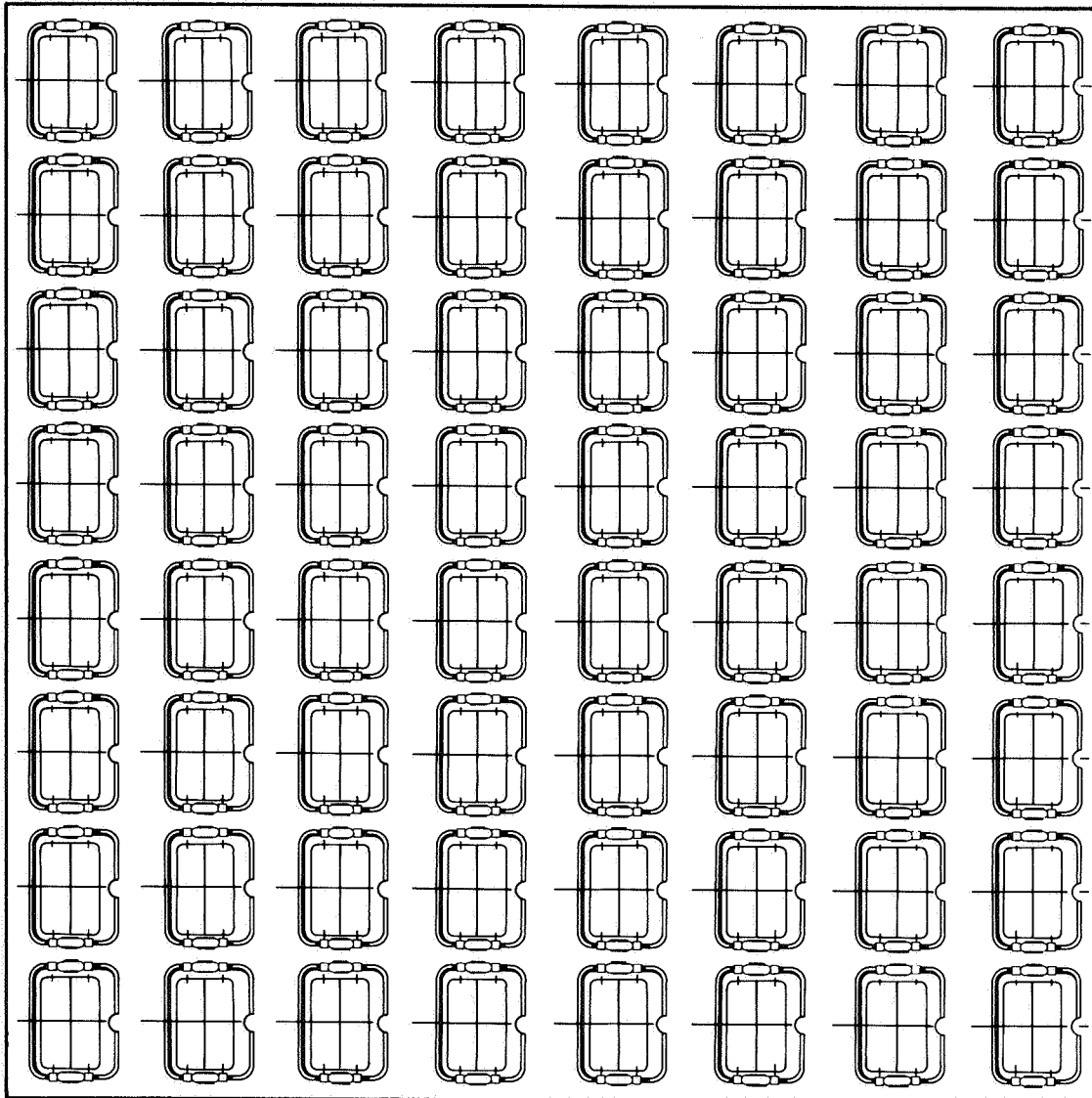
Figure III-67.- 64-module panel layout.
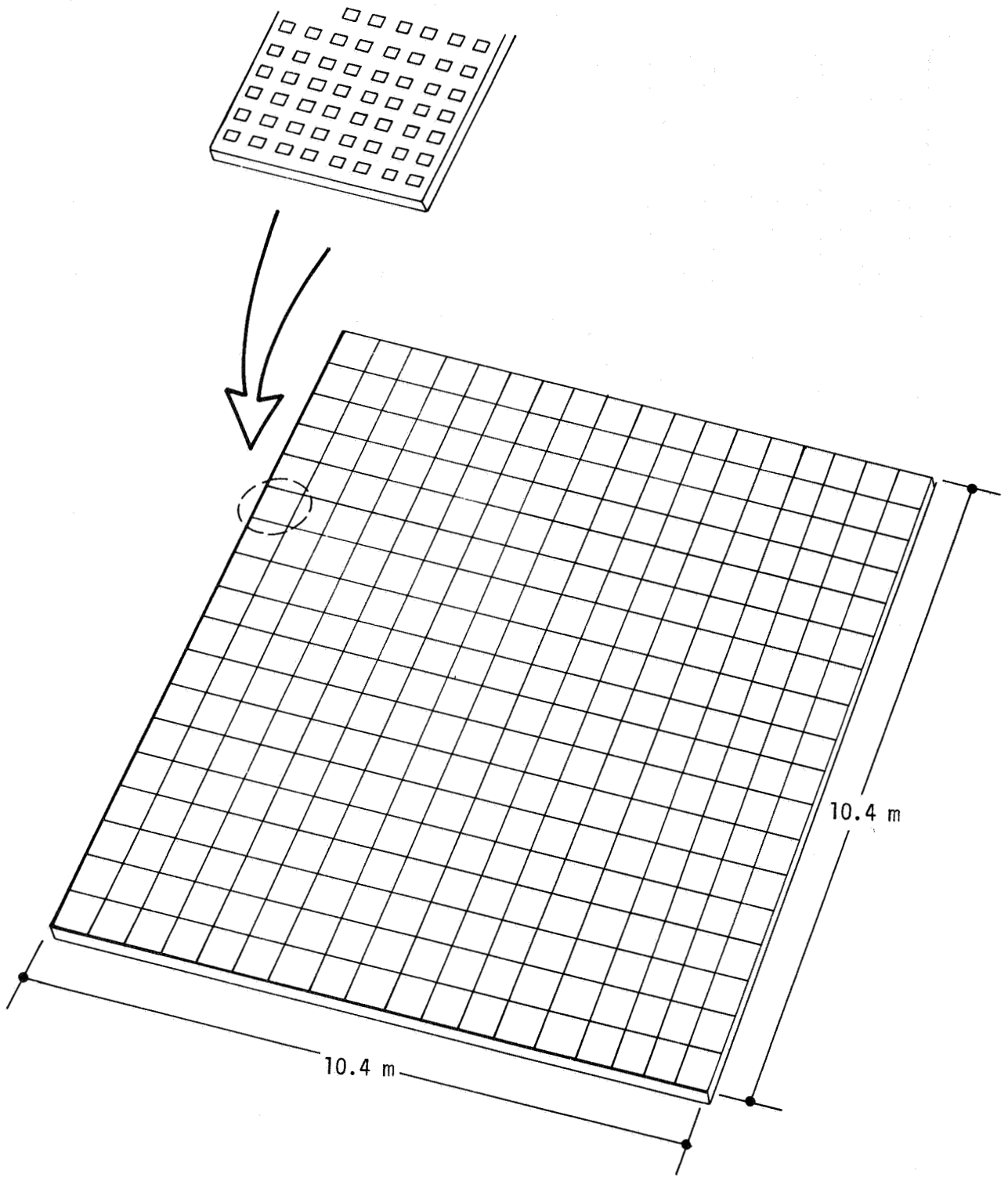
Figure III-68.- Subarray assembly (324 panels, 20 736 modules).

phase information to many thousands of solid-state devices rather than to a single tube.

One of the fundamental problems with solid-state devices is the low operating voltage that must be distributed throughout the antenna. Four methods of delivering this voltage have been investigated as part of the overall system studies (refs. 46 and 47).

a. High dc voltage (44 kilovolts) with dc/dc converters within the antenna

b. High ac voltage (100 kilovolts) with dc/ac converters in the solar array and ac/dc converters in the antenna

c. Low dc voltage (5.5 kilovolts) with no converters

d. Moderate dc voltage (8.6 kilovolts) with no converters

Two parameters, mass and I^2R losses, determine the relative merits of the four voltage-distribution techniques. A comparison of the performances of these techniques with that of the reference klystron SPS configuration is shown in table III-19. Each system has been normalized to provide 2.5 gigawatts of dc power out of the rectenna.

The results indicate that the moderate dc voltage (8.6 kilovolts) system with no dc/dc processing has the best performance of the four solid-state power-distribution schemes. The reference klystron configuration has the best overall performance, as would be expected.

The total satellite weight with the solid-state microwave antenna and the 8.6-kilovolt dc voltage-distribution system is 3505 tonnes heavier (12.5 percent) than the klystron system normalized to provide 2.5 gigawatts output power. However, the klystron system is being penalized by operating at one-half its power capability, particularly with regard to electricity costs (mills per kilowatthour). An interesting point from a preliminary costing analysis is that the "sandwich" concept was developed to eliminate the dc power-distribution system and thus reduce satellite weight. The "sandwich" system optimizes to an output power of approximately 1.15 gigawatts. In comparing the two solid-state approaches, the cost penalty incurred by reducing the output power to 1.15 gigawatts for the sandwich concept may have a greater economic impact than accepting the power-distribution weight penalty (and associated cost increase) in the separate solid-state antenna system.

5. SANDWICH SYSTEM

A number of "sandwich" concepts have been investigated (refs. 48 and 49), with the major alternative configurations summarized in figure III-69. The one currently favored, because of less overall volume and best control features, is similar to concept 5 (fig. III-69(e)), although with only two transmitting antennas. This approach is based on rigid coupling of two

177

TABLE III-19.- COMPARISON OF WEIGHTS AND LOSSES FOR VARIOUS VOLTAGE-DISTRIBUTION SYSTEMS

Parameter	Reference klystron system (normalized to 2.5 GW)	Solid-state (2.5 GW) systems			
		44 kV dc	100 kV ac	5.5 kV dc	8.6 kV dc
Solar array					
Mass, t	13 210	14 120	13 853	15 674	15 252
Power, MW	4540	4853	4761	5387	5240
Power distribution system[a]					
Efficiency, percent	0.901	0.886	0.903	0.798	0.8202
Losses, MW	450	553	461	1087	940
Mass, t	1735	7746	9803	4870	2881
dc power into solid-state devices, MW . . .	4090	4300	4300	4300	4300
Microwave system and rotary joint[b]					
Efficiency, percent	0.63	0.60	0.60	0.60	0.60
Mass, t	8015	7700	7700	7700	7700
Power, MW	2576	2576	2576	2576	2576
Grid interface					
Efficiency, percent	0.97	0.97	0.97	0.97	0.97
Power, MW	2500	2500	2500	2500	2500
Total satellite					
Mass,[c] t	28 011	36 070	38 254	34 457	31 516

[a] Solar array and antenna.
[b] Excluding power distribution.
[c] Includes 22 percent growth.
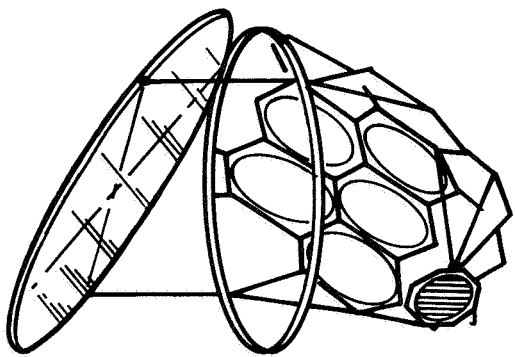
(a) Concept 1: flat primary/
faceted secondary.
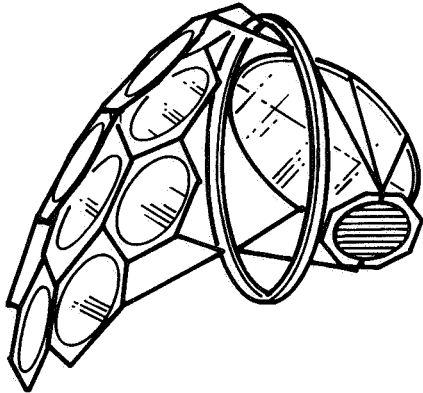
(b) Concept 2: flat secondary/
faceted primary.
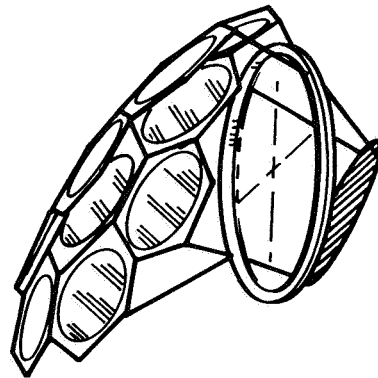
(c) Concept 3: inclined antenna/
single faceted reflector.
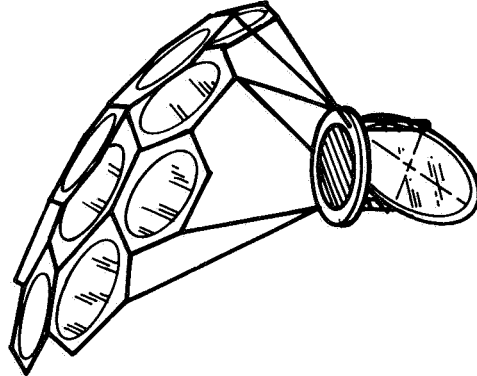
(d) Concept 4: rf reflector/
single multifaceted reflector.
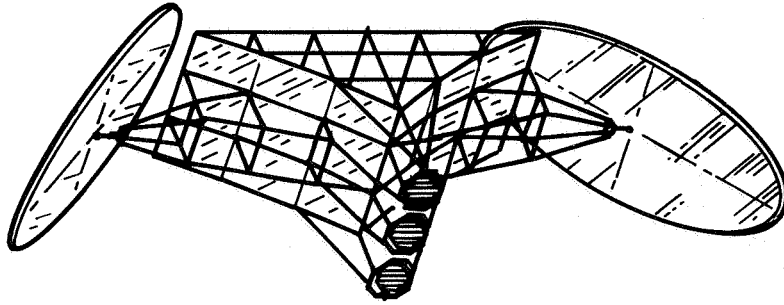
(e) Concept 5: multiple-
antenna concept.

Figure III-69.- Alternative solid-state-sandwich concepts.

179

concept 2 antennas to enable sharing a common location in geosynchronous orbit (fig. III-70).

The baseline single-antenna concept is also an important consideration when designing the overall sandwich concepts in the determination of the amplitude taper across the array. Unlike the reference concept, in which very high power klystron sources ($\sim$70 kilowatts) are used and a sloping taper is a natural feature, the main objectives in the case of a solid-state sandwich are to have as large a number of identical components as possible and to minimize the size of the satellite. A comparison of a 10-decibel (Gaussian) and 0-decibel (uniform) taper is thus in order. For the latter, all amplifiers carry the same power level, and the spacetenna diameter is a minimum for a given beam width. As a first-order comparison, the salient features of a typical 0-decibel sandwich and a 10-decibel tapered sandwich are shown in table III-20. (Multibandgap solar cells are assumed in this study summary, but the chart is for comparison purposes only.) The 10-decibel taper system has a smaller rectenna but higher electricity costs because of higher satellite costs. In conclusion, the sandwich configuration is not compatible with a tapered antenna. In table III-21, the characteristics of a standard GaAs-based sandwich are compared with those of a multibandgap cell alternative.

a. Sandwich Concept

The GaAs sandwich concept has the nominal characteristics described in table III-22 with an effective concentration ratio of 5.2. The preliminary efficiency chain of the sandwich is summarized in figure III-71. Several factors such as summer solstice, seasonal variation, and reflector reflectivity degradation are not included; these factors may reduce the available power from 1.15 gigawatts to 0.92 gigawatt at the grid interface. Analyses into these effects are underway. It should be noted that higher amplifier base temperatures (398 K (125° C)) are required in the sandwich concept because the amplifiers in the sandwich are relatively small (5 to 6 watts) and are cooled by their own beryllium oxide radiator disks, which radiate heat in only one direction.

b. Design Considerations

The solid-state arrays are subdivided into square subarrays of 5 by 5 meters each. This subarray size is sufficiently small to keep the grating-lobe peaks to less than 0.01 mW/cm^2 under worst case antenna tilts as shown in figure III-72. This limitation implies a mechanical antenna-attitude-control accuracy of ±2' of arc, or a total swing of 4' of arc. It is expected that the major-axis fluctuations can be controlled to this accuracy using conventional star sensor and Earth-edge sensor plus inertial attitude control systems, with ion thrusters providing the required impulses. The associated microwave scattered power loss is 10 megawatts as shown in figure III-73 for an antenna tilt of 2 arc-minutes and a random subarray tilt of 3 arc-minutes.

All amplifiers within the 5- by 5-meter subarray are controlled together; i.e., they are fed in phase. A diagrammatic view from the

CR = 6

8-mirror
primary
reflector

14 750 m

7200 m

Solid-
state
solar cell
field,
1830 m
diam

5850 m

Elliptical
reflector

4350 m
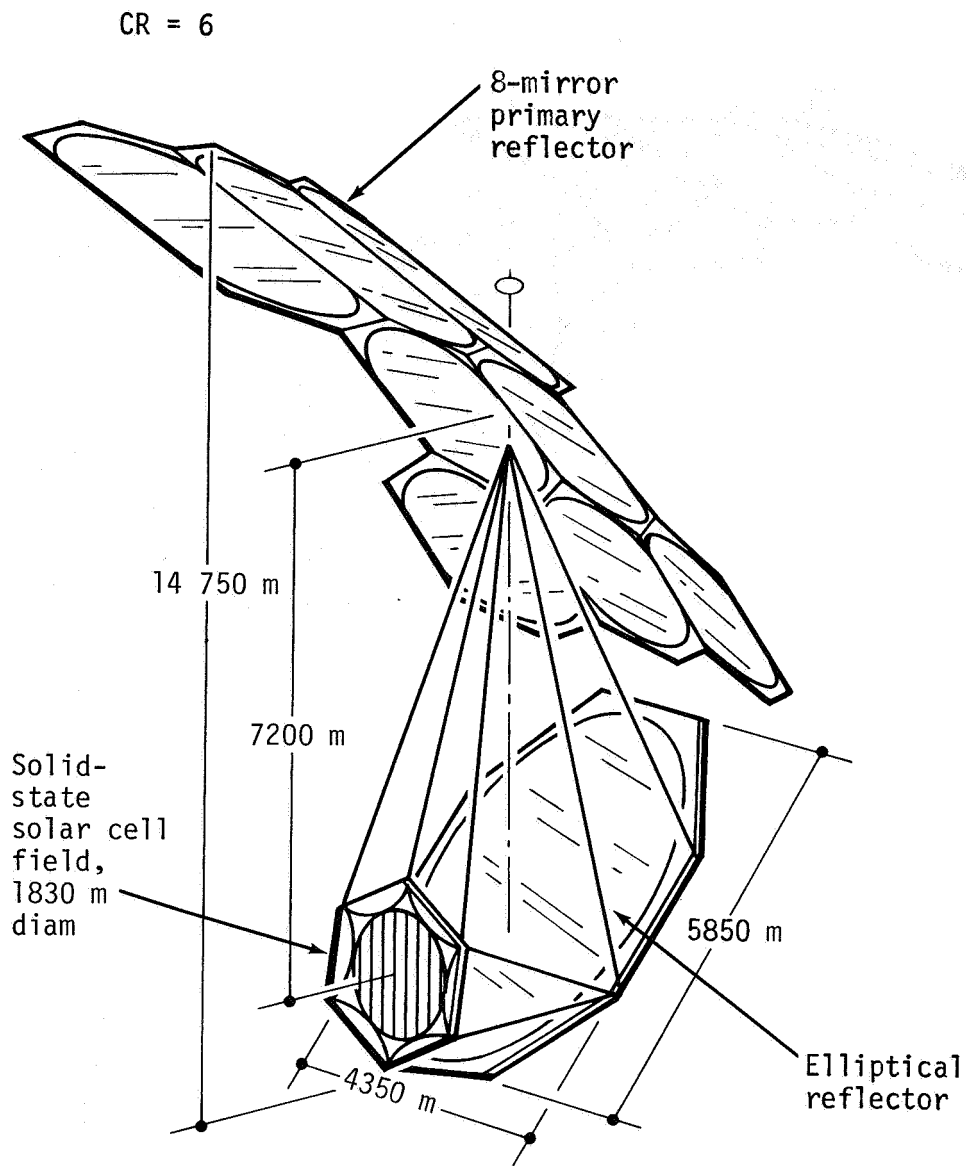
(a) Single.

Figure III-70.- Solid-state-sandwich concepts.

181
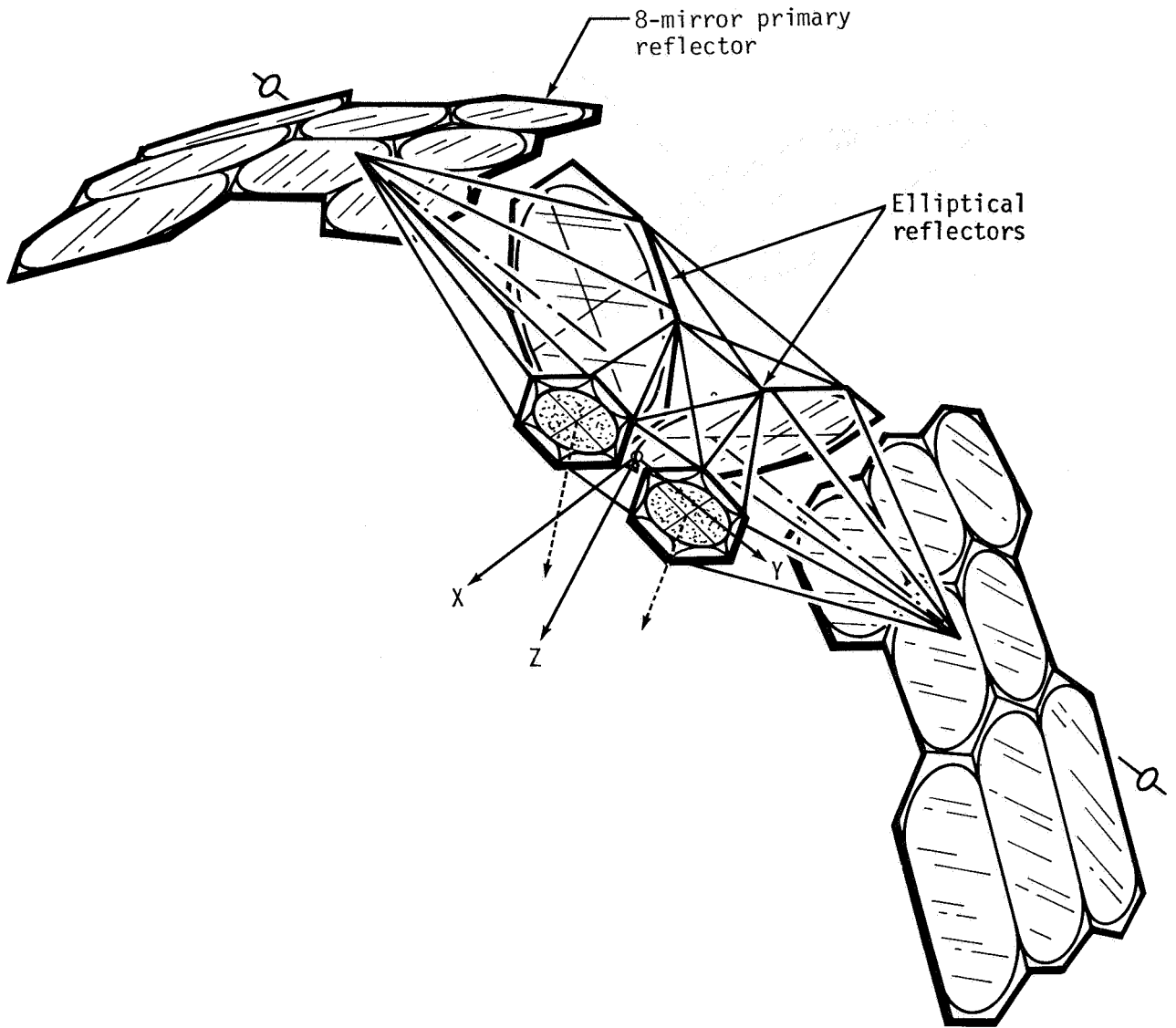
(b) Dual.

Figure III-70.- Concluded.

TABLE III-20.- SOLID-STATE-SANDWICH CONCEPT COMPARISON OF
0- and 10-DECIBEL ANTENNA POWER TAPER

Characteristic	Value for antenna power taper of -	
	0 db	10 dB
Type of solar array	MBG[a]	MBG
Maximum effective concentration ratio	6.0	6.0
Amplifier efficiency	0.8	0.8
Maximum antenna power density, W/m^2	1235	1235
Antenna diameter, km	1.578	1.588
Total transmitted power, GW	2.418	2.049
Power at utility interface, GW	1.591	1.127
Rectenna boresight diameter, km	5.600	4.929
Total satellite mass, kg	10.13×10^6	13.30×10^6
Cost, $		
Satellite	0.796×10^9	0.963×10^9
Construction operations	0.079×10^9	0.096×10^9
Transportation	0.598×10^9	0.798×10^9
Rectenna	0.985×10^9	0.763×10^9
Total[b]	2.789×10^9	3.030×10^9
Installation[c]	1759	2689

[a]MBG = multibandgap.
[b]Includes management and contingency costs.
[c]Dollars per kilowatt at utility interface.

TABLE III-21.- RECOMMENDED SOLID-STATE-SANDWICH
CONCEPT CHARACTERISTICS

Characteristic	Value for option	
	Secondary	Primary
Solar array type	MBG	GaAs
Effective CR	5.2	5.2
Solar array temperature, K (°C)	473 (200)	473 (200)
Amplifier base temperature, K (°C)	398 (125)	398 (125)
Amplifier efficiency	0.8	0.8
Antenna taper ratio, dB	0	0
Antenna diameter, km	1.63	1.83
Power at utility interface, GW	1.53	1.15
Rectenna boresight diameter, km	5.4	4.76

TABLE III-22.- NOMINAL CHARACTERISTICS
OF GaAs-SANDWICH CONCEPT

Uniform illumination effective CR	5.2
Solar cell temperature, K ($^\circ$C)	473 (200)
Solar cell efficiency	0.1566
Solar cell packaging factor	0.8547
Amplifier efficiency	0.8
Amplifier base temperature, K ($^\circ$C)	398 (125)
Antenna ohmic efficiency	0.96
Antenna power density, W/m^2	695.8
Antenna diameter, km	1.83
Antenna area, km^2	2.63
Total transmitted power, GW	1.82
Power at utility interface, GW	1.15
Rectenna diameter, km	4.76
Rectenna area, km^2	16.67

Equivalent solar energy incident upon solar cells (excludes summer solstice and seasonal variations)	→	Effective concentration ratio	→	Solar cell efficiency at AMO 473 K (200° C)	→
3.55 GW		5.2		.1566	
		18.46 GW		2.89 GW	

Array package factor	→	Photovoltaic array power distribution	→	Antenna power distribution	→	dc-rf conversion	→
.8547		.99		.99		.8	
2.47 GW		2.44 GW		2.42 GW		1.93 GW	

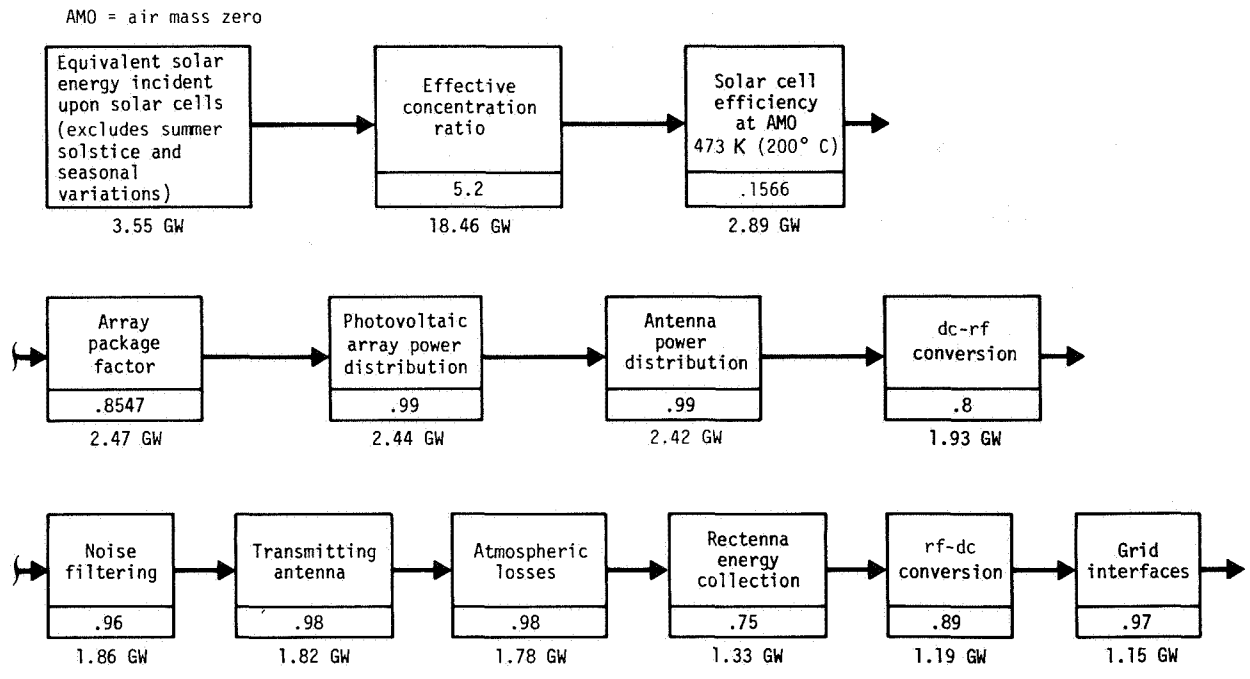| Noise filtering	→	Transmitting antenna	→	Atmospheric losses	→	Rectenna energy collection	→	rf-dc conversion	→	Grid interfaces	→
.96		.98		.98		.75		.89		.97	
1.86 GW		1.82 GW		1.78 GW		1.33 GW		1.19 GW		1.15 GW	

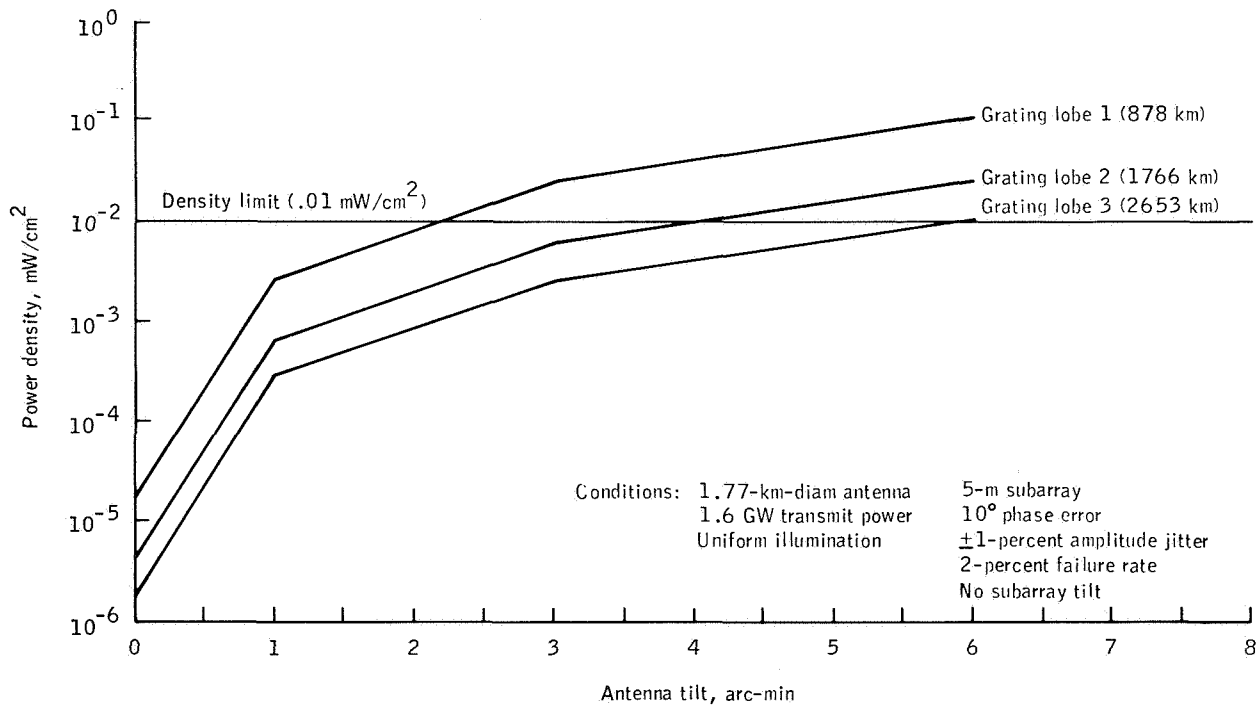Figure III-71.- Efficiency chain for sandwich configuration.

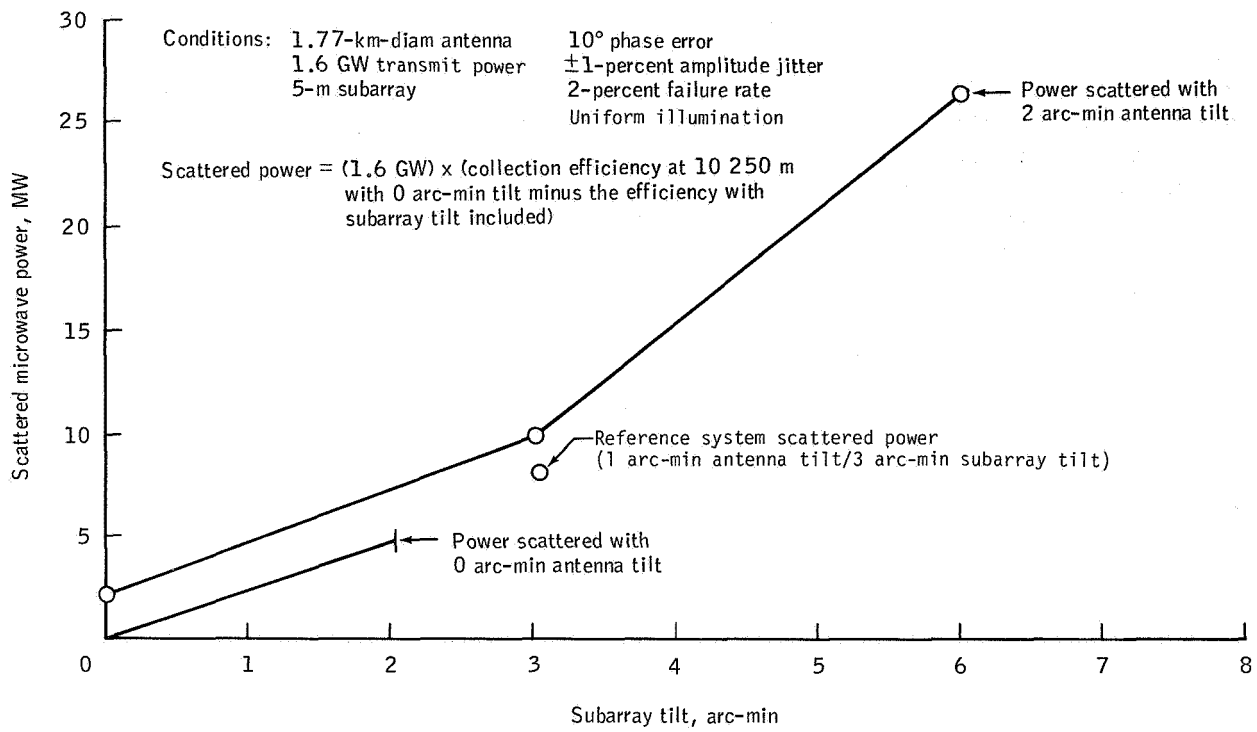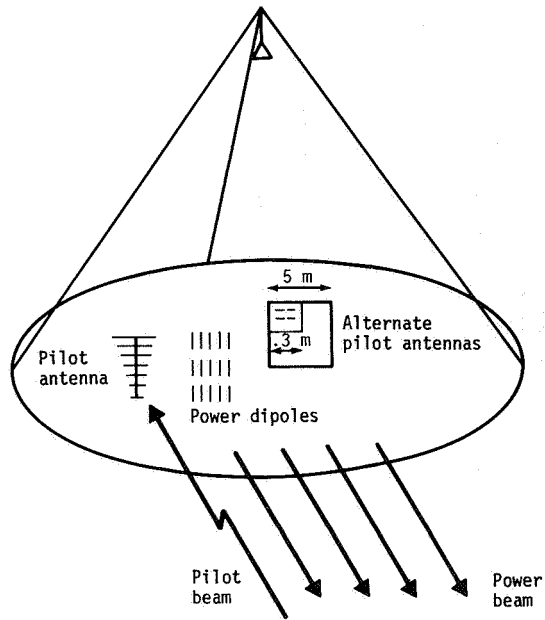Figure III-72.- Effects of antenna tilt on power density at the first three grating lobes.

186

Figure III-73.- Effects of subarray tilt on microwave scattered power.

bottom of the solid-state arrays is illustrated in figure III-74(a). Power dipoles radiate downward in the "power beam," and a high-gain (in this case, a yagi) pilot antenna receives a pilot beam coming from the ground. The received pilot-beam signal is then processed to direct the power beam. An alternate pilot antenna is shown in the square insert. The receiver antenna is orthogonally polarized with respect to the power dipoles to minimize interference from the power signal. The pilot signal received by the antenna is amplified, filtered, and processed in a phase conjugation circuit, which receives a phase reference signal from the rear of the array (fig. III-74(b)). The phase reference antennas are also orthogonally polarized with respect to the power dipoles. A reference-signal transmitter is located somewhere at the rear of the aperture, and sufficiently above to allow reception with a high-gain reference-signal-receiver antenna. An approximate range of reference transmitter heights (H) is indicated also in figure III-74(b). The transmitter should be mounted as low as possible, but gain variations at the receiving point are of concern.

An artist's representation of the sandwich configuration is shown in figure III-75. The solid-state sandwich has an element spacing of 7.81 centimeters.

c. Reference Phase Distribution

The phase reference signal is distributed via rf over the solar array/microwave array as shown in figure III-76. From the shaped-beam illuminator antenna, the rf signal is distributed over a cone with maximally 90° beam width (θ_i). The illuminator may be a corrugated, phase-corrected horn or a synthetic-beam array using multiple weighted generating beams. The latter approach has the advantage of very tight control over the amplitude function, so that all reference pickup antennas receive the same signal strength, and of very high reliability because a large number of distributed transmitters is used with built-in redundancy. Only the local oscillators and driver amplifiers need to be made redundant. However, variations in the structural integrity of the array can be removed modulo 2π (12.24 centimeters) since bandwidth is not a problem with the reference phase signal. The phase at each subarray pickup point is normalized with respect to a perfectly flat uniform aperture by means of a servoloop shown in figure III-77. For each subarray center location, a phase-delay differential ("reference standard") is computed; this differential occurs for the two generating frequencies f_{r1} and f_{r2} if the receiving antenna is located on a perfect plane. These delays can be calculated and tuned in the laboratory to fractions of a degree. The output of the phase bridge then drives a phase shifter until the path-delay differential equals that of the reference standard. Since this circuit is used at every subarray, the subarray center points are electrically normalized to show phase $\phi = \phi_0$ constant across the entire array. By this means, the conjugation circuit is provided with the required reference phase. This concept does not account for any phase distortions due to structural interference of the phase reference signal.

(a) Bottom.
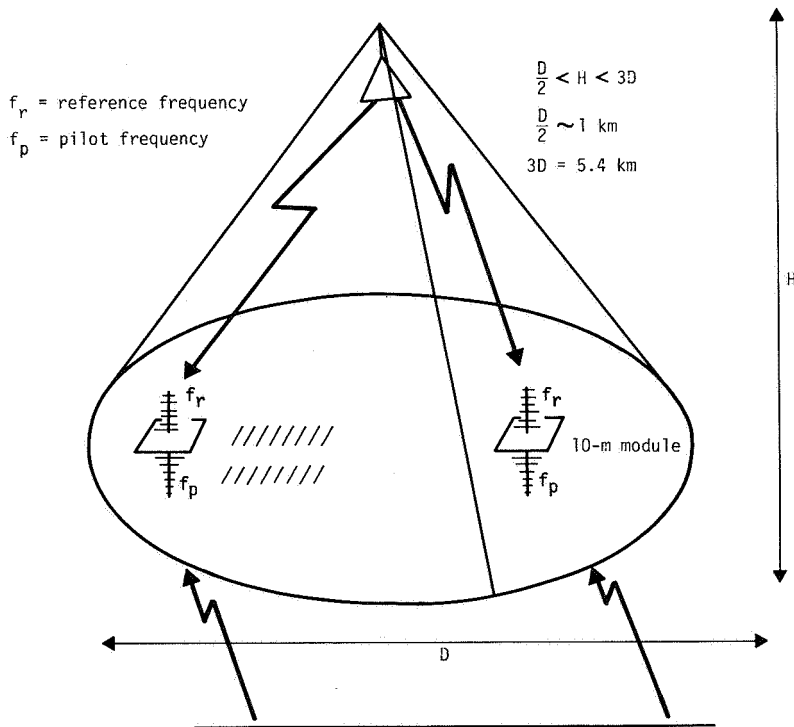
(b) Top.

Figure III-74.- Spacetenna total view.

189

View from Sun

GaAs solar cells
(.252 kg/m^2)

7.81 cm

7.81 cm

Mass density
1.68 kg/m^2

Dipole (4098)

Solid-state amplifier

Berlox radiator

Riser stem

Fiberglass truss

View from Earth

Solar cells

Top of amplifier

Ground plane

3.5 cm

1.0-cm honeycomb sandwich
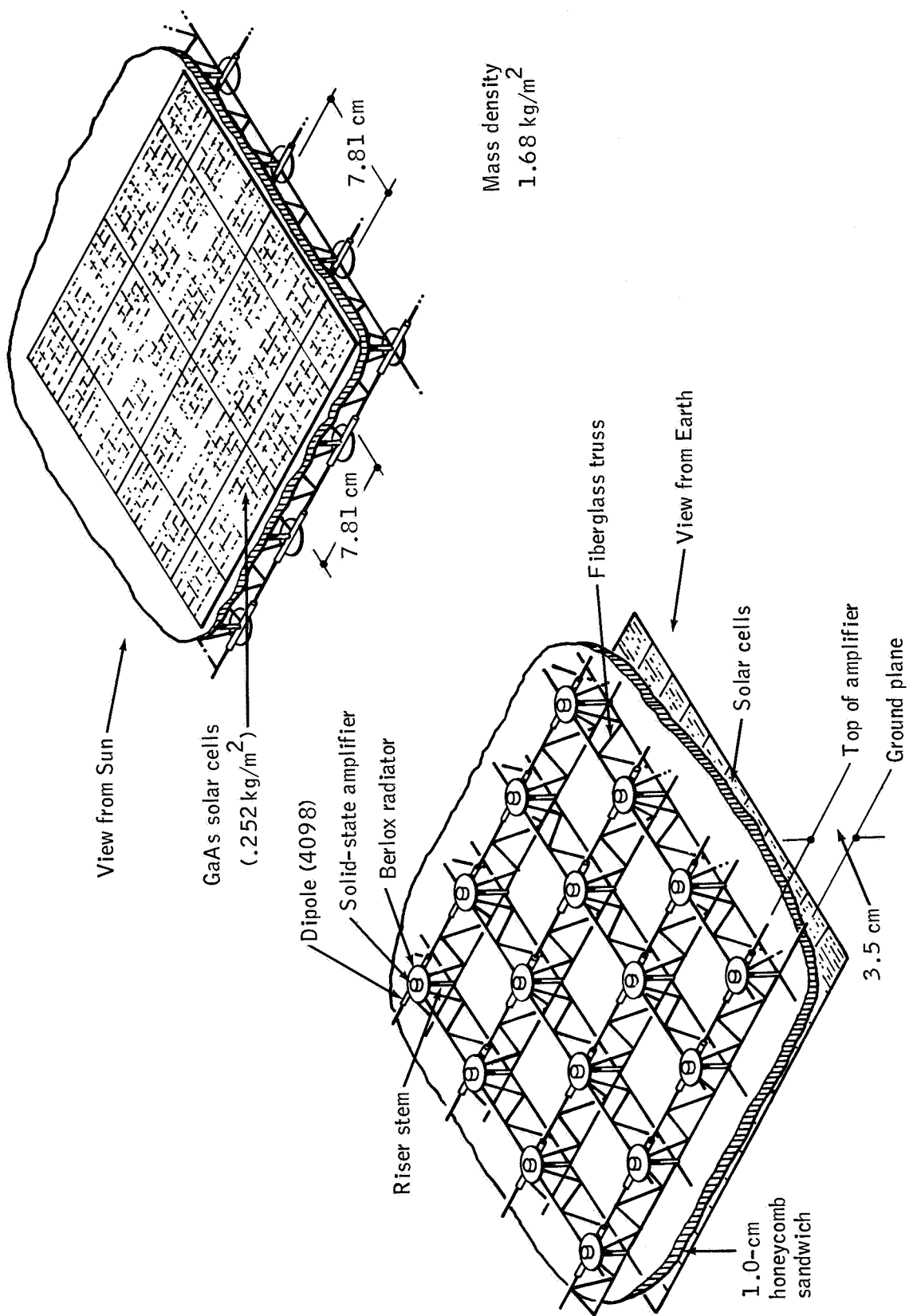
Figure III-75.- Satellite sandwich antenna/solar cell panel configuration (preliminary).

190
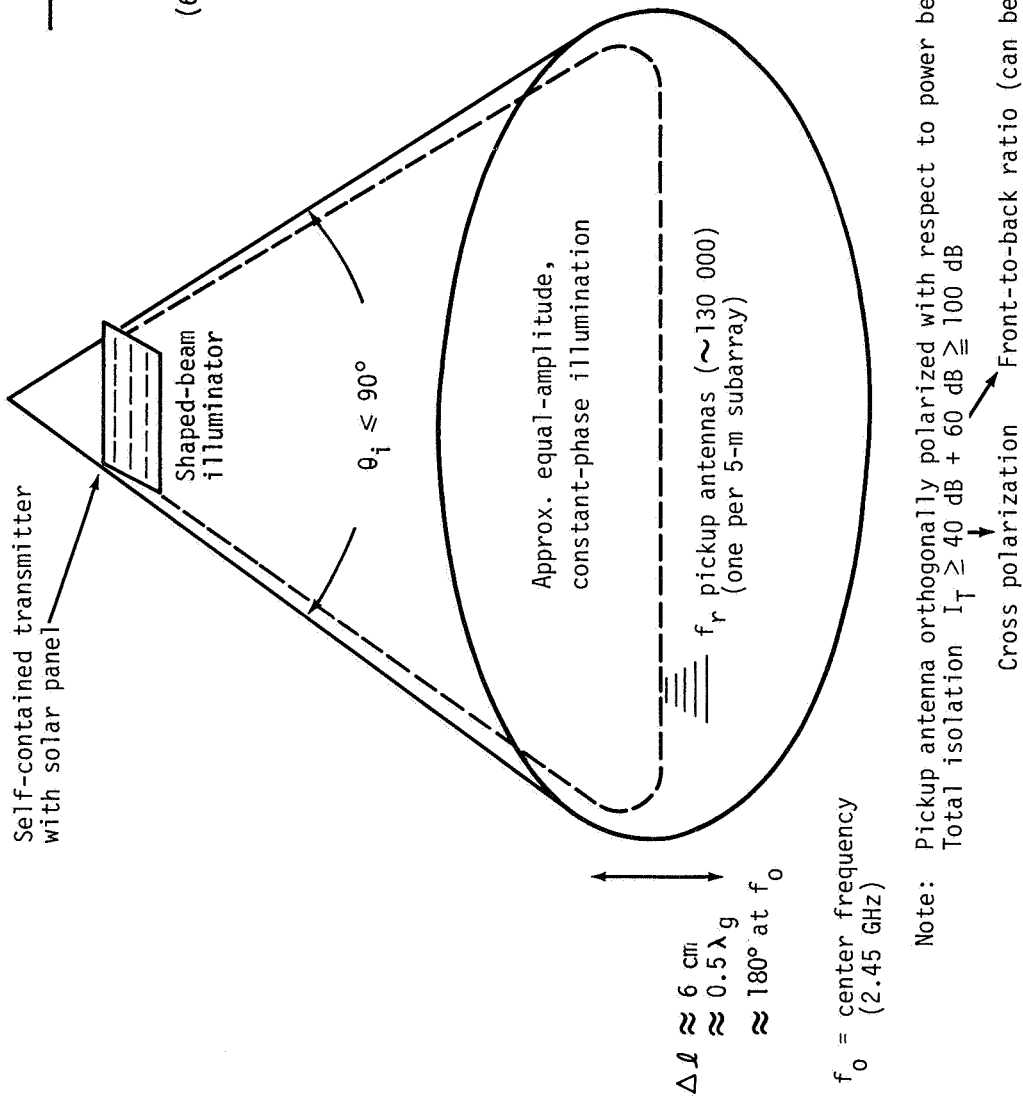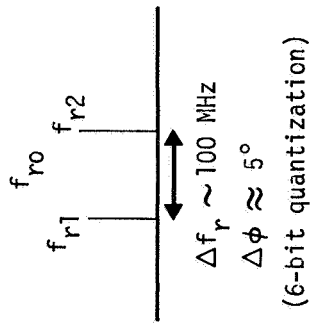
Figure III-76.- Phase reference-signal distribution system for solid-state-sandwich concept.

Self-contained transmitter with solar panel

Shaped-beam illuminator

$\theta_i \leq 90°$

Approx. equal-amplitude, constant-phase illumination

f_r pickup antennas ($\sim$130 000)
(one per 5-m subarray)

$\Delta \ell \approx$ 6 cm
$\approx 0.5\lambda_g$
$\approx 180°$ at f_o

f_o = center frequency
(2.45 GHz)

f_{r1} f_{ro} f_{r2}

$\Delta f_r \sim$ 100 MHz
$\Delta \phi \approx 5°$
(6-bit quantization)

Note: Pickup antenna orthogonally polarized with respect to power beam
        Total isolation $I_T \geq$ 40 dB + 60 dB $\geq$ 100 dB
                                    ↑   ↑
                          Cross polarization   Front-to-back ratio (can be made >100 dB)

191

Figure III-77.- Reference-signal control loop.

L.O. = local oscillator

IV. CRITICAL SUPPORTING INVESTIGATIONS

In this section, the activities accomplished in several technology areas are summarized. The work has been sponsored by the DOE/NASA SPS Concept Development and Evaluation Program and involves individual contractual efforts, generally of less than $100 000 in size.

A. DESIGN AND BREADBOARD EVALUATION OF THE SPS REFERENCE PHASE CONTROL SYSTEM

Lockheed Engineering and Management Services Company (LEMSCO), Inc., has been under contract with JSC since February 1979 to design, breadboard, and test elements of the current baseline phase control system. The overall contractual effort includes the following tasks.

1. Design, fabricate, and test breadboard elements of the master slave returnable timing system. This system is baselined as the reference phase distribution technique for the SPS.

2. Design, fabricate, and test breadboard power transponder units (without the klystron power amplifier) and the pilot signal transmitter (ground station unit).

3. Integrate the MSRTS distribution system with at least two power transponder units and conduct end-to-end system performance evaluations.

4. Evaluate high-power klystron noise-reduction phase-lock-loop performance and establish output phase noise characteristics (using 1-kilowatt L-band klystron obtained on surplus from the NASA Goddard Space Flight Center).

In the following discussion, the accomplishments and current status of the LEMSCO effort are described. The MSRTS technique as described by Lindsey (ref. 28) is proposed as a potential method of accurately transferring phase from the reference pilot receiver at the center of the SPS microwave array antenna to each conjugation point (power tube) in the SPS array. A small-scale breadboard of this type of distribution technique has been built and tested in the JSC Electronic Systems Test Laboratory (ESTL). The results are summarized here. A simplified functional diagram of the MSRTS is shown in figure IV-1; its operation is described in Section III.B.2. In the SPS application, the choice of distribution frequencies is limited by the modulo 2π phase ambiguity at the slave node. This ambiguity is manifested at frequency 2ω and corresponds to a modulo π phase ambiguity at the actual distribution frequency. Thus, the distribution frequency must be an even submultiple of the frequency desired for phase conjugation to eliminate the π ambiguity (i.e., any even multiple of π is modulo 2π; thus, no ambiguity exists). The current SPS baseline concept embodies a four-level phase distribution tree using the MSRTS for phase transfer accuracy. The reference-signal phase is maintained throughout the system by using the slave signal at each node of the tree as the master reference for transmission to the next node. Currently, nine MSRTS electronic units have been fabricated.
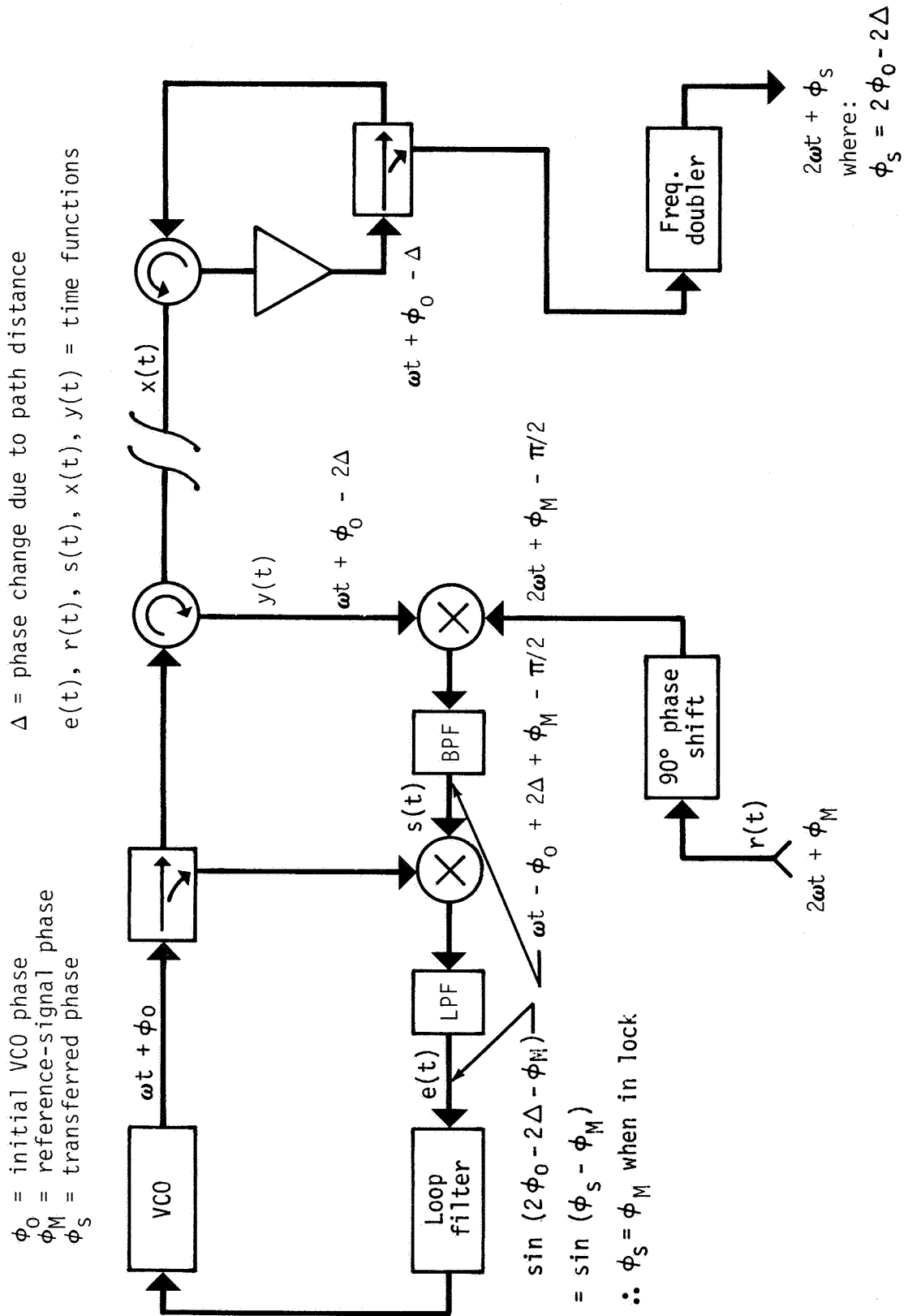
Figure IV-1.— Simplified functional diagram of MSRTS.

194

Initial testing was accomplished on three units, and tests are in progress using a four-level (node) network involving five MSRTS units.

The MSRTS detailed circuitry at each node of the SPS, the system test configurations, and the test results are provided in reference 50. A typical test-configuration block diagram is shown in figure IV-2. Data were obtained by interchanging several cables of different (arbitrary) lengths for cables A and B shown in the figure. The statistical properties of the resulting phase errors between the final nodal point (third level) and the reference (source) are shown in figure IV-3. Because of the relatively small samples of cable combinations (30 possible combinations), a firm conclusion of phase error distribution is not possible. However, for the large numbers involved in the SPS (101 552 points), the error distribution is assumed to be Gaussian with little or no reservation. The observed rms phase error was 4.2° for this particular test. Several similar types of tests were conducted using the MSRTS units in different tree configurations.

On the basis of these initial tests, it can be concluded that satisfactory MSRTS performance can be achieved using readily available components under these closely controlled laboratory-type conditions. However, it must be pointed out that this performance was achieved only after numerous circuit modifications were made to account for the nonideal behavior of these components. For example, port-to-port isolation specifications for the mixers and circulators used in the breadboard MSRTS units are on the order of 20 to 30 decibels. External balancing and leakage-cancellation circuits were required (as discussed in ref. 50) to increase the effective isolation to approximately 40 to 50 decibels to obtain the performance measured.

Further testing is required to determine feasibility of the MSRTS concept for practical applications such as the solar power satellite. For example, additional tests must be performed to determine sensitivity of various MSRTS components to temperature variations and other environmental factors. System tests integrating the MSRTS distribution system and power transponder units may uncover other potential problem areas.

The power transponder breadboard design is completed, and all parts have been procured. The completion of all testing is scheduled for the end of 1980. A functional block diagram of the pilot signal transmitter is shown in figure IV-4, and block diagrams of the pilot receivers (central and conjugating) are shown in figures IV-5 and IV-6. It should be noted that the central pilot receiver is somewhat different in design since it must establish the initial reference signal for distribution by the MSRTS to the other pilot receiver/conjugation units. This difference is seen mainly in that a stable local reference is provided for the first and second local oscillators in the PN code-tracking branch of the central pilot receiver. In the pilot/ conjugation receivers, these local oscillator signals are derived from the phase reference distribution signal provided by the MSRTS distribution system. One further point of interest involves the phase-lock loop around the "simulated" power amplifier. One of these units will be integrated and evaluated using the 1-kilowatt L-band klystron as the power amplifier shown in

PTU = phase tracking unit
IRU = interface return unit
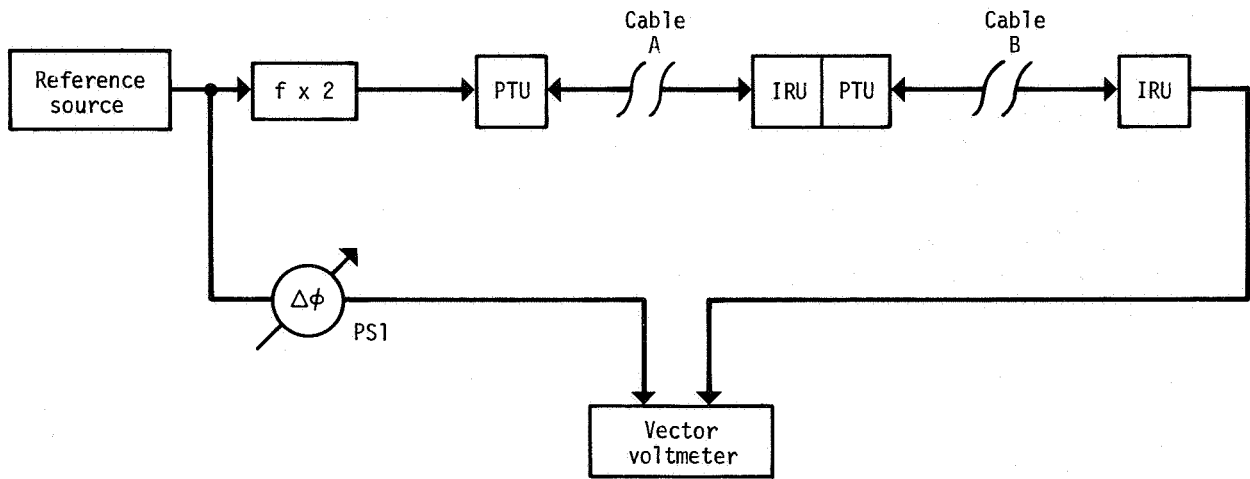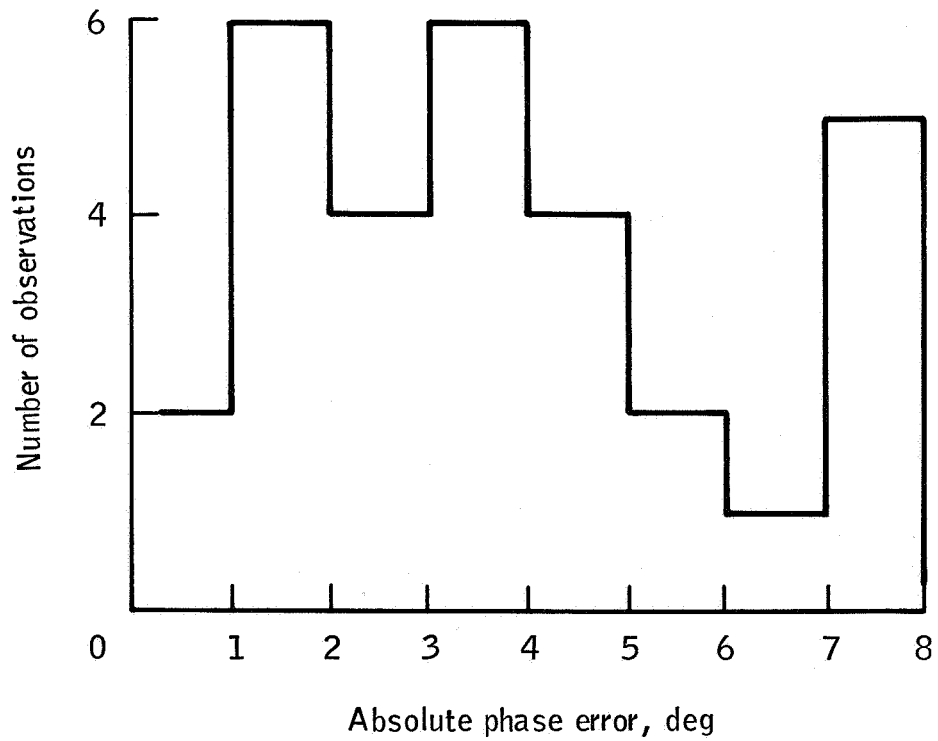

Figure IV-2.- Three-node test configuration.

Std. dev. of 30-trial sample = 4.2°

Figure IV-3.- Histogram of three-node test results.
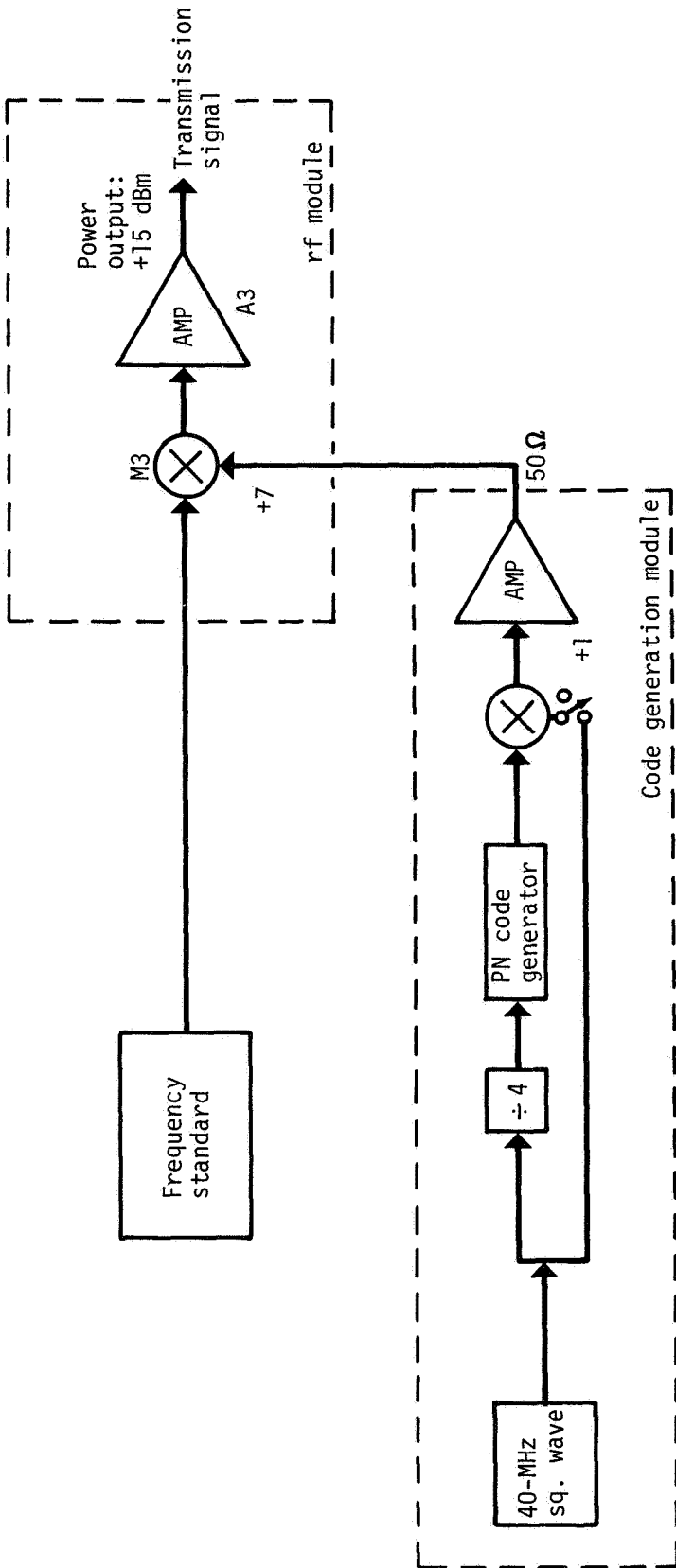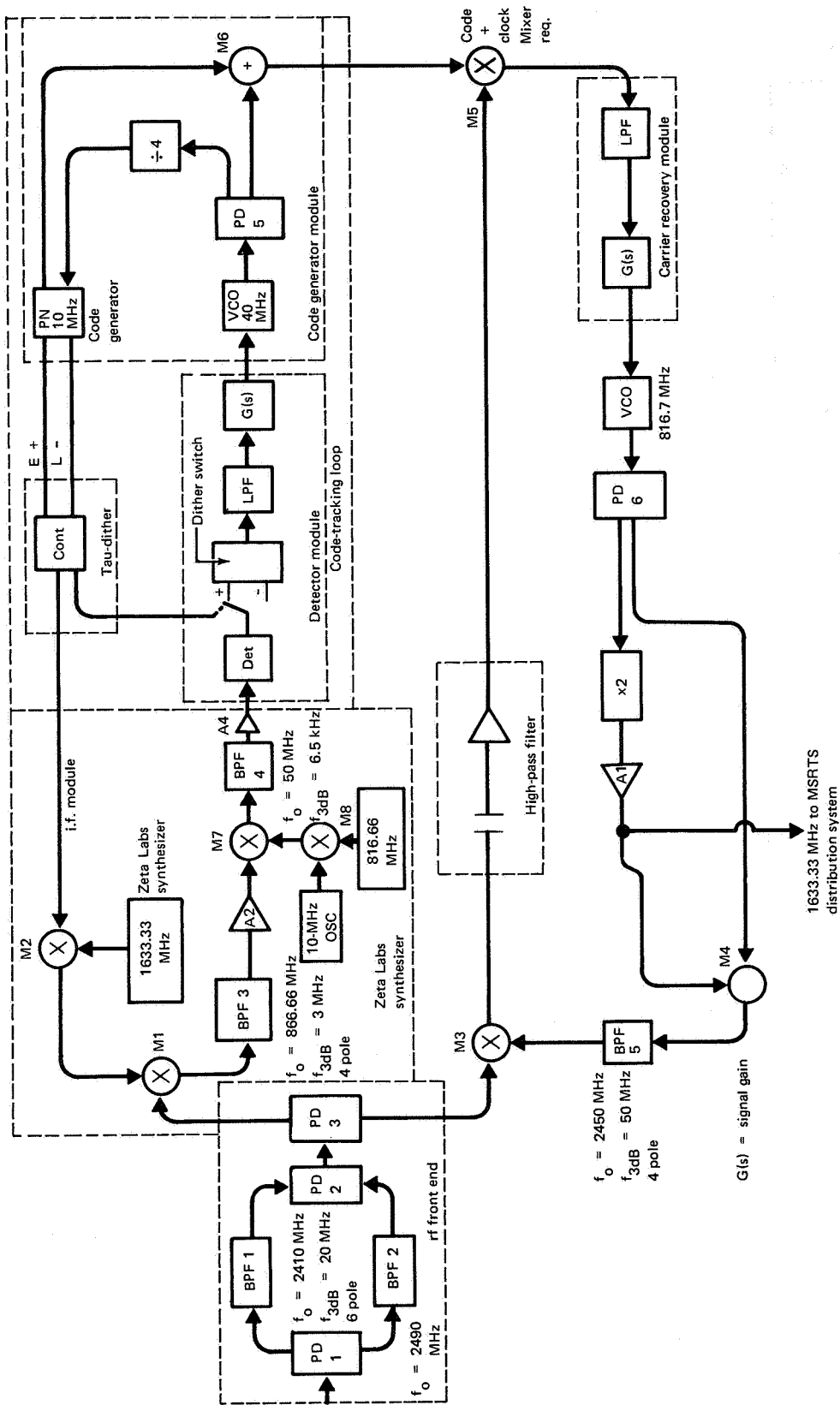
Figure IV-4.- Pilot-transmitter block diagram.

197

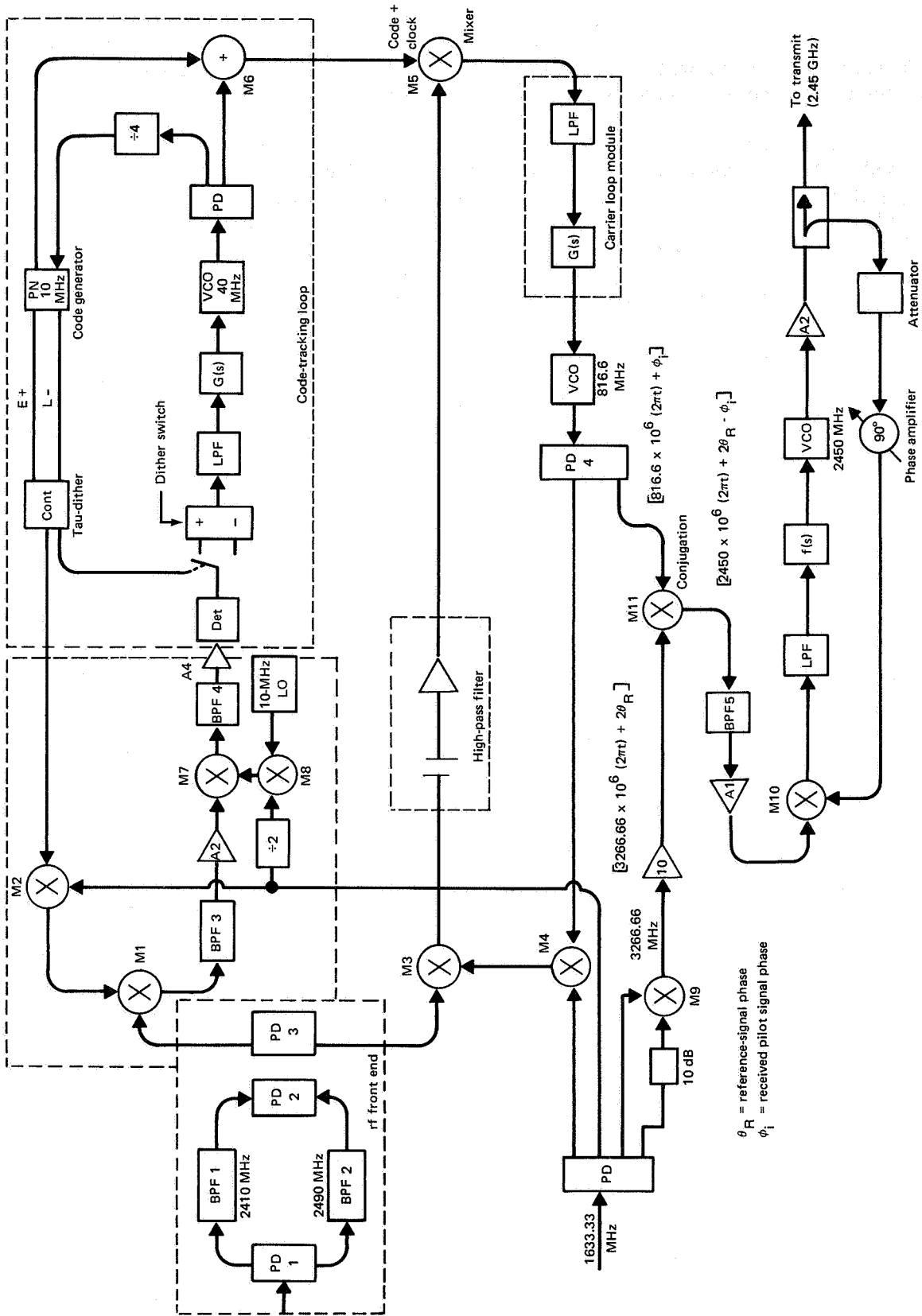Figure IV-5.— Central pilot receiver block diagram.

Figure IV-6.- Pilot/conjugation receiver block diagram.

θ_R = reference-signal phase
ϕ_i = received pilot signal phase

199

the block diagram. Phase noise characteristics with and without the phase-lock loop activated will be obtained to determine effectiveness of reducing low-frequency phase noise with phase-lock-loop techniques.

Finally, a series of overall end-to-end system performance tests is planned. These tests will use the integrated MSRTS and pilot receiver/conjugator units, together with the pilot transmitter. The tests are designed to evaluate the accuracy of the conjugated phases, effects of random variations in pilot transmitter to pilot receiver path lengths, system noise effects, effects of power signal interference, and simulated ionospheric disturbance effects. A typical system test configuration is shown in figure IV-7. In this configuration, individual path lengths, signal levels, and/or other effects can be injected into the system under controlled laboratory conditions and thus detailed engineering evaluation of system response can be performed. If performance is seriously degraded in certain instances, potential mitigating strategies can be evaluated. The system-level tests are scheduled to begin in September 1980.

B. FIBER OPTICS LINK ASSESSMENT

The Boeing Aerospace Company has been under contract to JSC since December 1979 to demonstrate the feasibility of a fiber optic link for transmission of a 980-megahertz analog signal. Potential application of fiber optic transmission links to the SPS phase control distribution system is attractive since fiber optics provide advantages over rf cabling in areas of weight, volume, flexibility, and, in particular, EMI susceptibility. However, incorporation of a fiber optic distribution system would introduce optical components of questionable reliability. An overall SPS reference phase control concept using fiber optic techniques is shown in figure IV-8 (ref. 51). The tasks accomplished were (1) analyses of existing optical fibers and components for potential use in the SPS phase distribution system concept, (2) design and construction of a breadboard optical link for laboratory evaluation, and (3) assembly and test of a two-way optical link at 980 megahertz of approximately 200 meters length. Figure IV-9 is a block diagram of the optical two-way link as it will be ultimately configured for system testing at the ESTL.

Several types of optical components and fibers were investigated. These are addressed in detail in reference 51. The selected link configuration incorporates an injection laser diode supplied by Nippon Electric Company (NEC) (NDL-3205P) for the emitter device. An avalanche photodiode was selected as the detector component, and an RCA device (C30908F) was chosen. Four fibers were evaluated during the fiber test phase of the program, and the Corning inside vapor phase oxidation (IVPO) fiber (product 5101) was selected for use in the dual-link configuration. Measurements of phase delay and attenuation of the 980-megahertz signal through each type of fiber were evaluated at a fixed temperature and for variable temperatures of the optical fiber. The basic test setup shown in figure IV-10 indicates the optical and electrical signal levels used in the tests. The results of signal phase changes as a function of temperatures for the Corning IVPO fiber at 60 megahertz for a 1-kilometer length are shown in figure IV-11. Data were obtained at signal frequencies of 60 and 980 megahertz.

200
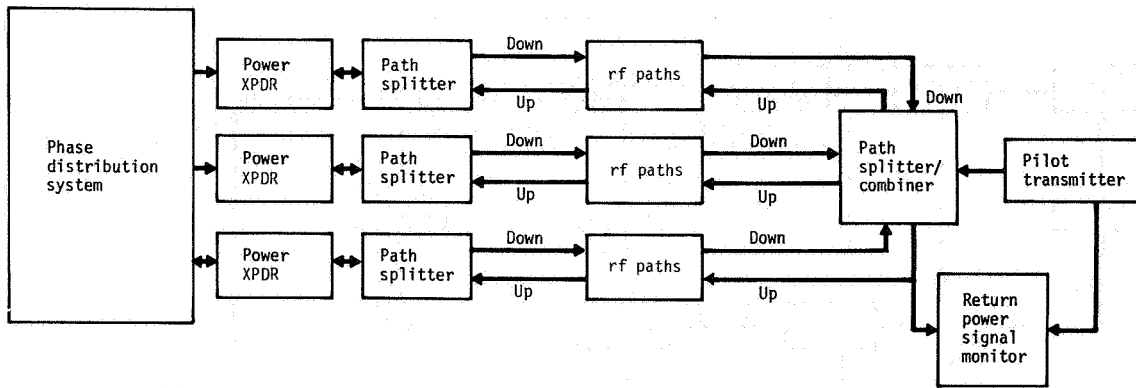
- Laboratory configuration allows highly accurate phase error measurements
- Radiofrequency path allows precisely controlled parameters
  - Pilot signal to power signal interference ratios
  - Fixed path-length differences
  - Path-length variations (slow and rapid) - simulating ionospheric/atmospheric effects

Figure IV-7.- Laboratory end-to-end system test concept.

A. Power divider

B. Phase control center line length compensation

C. Fiber optic transceiver two-way link

D. Klystron phase compensation loop
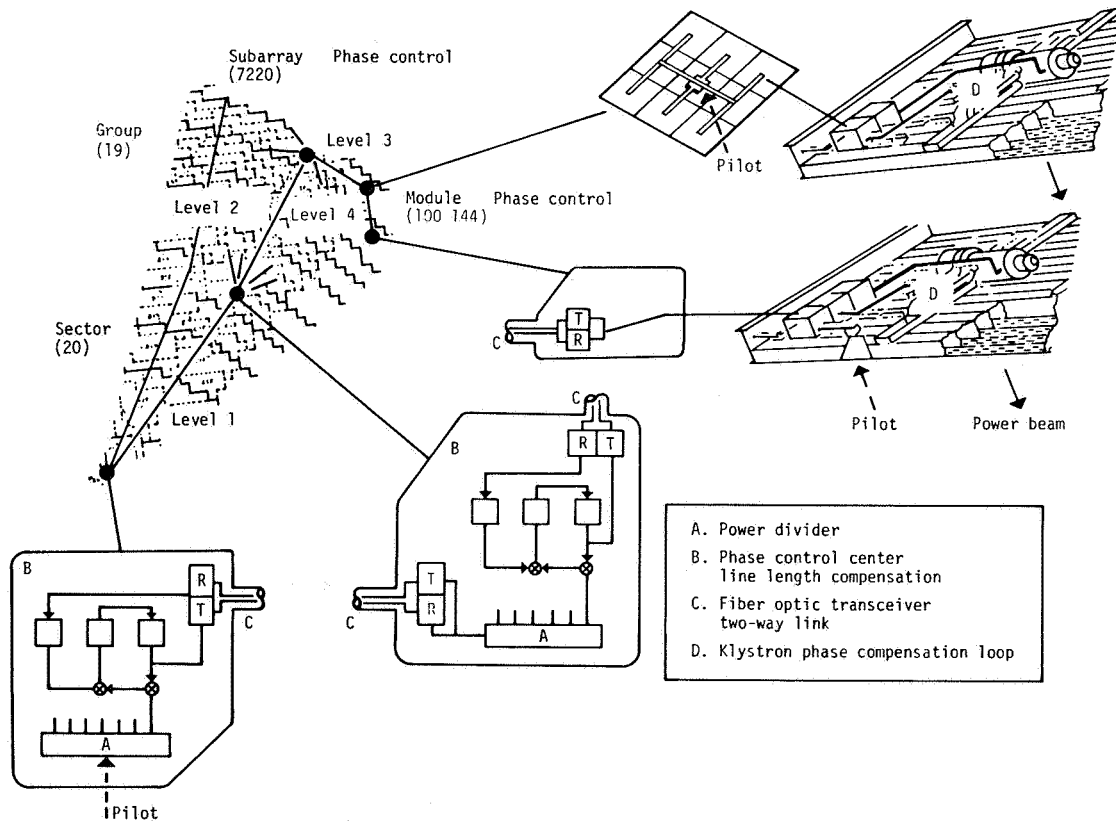
Figure IV-8.- SPS reference phase control system.

201
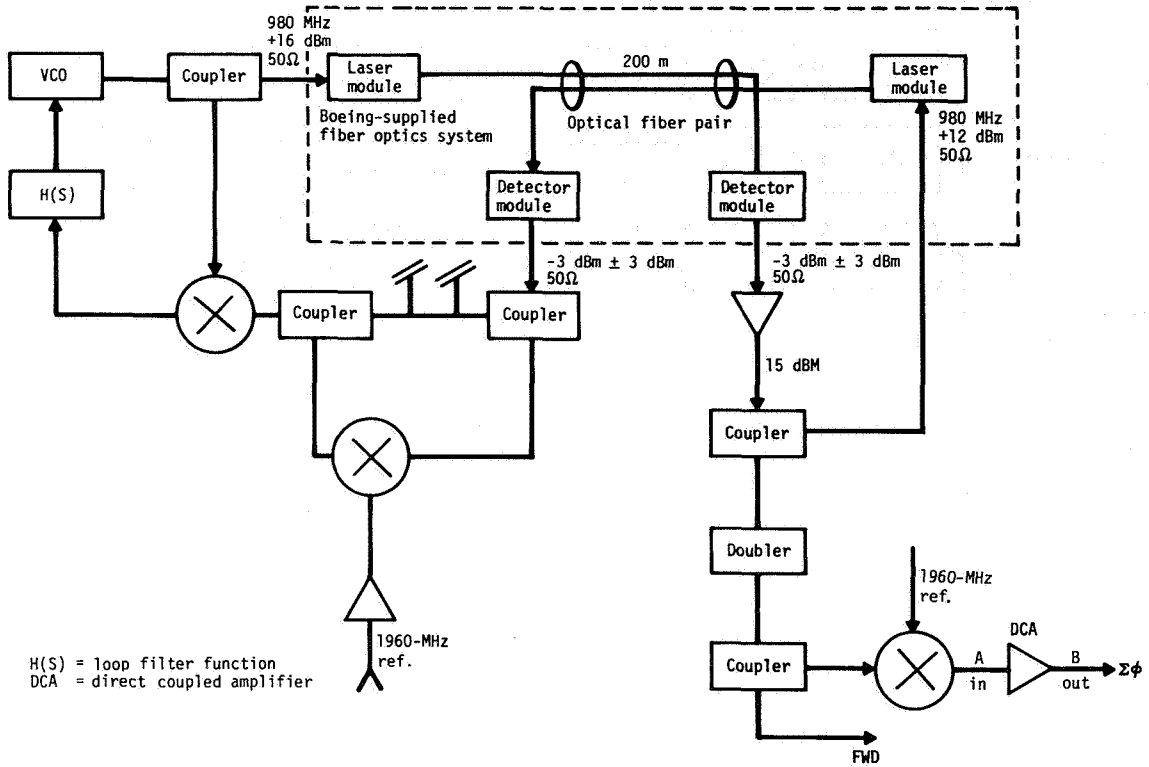
Figure IV-9.- SPS fiber optics dual-link system.
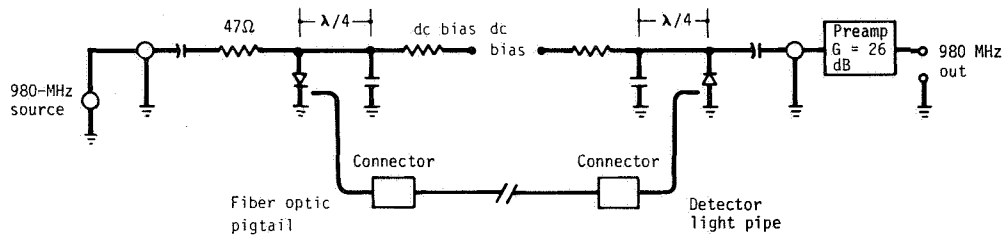
Emitter	Fiber	Detector
NEC injection laser diode	Corning IVPO, graded index	RCA avalanche photodiode
Bias coupled through quarter-wave microstrip	Length = 303 m	Bias coupled through quarter-wave microstrip
I_{bias} = 88 mA dc	Atten = 3.9 dB/km	V_{bias} = 180 V dc
	BW = 870 MHz-km	
Optical power = 437 μW at emitter pigtail	N.A. = 0.218	Optical power = 228 μW at detector light pipe
V_{980MHz} = 0.7 V rms		V_{980MHz} = 135 mV rms out of preamplifier
	BW = bandwidth	
	N.A. = numerical aperture	

Figure IV-10.- Initial SPS 980-megahertz fiber optics link test.
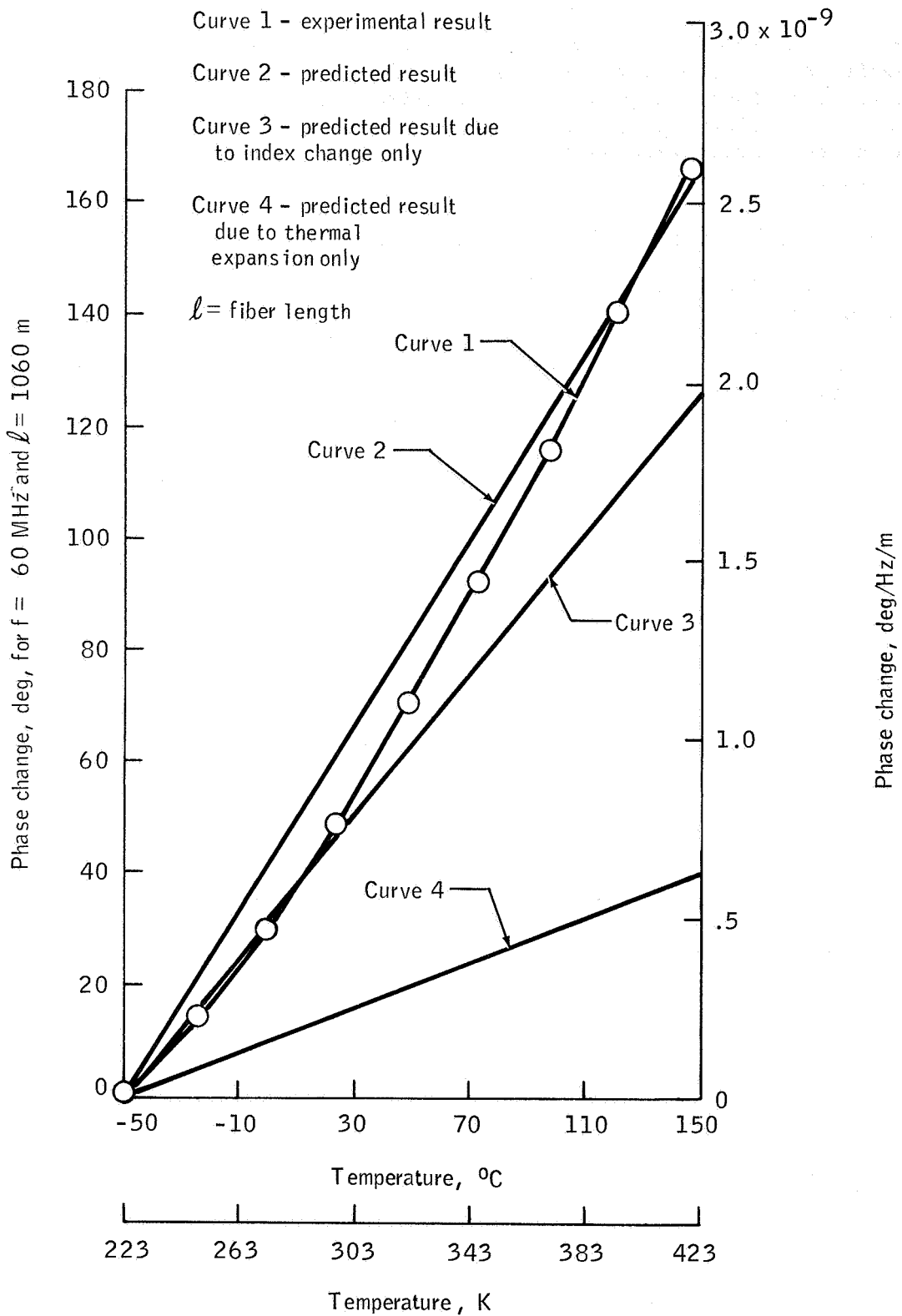
Figure IV-11.- Phase delay as a function of temperature for IVPO fiber.

The two-way link was fabricated and tested to verify satisfactory transfer of the 980-megahertz signal. The received signal was observed, and its amplitude and phase appeared extremely stable and essentially noise free. These fiber optic links should be suitable for use in the closed-loop phase distribution system testing planned for the summer of 1980 at the ESTL.

C. S-BAND ACTIVE RETRODIRECTIVE ARRAY PHASE ERROR EVALUATION

The Jet Propulsion Laboratory is scheduled to perform a series of tests using the active retrodirective array system which they have been developing. The tests (scheduled for early March 1980) have had to be rescheduled because of unavoidable delays in obtaining certain components for the array fabrication. Much of the system hardware has been fabricated, and individual units have been checked out in a bench test configuration. The basic system configuration to be evaluated is shown in figure IV-12. The system will be erected in an anechoic chamber and tests conducted to establish accuracy of the retrodirective beam-forming and pointing functions.

1. PROCEDURE

The pilot source assembly, consisting of the pilot source and a receiver diplexed to the same antenna, will be moved in an arc about the ARA midpoint to verify retrodirective scanning of the ARA. Since the 3-decibel beam width of the individual ARA elements is about $8°$, the pilot source assembly will be moved through an arc of about 2 meters between half-power points. Since a positioner and its automatic pattern recorder cannot be used, it will be necessary to measure receiver output as a function of scan angle at many points on the arc. The measurement will be repeated with the ARA elements displaced from their nominal positions in both a regular and random manner.

The pattern produced by the ARA will be measured by moving a small antenna in an arc about the ARA midpoint while the pilot source remains fixed along the ARA boresight. This is a qualitative measurement only; the pattern produced by an eight-element ARA is not a reliable indication of the pattern of an array composed of many thousands of elements.

2. EXPERIMENTAL RESULTS

Plans to construct and evaluate an eight-element active retro-directive array could not realized because of lack of resources. As a result, experimental data are available only from the bench tests of the phase control system electronic modules. Results of these tests indicated that proper phase conjugation was achieved; however, phase ambiguities were present as a result of the frequency dividers. Although the ambiguity problem must be corrected for "central phasing" to be a workable concept, the tests were beneficial in identifying sources of phase error such as mixer imbalance, mismatch, etc. A final report covering the bench test results will be prepared by JPL.

Figure IV-12.— Beamed rf power technology: eight-element experimental active retrodirective array block diagram.

Legend:

R-T = RCVR-XMTR-diplexer assy

φC = Phase conjugator

φRR = Phase reference regenerator

φ_0 = Reference phase

2PLX = Diplexer

205

D. ANTENNA ELEMENT EVALUATION

        The Boeing Aerospace Company has been under contract to JSC since
July 1979 to better define the electronic aspects of the SPS waveguide slot
array. The specific objectives of the program and the status of results were
presented at the SPS microwave workshop held at JSC in January 1980 (ref. 52).
The following material is a summary of the objectives and status of this task.
The objectives are

        1. To build a full-scale, half-module, 10-stick array, the design
            parameters for which are to be determined by analytical consider-
            ations tempered by experimental data on a single slotted radia-
            ing stick

        2. To experimentally evaluate the completed array with respect to
            antenna pattern, impedance, and return loss

        3. To measure swept transmission amplitude and phase to provide a
            data base for design of a pilot receiving antenna

    1. THEORY AND PROCEDURE

        The first step in module design is to fix the gross dimensions,
including the module length and width, and the dimensions of the radiating
sticks and the feed waveguide. Because the feedguide is a standing-wave de-
vice in which the coupling slots must be spaced by $\lambda_g/2$, where λ_g is the
guide wavelength, and because λ_g is a function of waveguide width, the
radiating-stick and feedguide dimensions are not independent.

        The SPS baseline design consists of a half module of ten 1.6-
meter-long sticks of 6- by 9-centimeter cross section. For these dimensions,
at the SPS frequency, the feedguide dimensions are also 6 by 9 centimeters.
To assess the desirability of the baseline configuration, it was decided to
configure the experimental module according to the baseline design. The com-
mercially manufactured waveguide which most nearly approximates the baseline
guide is WR-340, with dimensions of 4.32 by 8.64 centimeters. Because this
waveguide was not available in sufficient quantity, the WR-284 waveguide was
used instead for the developmental module. Because this waveguide is narrower
than the baseline, and because it would be used for both the radiating sticks
and the feedguide, the design frequency of the developmental module was in-
creased from 2.45 to 2.86 gigahertz.

        The design of the waveguide stick entails the assignment of
values to both the slot offset from the waveguide centerline and the slot
length. The slot length ℓ is chosen so that the slot is resonant at the
design frequency. The slot offset is chosen to give the desired slot con-
ductance, which is determined by impedance matching considerations. Thus,
for a waveguide stick containing N identical shunt slots, the desired value
of normalized slot conductance g is just g = 1/N.

        For a single isolated stick, the choice of slot length and slot
offset is relatively straightforward. The slot length is given to good

approximation by $\ell = \lambda_o/2$, where λ_o is the free-space wavelength. The conductance and the slot offset are related to sufficient accuracy by a well-known equation. Tentative radiator stick dimensions in the WR-284 waveguide are (ref. 52): slot spacing, 7.62 centimeters; slot length, 5.03 centimeters; slot width, 0.317 centimeter; slot offset, 0.475 centimeter; and number of slots, 18 or 20. Where several sticks are placed in close proximity, however, as they are in the SPS module, the design problem is exaggerated by mutual coupling between the sticks; that is, the slots in any particular stick are loaded by the slots in the neighboring stick and will necessarily exhibit resonant frequencies and conductances which differ significantly from those predicted by single-stick equations.

Because of the mutual-coupling problem, the choice of slot length and offset has been pursued in an iterative manner beginning from the single-stick analytical values. Data for several iterations with two waveguide sticks are shown in table IV-1. Because the slot offsets, once machined, are fixed, stick impedance in these data are varied by changing the number of slots by means of a sliding short circuit in the waveguide.

The radiating waveguide sticks are fed in phase by a feed waveguide the axis of which is perpendicular to those of the radiating sticks. Like the radiating sticks, the feedguide supports a standing wave. The power is coupled from the feedguide to each radiating stick through a resonant (length, $\lambda_o/2$) coupling slot, which is inclined to the feedguide axis. The transformed radiating-stick impedance encountered by the feedguide is proportional to $\sin^2 2\theta$, where θ is the inclination angle. The phase of the power coupled to the stick is inverted as the coupling slot is reflected in the feedguide axis. For maximum power transfer to the 10 radiating sticks, each stick must present an impedance to the feedguide of one-tenth the feedguide characteristic impedance. This value dictates a rather small coupling-slot inclination of about 7°. To maintain proper phasing of the radiating sticks, the coupling slots are alternately reflected in the feedguide axis.

The receiving antenna receives a pilot signal from Earth with phase information to keep all modules in phase. For symmetry, the pilot signal should originate from the center of the SPS Earth receiving array. Ionospheric phase shift and Faraday rotation indicate that the pilot signal should be centered on the SPS power frequency with the phase information in symmetrically disposed sidebands. The purposes of the receiving-techniques evaluation were as follows.

    a.   To conduct a shared receiving antenna compared to separate receiving antenna study to determine feasible pilot-beam budget and receiving-antenna constraints due to power module

    b.   To design and select a pilot-beam receiving-antenna technique compatible with a power beam array which must allow simultaneous transmission of an S-band carrier and reception of the anticipated pilot-beam spread-spectrum signal

TABLE IV-1.- ITERATIVE DESIGN PROCEDURE FOR
RADIATING-STICK PARAMETERS

Stick no.	No. of slots[a] for best match		Slot offset,[c] cm	Slot length, cm	Comments
	Single stick	Dual stick[b]			
1	22	20	0.457	5.18	Resonance at 2800 MHz; slot excessively long
2	16	14	.508	4.927	Resonance at 2880 MHz; slot excessively short; excessive conductance per slot
3	18	16	.475	5.029	Resonance at 2875 MHz
4	18	18	.457	5.08	Resonance at 2860 MHz[d] expected

[a]Sliding short-circuit measurement: VSWR at resonance = 1.1.
[b]Nonduplicate sticks are used to approximate mutual-coupling effect.
[c]Affects slot conductance primarily.
[d]Desired frequency for matching of feedguide and radiating-stick guide (WR-240).

The pilot-beam analysis established that very small, low-gain pilot receiving-antenna elements embedded in the transmitting array are significantly superior to any scheme of diplexing, because (a) the total system power losses are two orders of magnitude lower using a separate antenna than with any state-of-the-art diplexing device; (b) the small antenna, because of its inherent broad bandwidth, is fully compatible with a spread-spectrum signal, whereas the transmit array is not; and (c) the small, low-gain antenna represents a much lower development risk than a diplexing device.

An important consideration in the pilot-link design is the isolation of the pilot receiver from noise inherent to the high-power downlink signal. With the dipole, isolation can be improved by rotating the antenna so that it is cross-polarized to the power transmitting antenna. An alternate noise-canceling scheme uses two dipoles per receiving antenna, as shown in figure IV-13. These are separated by $\lambda_o/4$ and can, therefore, be connected to pass, as would a directional coupler, radiation coming from the Earth while rejecting that which is earthbound. One of the candidate receiving antennas in figure IV-13, the slot, or "credit-card" receiving antenna, has been built and sweep-tested. It consists of a 4.44- by 0.157-centimeter Teflon-glass microcircuit board short-circuited around three edges to form a low-impedance waveguide cavity.

The antenna pattern of the breadboard slotted-array module was measured on one of the six antenna ranges at Boeing. Besides observing the far-field rule $R > 2D^2/\lambda \geq 55$ meters, where R is range and D is antenna diameter, high paths and sharp-beam range illuminators were employed to minimize multipath errors. For the ranges at the Boeing Developmental Center, multipath errors at beam center are estimated to be well under ± 0.1 decibel. Gain is measured using a Scientific Atlanta SA-1740 precision amplifier-receiver and SA-12-1/70 standard-gain horn. Measurement accuracies are estimated on the basis of total root-sum-square (rss) errors to be ± 0.4 decibel or ± 9 percent in power.

The antenna efficiency is obtained from the experimental measurement of gain G, with respect to a reference horn, and of directivity D. Since the directivity is the gain of a lossless antenna, the ratio of these values represents the efficiency of the antenna. The gain is obtained from the measured value of incremental gain above a calibrated standard horn. The directivity is expressed as the ratio of the maximum radiation intensity U_{max} to the average radiation intensity $\bar{U} = 1/4\pi \iint U(\theta,\phi)d\Omega$, where θ is azimuth angle variable, ϕ is elevation angle variable, and Ω is angular space.

The directivity measurement is performed separately by rotating the antenna continuously through selected azimuth and elevation angles and integrating the far-field contributions over a solid sphere to obtain the directivity with reference to an isotropic radiator as $D = U_{max}/\bar{U}$. The efficiency is obtained from the ratio of these two separately measured experimental values, $\eta = G/D$. With currently available antenna range accuracy, this measurement is typically determined to ± 0.4-decibel accuracy. The resulting efficiency value will give an indication of ohmic losses in the waveguide feed system and in the radiating sticks. Since in the SPS baseline

209
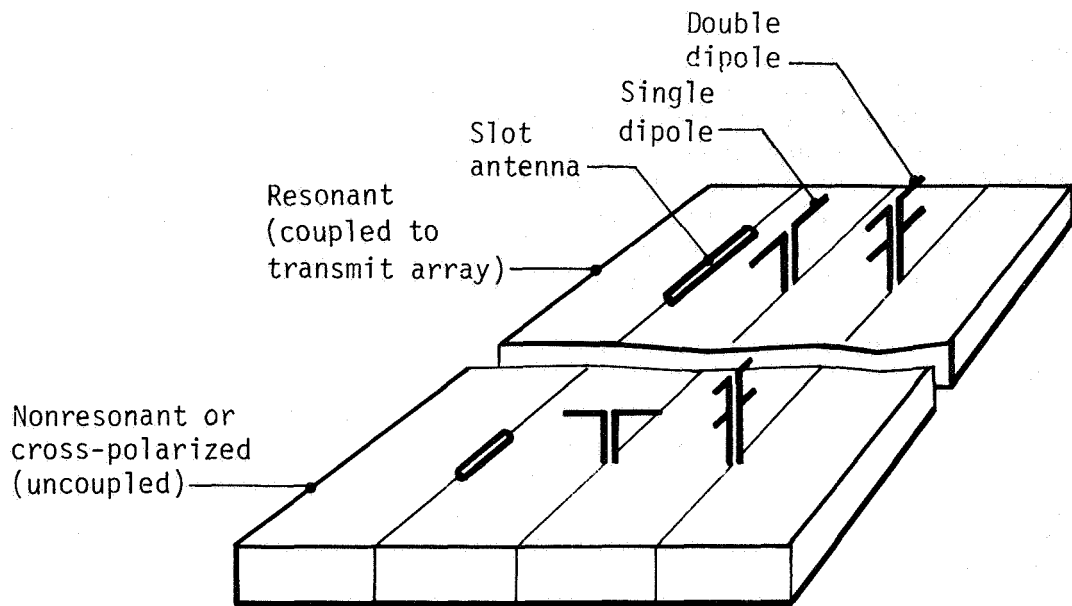
Figure IV-13.- Potential SPS pilot-link receiving-antenna configurations.
The double-dipole configurations afford partial noise cancellation.

design, this loss is estimated to be less than 0.1 decibel, the antenna range measurement can only provide a crude verification.

2. EXPERIMENTAL RESULTS SUMMARY

State-of-the-art antenna gain measurements (30.56 ± 0.35-decibel accuracy) were adequate to bracket the aperture efficiency to 85.7 ± 7 percent, indicating good agreement for a 200-slot module based on the theoretical directivity of 31.23 decibels. Predicted efficiency values for a full-scale SPS array, based on extrapolation of the preceding results, would yield an efficiency in excess of 95 percent when accounting for recoverable scattering losses.

The ohmic efficiency based on a measured value of gain and directivity was 87.9 percent, with a tolerance of +20.9 and -14.7 percent. The expected ohmic efficiency is 96.6 percent based on rough measurements of loss and mismatch. Improved methods for directivity and calorimetric measurement of loss are indicated for the next phase of this program.

A small printed-circuit receiving antenna was inserted into the array through slots cut from the common walls of adjacent sticks. The initial performance of this co-polarized "credit-card" antenna revealed significant mutual coupling with the adjacent array slots, an indication that a cross-polarized subresonant slot or dipole antenna may be required.

Additional tests were conducted at the JSC anechoic chamber to evaluate the transmission bandwidth and harmonic attenuation of the slotted-waveguide transmitting antenna. The 3-decibel bandwidth was found to be 140 megahertz (i.e., 2860 ± 70 megahertz), which agrees with the test results obtained at Boeing but is considerably broader than expected (approximately 2860 ± 20 megahertz). Results of the harmonic pattern measurements indicated that many lobes existed at each harmonic frequency from the second through the fifth harmonic. The peak level of these lobes relative to the fundamental frequency peak gain ranged from -14 to -24 decibels. These results indicate that the harmonic frequencies will be radiated in many directions with relatively high gain.

E. SOLID-STATE ANTENNA POWER COMBINER

The Boeing Aerospace Company has been under contract to JSC since July 1979 to investigate concepts applicable to the solid-state SPS configuration which may be required to sum the outputs of many relatively low power devices with extremely low loss in the combining process. To avoid the power-combining losses associated with circuit hybrids, it was proposed that the power from multiple solid-state amplifiers be combined by direct coupling of each amplifier's output to the radiating antenna structure. The resulting savings in transmitter efficiency ranges from 4 to 10 percent depending on the configurations being compared. The selected power-combining antenna consists of a unique printed (metalized) microstrip circuit on a ceramic-type dielectric substrate, which is backed by a shallow, lightweight aluminum cavity that sums the power of four microwave sources. The antenna behaves like two one-half-wavelength slotline antennas coupled together by

way of their common cavity structure. A significant feature of the antenna configuration selected is that the radiated energy is summed to yield a single radiated output phase, which represents the average insertion phase of the four power amplifiers. This energy may be sampled, and, by comparison with the input signal, one can correct for phase error to maintain the insertion phase of all solid-state power-combining modules at exactly the same value. This procedure ensures that the insertion phase of each SPS power-combining antenna module is identical even though the power amplifiers are fabricated to relatively loose (low cost) insertion phase requirements.

1. PROGRAM SUMMARY

A detailed review of the solid-state antenna power combiner program was presented at the SPS microwave workshop held at JSC in January 1980 (ref. 53). The following material is a summary of this program and was extracted from reference 53.

The program entailed the design and fabrication of a four-feed microstrip antenna and a stripline antenna-phasing network which was integrated with four transistor amplifiers to demonstrate that the total solid-state module (amplifiers plus antenna) operates as an efficient power-combining-radiating system. The antenna developed was evaluated for gain, pattern, and efficiency on the antenna range with and without the amplifiers. The amplifiers are connected directly to the antenna without benefit of isolators so that their interaction with the antenna is unimpeded. The combined output power of the amplifiers is approximately 0.5 watt.

Figure III-62 contains a sketch of the power-combining microstrip antenna which was evaluated. The dielectric substrate is metalized on both sides. The underside, within the cavity, contains the four microstrip feedlines, which are coupled to the two radiating slots on the top side by way of two narrow slotlines. To feed the antenna, two of the rf inputs are required to be 180° out of phase with the remaining two. An antenna feed network is thus required to provide the four 0°-180° equal-amplitude outputs.

The antenna feed network, the power amplifiers, and the microstrip antenna are connected as indicated in figure IV-14. The four cables connecting the amplifiers and the antenna are required to have equal electrical lengths as are the cables connecting the antenna feed network and the amplifiers. This requirement is necessary to retain proper phasing of the antenna.

Three solid-state antenna module feed networks were assembled, and measurements were made on all units. Two of the feed networks were used to accomplish the antenna range tests. The stripline feed network consists of two 0°-180° hybrid ring junctions fed by a single in-phase two-way power divider. The circuit metalization pattern is etched into the top circuit cover plate as a label for the finished feed.

The insertion loss and insertion phase measurements over a 500-megahertz bandwidth indicate that at the design frequency, the insertion loss

212
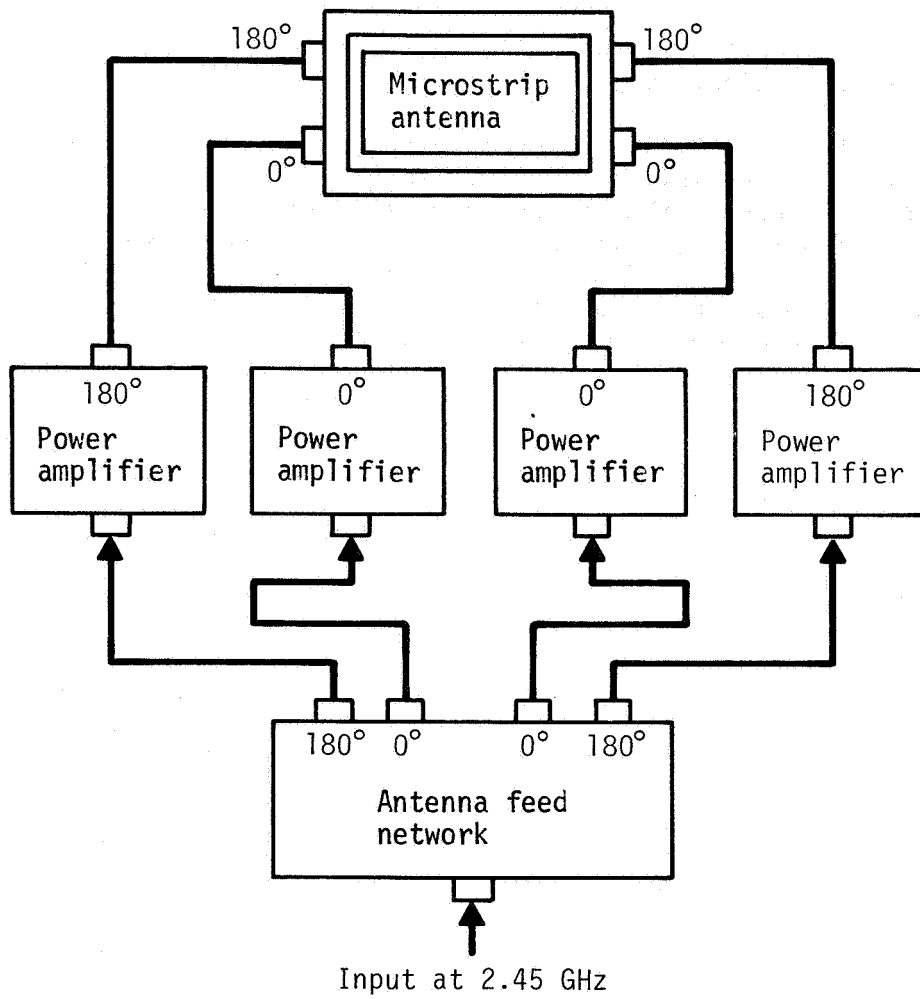
Figure IV-14.- Power-combining antenna, feed network, and power amplifier block diagram.

213

of all ports is nearly equal. The insertion phase error window at 2.45 gigahertz is 1.5° wide, or ±0.75°.

The four 2.45-gigahertz power amplifiers were supplied by Tron-Tech, Inc., of Eatontown, New Jersey. As can be seen from table IV-2, the amplifiers meet many of the small-signal specifications but are out of specification on others. More tests are scheduled to determine amplifier performance under the required drive condition needed to yield 0.5 watt of output power. Until these additional tests are completed, it is premature to speculate on the degree of suitability of the four amplifiers.

A four-feed microstrip antenna was developed which appeared suitable for the task at hand. It evolved through a series of steps which began with a microstrip to slotline coupler and graduated from a single-feed slotline antenna to a dual-fed slotline antenna and, finally, the four-feed design. The antenna substrate is 16.77 square centimeters and is backed by a 6.35- by 6.35- by 0.762-centimeter cavity, which couples the radiating slots together.

The antenna, when fed by the feed network described earlier, exhibits a bandwidth at the 15-decibel loss points of approximately 100 megahertz. A preliminary pattern taken with the antenna on the range is shown in figure IV-15. The peak gain as measured is approximately 8 decibels not accounting for 0.43 decibel of feed network and cabling losses. The pattern is orderly, with the first side lobes approximately 23 decibels down. A second, "cleaned-up" model was fabricated to initiate full range testing with and without the power amplifiers.

The primary purpose of the antenna range testing was to determine the efficiency of the four-feed antenna with and without the amplifiers. The efficiency is derived by dividing the antenna gain G by the antenna directivity D. The antenna gain will be determined by a three-antenna method in which antenna spacing is measured to better than 0.5 percent. This method is expected to yield gain accuracies of ±0.3 decibel.

The antenna directivity D is defined as the ratio of the peak radiated power to the average isotropic radiated power (average power radiated over the unit sphere). To determine the average isotropic radiated power, one must measure and total the radiated power over the spherical surface with the unknown antenna at its center, and average that value by dividing by the number of measurements. Typically, a 2° by 2° cell is employed which requires 16 200 measurements. The error associated with the directivity measurement is approximately ±0.25 decibel.

The antenna feed system insertion loss is measured on the automatic network analyzer (HP 8542B), which is periodically certified by Hewlett-Packard using standards traceable to NBS to an accuracy of ±0.15 decibel (±3.51 percent) for devices of low insertion loss. Thus, when the feed system insertion loss is subtracted from the measured gain, the feed system measurement uncertainty will be added to the previously stated uncertainties.

TABLE IV-2.- AMPLIFIER SPECIFICATIONS AND SMALL-SIGNAL
MEASURED VALUES

Parameter	Specification	Small signal[a]
Frequency, GHz	2.45	2.45
Power output at 1-dB gain compression, dBm	21	(b)
Gain, dB	[c]6	7.76 to 8.18
Gain match, dB	[d]-0.5	±0.21
VSWR		
Input	[d]2.5:1	[e]3.65:1
Output	[d]1.5:1	[f]1.66:1
Phase match, deg	[d]±5	±2.4
Phase control, deg	[c]±10	[g]±2
Gain control	(h)	(i)
Infinite VSWR save at full power	--	(j)

[a]Measured by Boeing Aerospace Company.
[b]Not measured.
[c]Minimum.
[d]Maximum.
[e]One unit.
[f]Two units.
[g]By varying B+ voltage according to Tron-Tech.
[h]By varying B+ voltage.
[i]Installed separate loss control, which yields ±1.5 decibels according to Tron-Tech.
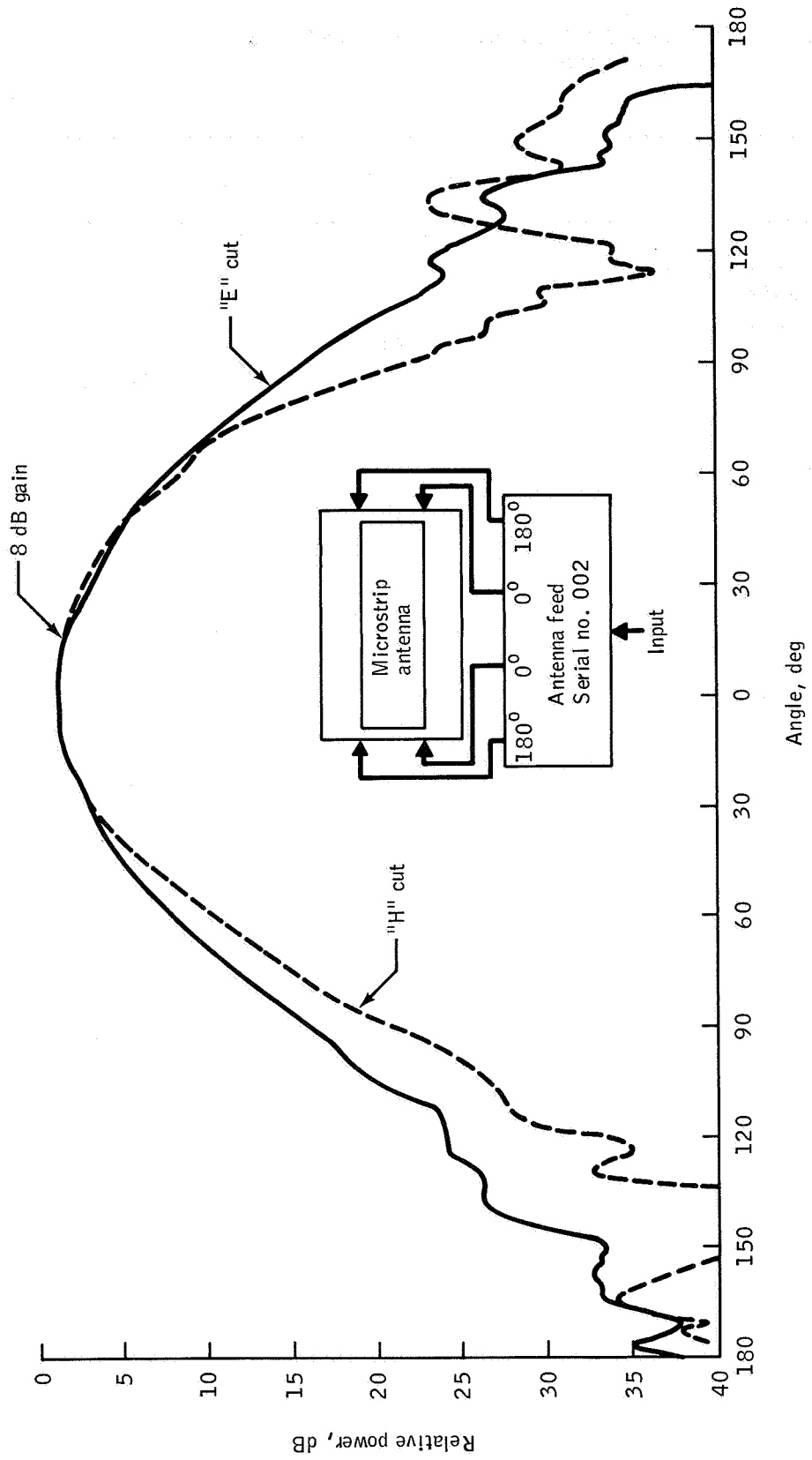[j]Verified by Tron-Tech.

Figure IV-15.— Antenna range gain pattern for the first power-combining microstrip antenna (feed network number 2).

The rss value of the combined efficiency is $\pm(0.30)^2 + (0.25)^2 + (0.15)^2 = \pm 0.42$ decibel = ± 10 percent. Cross-polarized radiation for the SPS application is considered wasted power; therefore, it is also measured and included when determining the antenna efficiency.

With the basic antenna characterized for gain, pattern, and efficiency, antenna range measurements were made with the solid-state power amplifiers inserted and operating with a combined output power of approximately 0.5 watt. The measurement of interest is the difference between the range received power with and without the inclusion of the solid-state power amplifiers. The difference should be equal to the gain of the amplifiers. This difference will verify the degree to which the antenna sums the available power of the four amplifiers. Pattern measurements will also be taken to compare with those taken without the power amplifiers. As a final test to verify the entire procedure, the integrated amplifier-antenna system will be tested for directivity and gain, and the overall efficiency will be calculated.

2. EXPERIMENTAL RESULTS

The antenna efficiency was measured as the ratio of the measured gain and the antenna directivity, both of which have inherent errors associated with their measurements. Part of the losses are attributed to the developmental nature of the antenna; a section of microstrip line, a nonoptimum dielectric substrate, and silver conducting epoxy were used in fabrication of the antenna. Accounting for these losses, which would not exist in an optimized combiner design, and for the measured cross-polarized component of radiation (~ 1 percent), the combining loss, to within the measurement accuracy of ± 0.33 decibel, is negligible.

Significant additional information on the performance of the combiner-radiator module was obtained by the incorporation of four carefully matched, low-cost silicon bipolar transistor amplifiers. When the four solid-state power amplifiers yielding a combined output power of 0.5 watt were added to the antenna, the output power was summed perfectly in the antenna beam without any measurable added loss over that obtained without the amplifiers. This result confirms the principal contention that all losses associated with the power-combining process are insignificant to within current measurement errors. The regularity of the measured E and H antenna patterns with and without the amplifiers also indicate that all the amplifiers are combining properly, with the added gain on the antenna range corresponding to the bench-measured amplifier gain to within 0.1 decibel.

F. SOLID-STATE AMPLIFIER DEVELOPMENT PROGRAM

The Radio Corporation of America performed early studies of a potential solid-state transmitter for SPS applications under the auspices of JSC. Later, RCA initiated a solid-state amplifier development program under contract to Rockwell International through MSFC.

In their early studies, RCA suggested that, in practice, solid-state device power output must be traded off against efficiency. Considering this

and other factors, RCA concluded that gallium arsenide rather than silicon appears to be the most favorable material and that some type of field-effect device would be best suited for combining high efficiency and ease of fabrication (ref. 9). Thermal and electrical designs for both Schottky barrier and junction-type field-effect transistors were generated to highlight considerations likely to influence the course of future work. Devices providing 4 watts of rf power at greater than 80 percent efficiency were considered feasible. An actual amplifier was constructed using commercially available devices with very good results; the amplifier provided 3 watts of rf power at an efficiency of 58 percent (ref. 33). The ensuing system definition study to make effective use of the solid-state devices resulted in a system concept that considered the direct conversion of sunlight into microwave power-generating modules. This general concept, referred to as the "SMART" concept by RCA, is later referred to by Rockwell and others as the "sandwich" concept. It was concluded that this type of system has a factor of merit (i.e., power in watts per weight in kilograms) advantage over the klystron reference system. Recommendations were made for further study of the sandwich concept and to continue studies of the factors affecting high-efficiency operation of microwave FET's and their associated circuitry.

The MSFC/Rockwell contract effort calls for demonstration of an amplifier having an output power of 5 watts, a gain of 8 decibels, and a power-added efficiency of 50 percent. Once this is accomplished, an effort will be conducted to increase the rf output power to 10 watts, the gain to 10 decibels, and the power-added efficiency to 65 percent (ref. 33). Commercially available GaAs FET's will be used.

Computer-aided analysis techniques are in use both for small-signal device characterization and to define the available trade-offs under large-signal operating conditions. Results, thus far, have been very impressive. When optimized for maximum efficiency at the SPS frequency (2.45 gigahertz), a power amplifier stage using a device designed for 12-gigahertz operation yielded a 71-percent power-added efficiency, an rf power output of approximately 1 watt, and a gain of about 11 decibels. Test results of power output and efficiency for conditions of maximum power and efficiency tuning are shown in figure IV-16 (ref. 33). Solid-state technology is in a state of rapid growth in both the microwave and the signal-processing areas. This growth has been stimulated on the one hand by the commercial computer industry and on the other by military interest in microwave solid-state devices. The SPS will reap tremendous benefits from the very large investments made in this technology.

G. MAGNETRON TUBE ASSESSMENT

The Raytheon Company has been conducting analytical and experimental assessments of crossed-field devices for application as the SPS microwave power amplifier. The first proposed use of the crossed-field directional amplifier in the solar power satellite dates back to 1970 (ref. 54). In recent years, JPL has suggested potential application of the microwave
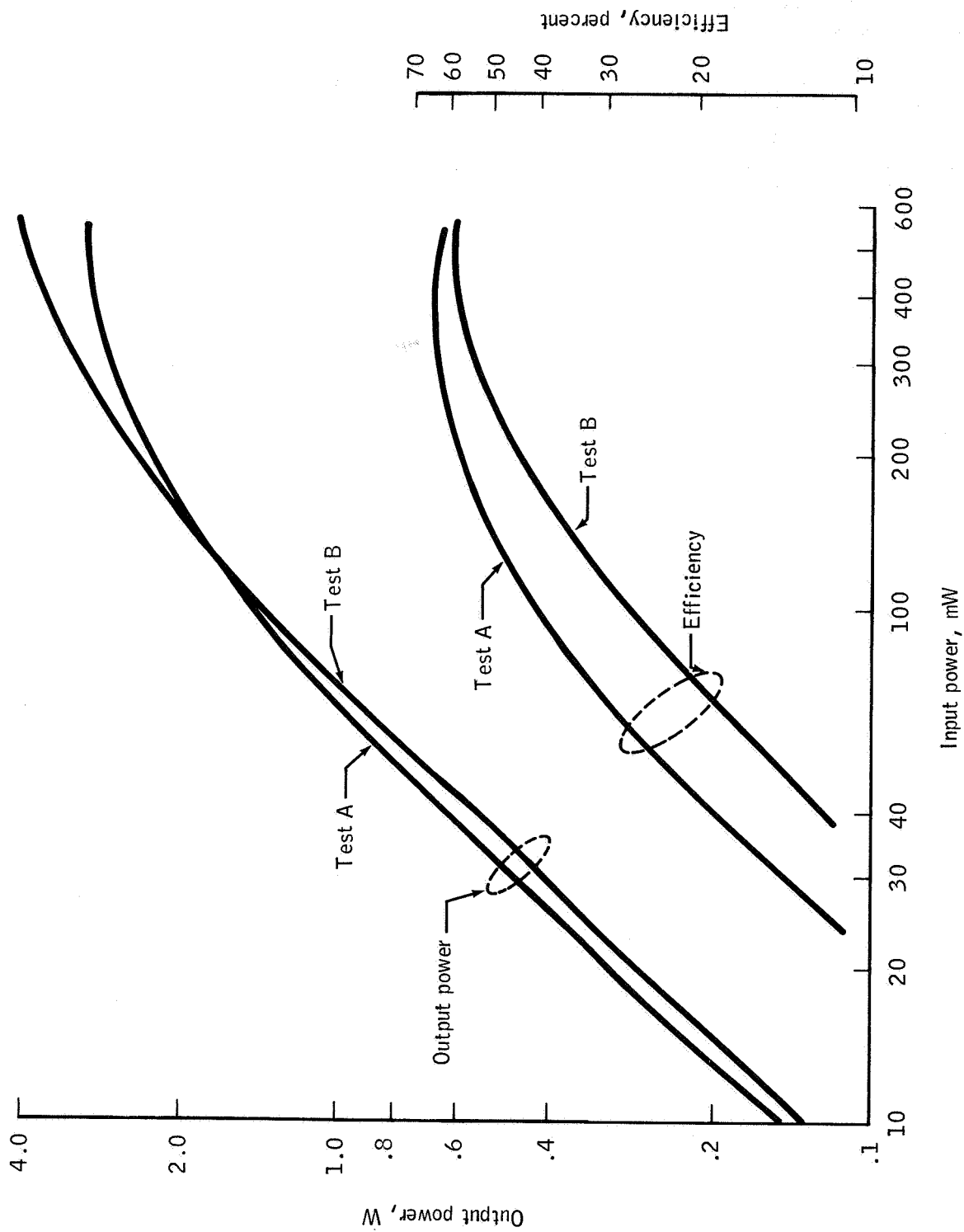
Figure IV-16.- Test results: maximum power and maximum efficiency
tuning.

219

oven magnetron as the SPS power amplifier, because of its inherent high efficiency, simplicity, relatively low mass, and high production volume and resulting low costs. Raytheon is currently under contract to MSFC to perform analytical and experimental evaluation of the characteristics of a microwave-oven-type magnetron that are pertinent to the SPS application (i.e., efficiency, output noise level, phase stability, and tube life (reliability)). A detailed summary of the work accomplished was presented at the SPS microwave system workshop held at JSC in January 1980 (ref. 25). Much of the information provided here is extracted from reference 25.

The current study involves a penetrating look at all interfaces associated with the magnetron directional amplifier. One of the most important developments of the current activity is the precise control of both the amplitude and the phase of the microwave power output from the amplifier by feedback control systems using phase and amplitude references. The output phase of any microwave generator in the SPS, regardless of kind, must be carefully controlled to prevent appreciable impact on the overall subarray phase budget, which must include many other factors.

The control of the output amplitude in the face of many factors that tend to change that amplitude is also essential for generating an efficient microwave beam. In the case of a crossed-field device, the output amplitude can be controlled to a predetermined value by another control loop which makes use of small electromagnets to boost or buck the residual field provided by permanent magnets. The overall schematic for the combined phase and amplitude control of the magnetron directional amplifier is shown in figure III-45.

The lack of historic data on the noise performance of CW crossed-field devices and the consequent inability to predict their behavior in the SPS application, where the noise level of the transmitter is a highly critical issue, understandably became a major factor in the selection of a generator for the SPS reference system. Even after the importance of this noise was realized, it was necessary to make special noise-measuring setups to obtain more sensitive measurements. Many measurements of signal-to-noise ratio over frequency ranges of as much as ±1000 megahertz either side of the carrier have been made on magnetron directional amplifiers with this equipment. Data were taken both with normal external power applied to the filament and with no filament external power applied. For the condition of no external filament power applied, a signal-to-noise ratio of 130 decibels in a 1-kilohertz noise bandwidth has been obtained.

It should also be noted that these low noise measurements have been observed on magnetrons made by different manufacturers and in different time periods, but not on all magnetrons that have been randomly selected. However, no statistical studies have been made nor probably should be made until more sensitive measuring equipment is available. In fact, it may be more effective to devote any limited future effort to better understanding the sources of noise in the magnetron.

Measurements of close-in phase-modulation noise added by the magnetron directional amplifier were also made when it was operating with a gain

220

of approximately 20 decibels. These measurements indicated a carrier-to-noise level that was typically 115 decibels in a 1-kilohertz bandwidth of noise in the range of 10 to 100 kilohertz removed from the carrier frequency. This value represents excellent performance.

In the harmonic generation area, there was no particular issue between the crossed-field and klystron device approach since it is known that both of these devices as well as all other classes of microwave generators produce harmonics. Measurements made on two representative tubes, designated as numbers 11 and 12, are given in table III-12 (ref. 25). These findings are somewhat better than had been anticipated. The unexpected anomaly of the significant energy at the fifth harmonic is an indication of the difficulty of the a priori assessment of the more complicated characteristics of any microwave generator.

An investigation of the application of carburized thoriated-tungsten cathodes to the design of a long-life SPS magnetron has been accomplished. It has been established from life test evaluations that the life of a carburized tungsten cathode is a very steep function of the operating temperature. The difference between life at 2000 K and 1900 K is a factor of 10. From the great body of design data based on many laboratory investigations as well as life test data, an operating temperature of 1900 K is associated with a potential life of 500 000 hours, or more than 50 years, if the cathode is made from 0.1-centimeter (0.040 inch) diameter wire that is 50-percent carburized. This is a reasonable design and a reasonable operating temperature for a cathode that could be used in a magnetron designed for SPS use.

Crossed-field electron tubes of the magnetron and amplitron type are properly recognized as the most efficient of microwave generator devices. The highest electronic efficiency, defined as the efficiency with which dc power is converted into microwave power, is associated with a high ratio of the magnetic field B to a design parameter B_0, which is proportional to frequency. However, the theoretical electronic efficiency is always degraded to some degree by the circuit efficiency and can be degraded by improper design of the interaction area and other design parameters as well. When the B/B_0 ratio is high and the tube otherwise properly designed, the measured electronic efficiency has exceeded 90 percent as exhibited by the commercially available 8684 magnetron. For reasons largely related to the physical size and cost of the permanent magnet, crossed-field devices are almost always designed in the range of $B/B_0 = 4$ to 6. This ratio applies to the microwave oven magnetron, the operating characteristics of which have recently been intensively evaluated.

When the permanent magnet is removed from a microwave oven magnetron and the device is operated in an electromagnet, the measured overall efficiency can be considerably increased as shown in figure IV-17. The value of 82 ± 1 percent efficiency was carefully measured after extensive preparation and precaution; then, a balance was made between the dc power input and the sum of the microwave power output and the power dissipated in the anode as an additional precaution. After taking a carefully measured circuit efficiency of 95 percent into account, the electronic efficiency was computed to be 85 percent. To this value may be added at least 1 and perhaps 2 percentage
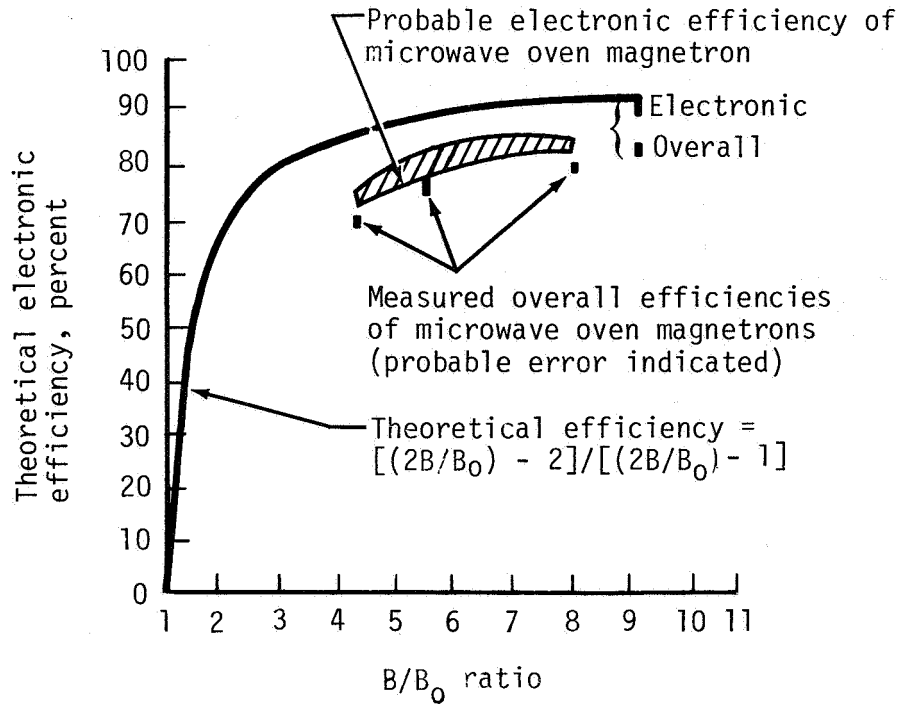
221

Figure IV-17.- Theoretical and experimentally observed electronic efficien-
cies of conventional microwave oven magnetron and 915-megahertz magnetron.
Electronic efficiency is efficiency of conversion of dc power into micro-
wave power. Overall efficiency includes circuit inefficiencies that can
be ascertained from cold-test data.

points to account for the amount of backbombardment power that was needed to heat the cathode to a temperature sufficient to provide the emission (i.e., no external filament power was used).

Although this efficiency may seem high, it is actually from 6 to 8 percent lower than it should be and considerably below that of the 8684 magnetron previously mentioned. The reason for the degraded efficiencies that seem to occur for all B/B_0 ratios is not fully understood. A contaminated field pattern does exist in the tube in the cathode-anode interaction area, and there may be some leakage current, although small, around the end shields; but there are probably other factors as well.

With one exception, there has never been a dedicated effort to maximize the efficiency of the crossed-field device. The one exception was an effort made on an amplitron device and resulted in an overall efficiency of 90 ± 3 percent. It, therefore, seems probable that if a dedicated effort was made to optimize the design of an SPS tube for efficiency, an efficiency of 90 percent could be achieved. The procedure would be to use high B/B_0 ratios, to make certain that design of the end shield and the polepiece was proper, to make certain that the cathode potential always remained at a neutral potential with respect to the vanes, to contour the vane tips, and to design for high circuit efficiency.

H. MICROWAVE IONOSPHERIC INTERACTION EXPERIMENT

As a result of the work being conducted on the SPS phase control system evaluation and various other concerns associated with the microwave signal propagation, it has become clear that the existing data base relating to ionospheric effects on microwave signal propagation is not adequate. During the microwave system workshop held at JSC in January 1980, this deficiency was clearly obvious. Since that time, JSC entered into a contract with the University of Texas Applied Research Laboratory (ARL) to conduct a field experiment obtaining data that can be used for initial modeling of the ionosphere, for both the natural and SPS-heated (simulated) states. A discussion of the potential effects of the ionosphere (both natural and heated) on microwave signal propagation and a review of the test activity and schedule follow.

The propagation of electromagnetic waves through the ionosphere is affected by the free charges there. The effects are frequency dependent, falling off as $1/f^2$ at very high frequency and above. The proposed SPS will have to transmit its energy and control information through the ionosphere. Although the proposed SPS frequencies will be very high (S-band), there may be some nonnegligible effects in certain areas.

One of the areas for which a potential problem exists is the "pilot signal." This is a signal between ground and satellite which acts as the phase reference for the SPS power signal. The pilot signal will be at a frequency (2.45 gigahertz) well above any local plasma frequency in the ionosphere. This frequency ensures that the local refractive index will differ only slightly from unity. However, this signal will have to go through the same spatial region as the power signal. The precise effects of this power

223

signal on the ionosphere and the manner in which the perturbated region will affect the pilot signal are unknown.

The major effect of the power signal on the ionosphere will be thermal. The deposition of only a very small fraction of the SPS power signal will represent a significant increase in the temperature. Although it is not possible to fully test these effects before an SPS launch, a very good approximation can be obtained by heating the ionosphere with rf energy from a ground site, such as the experimental facility at Platteville, Colorado. Measurements of the effects created by this heater can be used to determine the effects of the given amount of heating on the pilot signal.

The refractive index of the ionosphere at a frequency f of 2.45 gigahertz can be approximated as

$$n = 1 - \frac{f_p^2}{2f^2}$$

$$= 1 - \frac{AN}{2f^2}$$

$$= 1 - 6.7 \times 10^{-12} \ cm^3/electron \times N \tag{25}$$

where f_p = plasma frequency

A = $8.06 \times 10^7 \ Hz^2-cm^3/electron$

N = electron density

The phase change of the pilot signal caused by the normal ambient ionosphere will be

$$\phi = \frac{2\pi}{\lambda} \int (n - 1)ds \tag{26}$$

where the integral is taken along the path s from the satellite to the ground. Substituting the value of n from equation (25) and the wavelength for the pilot signal frequency (2450 megahertz), 12.245 centimeters, for λ, the following is obtained.

$$\phi = \frac{2\pi}{12.245} \int \left[(1 - 6.7 \times 10^{-12}N) - 1 \right] ds$$

$$= \frac{2\pi}{12.245} \int (-6.7 \times 10^{-12})N \, ds$$

$$= -(2\pi) \times (5.5 \times 10^{-13}) \int N \, ds \qquad (27)$$

The quantity $N_c \equiv \int N \, ds$ is called the electron columnar content and is usually expressed in total electron content units (TECU's), which are 10^{12} electrons/cm^2. This integration is done because the columnar content of the ionosphere along a vertical path varies from about 5 TECU's at night to 50 to 100 TECU's during the day. In TECU's,

$$\phi = -2\pi \times 0.55 N_c \qquad (28)$$

The ambient ionosphere will therefore cause the pilot signal to be changed by about 3 cycles at night and 25 to 50 cycles in daytime. This effect should be slowly varying and not pose any serious difficulties.

The pilot signal will go through a region of the ionosphere which is perturbed by the power beam. This perturbed region may differ from the ambient ionosphere in two important respects. First, there may be a large-scale change in the electron density. This change would cause the region to act as a lens in either focusing or defocusing the beam depending on whether a net decrease or increase in electron density, respectively, occurred. Second, there would be an increase in the small-scale turbulence which would increase the scattering.

Since the daytime phase shift will be many cycles, it will require only a small percentage change in the columnar content to create a cycle change. If this change occurs gradually over a large area, the energy will be deflected and focused. The variation can be thought of as imposing an extra length in the path proportional to the variation in columnar electron content.

$$\Delta h = \frac{\Delta \phi}{2\pi} \lambda$$

$$= (6.7 \text{ cm/TECU}) \Delta N_c \qquad (29)$$

225

As can be seen in figure IV-18, a linear slope will amount to a deflection of the energy. If the slope in N_c change is

$$s = \Delta N_c/h \qquad (30)$$

then the deflection angle will be

$$\Delta\ell/h = (6.7 \text{ cm/TECU}) \times s \qquad (31)$$

A 1-TECU change over 1 kilometer would give a deflection of 6.7×10^{-5} radian, or 3.8×10^{-3} degree. A quadratic charge dependence of ΔN_c with distance from the center will generate a focusing. If

$$\Delta N_c = ah^2 \qquad (32)$$

then

$$\Delta\ell = (6.7 \text{ cm/TECU})ah^2 \qquad (33)$$

and the phase acts like that coming from a parabolic reflector with focal distance approximately equal to the radius of curvature

$$R = \frac{1}{2a \times 6.7 \text{ cm/TECU}} \qquad (34)$$

If a is 1 TECU/km^2, then R will be approximately 7500 kilometers.

These changes will probably have little effect on the pilot signal. However, it is unclear whether small-scale gradients in N_c may not be larger than those used in the preceding discussion. If the spatial extent of the gradient is very small, the previously described treatment becomes invalid. The wave nature of the radiation will then be of major importance, and the effects can be most easily thought of as resulting from a scattering process. A rough scale length which will divide the two regions will be the final Fresnel zone radius

$$r_o \equiv \sqrt{\lambda A} \qquad (35)$$

Incoming plane waves

Large-scale ionospheric irregularity

$\Delta \ell$

h

Outgoing phase fronts
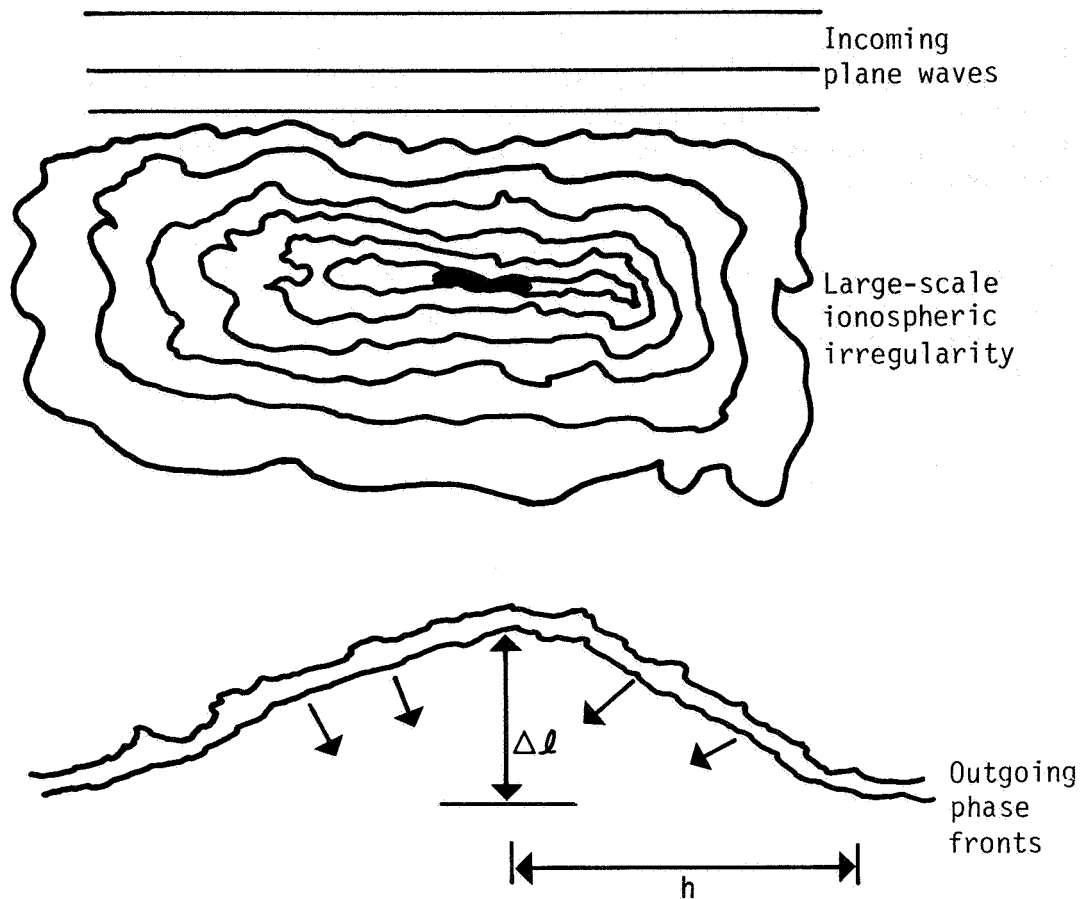
Figure IV-18.- Large-scale ionosopheric irregularity deflecting and focusing pilot signal.

where λ is the wavelength and A is the distance from the scattering region to the receiver. For scattering at a 300-kilometer altitude, r_o is about 200 meters. This relationship means that variations smaller than $2r_o$, or about 0.5 kilometer, will act as a large volume with some scattering density per unit volume.

The received wave will be the superposition of the direct-path wave and the sum of all the waves scattered from the volume (fig. IV-19). This problem has been extensively studied. Briggs and Parkin (ref. 55) found that the rms phase variation from isotropic irregularities scattering in the ionosphere was

$$\phi = \pi^1 \ r_e \lambda \sqrt{L_1 \times L_2} \ \Delta N_{rms} \tag{36}$$

where r_e = the classical radius of the electron (2.8×10^{-13} centimeter)

λ = the wavelength

L_1 = the inner scale length of variations

L_2 = the thickness of the irregularity region

ΔN_{rms} = the rms density perturbation

If one assumes a 1-percent variation in daytime, an ambient density of 10^7 electrons/cm^3, a 30-meter inner scale length, and a 30-kilometer thickness, then

$$\phi = 4.2 \times 10^{-2} \ \text{radian}$$

$$= 2.4° \ \text{rms} \tag{37}$$

Of course, the variation in an extremely turbulent region might be larger than 1 percent, which is typical of scintillation regions. In addition, a better estimate of effects on a particular signal may be made if the full spatial spectrum of the turbulence is given.

The experiment conducted by ARL was designed to measure the intensity of the electron density turbulence structure in both the natural ionosphere and the heated region. Heating was accomplished by using the ITS heater facility at Platteville, Colorado, to deposit rf energy into the F-region of the ionosphere.

The tests were conducted in the second week in April 1980, and the final report including a mathematical model of the ionospheric perturbation will be completed by December 1980. Both disturbed and unheated regions of the ionosphere were probed with signals from the U.S. Navy Navsats.

Figure IV-19.- Small-scale ionospheric irregularities acting as volume scatterer of pilot signal.

The Navsats carry radio beacons at 150 and 400 megahertz. The 400-megahertz signal is used to navigate from observations of the Doppler curve. This m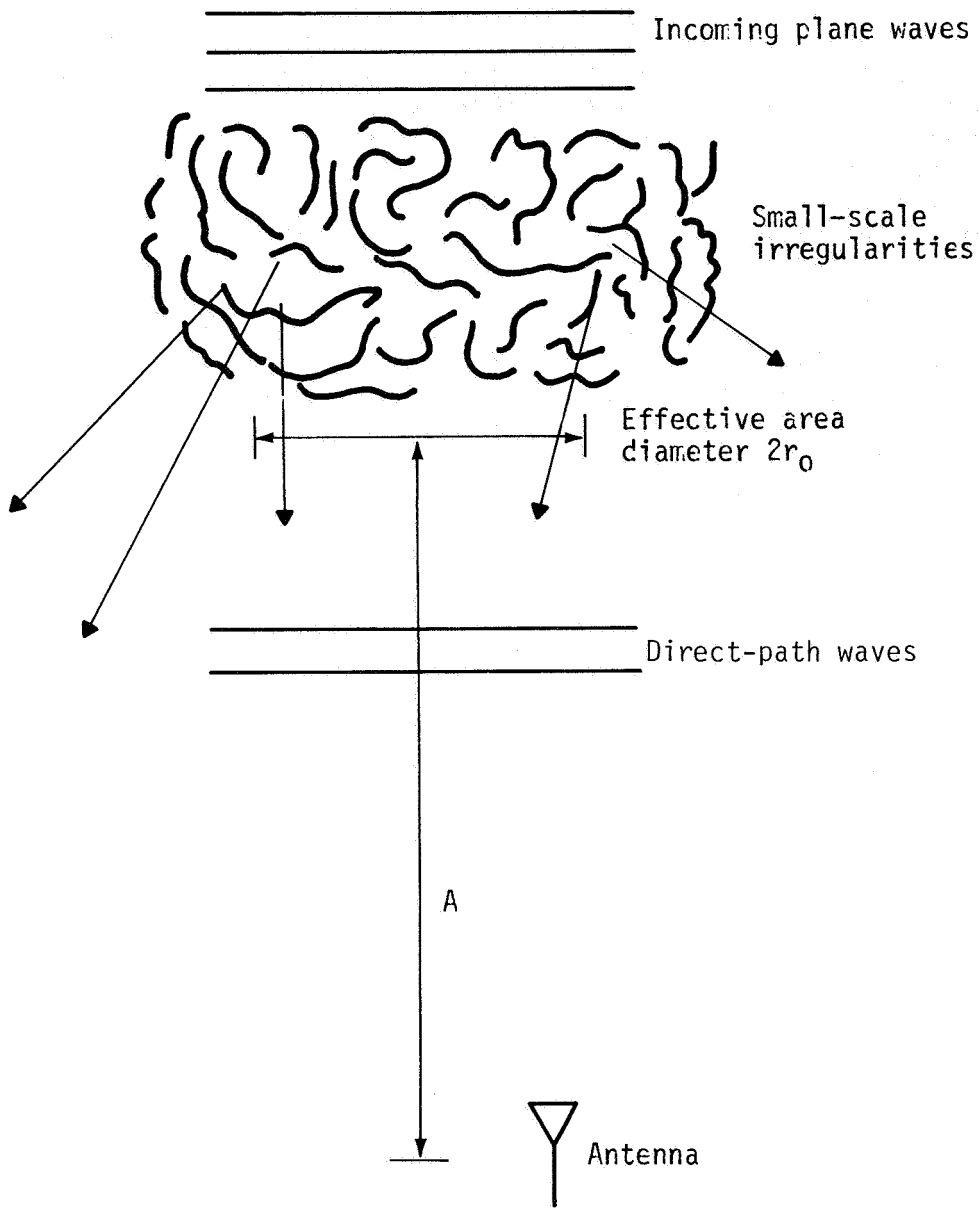easurement is significantly contaminated by propagation effects as the signal passes through the ionosphere. A 150-megahertz signal is also transmitted to measure and remove the dispersive effect of the ionosphere. For the current problem, the priorities were reversed and the measurement of the ionospheric propagation effects were of primary interest.

The standard two-frequency navigation receiver for Navsats (geoceiver) generates a signal with frequency proportional to the rate of change of the columnar content (N_c) along the line of sight as the satellite sweeps by in the sky. The ARL geoceiver was modified to generate several analog signals including the refraction phase and the automatic gain control (AGC) voltages for the 150- and 400-megahertz signals. The refraction data were converted to the audiofrequency range by an external circuit, and this signal along with the AGC voltages were then recorded on magnetic tape.

An advantage to this procedure is that the signal generated by the ARL geoceiver has eight times the phase change per N_c charge as the signal later counted by the internal circuit. Thus, both time and N_c resolutions are improved by this modification.

After the preliminary evaluation was completed, the data were digitized at a high rate in the ARL computer center. These data then formed the basis of a detailed characterization of the electron density perturbations in the heated and unheated regions. The initial results were reviewed at JSC in October 1980.

Tentative conclusions based on the initial data evaluation follow.

(1) The electron density across the heated region will consist of both large-scale and small-scale variations.

(2) The phase variation across the heated region will be less than $10°$ peak for large-scale disturbances and less than $1°$ rms for small-scale disturbances.

(3) Amplitude scintillations observed near the heated region cannot be attributed solely to multipath conditions.

A statistical characteristic of the turbulence as a function of electron field intensity and other variables will be developed and the effects on the SPS power signal and pilot signal will be evaluated. These results will be included in the final report scheduled for distribution in January 1981.

V. SYSTEM CONCLUSIONS AND REMAINING ISSUES

A. CONCLUSIONS

As a result of the numerous analytical and experimental evaluations which took place during the DOE/NASA Concept Development and Evaluation Program, certain conclusions can be reached on the microwave PTAR system. These conclusions were presented and discussed as part of the system workshop held at JSC in January 1980. The conclusions listed here apply to the overall microwave PTAR system. More detailed conclusions are presented for each subsystem in Section III.

1. MICROWAVE POWER TRANSMISSION

Transferring gigawatt power levels between two points using microwaves is feasible.

2. SINGLE COMPARED TO MULTIPLE ANTENNAS

Each SPS microwave power transmission system should use one transmit antenna with contiguous radiating subarrays rather than multiple separate antennas.

3. FREQUENCY

The power transmission frequency of 2.45 gigahertz has been determined to have advantages for power transmission and reception based on system trade-offs including (a) transmit antenna and rectenna sizing, (b) propagation effects through the atmosphere, (c) hardware technology projections, and (d) ISM band utilization.

4. MICROWAVE SYSTEM SIZING

Transmit antenna size (1 kilometer), rectenna size (10 kilometers minor axis), and power delivered to the utility grid (5 gigawatts) have been determined on the basis of minimum cost of electricity per kilowatthour. The trade-offs were based on a maximum rf power density limit on the transmit antenna of 23 kW/m^2 (tube configuration), a maximum power density through the ionosphere of 23 mW/cm^2, and the current projections of microwave system efficiencies. A microwave system using solid-state power amplifiers will have a different thermal limit and different system efficiencies, resulting in different system sizes.

5. TYPE OF TRANSMITTING ANTENNA

The transmitting antenna should be a phased array using slotted-waveguide feed techniques to meet the requirement of maximum power-transfer efficiency.

231

6. TYPE OF RECEIVING ANTENNA

An SPS rectenna concept theoretically capable of recovering all rf energy impinging on its surface with direct rf-to-dc conversion provides the required maximum conversion efficiency.

7. ANTENNA CONSTRUCTION AND SUBARRAY ALINEMENT

Construction of a 1-kilometer-diameter antenna array with a ±1-arc-minute flatness tolerance appears to be within the state of the art if low-CTE materials are used. Antenna subarray alinements, both initially and operationally, can be maintained to ±3 arc-minutes by the use of azimuth-elevation mounts and laser measurement techniques.

8. POWER BEAM STABILITY

On the basis of analytical simulations and experimental evaluations, it appears feasible to automatically point and focus the power beam with minimum wander (±250 meters) and automatic fail-safe operation (rapid beam defocusing).

B. REMAINING ISSUES

In addition to the preceding conclusions, certain remaining issues have been identified and must be addressed in any follow-on program. These issues are for the overall microwave PTAR system.

1. Microwave PTAR system performance

2. Noise and harmonic characteristics

3. Antenna transmission efficiency

4. Beam-forming accuracy

5. Beam-pointing accuracy

6. Beam security

7. Power beam/pilot beam isolation

8. Effects of ionospheric/atmospheric disturbances on pilot signal

9. Mechanical alinement/tolerances

10. End-to-end system efficiency

11. Corona (tube configuration only)

12. Multipacting (tube configuration only)

13. Plasma (tube configuration only)

232

14. RFI effects on selected hardware

15. Unit costs

16. Alternate technologies

    a. Solid state

    b. Magnetron

17. Possible new technologies

    a. Photoklystron

    b. Gyrocon

More detailed issues identified for each subsystem are discussed in Section III.

Lyndon B. Johnson Space Center
    National Aeronautics and Space Administration
      Houston, Texas, November 12, 1980
        953-36-00-00-72

APPENDIX - WORKSHOP ON MICROWAVE POWER TRANSMISSION SYSTEM
FOR THE SOLAR POWER SATELLITE, REVIEW PANEL FINAL REPORT

INTRODUCTION

The Solar Power Satellite (SPS) Workshop on Microwave Power Transmission and Reception was held at the NASA Lyndon B. Johnson Space Center (JSC) in Houston, Texas, on January 15 to 18, 1980. The objectives of this workshop were (1) to assess and critique the assumptions, methodologies, and conclusions of the NASA SPS studies and (2) to identify and assess critical issues and make recommendations for follow-on work.

The workshop review panel consisted of individuals with expertise and experience in each of the areas relevant to the SPS microwave system. Dr. Robert C. Hansen of R. C. Hansen Inc. and Professor Bernard D. Steinberg of the University of Pennsylvania both provided expertise in the area of microwave beam shaping and phase control. Professor Aldo V. da Rosa of the Stanford University Radioscience Laboratory was the expert on microwave-ionosphere interactions. Mr. Harry Goldie of Westinghouse and Dr. Paul Tallerico of the Los Alamos Scientific Laboratory contributed in the area of high-power microwave tubes. Professor William L. Wilson, Jr., of Rice University provided expertise in the area of solid-state microwave devices and waveguides. Dr. John W. Freeman, Rice University Professor of Space Physics and Astronomy, and chairman of the workshop, represented a broad knowledge of the SPS concept and its historical development and of microwave energy conversion devices.

The format of the workshop consisted of presentations by NASA and contractor personnel in each of the following areas: system performance, phase control, power amplifiers, radiating elements, rectenna design, solid-state devices, and planned program activities. These presentations were arranged by Mr. R. H. Dietz of JSC. A large amount of material was presented. Following each day's presentation, the review panel met privately and discussed the material that was presented. They also met for the entire afternoon of the last day to discuss their conclusions. Administrative arrangements were made by Texas A. & M. University under the direction of Dr. Richard E. Thomas, Director, Center for Strategic Technology.

The format of this report consists of a brief summary of the reference system, a presentation of general conclusions by the panel, specific conclusions in each of the major topic areas (including a discussion of solid-state microwave devices under the heading "Microwave Amplifiers"), and a summary.

235

SUMMARY OF THE REFERENCE SYSTEM

According to the DOE/NASA reference system report (ref. 1), the SPS microwave system could consist of a large array (about 100 000) of high-power klystrons grouped into subarrays and feeding an array of slotted waveguides (spacetenna). Solid-state microwave amplifiers have also been investigated. The high-power klystrons would be powered by 40-kilovolt powerlines from a series/parallel solar cell array.

The klystrons would be phase controlled at the subarray or individual klystron level in such a manner as to produce as nearly as possible a parallel-beam, plane wavefront launched from the 1-kilometer-diameter spacetenna and directed at a 10-kilometer-diameter rectenna located on the surface of the Earth. Phase control would be accomplished by a retrodirective pilot beam launched from the center of the rectenna and phase conjugated with the help of an onboard phase reference signal to provide the proper phase angle for each subarray or klystron.

Main beam conversion to direct-current (dc) electricity at the ground would be accomplished by rectifier-filter circuits attached to each dipole antenna in the rectenna array. The dc power output from the rectenna would be about 5 gigawatts.

The primary constraining factors on the beam power are the 21-kW/m^2 heat dissipation limit on the spacetenna and the hypothetical 23-mW/cm^2 power density limit on heat-balance disturbances to the ionosphere. The main beam operating frequency of 2.45 gigahertz has been chosen. The overall microwave system efficiency for the reference system is estimated by NASA to be 61.1 percent. Microwave power levels at the rectenna edge are constrained to 1 mW/cm^2 and are less than 0.1 mW/cm^2 beyond 0.7 kilometer from the rectenna edge. For further details on the reference system, see references 1 and 5.

GENERAL CONCLUSIONS BY THE PANEL

First and foremost, the review panel wishes to indicate that it is impressed with the large quantity of excellent work which has been done on the SPS microwave system. Given the relatively short time that the system has been under study and the modest funding available, the results to date are impressive. The dedication of a number of individuals is clearly apparent.

The panel believes that a microwave power transmission system for the SPS is probably technically feasible, given sufficient resources in terms of funding and time. Perhaps the best phrase to describe the panel's attitude is "cautious optimism." It is likely, however, that the final system will bear little resemblance to the present reference system. The panel feels that it is imperative that NASA not become locked on to the reference system as a basis for all future design. In some areas, such as the retrodirective phase control system and rectenna design, the review panel questions the present reference system approach.

The panel believes that top priority should be given to determining a hard upper limit for the permissible microwave power density which can be sent through the ionosphere. The number being used, 23 mW/cm^2, is based on an obsolete theoretical foundation and is without experimental support, and yet it is the constraining parameter in a number of the SPS design areas. Sufficient funds and resources should be allocated so that this question can be answered as soon as possible.

There should be more emphasis on systems engineering in the SPS and microwave system design. Sensitivity trades should be employed more frequently to reveal optimum design parameters and directions. Design decisions made early in the program do not appear to have been subject to continued scrutiny and review. Updating the design approaches and major reviews of the overall concept should be done on a frequent basis. A systems-level failure analysis should be done. There should be some effort expended toward ensuring that the entire system will fail gracefully, and not in a catastrophic manner. Detailed design work has gotten ahead of systems-level planning in some areas.

The design philosophy appears to be based solely on optimizing the efficiency of each individual component of the system. More emphasis is needed on evaluating the cost sensitivity of the design, with the possibility of achieving a slightly less efficient system that is considerably less expensive. One area in which this is particularly true is the rectenna. A lower cost rectenna, if it could be achieved, might allow one satellite to use widely separated rectennas, with the beam shifting from one to the other as the peak load shifts.

It would be useful to attempt to feed innovative or novel ideas into the design concept from time to time, rather than trying always to refine the original reference design. The panel feels that some of the major electronics and communications companies should become involved in the microwave system design, since some of the design concepts do not appear to be up to contemporary standards for equivalent military systems.

The panel feels that any experimental work at this stage of the SPS systems development should be very carefully considered. In some instances, some hard data are needed before further planning can be undertaken. Breadboarding a particular system, however, just to demonstrate a concept, does not seem warranted until further systems review has been accomplished. Microwave systems are critically dependent on the precise configuration and components which are used in their construction. Building a system in the laboratory that does not resemble the deployed system will not yield much useful information and is probably a waste of resources.

The problem with radiofrequency (rf) interference from the SPS microwave system appears to the panel to be severe and not adequately addressed at this time. Not only are the noise sidebands from the transmitter uncomfortably close to the maximum limits set by the radio astronomers, but the harmonic radiation from the SPS as well as reradiation from the rectenna appear particularly bothersome. At the power levels envisioned with this concept, intermodulation products between harmonics and many other rf sources

237

will be a major concern. There does not appear to be enough emphasis at the systems planning level for controlling the harmonic generation and radiation problem.

It was apparent from the workshop presentation that not enough attention has been paid to the problem of security and antijamming. State-of-the-art cryptography and National Security Agency security standards should be built into the system design from the outset. Coordination with appropriate agencies should begin now so that a smooth integration of their requirements into the SPS system can be achieved.

Finally, the panel feels that the project organization and structure could be improved in the next phase of the program. Greater coordination is required between the various contractor efforts. In view of the large number of design areas now needing work, it is possible that the concept of two parallel programs has outlived its usefulness. There should be a single NASA program office in charge of the SPS system which could oversee the development of the entire project.

SPECIFIC CONCLUSIONS ON MAJOR TOPIC AREAS

Beam Forming and Control

Phase control for beam forming is crucial to successful operation of the SPS. Phase control is more critical than many of the other subsystems and components because failure to function within tolerances can cause a sudden and complete loss of power transfer to the ground. The design must have some kind of redundancy or protection at the subsystem level to prevent catastrophic failure.

The reference system - The current LinCom scheme for achieving reference phase control has a major disadvantage. The power transmitters at 2.45 gigahertz tend to interfere with the onboard pilot receiver. This interference is suppressed by the use of a high-rejection-ratio/narrow-band notch filter, by separating the sidebands of the pilot waveform, and by the use of the spread-spectrum antijamming improvement ratio. This approach is unacceptable because long-term stability of the deep notch filter is unlikely with existing technology. Use of the spread spectrum to achieve rf interference suppression is very beneficial. Spread spectrum should also be added to the system for antijamming and antispoofing. It is recommended that this approach be continued, provided the notch filter problem can be solved, and that the use of spread spectrum be expanded for antijamming protection also.

Alternative phase control systems - The broadcast onboard reference signal idea presented by Rockwell International appears feasible. It is rugged, resilient, and relatively simple. It should be pursued. Any scheme which will lower the microwave parts count in the phase control system should be given a high priority for further study. It would be desirable, if possible, to eliminate the uplink pilot system for beam forming. This step would eliminate possible ionosphere problems and reduce the possibility that the SPS

238

would suffer sudden and complete loss of function if the uplink should suddenly fail or be interrupted.

Ground-based pilot systems that have most of the sophisticated hardware and subsystems on the ground are the best of the pilot signal types and should be pursued further. There are two very severe problems, however. First, on the order of 150 to 200 decibels isolation is needed from the downlink signal. This is an extremely difficult task. Second, as the system ages, tuning drifts and changes in impedance levels will take place. As many components as possible should be under closed-loop control to compensate for phase changes due to drift. Every circuit shown to the review panel had some open-loop parts in the phase control scheme. It must be demonstrated that any proposed system can overcome these problems.

An even more subtle phase drift problem exists. Certain components under the closed-loop subsystem will, when they age and mistune, produce phase changes in the larger part of the system to which they belong; for example, the voltage-controlled oscillator (VCO) phase-lock loop that is frequency controlled. When the free-running frequency of the VCO drifts, its closed-loop frequency does not shift, which is proper. However, the loop bias voltage needed to maintain the correct frequency will change to compensate for the drift. This change will be reflected directly as a phase-shift change in the path through the phase-lock loop. Work should be undertaken to investigate the effects of aging on any system performance. All contractors should examine the aging tolerances of their systems.

Separation of steering and phase control - The one-sigma error of the attitude control system is several times larger than the required steering accuracy. The gimbal-angle steering error could be reduced to acceptable levels by using a monopulse aiming system. A secure coded transmitter on the ground would be received by a line of a few horns dispersed across the face of the spacetenna. The baseline should be roughly 200 meters. This link margin should allow a monopulse improvement factor of about 50, plus antijamming capability. The actual power module phasing could then be performed independently by a system that only needs to keep the surface of the module phase center flat. Thus, beam steering would be accomplished with one system, and phase control and surface flattening would be achieved with another. The pointing of the beam in the axis normal to the gimbal axis may also need some improvement. For this function, another monopulse set may be used. The monopulse outputs could be used either to control the phase of the power modules or to drive small correction drive motors or thrusters. If the two functions of beam steering and phase control could be thus separated, a wider range of options would be available for the choice of the phase control system.

Phase and amplitude error estimation - The SPS spacetenna array of power modules will have a statistical error distribution over each subarray in the system. However, the phase at the center of each subarray will have a different statistical error distribution. A probabilistic random error theory should be developed to analyze this problem so that accurate tolerance values can be developed. Monte Carlo computer simulations are risky for two reasons.

239

First, an array with more than a hundred thousand elements cannot be realistically simulated. Second, many computer runs must be made to establish the probability distribution function value. With only a few dozen runs, only smoothed values are obtained. Monte Carlo should be used as an adjunct to probabilistic formulas.

Far side lobes - The beam patterns generated thus far may be somewhat optimistic in the far-out side lobes. Excluded from the analysis of the radiation pattern has been the effect of position errors in the phase centers of the subarrays and modules. In particular, the effect of these errors on the distant side lobes has not been calculated. There is some angle away from the main lobe beyond which the side-lobe pattern begins to deviate from the design pattern and tends toward the side-lobe properties of a random array. This angle should be calculated and the effect determined. If the subarrays are rigid and ideally manufactured, and if all the in-plane distortion is associated with their relative positions, then the average side-lobe level beyond the angle mentioned previously is below the main lobe by 38 decibels plus the relative gain of the subarray patterns in that angular region.

If there is also distortion in the subarray, then the problem becomes somewhat less obvious. The subarray levels probably become worse, although there might be a situation in which they would be improved by about 12 decibels (100 000 modules in contrast to 7000 subarrays). This effect should be studied. Even if the subarray is rigid, however, manufacturing and installation tolerances on the modules within the subarray will introduce a priori unknown position errors which will affect the average far-out side-lobe level. Thus, it is possible that power which is lost to the side lobes may be somewhat higher than predicted. This effect should also be given some consideration.

Beam taper - To achieve a high beam efficiency, an array amplitude taper of 8 to 10 decibels is indicated. This taper should not be approximated in a stairstep fashion by subarrays of constant amplitude. Instead, each subarray should have its own amplitude taper in both coordinates to obtain the smoothest approximation to the desired array excitation. Of course, with square subarrays, a circularly symmetric array excitation cannot be exactly realized, but the stairstep can be bettered as it produces higher side lobes than necessary. In choosing the overall excitation function, distributions which are easy to integrate should be avoided. Instead of easy mathematics, the design should be based on good physics. The antenna art now designs distributions by placing zeros at the proper places for shaping the side-lobe envelope. There are, in fact, rotationally symmetric distributions with low Q, adjustable side-lobe level, and high efficiency. A more advanced design process would construct a distribution that optimizes beam efficiency subject to constraints on distribution edge pedestal and on side-lobe envelope. Such an optimization can be formulated as the ratio of two quadratic Hermitian forms; exact solutions can be calculated. For a program of the importance (and size) of the SPS, crude handbook array distributions are not adequate. At least a distribution with proper zeros should be used, and eventually a constrained synthesis should be employed to optimize beam efficiency. An improvement of 1 or 2 percent can easily pay for good antenna design.

Lattice design - Regarding the spacetenna array element lattice, examination of the effective area of an element in an array or an examination of the element active gain which is equivalent, shows that, for small arrays, the lattice should be square with half-wave spacing to maximize gain. As the size of the array increases, the element spacing may be increased without serious gain loss. In the limit of an infinitely large array, the element spacing can be just under one wavelength in a square lattice or 15 percent larger in a hexagonal lattice without any gain decrease. That is to say, the effective area of half-wave dipoles or slots is sufficient to allow these larger spacings in an infinite array as was shown rigorously in reference 56. Thus, since the spacecraft antenna is very large in wavelengths, the slot spacing can, in principle, be made nearly one wavelength except for the elements near the edge. The practical implications are that the waveguides can be operated closer to cutoff to increase slot spacing and that the waveguides need not be contiguous but can be separated. This configuration reduces the weight and complexity of the antenna.

Miscellaneous items - Another consideration which should be included in the system design and evaluations is mutual coupling among the active elements which may have pronounced effect on the phase control system and its behavior. These effects should be studied now. More studies should be undertaken to determine whether phase control at the subarray, rather than the power module, level would be sufficient. Such control could have some significant cost advantages. Ionospheric effects on the pilot beam are totally unknown, both in magnitude and in temporal behavior. These effects should be studied as soon as possible. Range measurements on the radiating elements will be difficult or impossible to accomplish to the 1-percent-accuracy level. Multipath effects are the major problem. However, it is the feeling of the panel that good range measurements are very important and are worth the investment early in the program. The scan time (1 minute) of the closed-loop system presented by Novar is probably excessively slow to provide the required control.

Although there was not complete agreement, the panel tended to favor a closed-loop phase control system over the retrodirective approach. The on-board broadcast phase reference system presented by Rockwell in connection with the solid-state-sandwich configuration seems appealing because of its freedom from ionospheric variations and interruptions. Work should proceed on both closed-loop and open-loop systems. None of the phase control systems presented are clearly superior at this time.

Microwave Amplifiers

There is still no definite answer as to which choice is optimum for the microwave power amplifier devices. At this time, the klystron looks most favorable, but either the solid-state or the magnetron source may look better later. The question of optimum power transmission voltage and amplifier size should be very carefully studied and reexamined. Some attempt should be made early to determine the maximum voltage which can be safely used in the SPS environment, as this has a significant bearing on many design decisions. If it is not possible to operate at 40 to 50 kilovolts, klystrons can not be used.

Better ohmic efficiencies will be obtainable with higher voltages, and the klystron efficiencies will increase as well. On the other hand, reliability of power-conditioning equipment and the klystron tubes themselves will probably decrease as the voltage increases. Some test of a high-voltage array, perhaps piggyback on a Space and Missile Systems Office (SAMSO) mission in geosynchronous orbit, should be considered. Tests in low Earth orbit will not be satisfactory since the two plasma environments differ significantly. Moreover, the SPS itself may significantly alter the geosynchronous-orbit plasma environment.

Noise and harmonics - One of the major problems with any of the power amplifiers being considered is that of noise and harmonic generation. It appears most likely that the klystron will have much less noise than either the field-effect transistor or the magnetron. The noise question should be answered at the device level first. Once a device has met the noise requirements, subarray tests should be started to examine the mutual-coupling behavior. Inasmuch as klystron characteristics do not scale well, no effort should be spent on developing a lower power klystron than that anticipated for actual use in the SPS.

Solid-state devices have to overcome problems of noise, efficiency, and high-temperature operation before they can become viable contenders in the SPS microwave system. The solid-state program should be aimed at getting answers to some of these more important questions before the devices are designed into an SPS system. Noise and harmonic generation, as well as optimum efficiency operation, can best be determined by a well-designed and well-executed computer model. A sophisticated model which takes into account all of the device parameters will be most useful in determining optimum performance. The development of this computer model should be tightly coupled with a device development program. Actual operating waveforms and efficiencies should be compared with the model to make it as realistic as possible. Once a good model has been built, global studies of device performance under various load conditions should be undertaken. Sensitivity studies should be made to determine the extent of load mismatch which would be permissible with these devices. Finally, harmonic generation and sensitivity to changes in the load at the second harmonic should be made to determine the degree of harmonic suppression that can be reasonably achieved.

Solid-state testing - As soon as reasonable solid-state devices can be fabricated, an extensive test program should be initiated for determining failure mechanisms and radiation sensitivity. Cooling and maximum allowed temperature are critical to the design of a solid-state microwave system. Further information on these parameters is needed. Cost may become a serious problem for the solid-state devices because of the large quantities that will be required.

Magnetrons - Injection-locked magnetrons may offer substantial promise from a cost point of view; however, substantial work is needed at the device level in the area of noise reduction and improved efficiency. The panel recommends further work in this area.

Klystron cooling - The panel is concerned about the long-term stability of the water-cooling design for the klystron. Corrosion and eventual leakage could be a major problem. Studies should be initiated soon to evaluate this problem. Of particular concern is electrolytic action among dissimilar metals and the effects of leaking water on the integrity of the rest of the SPS system.

Device efficiency - In most of the efficiency budgets produced so far, only the most optimistic predicted values have been used for the estimates of dc to rf conversion. A more conservative approach would be to use demonstrated efficiencies, with the variabilities of loading and performance included in the model. The best estimate and the worst estimate should be compared so that the expected range of system performance can be determined. For the klystron, the power lost in the collector power supply should be included in the efficiency estimate; otherwise, comparisons with other devices are not valid.

Ground-Based Exploratory Development recommendations - In summary, the Ground-Based Exploratory Development (GBED) Program should aim at producing a high-efficiency, high-power klystron. This tube should then be evaluated carefully for its noise and efficiency characteristics. Phase-locked magnetron development should continue at the device level, with particular emphasis placed on noise reduction and efficiency enhancement. The solid-state amplifier should be developed further with emphasis on research at the device level rather than at the systems level. Work on innovative concepts such as the photoklystron should be encouraged.

Radiating Elements

Materials - The principal problem the panel identified in the radiating-element area is related to materials. Aluminum appears attractive except for its poor thermal-expansion characteristics. Work should be initiated to determine whether there are any manufacturing or design techniques which would ameliorate this to some degree. An estimate should be made of the maximum thermal distortions which can be expected, and these should be fed back into the antenna radiating pattern calculations. Arbitrarily picking a number of 0.64 centimeter (1/4 inch), as was done in the study, does not seem realistic enough.

Problems of I^2R losses should also be addressed early so that potential later snags can be avoided. Whatever manufacturing technique is finally selected, low loss must remain one of the fundamental requirements. A set of principles should be developed for use in guiding the mechanical design.

Although low coefficient of thermal expansion composites were mentioned frequently during the workshop, no evidence was presented to indicate that these materials would in any way be suitable for microwave circuitry on the SPS. Obvious problems include outgassing from the epoxies, conductor adhesion problems, and fabrication techniques. Because little is known about

these materials currently, they should not be given extensive consideration in the SPS design.

Multipacting – The multipacting problem was mentioned frequently. Although this phenomenon is fairly well understood, data currently are insufficient to enable predicting whether it will be a problem in the microwave system radiator. A set of experiments should be defined which will permit reasonable estimation of the extent of the problem in the SPS environment. This includes outgassing tests on the epoxy composite.

Testing – Many types of tests must be performed on both the power modules and the subarrays before their microwave performance will be known with certainty. In particular, it is important to determine either the radiating power efficiency or the antenna gain. Measurement of either of these to an accuracy of 1 or 2 percent is extremely expensive, and perhaps not even feasible. The large size of the subarray means that a very large range must be used for far-field testing. There is no existing range that has sufficiently low multipathing to allow such accurate measurements. Most anechoic chambers have background levels higher than -50 decibels. For a 1-percent-accuracy measurement, the background must be lower, as the low-level side lobes can have a significant effect on the antenna gain. One alternate approach would be to measure antenna patterns and waveguide losses separately. The antenna pattern would require a high-quality anechoic chamber and many pattern cuts. Waveguide attenuation losses could be made on long sections of guide. These measurements, coupled with carefully measured impedance characteristics of the entire subarray, would be sufficient to characterize the entire spacetenna performance.

Harmonics – Finally, the problem of harmonic interaction with the radiating structure needs to be addressed. It will not be feasible to place filters, circulators, or much else between the power amplifier and the radiating element without introducing unacceptable losses. Thus, harmonic suppression on the SPS itself must be achieved with the design of the radiating elements.

The Rectenna

The rectenna was given much early work and development but has been neglected in more recent SPS history. This does not seem to be a good idea, as the present microwave system rectenna concept needs considerably more work. The major problems which the panel sees are those of weather protection, parts count, and harmonic reradiation. The demonstrated efficiencies at Goldstone have shown that the basic concept is reasonable but have not answered the question of scaling this approach to SPS power levels and larger mass-produced arrays.

Harmonics – The main concern of the panel was that of harmonic generation and reradiation from the individual rectenna elements. The amount of harmonic suppression possible with any economically reasonable filter placed on 10^{10} individual elements does not seem to be sufficient to limit the harmonic signals to an acceptable level. The only logical approach is to seek

244

ways to lower the number of individual receiving elements so that more care can be exercised in their design and construction. The Rensselaer Polytechnic Institute work was pointing in that direction, and the panel feels that a lot more effort should be expended toward further developing microwave-concentrating schemes such as the Boeing hogline.

Weather protection - It is a certainty that some form of weather protection or radome will be needed over all of the active elements in the rectenna. This feature, which has not really been considered in current rectenna designs, must be considered from the outset, as it will have significant effects on the physical construction of this costly component of the microwave system.

Element lattice design - With regard to the rectenna element lattice design, the narrow beam width, the high gain, the active element impedance, and the active element pattern that are characteristic of a large phased array arise from the fact that the elements are phase-coherently combined by a microwave network. The rectenna has external mutual coupling but not internal rf connections. Thus, the external mutual coupling affects the impedance of each element. But such an array, in which each element is connected to an independent resistive load, does not have the narrow beam width, the high gain, etc., of the phased array. This is fortunate for it allows realistic tolerances to enable satisfactory performance. There is, however, a corollary. The internal mutual coupling which increases element capture area as spacing increases, up to grating-lobe appearance, is not operative. Thus, for a half-wave slot or dipole over a ground plane, the effective area appears to be that of the isolated element, which is 0.261 times the square of the wavelength. Thus, the rectenna lattice should be square with a spacing just above one-half wavelength. However, it is not necessarily true that the element effective area is square, which may require an adjustment of the lattice. Clearly, more work should be done on this problem, but conventional unit cell active impedance approaches appear to be useless.

Cost effectiveness - The rectenna is currently a major cost factor in the total SPS system. As such, it should be subjected to careful cost-effectiveness-sensitivity studies, which might point toward a slightly less efficient system but with substantial cost savings. For example, at the outer edge of the rectenna, the cost in dollars per watt appears to be higher than that for surface-deployed solar cells at the SPS solar cell cost. In other words, it would be more cost effective to replace a substantial fraction of the outer area of the rectenna with solar cells.

SUMMARY

In summary, it is the consensus of the microwave power transmission and reception workshop review panel that a 5-gigawatt SPS microwave power transmission system is probably technically feasible. However, a large amount of work will be necessary in a number of areas to establish certainty and to determine system efficiency, reliability, rf compatibility, security, safety, longevity, and cost.

The panel believes that the final system will not resemble the current reference system and urges NASA to recognize this in all future planning. The GBED appears too heavily locked into the reference system.

RECOMMENDATIONS

The panel recommends more attention to systems engineering and failure analysis. There should be more sensitivity studies to optimize cost effectiveness. Attention should be paid to system security and antijamming features. There should be periodic overall design reviews to update critical design parameters.

In view of the magnitude and potential importance of the SPS, the panel recommends major program management status and a single program office within NASA for greater coordination of the contractor effort. Finally, the panel applauds the outstanding effort to date by the SPS team and is impressed with the very good progress which has been made thus far.

REFERENCES

1. Satellite Power System: Concept Development and Evaluation Program, Reference System Report. Rep. DOE/ER-0023, Department of Energy, Oct. 1978. (Also available as NASA TM-79762, 1979.)

2. Satellite Power System Concept Development and Evaluation Program Plan, July 1977-August 1980. NASA TM-79400, 1978.

3. Solar Power Satellite System Definition Study - Phase III, Final Report. Volume III - Laser SPS Analysis. Rep. D180-25969-3, Boeing Aerospace Co. (Contract NAS 9-15636), June 1980.

4. Satellite Power System: Concept Development and Evaluation Program, Volume I - Technical Assessment Summary Report. NASA TM-58232, 1980.

5. Dietz, R. H., coordinator: Solar Power Satellite Microwave Power Transmission and Reception, A Workshop Held at Lyndon B. Johnson Space Center, January 15-18, 1980. NASA CP-2141, 1980.

6. Arndt, G. D.; and Monford, L. G.: Solar Power Satellite System Sizing Tradeoffs. NASA TP-1804, 1981.

7. Chie, C. M.: A Ground Based Phase Control System for the Solar Power Satellite, Volume IV, Final Report. LinCom Corp. (Contract NAS 9-15782). NASA CR-160458, 1980.

8. Ott, J. H.; and Rice, J. S.: Digital SPS Phase Control Using Traveling Wave Interferometry. Novar Electronics Corp., Oct. 1978.

9. Belohoubek, E. F.; Ettenberg, M.; et al.: Final Report, Analysis of S-Band Solid-State Transmitters for the Solar Power Satellite. RCA Laboratories, David Sarnoff Research Center (Contract NAS 9-15755). NASA CR-160320, 1979.

10. Gutmann, Ronald J.; and Borrego, Jose M.: Solar Power Satellite Rectenna Design Study: Directional Receiving Elements and Parallel-Series Combining Analysis. Rensselaer Polytechnic Institute (Contract NAS 9-15453). NASA CR-151866, 1978.

11. Arndt, G. D.; and Berlin, L. A.: Microwave System Performance for a Solar Power Satellite During Startup/Shutdown Operations. Proceedings of Fourteenth Intersociety Energy Conversion Engineering Conference, Vol. 2, American Chemical Society (Washington, D.C.), 1979, pp. 1500-1505.

12. Solar Power Satellite System Definition Study - Phase II. Volume II - Reference System Description. Boeing Aerospace Co. (Contract NAS 9-15636). NASA CR-160443, 1979.

247

13. Microwave Power Transmission System – SPS System Evaluation – Phase III, Vol. I. Rep. D180-24635-1, Boeing Aerospace Co. (Contract NAS 9-15196), Mar. 1978.

14. Solar Power Satellite System Definition Study – Part II. Volume IV – Microwave Power Transmission Systems. Boeing Aerospace Co. (Contract NAS 9-15196). NASA CR-151668, 1977.

15. Duncan, Lewis M.; and Gordon, William E.: Ionosphere/Microwave Beam Interaction Study, Final Report. Rice University (Contract NAS 9-15212). NASA CR-151517, 1977.

16. Maynard, O. E.; Brown, W. C.; et al.: Microwave Power Transmission System Studies, Volume 2: Introduction, Organization, Environmental and Spaceborne Systems Analyses. Raytheon Co. (Contract NAS 3-17835). NASA CR-134886, vol. 2, 1975.

17. Rush, C. M.: Ionospheric Disturbance Overview. Paper presented at Satellite Power System (SPS) Program Review (Lincoln, Nebr.), Apr. 22-25, 1980. Rep. DOE/ET-20175-1, Department of Energy, Apr. 1980, p. 64.

18. Gordon, William E.; and Duncan, Lewis M.: Ionosphere/Microwave Beam Interaction Study, Final Report. Rice University (Contract NAS 9-15212). NASA CR-151821, 1978.

19. Arndt, G. D.; and Leopold, L.: Environmental Considerations for the Microwave Beam From a Solar Power Satellite. Proceedings of Thirteenth Intersociety Energy Conversion Engineering Conference, Vol. 1, Society of Automotive Engineers (Warrendale, Pa.), 1978, pp. 195-200.

20. Dickinson, R. M.: Beamed Microwave Power Transmitting and Receiving Subsystems Radiation Characteristics. Rep. 80-11, Jet Propulsion Laboratory (Contract NAS 7-100), June 15, 1980.

21. Dickinson, Richard M.: Rectenna Array Measurement Results. Solar Power Satellite Microwave Power Transmission and Reception, A Workshop Held at Lyndon B. Johnson Space Center, January 15-18, 1980. NASA CP-2141, 1980, pp. 307-316.

22. Tracking and Data Relay Satellite System – System Design Report, Volume III. Rep. 2900-200-003-002, TRW Inc., Mar. 26, 1979.

23. Lindsey, W. C.; Kantak, A. V.; Chie, C. M.; and Booth, R. W. D.: SPS Phase Control System Performance Via Analytical Simulation. LinCom Corp. (Contract NAS 9-15725). NASA CR-160582, 1979.

24. Lindsey, W. C.; Scholtz, R. A.; and Chie, C. M.: SPS Pilot Signal Design and Power Transponder Analysis, Phase III Final Report – Volume II. LinCom Corp. (Contract NAS 9-15782). NASA CR-160537, 1980.

25. Brown, William C.: Progress Report on the Adapting of the Crossed-Field Directional Amplifier to the Requirements of the SPS. Solar Power Satellite Microwave Power Transmission and Reception, A Workshop Held at Lyndon B. Johnson Space Center, January 15-18, 1980. NASA CP-2141, 1980, pp. 214-222.

26. Achievable Flatness in a Large Microwave Power Antenna Study, Final Report. General Dynamics Corp., Convair Div. (Contract NAS 9-15423). NASA CR-151831, 1978.

27. Lindsey, W. C.; and Kantak, A. V.: Automatic Phase Control in Solar Power Satellite Systems, Final Report. LinCom Corp. (Contract NAS 9-15237). NASA CR-151856, 1978.

28. Lindsey, W. C.: A Solar Power Satellite Transmission System Incorporating Automatic Beamforming, Steering and Phase Control. Rep. TR-7806-0977, LinCom Corp. (Contract NAS 9-15237), June 1978.

29. Solar Power Satellite System Definition Study - Phase I. Volume III - Reference System Description. Boeing Aerospace Co. (Contract NAS 9-15636). NASA CR-160372, 1979.

30. Schroeder, K. G.: White Paper on Experimental Studies Leading to a Solid State Retrodirective Phased Array for Microwave Power Transmission From a Solar Power Satellite. Rockwell International, Nov. 1979.

31. Nandi, A. K.; and Tomita, C. Y.: Ionospheric Effects in Active Retrodirective Array and Mitigating System Design. Solar Power Satellite Microwave Power Transmission and Reception, A Workshop Held at Lyndon B. Johnson Space Center, January 15-18, 1980. NASA CP-2141, 1980, pp. 159-168.

32. Nalos, E. J.: High Efficiency SPS Klystron Design. Solar Power Satellite Microwave Power Transmission and Reception, A Workshop Held at Lyndon B. Johnson Space Center, January 15-18, 1980. NASA CP-2141, 1980, pp. 175-184.

33. Weir, David G.: Solid State Device Technology for Solar Power Satellite. Solar Power Satellite Microwave Power Transmission and Reception, A Workshop Held at Lyndon B. Johnson Space Center, January 15-18, 1980. NASA CP-2141, 1980, pp. 358-366.

34. Solar Power Satellite System Definition Study - Phase II. Volume II - Reference System Description. Rep. D180-25461-2, Rev. A, Boeing Aerospace Co. (Contract NAS 9-15636), Dec. 1979.

35. Lunden, C. D.; and Lund, W. W.: Solar Power Satellite Antenna Element Evaluation, Final Report. Rep. D180-25940-1, Boeing Aerospace Co. (Contract NAS 9-15636C), Feb. 1980.

36. Brown, W. C.: Microwave Beamed Power Technology Improvement. Monthly Progress Report no. 19, JPL Contract 955104, Raytheon Co., Jan. 1980.

37. Nalos, Ervin J.: Evaluation of "Thick Wall" Wave Guide Element. Solar Power Satellite Microwave Power Transmission and Reception, A Workshop Held at Lyndon B. Johnson Space Center, January 15-18, 1980. NASA CP-2141, 1980, pp. 245-252.

38. Schroeder, K. G.; Carlise, R. L.; and Tomita, C. Y.: The Resonant Cavity Radiator (RCR). Solar Power Satellite Microwave Power Transmission and Reception, A Workshop Held at Lyndon B. Johnson Space Center, January 15-18, 1980. NASA CP-2141, 1980, pp. 235-244.

39. Brown, William C.: Method for Precision Forming of Low-Cost, Thin-Walled Slotted Waveguide Arrays for the SPS. Solar Power Satellite Microwave Power Transmission and Reception, A Workshop Held at Lyndon B. Johnson Space Center, January 15-18, 1980. NASA CP-2141, 1980, pp. 253-255.

40. Freiley, A. J.; Batelaan, P. D.; and Bathker, D. A.: Absolute Flux Density Calibrations of Radio Sources: 2.3 GHz. Jet Propulsion Laboratory (Contract NAS 7-100). NASA CR-156132, 1977.

41. Kozakoff, D. J.; Schuchardt, J. M.; and Ryan, C. E.: Considerations for High Accuracy Radiation Efficiency Measurements for the Solar Power Satellite Subarrays. Solar Power Satellite Microwave Power Transmission and Reception, A Workshop Held at Lyndon B. Johnson Space Center, January 15-18, 1980. NASA CP-2141, 1980, pp. 256-265.

42. Woodcock, G. R.; and Andryczyk, R. W.: Rectenna System Design. Solar Power Satellite Microwave Power Transmission and Reception, A Workshop Held at Lyndon B. Johnson Space Center, January 15-18, 1980. NASA CP-2141, 1980, pp. 281-290.

43. Gutmann, Ronald J.: Rectenna Session: Micro Aspects. Solar Power Satellite Microwave Power Transmission and Reception, A Workshop Held at Lyndon B. Johnson Space Center, January 15-18, 1980. NASA CP-2141, 1980 pp. 291-299.

44. Few, A.: Macro Aspects. Paper presented at SPS Workshop on Microwave Power Transmission and Reception (Houston, Tex.), Jan. 15-18, 1980.

45. Solar Power Satellite System Definition Study - Phase III. Volume IV - Solid State SPS Analysis. Rep. D180-25969-4, Boeing Aerospace Co. (Contract NAS 9-15636), June 1980.

46. Solar Power Satellite System Definition Study - Phase II. Volume IV - Microwave Power Transmission Systems. Boeing Aerospace Co. (Contract NAS 9-15636). NASA CR-160565, 1979.

47. Solar Power Satellite System Definition Study - Phase III. Volume II - Final Briefing. Rep. D180-25969-2, Boeing Aerospace Co., Grumman Aerospace Corp., and Mass Science Northwest (Contract NAS 9-15636), June 1980.

48. Maynard, Owen E.: Solid State SPS Microwave Generation and Transmission Study. Raytheon Co. (Contract NAS 8-33157), Apr. 1980.

49. Satellite Power System (SPS) Concept Definition Study, Exhibits D and E. Rep. SSD-80-0062, Rockwell International (Contract NAS 8-32475), July 1980.

50. Vanelli, J. C.: Design and Testing of a Master Slave Returnable Timing System for the Solar Power Satellite. Rep. LEC-10474, Lockheed Electronics Co., Dec. 1979.

51. Solar Power Satellite (SPS) Fiber Optic Link Assessment, Final Report. Boeing Aerospace Co. (Contract NAS 9-15636). NASA CR-160575, 1980.

52. Lunden, C. D.; Lund, W. W.; and Nalos, E. J.: SPS Antenna Element Evaluation. Paper presented at SPS Workshop on Microwave Power Transmission and Reception (Houston, Tex.), Jan. 15-18, 1980.

53. Fitzsimmons, G. W.: SPS Solid State Antenna Power Combiner. Solar Power Satellite Microwave Power Transmission and Reception, A Workshop Held at Lyndon B. Johnson Space Center, January 15-18, 1980. NASA CP-2141, 1980, pp. 338-347.

54. Brown, W. C.: High Power Microwave Generators of the Crossed-Field Type. J. Microwave Power, vol. 5, no. 4, Dec. 1970, pp. 245-259.

55. Briggs, B. H.; and Parkin, I. A.: On the Variation of Radio Star and Satellite Scintillations With Zenith Angle. J. Atmospheric Terrest. Phys., vol. 25, June 1963, pp. 339-366.

56. Oliner, A. A.; and Malech, R. G.: Mutual Coupling in Infinite Scanning Arrays. Microwave Scanning Antennas, R. C. Hansen, ed., Volume II, Array Theory and Practice, ch. 3. Academic Press, 1966, pp. 195-335.

1. Report No. NASA RP-1076	2. Government Accession No.	3. Recipient's Catalog No.
4. Title and Subtitle SATELLITE POWER SYSTEM: CONCEPT DEVELOPMENT AND EVALUATION PROGRAM VOLUME III - POWER TRANSMISSION AND RECEPTION TECHNICAL SUMMARY AND ASSESSMENT		5. Report Date July 1981
		6. Performing Organization Code
7. Author(s) R. H. Dietz, G. D. Arndt, J. W. Seyl, L. Leopold, and J. S. Kelley		8. Performing Organization Report No. S-507
9. Performing Organization Name and Address Lyndon B. Johnson Space Center Houston, Texas 77058		10. Work Unit No. 953-36-00-00-72
		11. Contract or Grant No.
12. Sponsoring Agency Name and Address National Aeronautics and Space Administration Washington, D.C. 20546		13. Type of Report and Period Covered Reference Publication
		14. Sponsoring Agency Code

15. Supplementary Notes

16. Abstract

Activities in the DOE/NASA Concept Development and Evaluation Program are discussed for the solar power satellite power transmission and reception system. A technical summary is provided together with a summary of system assessment activities. System options and system definition drivers are briefly described. Major system assessment activities have been in support of the reference system definition, solid-state system studies, critical technology supporting investigations, and various system and subsystem trade-offs. These activities are described together with reference system updates and alternative concepts for each of the subsystem areas. Conclusions reached as a result of the numerous analytical and experimental evaluations are presented. Finally, remaining issues for a possible follow-on program are identified.

17. Key Words (Suggested by Author(s)) RF transmission efficiency Antenna Ionospheric disturbances Microwave Wave propagation	Rectenna Solid-state devices Phase control RF power amplifiers	18. Distribution Statement Unclassified - Unlimited Subject Category 44
19. Security Classif. (of this report) Unclassified	20. Security Classif. (of this page) Unclassified	21. No. of Pages 277 22. Price* A13

*For sale by the National Technical Information Service, Springfield, Virginia 22161